DYNAMIC RESPONSE OF POST-TENSIONED TIMBER FRAME BUILDINGS

by

DENIS PINO MERINO

Supervisors:

ASSOC. PROF. STEFANO PAMPANIN
PROF. ANDREW BUCHANAN
DR. DAVID CARRADINE

A THESIS SUBMITTED
IN PARTIAL FULFILMENT OF THE REQUIREMENTS FOR THE
DEGREE OF MASTER OF ENGINEERING

CIVIL AND NATURAL RESOURCES ENGINEERING
CHRISTCHURCH, NEW ZEALAND
SEPTEMBER 2011

The dissertation entitled “Dynamic response of post-tensioned timber frame buildings”, by Denis Pino M., has been approved in partial fulfilment of the requirements for the Master Degree in Earthquake Engineering.

Stefano Pampanin

Andrew Buchanan

David Carradine

Abstract

An extensive research program is on-going at the University of Canterbury, New Zealand to develop new technologies to permit the construction of multi-storey timber buildings in earthquake prone areas. The system combines engineered timber beams, columns and walls with ductile moment resisting connections using post-tensioned tendons and eventually energy dissipaters.

The extensive experimental testing on post-tensioned timber building systems has proved a remarkable lateral response of the proposed solutions. A wide number of post-tensioned timber subassemblies, including beam-column connections, single or coupled walls and column-foundation connections, have been analysed in static or quasi-static tests.

This contribution presents the results of the first dynamic tests carried out with a shake-table. Model frame buildings (3-storey and 5-storey) on one-quarter scale were tested on the shake-table to quantify the response of post-tensioned timber frames during real-time earthquake loading. Equivalent viscous damping values were computed for post-tensioned timber frames in order to properly predict their response using numerical models. The dynamic tests were then complemented with quasi-static push and pull tests performed to a 3-storey post-tensioned timber frame.

Numerical models were included to compare empirical estimations versus dynamic and quasi-static experimental results. Different techniques to model the dynamic behaviour of post-tensioned timber frames were explored. A sensitivity analysis of alternative damping models and an examination of the influence of designer choices for the post-tensioning force and utilization of column armouring were made.

The design procedure for post-tensioned timber frames was summarized and it was applied to two examples. Inter-storey drift, base shear and overturning moments were compared between numerical modelling and predicted/targeted design values.

Keywords: timber buildings, post-tensioning, shake-table, dynamic, seismic, earthquake, Laminated Veneer Lumber (LVL)

Acknowledgements

I would first like to thank my supervisors Associate Professor Stefano Pampanin, Professor Andy Buchanan and Dr. David Carradine for giving me the chance of participating in this research project and for their support.
I would like to thank Professors Athol Carr and Bruce Deam for their advice. I also acknowledge my friend and colleague Michael Newcombe for his guidance
Finally, I would like to thank Professor Ulrike Kuhlmann and the Institute for Construction and Design of the University of Stuttgart for their help.

Dedication

This thesis is dedicated to my parents:

Silvia Merino Pastene & Leonardo Pino Cadiz

And to my wife:

Christine Bader

Table of contents

List of tables

List of figures and illustrations

List of symbols, abbreviations and nomenclature

a	=*Acceleration*
A_g	=*Gross area*
A_o	=*Sinusoidal excitation amplitude*
A_{pt}	=*Area of post-tensioning steel*
A_{sh}	=*Horizontal shear area*
A_{sv}	=*Vertical shear area*
b	=*Width of the member*
c	=*Neutral axis depth*
C	=*Compressive force*
C_d	=*Seismic coefficient*
C_o	=*Damping matrix*
d	=*Displacement*
D	=*Dead load*
E	=*Characteristic elastic modulus*
E_{con}	=*Effective elastic modulus of the timber connection*
E_D	=*Total energy dissipated during a complete cycle*
E_{eff}	=*Effective elastic modulus of the timber connection*
E_{para}	=*Mean parallel to grain elastic modulus of the timber*
E_{pt}	=*Elastic modulus of the post-tensioning tendons*
E_s	=*Equivalent strain energy at the maximum displacement of the cycle*
E_t	=*Mean parallel to grain elastic modulus of the timber*
f	=*Frequency*
F	=*Force*

f'_b =*Characteristic bending stress for timber*

f'_c =*Compression parallel to the grain*

f'_p =*Characteristic perpendicular to grain compressive stress for timber*

f'_s =*Characteristic shear stress for timber*

f'_t =*Characteristic tension stress for timber*

F_k =*Applied force of the k^{th} floor*

f_{po} =*Initial stress for post-tensioning tendons*

f_{pu} =*Ultimate stress for post-tensioning tendons*

f_{py} =*Yield stress for post-tensioning tendons*

F_y =*Yielding force*

g =*Gravity acceleration*

G =*Shear modulus*

h =*Height of the member*

H =*Inter-storey height*

h_1 =*Height of the first floor*

h_b = *Height of a beam*

h_c =*Height of a column*

h_e =*Effective height of the equivalent SDOF system*

H_i =*Height of the i^{th} floor*

H_n =*Height to the n^{th} floor (the roof)*

K =*Stiffness matrix*

K_e =*Effective stiffness*

K_i =*Initial stiffness*

k_o =*Elastic stiffness*

k_μ =*Force reduction factor, elastic to inelastic spectrum*

K_o =*Initial stiffness matrix*

K_t =*Tangent stiffness matrix*

L =*Length*

L_b =*Bay length*

L_{cant} =*Length of a cantilever (or shear span)*

L_p =*Plastic hinge length*

L_s =*Length of a spring*

m =*Mass*

M =*Mass matrix*

M_b =*Moment of the beam*

M_c =*Moment at the centreline of the column*

Mt =*Moment*

m_e =*Effective mass*

m_i =*Mass of the* i^{th} *floor*

M_o =*Overturning moment*

M_{pt} =*Moment contribution due to post-tensioning*

M_s =*Moment contribution due to non-prestressed steel or energy dissipation*

Mw =*Seismic magnitude*

Mn =*Nominal moment capacity*

N =*Normal axial force*

Q =*Live load*

r =*Bi-linear factor(post-yielding stiffness divided by initial stiffness)*

R =*Return period*

t =*Time*

T =*Tension force*

T_e =*Elastic period*

T_n =*Natural period of the structure*

T_{pt} =*Tension force from the post-tensioning*

v =*Velocity*

V =*Volume*

V_B =*Total base shear*

V_{jh} =*Horizontal joint shear force*

V_{jv} =*Vertical joint shear force*

$V_{s,i}$ =*Storey shear of the* i^{th} *floor*

w =*Sinusoidal excitation frequency*

Z =*Zone factor, New Zealand code*

α , β =*Coefficients for Cauchy damping*

γ =*Coefficient applied to ductility for correction of elastic damping*

γ_t =*Joint-panel deformation*

κ =*Correction coefficient for elastic damping*

μ =*Ductility*

μ_k =*Coefficient of kinetic friction*

μ_s =*Coefficient of static friction*

γ_h =*Horizontal joint deformation*

γ_v =*Vertical joint deformation*

Δ =*Displacement of member*

δ_1 =*Inelastic mode shape for the first floor*

δ_c =*Inelastic mode shape evaluated at the critical level*

Δ_c =*Inelastic Displacement profile evaluated at the critical level*

Δ_d =*Design displacement of structure*

Δ_{dec} =*Displacement of a monolithic member*

$\Delta_{elastic}$ =*Elastic displacement*

δ_i =*Inelastic mode shape for the* i^{th} *floor*

Δ_i =*Displacement of the* i^{th} *floor*

Δ_{mon} =*Displacement of a monolithic member*

Δ_p =*Plastic displacement*

Δ_{pt} =*Displacement of post-tensioning tendon due to a gap opening*

Δ_s =*Displacement of energy dissipation due to a gap opening*

$\Delta_{T,5}$ =*Displacement for period T on a 5% damped displacement spectra*

$\Delta_{T,\xi}$ =*Displacement for period T on a damped displacement spectra*

Δ_y =*Yield displacement*

ε =*Strain*

ε_c =*Equivalent strain*

ε_t =*Timber strain*

ø =*Strength reduction factor*

$ø_{dec}$ =*Decompression curvature*

$ø_{mon}$ =*Curvature of a monolithic member*

$ø_o$ =*Over-strength factor*

$ø_{pt}$ =*Nominal Diameter*

$ø_y$ =*Yield curvature*

$ø_u$ =*Ultimate curvature*

θ =*Rotation*

θ_b =*Contribution to the rotation from the beam*

θ_c =*Contribution to the rotation from the column*

θ_{con} =*Contribution to the rotation from the connections*

θ_d =*Inter-storey drift*

θ_{dec} =*Rotation at the decompression point*

θ_{imp} =*Imposed rotation on a connection (gap opening)*

θ_j =*Contribution to the rotation from joint (panel zone)*

θ_u =*Rotation at the ultimate point*

θ_y =*Rotation at the yielding point*

λ =*Re-centering ratio*

ξ =*Damping*

ξ_{el} =*Elastic damping*

ξ_{eq} =*Equivalent viscous damping*

ξ_{hyst} = *Hysteretic damping*

ρ =*Specific mass*

σ =*Stress*

Chapter One: **INTRODUCTION AND SCOPE OF RESEARCH**

1.1 Introduction

Timber structures are highly attractive due to the versatility, architectural aesthetics, environmental and economic benefits. However, size limitations, strength capacity and costs have restricted the use of timber in multi-storey commercial buildings where large dimensions (long-spans and open space) are required.

Current multi-storey construction with timber is basically covered by plywood shear wall systems; most of the constructions are of a residential type where an important number of partitions are required and where long spans are not necessary. On the other hand commercial buildings require a maximization of open areas and therefore the number of walls is reduced, where typically frames are the solution adopted. There are some alternatives using solid timber frames for commercial buildings, most of them created in the 1990's and summarized by Buchanan et al. [1991]. The main ideas of those solutions are to concentrate non-linear behaviour on ductile connections usually comprised of steel rods and steel plates. These solutions have not been widely adopted due to brittle failures obtained as a consequence of high variability of timber strength used (GLULAM) and due to complex connection detailing [Fairweather, 1992].

Based on emerging technology developed in the precast concrete industry [Priestley, 1991; Priestley *et al*., 1999; Pampanin, 2005; NZCS, 2010], new solutions for multi-storey timber buildings are currently being developed at the University of Canterbury. The study of new technologies that uses timber has been strongly supported by the New Zealand government and private companies due to life-cycle performance, energy efficiency, and sustainability considerations. Therefore, timber construction implies a low environmental impact helping to comply with the Kyoto Protocol [Baumert *et al*., 2002]. In particular the feasibility, costs and construction process of proposed post-tensioned timber systems have been analysed by Halliday [1991], Smith [2008a] and Smith et al. [2008b].

The performance of initial tests suggests a high probability of success for verifying the robustness of the system under the most severe code requirements.

The implementation of performance-based seismic engineering (PBSE) into structural design practice has shown that different levels of structural damage and business downtime lead to financial losses, indicating that construction decisions need to consider a life-cycle cost-analysis rather than only the initial construction costs [Krawinkler, 1999]. This has led to the development of high performance structural systems capable of limiting damage to desired levels in a seismic event, rather than only preventing the collapse of the structure.
The actual tendency is to increase the performance requirements of the buildings, thereby not allowing the near collapse condition and ensuring an operational response for most of the cases. *Figure 1-1* shows the vision of the performance and hazard seismic levels presented in the design code of the structural engineers association of California SEAOC Vision 2000 [SEAOC,1995] modified (arrows) by the tendency to ensure better seismic performance.

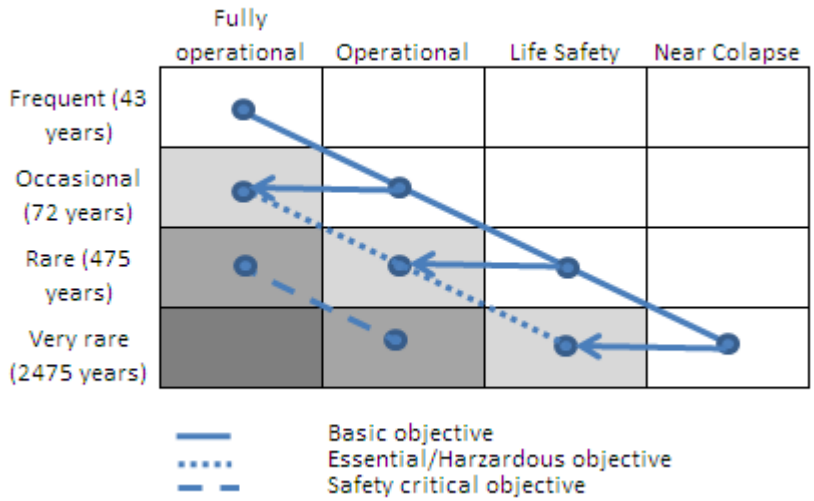

Figure 1-1 Performance design objective matrix [SEAOC, 1995] and modified basic objective curve (arrows) as proposed by [Pampanin, 2010]

A post-tensioned timber building complies with the requirements of low environmental impact construction and satisfies the PBSE philosophies. The proposed system combines glued laminated timber (Glulam) or laminated veneer lumber (LVL) or other similar engineered wood solutions, e.g., Cross-Laminated Timber (Cros-Lam or X-Lam) with post-tensioned steel strands and optional energy dissipation devices. In particular focus in New Zealand has been given to the use of LVL, an engineered wood product that increases the natural strength capacity of timber up to four times, reaching 40MPa in compression, thus making it capable of competing with concrete as a building material for long-span and multi-storey structures. Post-tensioned tendons (or threaded bars) help develop moment resisting connections, decrease beam deflections and provide re-centering action following a seismic event. Non-prestressed reinforcement can be also included and installed internally or externally (plug & play). Mild steel bars, in addition to providing stiffness and moment capacity, increase ductility, and seismic energy absorption of the structure. For simplicity, they are often referred to as energy dissipaters (as opposite to the post-tensioned tendon which cannot dissipater energy), though their use can be also well exploited in a non-seismic region as traditional reinforcing bars connecting timber elements.

As summarized by Buchanan et al. [2009] "*This new system gives opportunities for much greater use of timber and engineered wood products in large buildings, using innovative technologies for creating high quality buildings with large open spaces, excellent living and working environments, and resistance to hazards including earthquakes, fires, and extreme weather events*".

Structural behaviour of timber structures has been analysed under seismic conditions for many researches such as [Ceccotti, 1990] and [Popovski *et al.*, 2002]. A common conclusion is the great influence of the connection type adopted on the seismic response. Ceccotti analysed timber structures with traditional nailed connections. In this study, the degradation of stiffness and reduction of energy dissipation during cyclic testing was highlighted and regarded as typical for this type of connections. On the other hand, Popovski studied the seismic performance of riveted connections in heavy timber construction (*Figure 1-2*) for different types of processed timber products (LVL, GLULAM, etc.). In Popovski's research, the connections were all designed to fail in the rivet yielding mode. From tests (*Figure 1-3*) it was shown that the connections were ductile during seismic loading. The riveted connections showed non-brittle behaviour and lower variability in strength than conventional connectors (nailed or bolted); however there was a clear cyclic degradation of strength and a reduction of energy dissipation.

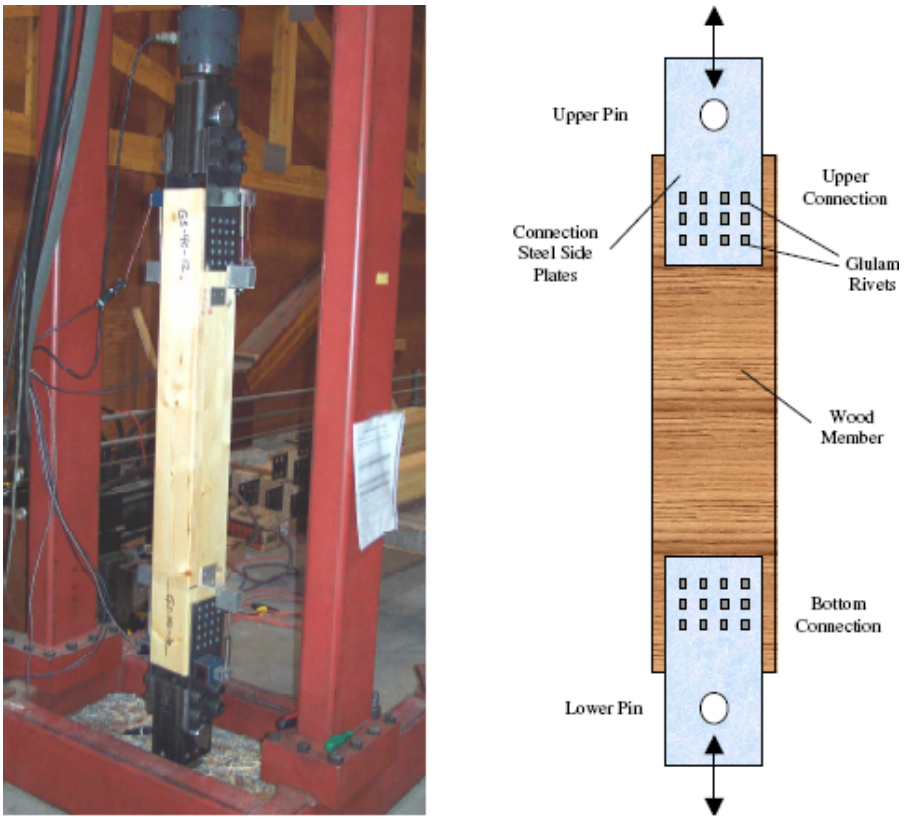

Figure 1-2 Test set-up for brace specimens with riveted connections [Popovski et al., 1995]

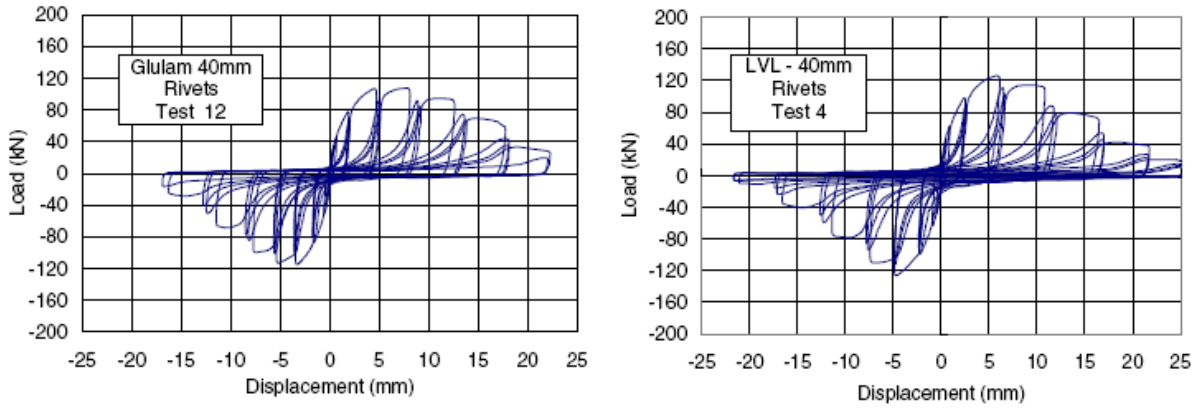

Figure 1-3 Test set-up for brace specimens with riveted connections [Popovski et al., 1995

The research presented in this document was carried out at the University of Canterbury and refers to the use of a post-tensioned timber connection, which has been proven to improve the seismic performance of traditional timber connections (as it will be explained in the following chapters). The solution proposed stands out for its simplicity and the capacity of avoiding residual deformations following a seismic event (due to the re-centering action of the unbonded post-tensioned tendons/bars).

Post-tensioned solutions recently developed at the University of Canterbury [Palermo *et al.*, 2005a; Smith *et al.*, 2007; Newcombe *et al.*, 2008a; Iqbal *et al.*, 2010] comprise the options of using post-tensioned timber walls or post-tensioned timber frames. The research described in this document is focused on the frame solution. *Figure 1-4* shows the beam-column joint of a post-tensioned solution that includes internal reinforcement (epoxied mild steel bars); this solution is considered as hybrid as it combines the tendons with an additional dissipation device. As mentioned, if non-prestressed reinforcement or supplemental dissipaters are required, they can be included internally or externally. The hybrid connection can be characterized (*Figure 1-5*) by a non-linear elastic part (as a contribution of the unbonded post-tensioned tendons) plus a bi-linear hysteretic part (given by the additional source of dissipation). During this research a pure post-tensioned timber solution (without any type of additional energy dissipation) was used, this decision was based on this connection being the simplest possible and the fact that it possesses the capacity of energy dissipation without any damage associated to it.

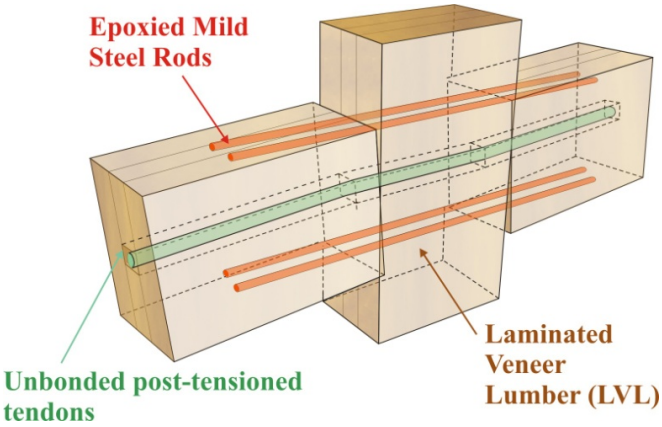

Figure 1-4 Beam-column connection, post-tensioned system with internal dissipation (Courtesy of M. Newcombe)

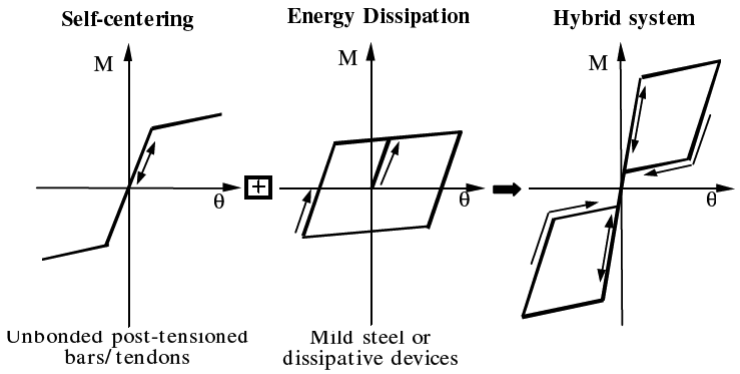

Figure 1-5 Hysteresis representation of hybrid configuration

Direct Displacement-Based Design (DDBD) is the most appropriate method to analyse post-tensioned rocking-dissipative timber structures considering that: a) damage is more strictly related to displacement, b) iterations on the initial stiffness would be required in a FBD c) calibration of force reduction factor (k_μ) would be necessary for the specific flag-shape hysteretic rule of these rocking-dissipative systems.

Non-linear behaviour, yielding and softening implies that for small increases of forces on the structure, a large increase in displacement could be obtained, and therefore displacement is the best way to describe the structural response until collapse. DDBD relies on the use of a Single-Degree-of-Freedom (SDOF) combined with secant stiffness and area-based equivalent viscous damping determined as the sum of the elastic and the hysteretic damping $\xi_{eq} = \xi_{el} + \xi_{hyst}$ [Priestley *et al.,* 2007]. The hysteretic contribution of the equivalent viscous damping of post-tensioned timber subassemblies have been so far obtained using the area-based approach through several quasi-static tests on beam-column subassemblies, column-to-foundation connection and single or coupled walls [Palermo *et al*., 2005a; Palermo *et al*., 2006a; Smith, 2006; Smith *et al*., 2007].The elastic damping contribution has instead not yet been investigated for post-tensioned timber buildings, and typically a constant value of ξ_{el} = 2% has been assumed. Computing the actual value of the equivalent viscous damping is required since a small increase of the assumed damping (***Figure 1-6***) may imply an important reduction of displacements. Hence, for a higher damping value, smaller member sizing is required to comply a deformation limit.

Figure 1-6 shows an example of the importance of computing accurately the value of the equivalent viscous damping particularly when other resources of supplemental damping are not used. In this case using the spectral displacements for "El Centro" earthquake it can be inferred that for a building of natural period T_n = 3sec the increase from 2% to 5% in equivalent viscous damping implies a reduction of around 65% of the expected lateral deformation of the building (it reduces from 370mm to 250mm). Therefore, an important reduction in the design forces demand and in the member sizing is achieved.

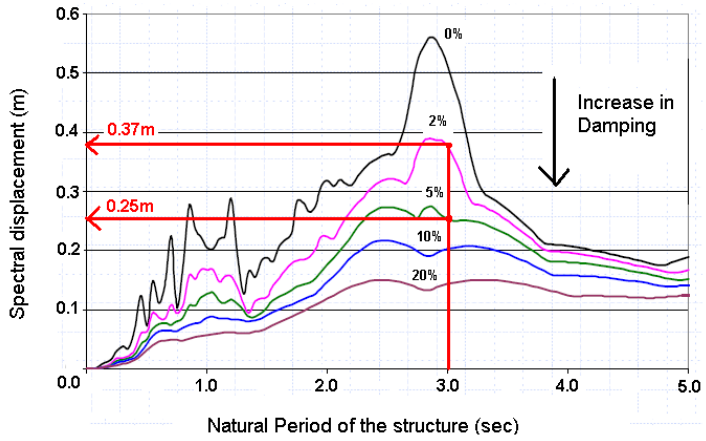

Figure 1-6 Spectral displacement, El Centro May 1940

1.2 Objectives and scope

The overall objective of this research is to validate the dynamic behaviour of post-tensioned timber frames. As part of this research, real-time shake-table tests were performed using LVL frames with post-tensioned connections. The specific objectives were:

- To monitor the general performance of post-tensioned timber frames during dynamic loading; drift (inter-storey deflection between adjacent levels divided by inter-storey height) capacity, level of damage, and residual displacements.
- To determine the influence of dynamic parameters in the response, i.e. amplification factors, type of damping, strain rate effects, and higher mode response. Sensitivity analyses were used to provide information required for proper modelling of post-tensioned timber frame structures subjected to dynamic forces.
- To determine the level of equivalent viscous damping for design of post-tensioned timber frames.
- To calibrate computer models in order to correctly represent the experimental results obtained.
- To review existing design procedures for post-tensioned timber frames, in particular the application of DDBD.
- To validate current design procedures (based on static and quasi-static tests), by testing post-tensioned timber buildings in a dynamic way.

1.3 Overview

Chapter two provide an overview and summary of the previous experimental tests undertaken on post-tensioned timber buildings at the University of Canterbury. While a wide number of post-tensioned timber subassemblies have been tested, at the time of performing this research no complete buildings had been tested. Additionally, as all performed tests were static or quasi-static, this investigation is the first to include dynamic response. Background literature regarding shake-table tests of buildings using alternative timber solutions is included.

Chapter three describes dynamic tests performed on a 1:4 scale post-tensioned timber frame building. Detailed description of the testing set-up is included as well as definitions of performed tests. The general behaviour of structure is described and the equivalent viscous damping computed. Variables that could affect damping values are discussed.

In Chapter four, quasi-static push and pull tests performed on a 1:4 scaled 3-storey post-tensioned timber frame are described and analysed, including test set-up and instrumentation. Frame lateral stiffness and variation of post-tensioning forces during testing are explained and quasi-static damping values are computed in order to be compared to dynamic damping.

Chapter five explains the current procedure to evaluate the response of post-tensioned timber frames subjected to lateral deformation (inter-storey drift). The main contributors to the inter-storey drift are defined and the procedure to compute their values is explained through formulation.

In Chapter six, different techniques to numerically model the dynamic behaviour of post-tensioned timber frames are explored. Rotational-spring models and Multi-spring models (non-linear elastic axial springs) are considered with the capacity of energy dissipation through hysteretic cycles or with a constant damping value added using a Rayleigh approach. Static and dynamic response from computer models are compared to the results obtained with quasi-static tests and shake-table tests respectively.

Chapter seven includes a sensitivity analysis on the effects on the seismic response using alternative damping models. Additionally, an examination is made of the influence of design choices in terms of post-tensioning force and column armouring.

Chapter eight includes a step by step analysis and design of two post-tensioned timber frames. The design procedure is summarized and some designer decisions are analysed. Time-history analyses are performed and results (floor acceleration, inter-storey drift, base shear, and overturning moment) are compared with those obtained through DDBD.

Chapter Two: **RECENT INVESTIGATION INTO BEHAVIOUR OF POST-TENSIONED TIMBER BUILDINGS**

2.1 Introduction

During lateral loading (due to earthquake or wind), traditional timber connections, i.e. nailed or steel dowels, may suffer moderate to extensive damage under inelastic demands, while a hybrid solution accommodates deformation demand at the beam-column interface. If correctly designed and detailed, negligible crushing of the LVL loaded perpendicular to the grain (column face) is expected.

Jointed ductile connections or hybrid configurations are the main idea behind the proposed system. During lateral displacement of the frame, a controlled rocking movement occurs at the beam-column interface (joint) and a gap at the beam-column interface opens and closes (*Figure 2-1*). When the gap opens the unbonded tendons elongate producing an increase in the post-tensioning force which prevents excessive gap-opening and provides an additional restoring force, ensuring minimal residual deformations after an earthquake. If additional non-prestressed steel (or dissipater devices) are included, they increase the connection stiffness and moment capacity and, importantly, could augment the overall energy dissipation of the system. To afford an effective re-centering and ensure a closing of the gap, the ratio of the moment capacity provided by the tendons (M_{pt}) over the moment capacity provided for the mild steel (M_s) defines the re-centering ratio, $\lambda = M_{pt}/M_s$, where λ = 1.15-1.25 is proposed, as has been done for precast concrete design [NZS3101:2006].

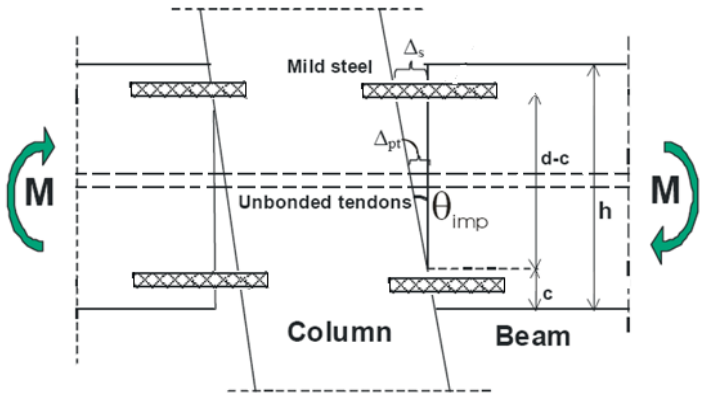

Figure 2-1 Jointed beam-column connection during lateral displacement (modified after Pampanin et al., 2001)

2.2 Developing of the post-tensioned timber system

The research program at the University of Canterbury started in 2005 with simple 2-dimension, 1:3 scale, beam-column subassemblies, followed by larger scale beam-column, column-to-foundation and single or coupled wall systems.
Figure 2-2 shows a beam-column connection configuration with post-tensioned only, the simplest possible connection and selected to be used during this research.

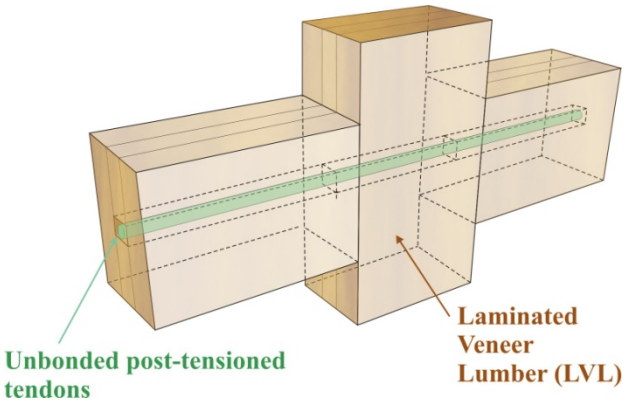

Figure 2-2 Jointed ductile beam-column connection, post-tensioned-only configuration (Courtesy of M. Newcombe)

The first results on quasi-static tests on the post-tensioned only configuration [Newcombe, 2005; Palermo *et al*., 2005a] showed a stable hysteretic behaviour, with non-linear elastic behaviour as a result of the gap opening and repositioning of the neutral axis. While hysteretic damping was displayed, this hysteresis does not imply damage, and energy dissipated is a consequence of timber capacity of recovering its original shape by the use of the strain energy stored. Re-centering was proven effective, with residual deformations being minimal. As previously mentioned, the apparent yielding point (*Figure 2-3*) corresponded instead to a relocation of the neutral axis once the gap is opened.

Following tests on a post-tensioned only solution, a hybrid solution using internal mild steel bars as additional reinforcement and dissipater devices was implemented (*Figure 2-4*). The deformed bars were machined down in order to confine and concentrate the plastic zone. Bars were fixed to beams and columns using epoxy.
The inclusion of reinforcing bars increased the lateral stiffness of the subassembly, the moment capacity of the beam-column connection and the amount of hysteretic energy dissipated. For the hybrid case the yielding point was actually the yielding of the dissipation devices. Negligible residual deformation was achieved. Non-visible damage on beam or column occurred during the test that reached 4.5% inter-storey drift.

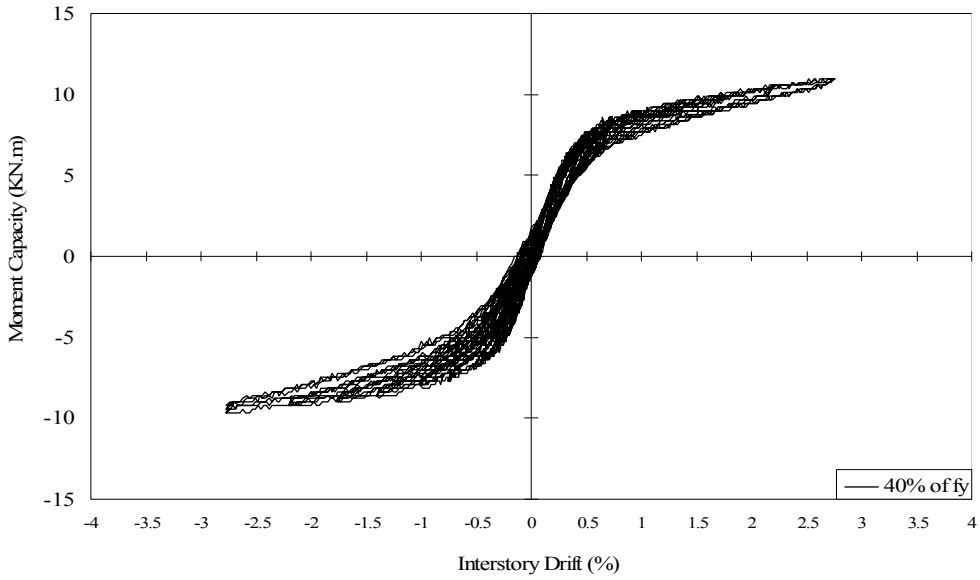

Figure 2-3 Moment capacity versus drift, post-tensioned only [Palermo et al., 2005]

Figure 2-4 Mild steel bars used as internal dissipaters [Palermo et al., 2006b]

Figure 2-5 shows the hysteresis curve recorded for hybrid configuration that includes internal mild-steel dissipaters. Stiffness degradation was observed, this degradation was probably due to bond degradation between reinforcing bars and LVL. Even when the degradation observed was much smaller than that observed for equivalent concrete solutions or nailed timber solutions, the idea of considering external dissipaters (as developed in the concrete version, Pampanin et al. [2005]) sounded attractive to avoid pinching and to easily replace the dissipater device; therefore it is considered a "plug and play" fuse.
A series of tests including a number of external dissipater configurations (*Figure 2-6*) were performed by Smith et al. [2006]. Dissipaters were installed using steel plates and epoxied rods creating a system which would increase energy dissipation with an easily removable and replaceable attached dissipater. The adopted solution was the one successfully proved with concrete structures or PRESSS-technology [Pampanin *et al.*, 2005]. The dissipater consisted of a simple mild steel bar epoxied within an external tube, acting as anti-buckling.

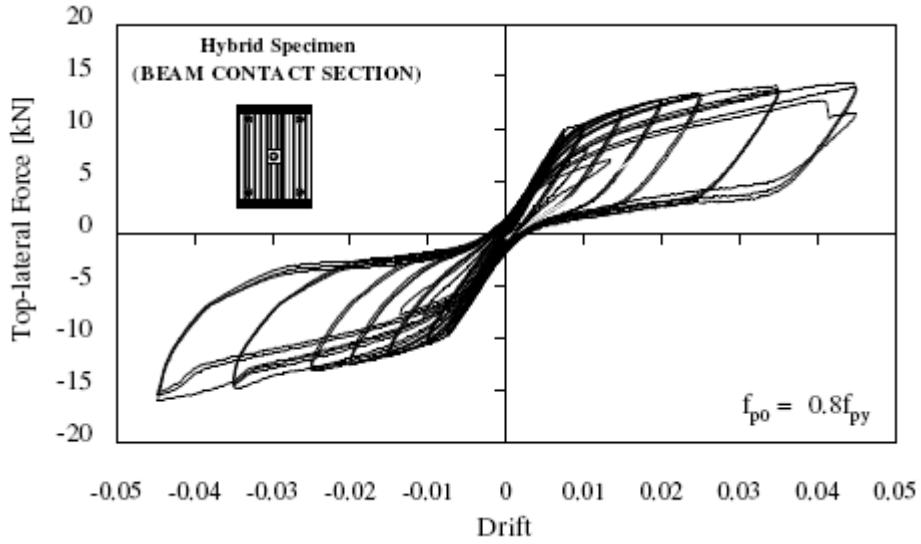

Figure 2-5 Hysteresis curve including post-tensioning and internal dissipaters [Palermo et al., 2006b]

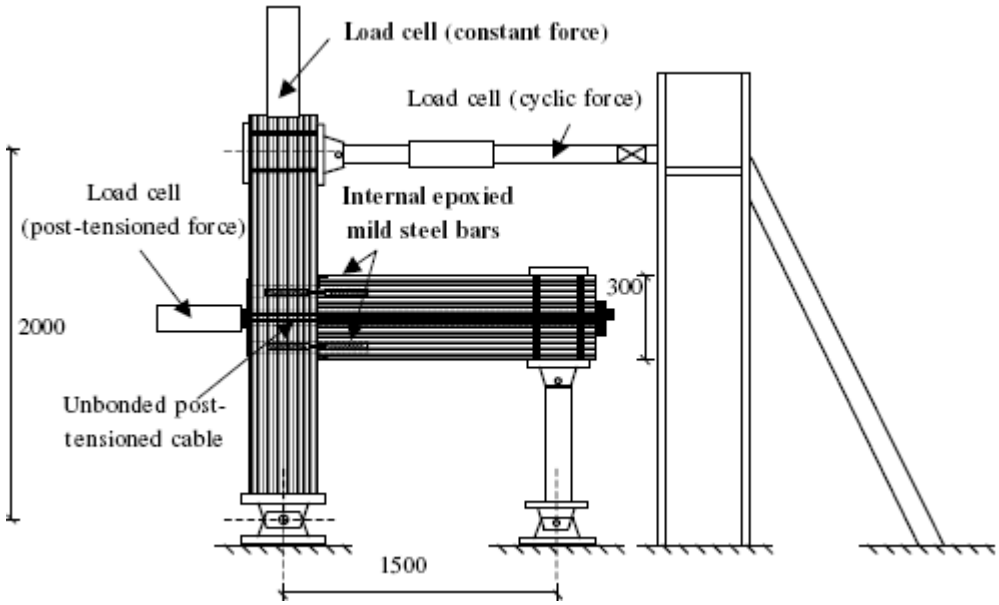

Figure 2-6 Test set-up for post-tensioned beam-column connection [Smith, 2006]

A pinned-pinned connection of the external dissipaters to the bracket and base plate was tested and rejected due to the occurrence of slipping as a consequence of hinge movement. An improved fixed-fixed solution was then tested (*Figure 2-7*); this configuration eliminated the slippage problems and showed an important increase in moment capacity and energy dissipation respective to the post-tensioned only solution (see *Figure 2-8*). The resultant flag-shape hysteresis loops proved to be very stable and exhibited no stiffness degradation (no bond deterioration being possible) and very satisfactory hybrid behaviour, e.g. re-centering and hysteretic dissipation.

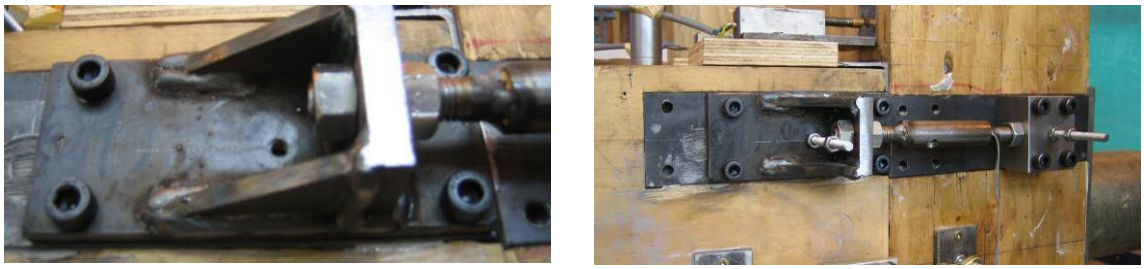

Figure 2-7 Beam-column connection, fixed-fixed dissipater attachment [Smith, 2006]

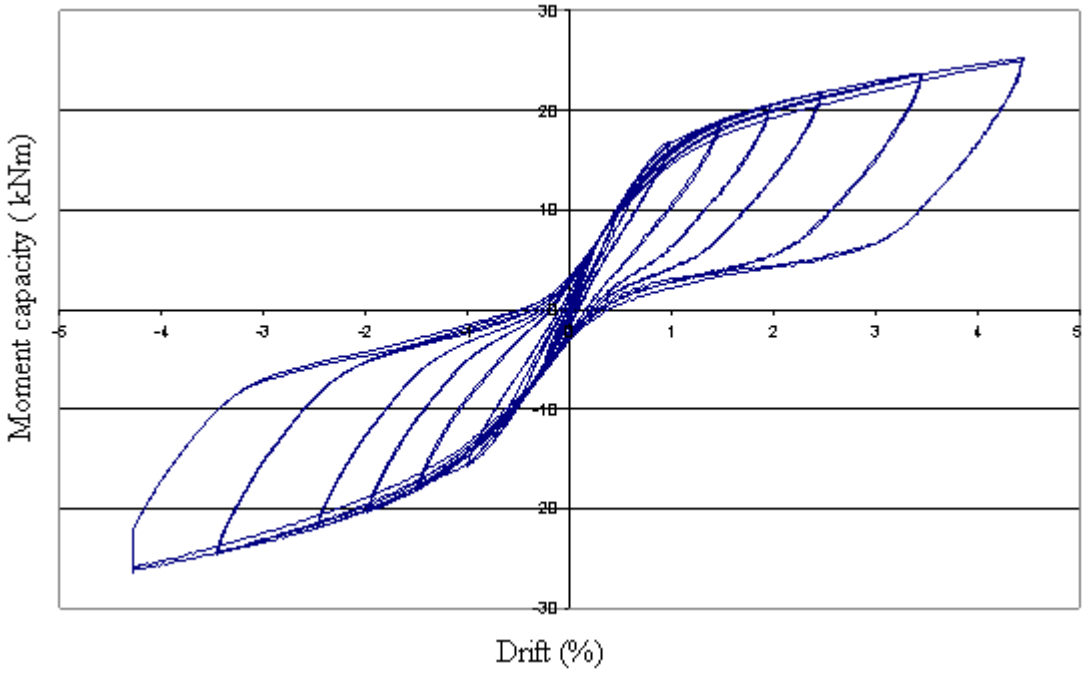

Figure 2-8 Moment capacity versus drift, external dissipater attached [Smith, 2006]

During the following years, a wide variety of rocking connections were tested including smaller scale specimens utilizing external and internal dissipation for beam-column connections, columns and walls (***Figure 2-9***). In general excellent seismic performance resulted [Palermo ***et al***., 2006b], and thus fomented the execution of test at bigger scale.

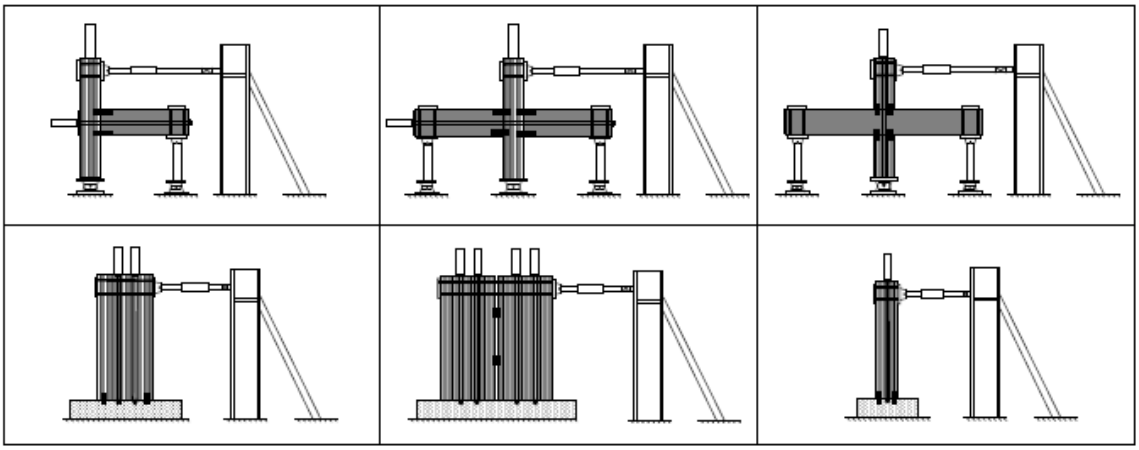

Figure 2-9 Interior and exterior beam-column subassemblies, single and coupled walls and columns specimens [Palermo et al., 2005a]

A full scale beam-column joint was designed and tested under quasi-static loading as part of a six-storey building being located in a high seismic zone in New Zealand [Iqbal *et al*., 2010] This investigation considered internal (*Figure 2-10*) and external beam-column joint subassemblies, with and without steel armouring plates, including and excluding external mild steel energy dissipaters, and considered different levels of post-tensioning force (*Figure 2-11*).

Figure 2-10 Full scale interior beam-column joint [Iqbal et al., 2010]

This full scale tests confirmed the previous results obtained from smaller scale subassemblies tests. In particular no visible damage was achieved at 2.5% inter-storey drift and re-centering action was effective. Post-tensioning losses at the end of each test were not greater than 2% of the initial post-tensioning value.

*Figure 2-12*a, shows a comparison between post-tensioned only versus hybrid solution (external "plug & play" mild steel energy dissipaters attached) both cases with steel armouring. There is clearly an important increase in energy dissipation and moment capacity when the hybrid solution is considered; additionally a small increase of stiffness is also achieved. Negligent residual deformations resulted.

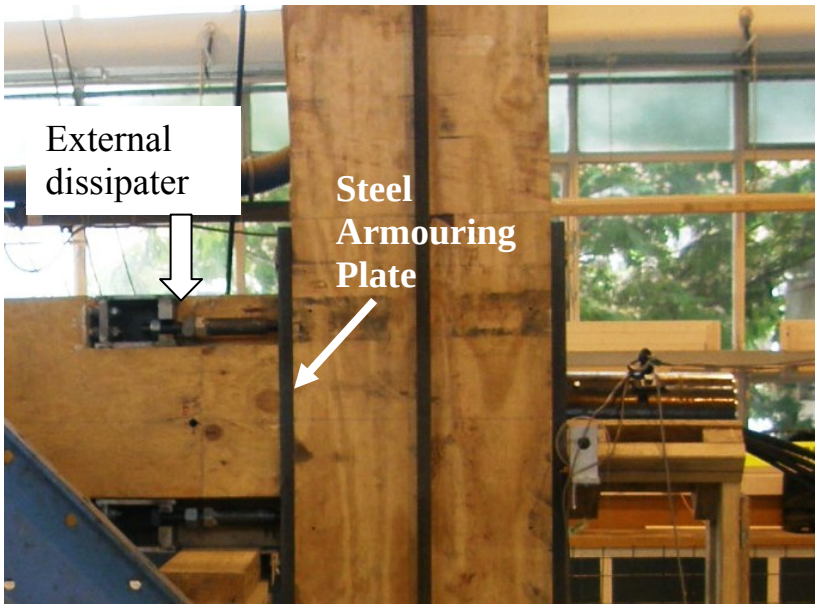

Figure 2-11 Full scale interior beam-column joint. Hybrid connection (post-tensioned tendons plus external energy dissipaters) with steel armouring [Iqbal et al., 2010]

Figure 2-12b compares armoured and unarmoured (timber against timber) for post-tensioned only configurations. In this case the armouring consisted on 30mm thick steel plates at beam-column interfaces to reduce perpendicular to the grain stress in compression.
The test that considered armouring shows a clearly increased stiffness over the configuration without armouring, but the energy dissipated was considerably smaller. Without the steel armouring, the column loaded perpendicular to the grain started to suffer damage at roughly 1% lateral drift. Even though the damage in the timber was minimal (2-4 millimetres), this generated an increase in energy dissipation, though not reliable because associated to material-related damage. Timber crushing on columns also creates a loss in post-tensioning force and thus implies a loss in lateral stiffness. The armoured case registered a loss on post-tensioning force around 2% meanwhile the unarmoured configuration lost approximately 9% of the initial post-tensioning force.

Additionally, in the same contribution by Iqbal et al. [2010] the effects of screws reinforcing in the joint-panel region were considered. It was noted that inclusion of screws did not change the stiffness of the subassembly but it helped reducing the losses of post-tensioning force.

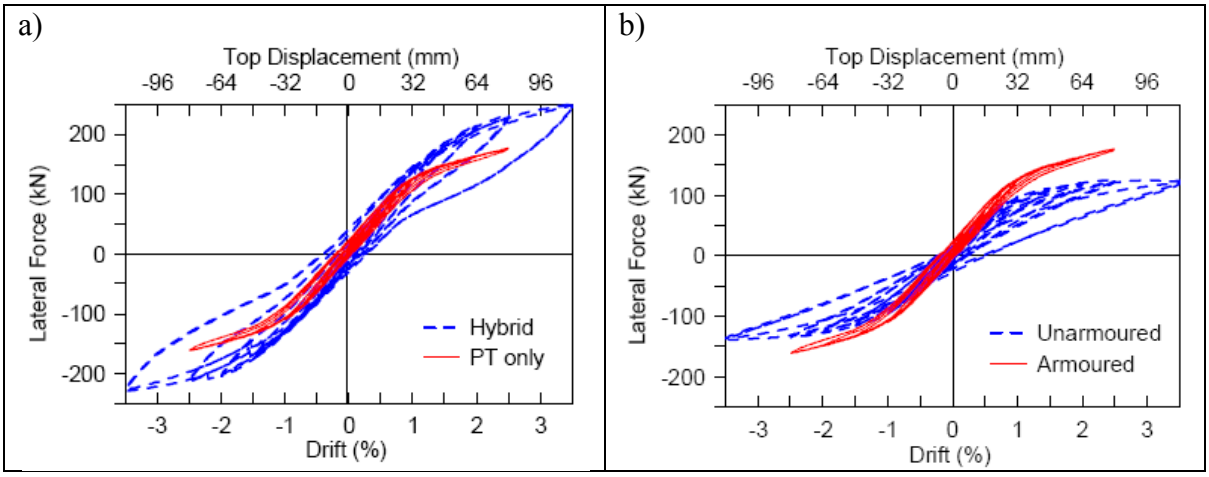

Figure 2-12 Full scale beam-column joint: a) Hybrid armoured configuration versus post-tensioned armoured configuration; b) Post-tensioned armoured configuration versus post-tensioned unarmoured configuration [Iqbal et al., 2010]

From the previous investigations, a summary of the most important points to take into consideration are as follows:

- The post-tensioning-only solution exhibits a robust non-linear hysteretic behaviour, due to the re-centering action of the unbonded post-tensioned tendons and has showed energy dissipation with no damage associated.
- Armouring of the beam-column connection can help reducing the stress demand perpendicular to the grain and increase the overall subassembly stiffness. However it reduces energy dissipation (damping).
- Hybrid solutions (combination of post-tensioned and non-post-tensioned reinforcing) increase section moment capacities and energy dissipation. For a specific drift of the structure the contributions to that drift will be the result of four factors; 1) deformation of beams, 2) deformations of columns, 3) panel zone deformation and 4) joint gap opening.
- The hybrid system is characterised by a flag shaped hysteresis loop during cyclic testing as a result of the combination of post-tensioning (non-linear elastic contribution) plus energy dissipaters (elasto-plastic or similar hysteresis).

All mentioned tests were performed in a static or quasi-static manner, meaning that the velocity and acceleration dependent parameters were not considered in the response. The effects of earthquakes and wind need to be analysed and understood in a dynamic mode before being confident about an equivalent static analyses.
Given that the objective of this research was to perform the first dynamic test on post-tensioned timber structures, literature regarding shake-table testing on timber structures is included in following sections.

2.3 Dynamic testing on timber buildings

Few researches have tested timber structures in a dynamic way, i.e. using a shake-table. These studies seem to have the common goal of validate under dynamic motion the development of alternative connection solutions capable of providing enhanced moment resistance, energy dissipation and ductility, when compared to more traditional timber connections with losses in stiffness and high flexibility.
The approach used by Heiduschke et al. [2008] to provide timber structures with these mentioned characteristics was to creating a strong reinforced joint through the use of bolts, glass-fibres and densified layers of laminated timber (*Figure 2-13*). The reasoning behind the use of the reinforced connection illustrated here was based on the low stiffness of traditional connections and the difference between moment capacities of members and connections. The reinforced connection used was proved to increase stiffness, moment capacity and energy dissipation.

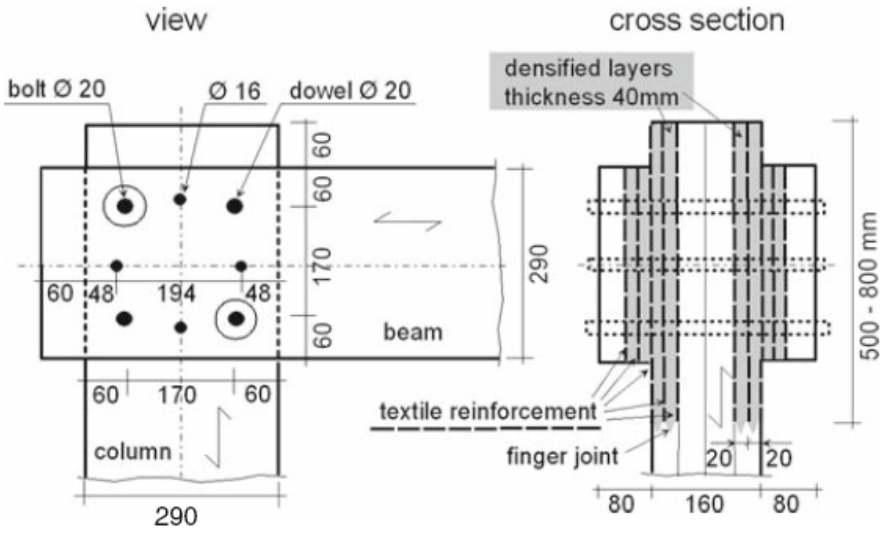

Figure 2-13 Densified and reinforced beam-column connection [Heiduschke et al., 2008]

Shake-table tests were performed on a 1:4 scale 2-storey timber-frame model building and on a full scale 2-storey timber-frame model building (*Figure 2-14*) incorporating the reinforced joint connections. Tests were divided on free-vibration tests and seismic tests. During tests it was possible to observe stiffness degradation due to the accumulation of damage at connections. The hysteresis response of the timber connection had a highly pinched shape (*Figure 2-15*); the achieved ultimate rotation was 2.4 times the yield rotation.
The obtained first-mode damping ratios, using the described configuration, ranged from 5% to 25% of critical damping, increasing depending of the level of sustained damaged. The energy dissipation recorded, was then attributed in its first stage (small deformation) to friction between beams and columns. At larger deformations, the dissipated energy was clearly attributed to the plastic deformation of wood and steel fasteners, therefore to unrecoverable damage.

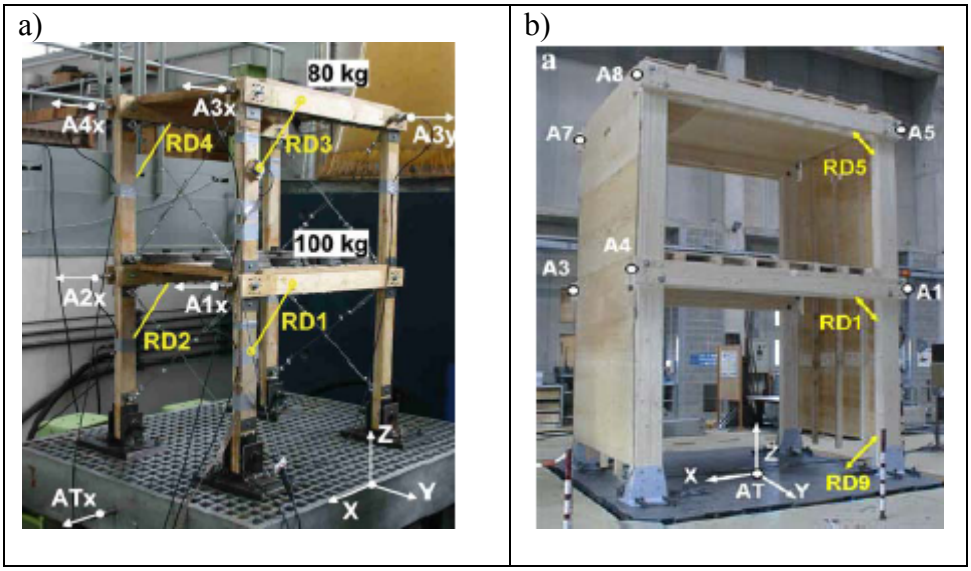

Figure 2-14 a) 1:4 scale model building b) Full-scale model building [Heiduschke et al., 2008]

The system was demonstrated to have limited self-centering capacity (residual deformations were recorded). This capability was explained based on the strain energy accumulated on the wood, used to restore the system to its original position. Once damage at connection was reduced (by limiting the large plastic excursion) residual deformations were minimised.
The studied concluded that it is possible to provide frames with moment-resisting joints in order to dissipate energy and provide a self-centering structure capable of undergoing large deformations. Beam and columns were kept elastic and the connections worked as dissipative links.

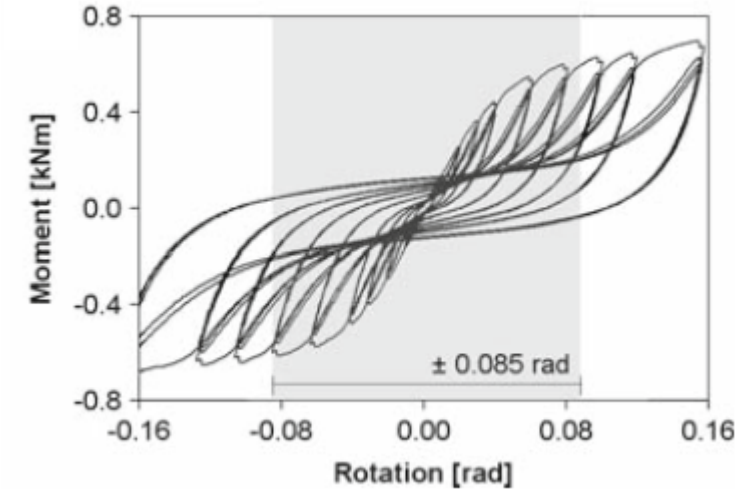

Figure 2-15 Moment rotation hysteresis from a cyclic test of a beam-column connection [Heiduschke et al., 2008]

Large-scale shake-table test have been performed to a number of timber structures, however, almost all of them were of the shear-walls type. One outstanding research is the NEESWood project [Lindt, 2010] which considered full-scale 3-D testing of timber shear-wall structures in a study that lasted four years. The NEESWood project's objectives were the development of mid-rise timber structures as an economic option to be applied in seismic regions in the United States.

The NEESWood project began in 2005, with the first benchmark structure tested in 2006 (***Figure 2-16***a). The two-storey three-bedroom 160m^2 wood-frame structure was designed based on an existing U.S. building code and tested at Buffalo's SEESL shake-table facility. This benchmark structure represented a typical 2x4in timber-framed house with dimensional lumber from the 1980's or 1990's located in California. The main structure consisted of a timber-framed house on wood joist floor with wood truss roof and concrete tile roofing. The exterior walls were covered by stucco over OSB sheathed shear-walls; the interior timber-framed walls were sheathed with gypsum wallboard. Typical corner hold-downs were used to prevent overturning of walls and to ensure a racking mode of deformation. The townhouse was subject to historical ground motions recorded during the 1994 Northridge Earthquake in California, reaching a peak ground horizontal acceleration of 0.84g and a peak ground vertical acceleration of 0.85g.
Even though the townhouse's seismic response was acceptable, a considerable amount of damage was registered. The damage registered at 2% of inter-storey drift included: cracking of the stucco, cracking and crushing of Gypsum wallboard, cracking and splitting of the anchoring system, and permanent differential movement of adjacent panels. Residual lateral deformation was also recorded.
The equivalent viscous damping of the structure was computed using a half-power bandwidth method, giving as a result an equivalent viscous damping of ξ = 15.4% for the first natural frequency.

In a second phase, the NEESWood project considered the same two-story townhouse structure but this time a fluid damper device connected with a chevron brace configuration was incorporated into key walls (***Figure 2-16***b). As a result of the increase of damping on the system, the seismic response was notably improved when compared to the conventional timber-framed wall configuration. Damage achieved was reduced and so were residual deformations.

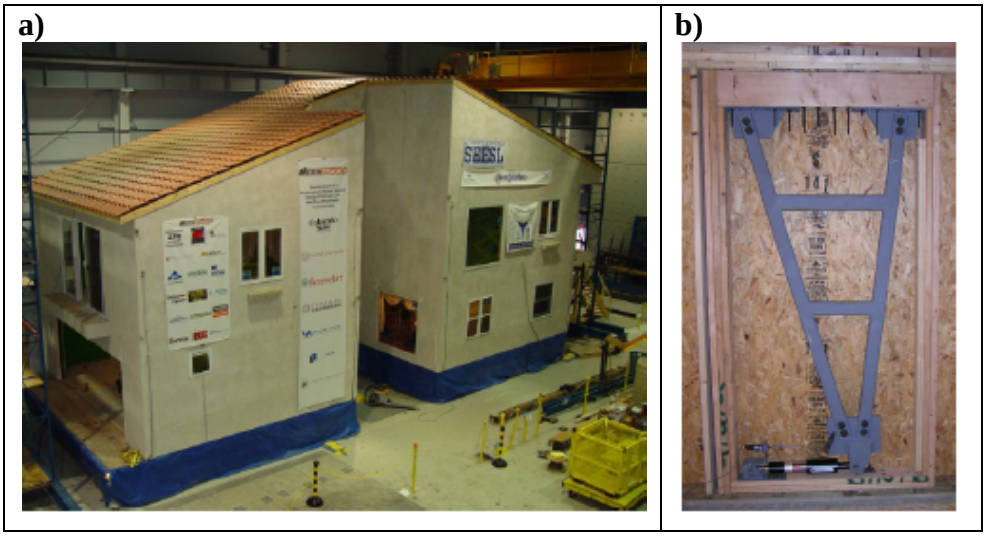

Figure 2-16 NEESWood Project: a) Shake-table test in 2006 b) Chevron-based modular damped wall [Lindt, 2010]

The Capstone building was tested on the E-defense shake-table in 2009 as part of the NEESWood project (*Figure 2-17*). The mid-rise, 6-storey, residential building of 1350m^2 was the ultimate test performed during the cited project [Lindt, 2010].
Performance-based seismic philosophy was applied to defined four levels of earthquake intensities representing particular performance levels expected and related with a probability of occurrence. The Capstone building was subjected to three levels of seismic intensity: a moderate earthquake; a design-basis earthquake (DBE); and a maximum credible earthquake (MCE).
The design was based on Direct Displacement Based Design (DDBD) approach [Priestley *et al*., 2007] that was extended to multi-story woodframe buildings. The building consisted of plywood shearwalls tied down with steel rods and supplied with additional dissipater devices included on walls. The building seismic response was reported as highly satisfactory, there was no structural damage while undergoing peak inter-story drifts of approximately 2% to 3%, additionally residual deformations were not significant.

Figure 2-17 Capstone test specimen, July 2009 [Lindt, 2010]

The mentioned projects are evidence of the continuing improvement of timber structures. There is an increasing requirement to provide timber structures with the capacity to withhold strong seismic events suffering only minimal damage. Costly repairs and downtime have to be avoided.

Accumulated damage and residual deformations are the best indicators of how well a structure has performed during an earthquake. A timber solution capable of resisting strong ground motions with minimal structural damage, negligible residual deformations, and being applicable to commercial and residential buildings is one of the primary objectives of the University of Canterbury's research.

Chapter Three: **SHAKE-TABLE TESTING OF 3-STOREY AND 5-STOREY POST-TENSIONED TIMBER FRAME BUILDINGS**

3.1 Introduction

This chapter provides a detailed summary of the dynamic response of two (5-storey and 3-storey), 1:4 scale, model buildings, constructed with post-tensioned timber frames. The aims of these tests were: a) to compute the parameters that define the dynamic response and b) to monitor the global behaviour of the structures under earthquake loading, in particular re-centering capacity and level of residual damage. Two types of tests were performed using either recorded ground motions (earthquake records) or sinusoidal tests with free vibration.

3.2 Materials

3.2.1 *Laminated Veneer Lumber (LVL)*

The experimental test used Nelson Pine LVL; *Table 3-1* summarizes the characteristic values used [Nelson Pine, 2003]. Stresses and strengths have been computed through testing full size specimens and considering the lower 5-percentile value determined with 75% of confidence. The value of the modulus of elasticity was not specified by the manufacturer and thus obtained by testing at the University of Canterbury [Cusiel 2009].

Table 3-1 Characteristic short duration modulus of elasticity and strength values [Nelson Pine LVL]

Parameter	Symbol	Value (MPa)
Modulus of elasticity parallel to the grain	E	10700(*)
Shear Modulus	G	500
Bending strength	f'_b	42
Shear strength	f'_s	6
Compression parallel to the grain	f'_c	35
Tension parallel to the grain	f'_t	22
Compression perpendicular to the grain	f'_p	12

(*) E-modulus value obtained by tests at University of Canterbury

3.2.2 *Post-Tensioned steel strands*

The experimental tests utilised 12.7mm, 7-wire strands (A_{pt} = 99mm^2) centred inside beams and *through columns for post-tensioning. The properties are listed in Table 3-2.*

Table 3-2 Post-Tensioning strand properties

Nominal Diameter	$ø_{pt}$	13mm
Nominal Area	A_{pt}	99mm^2
Nominal Ultimate Stress	f_{pu}	1862MPa
Elastic Modulus	E_{pt}	197000MPa
Yield Stress	f_{py}	1530MPa

3.3 Geometry and similitude requirements

3.3.1 *Geometry of model buildings*

The model building (*Figure 3-1*a) is based on a portion of a realistic 5-storey prototype structure with plan dimensions in the North-South direction of 16m and in the East-West direction of 12m (*Figure 3-1*b). The prototype building was assumed to be a shear-wall type in the North-South direction and a frame type in the East-West direction. The model (test specimen) building thus represents the main seismic resisting system in the East-West direction. In plane the post-tensioned timber frame has two bays that span for 6m and the interstorey height is 3.2m.

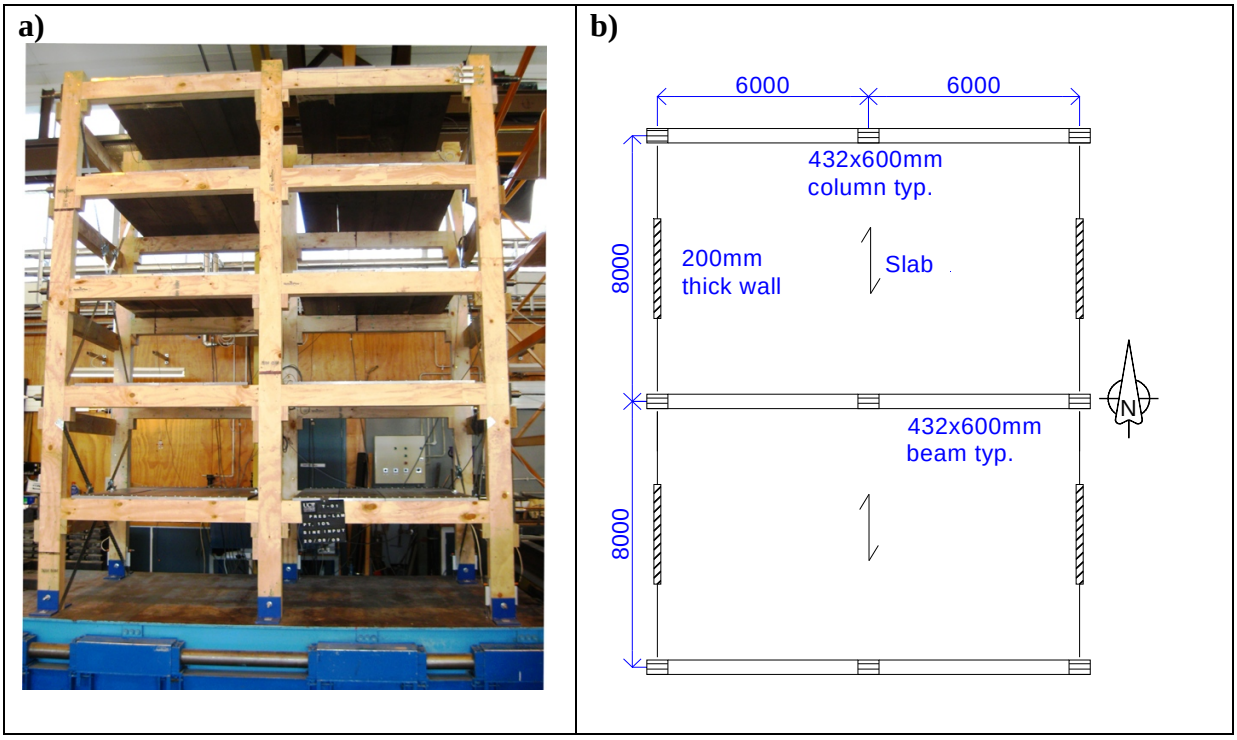

Figure 3-1 a) 5-storey 1:4 scale model building on shake- table b) Plan section of prototype building

The prototype building was designed according to the New Zealand code NZS1170:2004 considering Wellington city seismicity, soil type C, 1/500 year event without near field factors. The prototype building was designed to avoid structural damage during lateral deformations smaller than 2.5% interstorey drift.
The gravity loads utilized were: dead load D = 2.9KPa and live load Q = 3KPa. This resulted in a floor mass for a frame under seismic load combination (D+0.3Q) of 367kN.
The seismic forces were obtained according to the Direct Displacement Based Design [Priestley *et al.*, 2007]. Frame sections and post-tensioning forces were then computed to withstand seismic lateral forces. The geometry, members' sizes and post-tensioning forces of the model building were obtained scaling down the prototype building.

A scale of 1:4 was used and values used for fulfilment of similitude requirements presented later. Although the model building is a 3D structure, it has been designed and prepared to be tested in one direction only as a 2D frame. Two symmetric post-tensioned frames were included in the testing direction, and were transversally connected using secondary beams and bracing elements to minimize torsion effects and to represent the walls in the North-South direction. The model building geometry is shown in *Figure 3-2*.

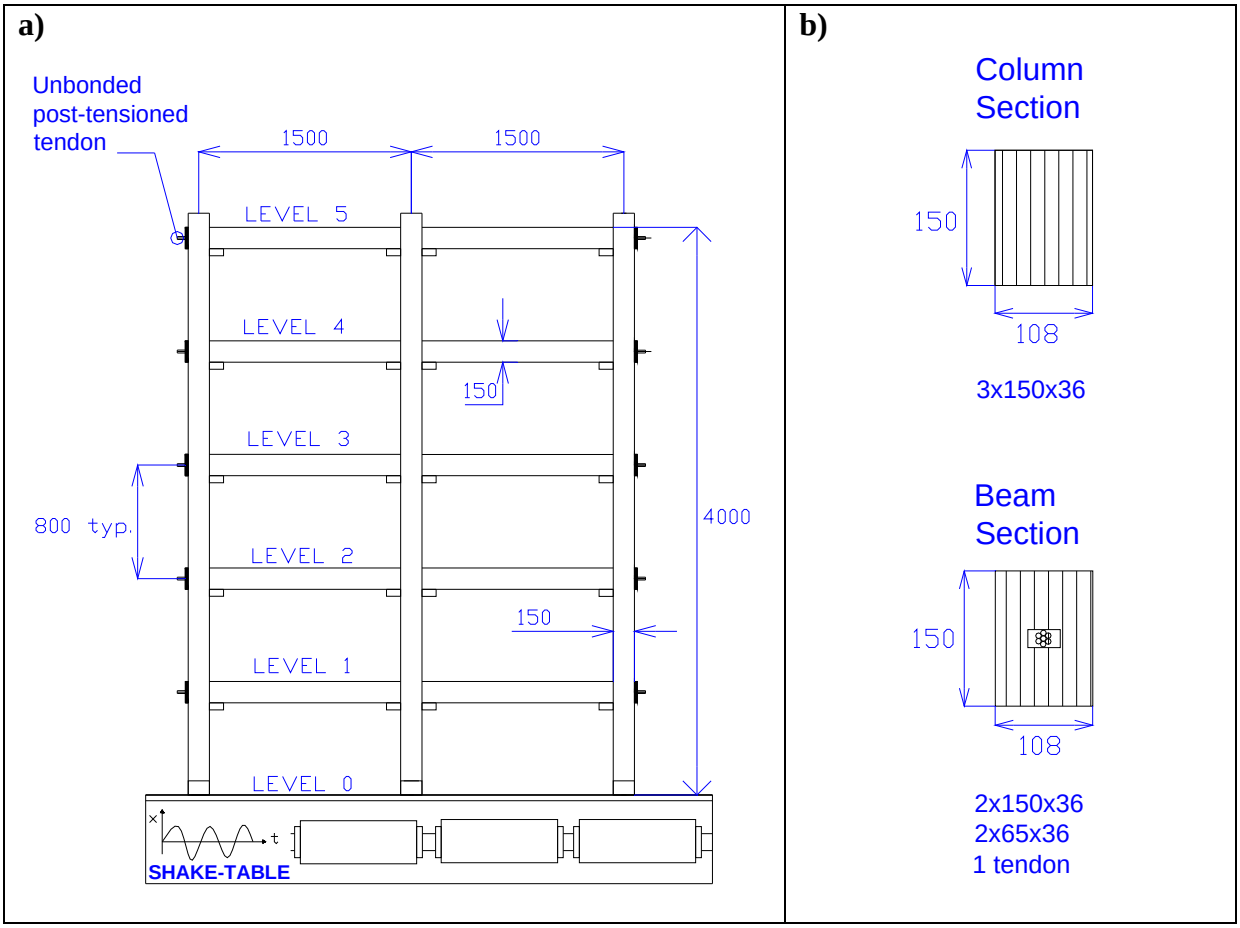

Figure 3-2 a) Model building global dimensions b) Beam and column cross section (units mm)

The global dimensions of the model building were 3m long and 1.5m wide. The inter-story height was 800mm resulting into a 4m total height for the 5-storey building, and a 2.4m height for the 3-storey building. Columns were solid sections made by three screwed pieces of LVL timber of 36x150mm; the column cross-section had dimensions of 108x150mm. The beams were hollow sections formed by 3 pieces of 36x150mm, a central cavity of 36x50mm was provided for the tendons. A single 7-wire strand (12.7mm diameter) was included as post-tensioning reinforcement per level per side. More details can be found in Appendix A.

3.3.2 *Similitude requirements*

Similitude rules comprise a quantitative relationship between the behaviour of the model building tested (scaled) and that of the prototype structure [Sullivan ***et al.***, 2004]. Satisfying all similitude requirements to have a perfect scaled replica would be impossible or extremely costly. The selection of a similitude law needs to be based on the parameters that need to remain constant to simplify requirements and to achieve a good representation of the system that is being emulated.

An accurate simulation of the stress-strain relationship of the material is a key point considering that the scaled material needs to demonstrate the same behaviour as the original material. Thus, considering the impossibility of scaling stress-strain relationships for timber, the best solution is to use a similitude law that keeps stress constant.

The Cauchy-Froude similitude law (***Table 3-3***) was selected to be used. This law not only keeps stress-strain constant, but it also maintains accelerations, which is an advantage point to be considered during shake-table tests. Since a scale of 1:4 was used, the value to use in the similitude law is $\lambda = 0.25$.

Table 3-3 Scale factors to satisfy the Cauchy-Froude similitude laws [Sullivan et al., 2004]

Parameter	Symbol	Scale factor
Modulus of elasticity	E	1
Length	L	λ
Area	A	λ^2
Volume	V	λ^3
Mass	m	λ^2
Displacement	d	λ
Velocity	v	$\lambda^{1/2}$
Acceleration	a	1
Weight	w	λ^2
Force	F	λ^2
Moment	Mt	λ^3
Stress	σ	1
Strain	ε	1
Time	t	$\lambda^{1/2}$
Frequency	f	$\lambda^{-1/2}$

3.4 General details and construction of model buildings

The construction process of a post-tensioned timber building stands out because of the simplicity, level of tolerances achieved, and rapid erection as observed in the construction of a 3-D test-building at larger scale, with post-tensioned frames, post-tensioned coupled wall and floors [Newcombe *et al.*, 2010a]. The beams and columns of the 1:4 scaled frame specimens were pre-fabricated and the complete frames were assembled as a "Lego" system on the ground where the post-tensioning was applied to each beam, and then the frames were lifted and placed on the shake-table. Longitudinal frames were connected using transversal beams and strip bracing. Steel weights were screwed to the top of the beams for each floor to provide the correct seismic mass, and finally the instrumentation was attached to the structure.

It is important to mention that every time that a change in the post-tensioning levels was implemented, the bolted (pinned) base connections between the columns and the shake-table were released, to avoid the generation of undesired loads on the frame.

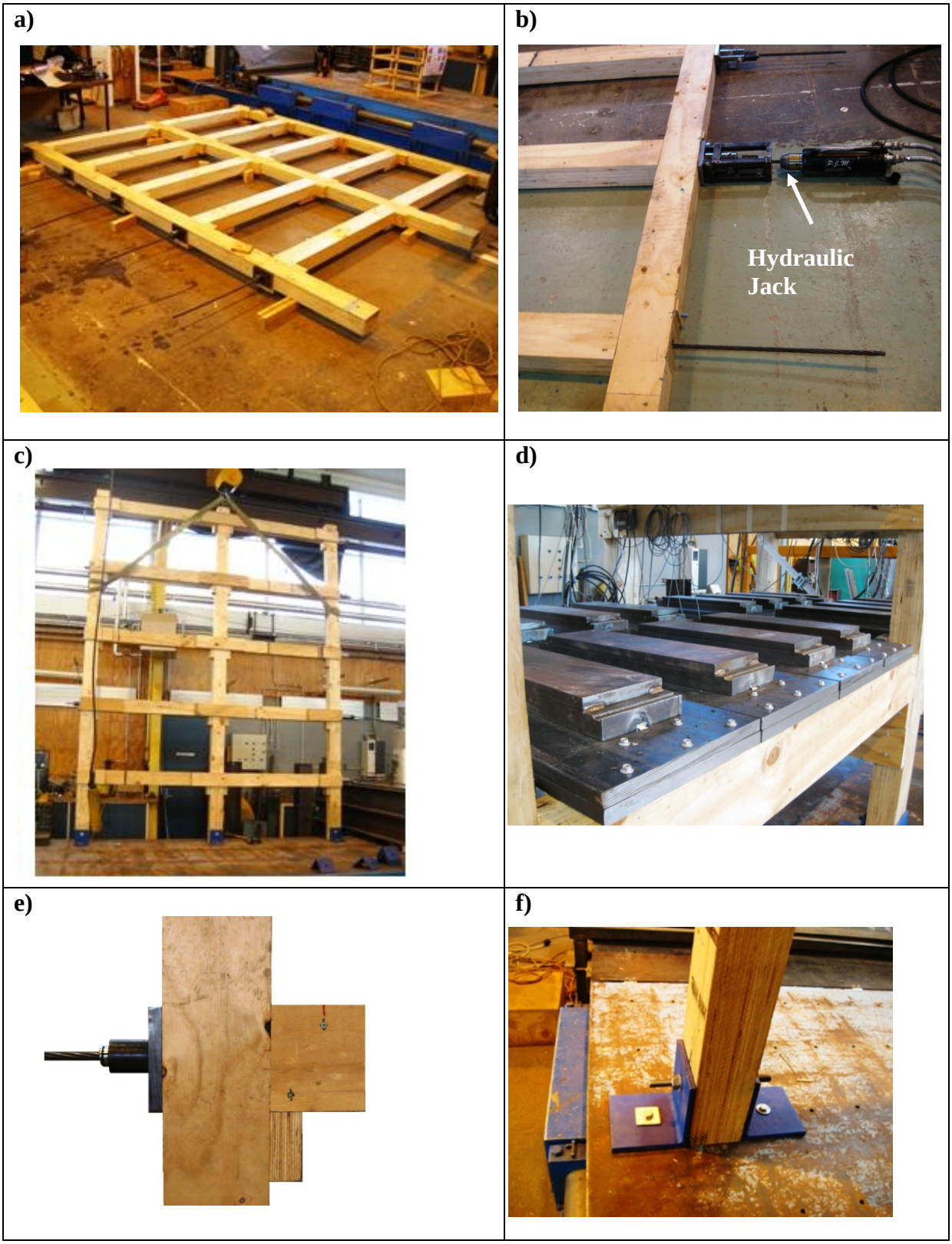

Figure 3-3 a) Frame assembled on ground b) Applying post-tensioning c) Frame lifted in place d) Added mass e) Beam-column connection detail f) Pin connection of column to shake-table

3.5 Set-up and instrumentation

3.5.1 *Shake-table device*

The shake-table at the University of Canterbury shown in *Figure 3-4* has a plan area of 2m wide by 4m long. The table, which has an unloaded mass of 5000kg, is constructed of 12mm steel plates connected on top of steel beams. The system is driven by a 280kN hydraulic actuator, powered by a 300Hp motor operating at 4000psi (28Mpa). The hydraulic actuator is controlled by a set of two Moog E072-054 servo-valves. More details on the shake-table original design and characteristics can be found in Ghee [1985].

The shake-table is a uniaxial earthquake ground motion simulator and has a payload capacity of 20tonnes and displacement amplitude of 130mm (total stroke of 260mm). The capacity of the servo valves limits the velocity of the table to approximately 242mm/s. This is defined as the saturation velocity of the table. As the table reaches saturation, the velocity gradient suddenly reaches zero, resulting in large table accelerations. These acceleration spikes can be very significant and in many cases they can be much greater than those expected from the desired acceleration command.
.

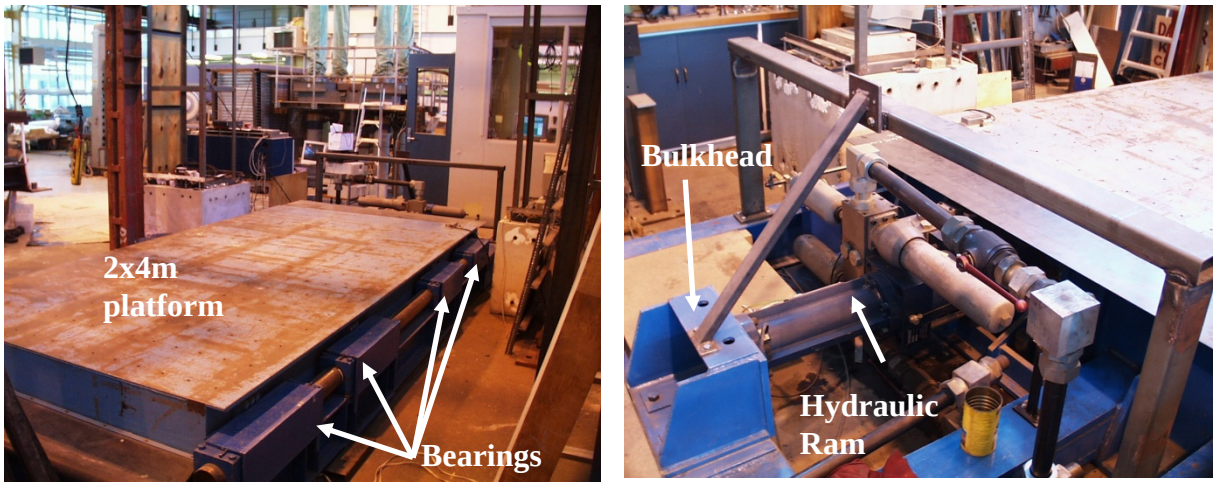

Figure 3-4 University of Canterbury shake-table

An external data acquisition system is used to capture and record both displacement and acceleration data from the table. The sample rate of the acquisition system is 90Hz. All connections between components are with standard coaxial cable.
Data acquisition for the shake-table is collected via a high speed logger and computer. A total of 64 channels can be logged at any one time, this being the number that limited the amount of instrumentation.

3.5.2 *Instrumentation*

The instrumentation of the scaled model building is shown in *Figure 3-5*. The South frame was fully instrumented; the North frame had instrumentation in particular locations just to compare the response between the two frames, and also measuring any possible torsion.

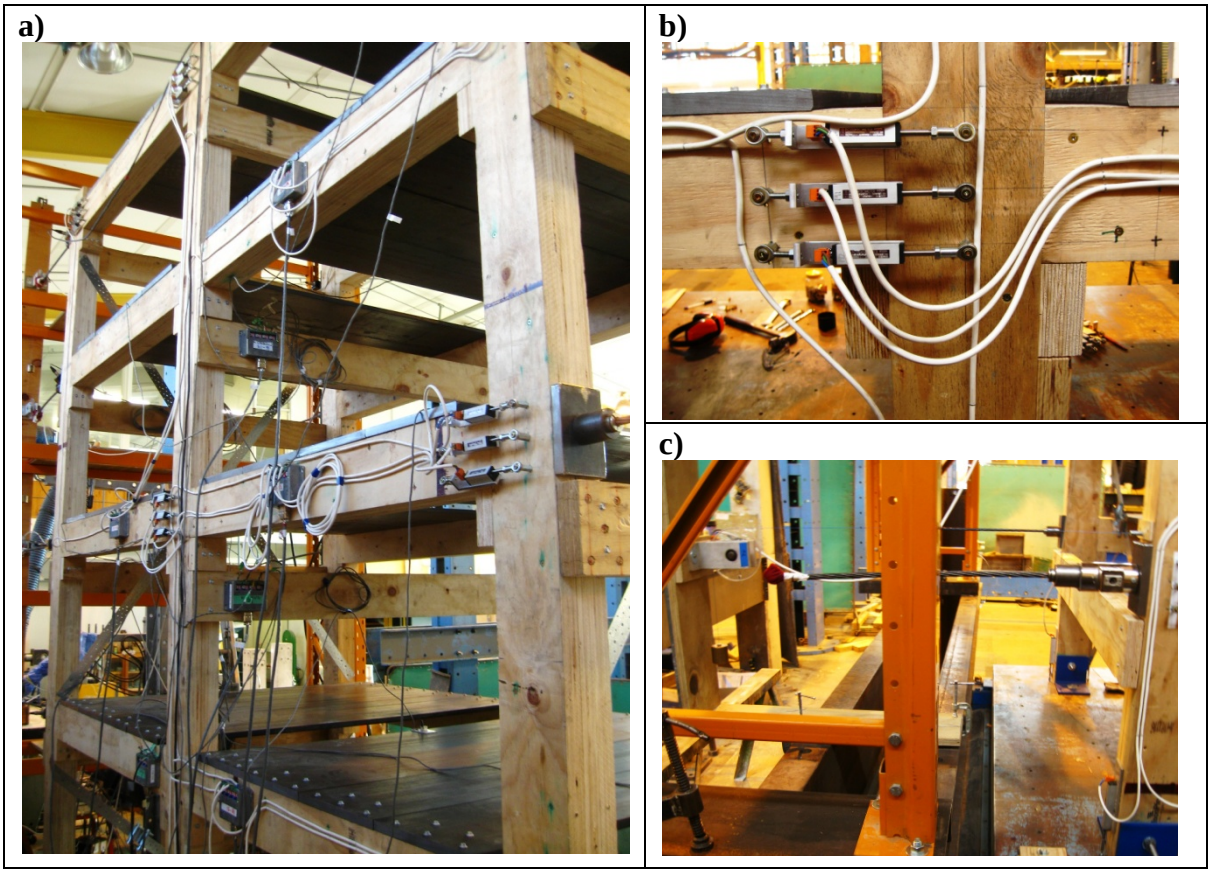

Figure 3-5 a) South frame instrumentation b) Linear potentiometers at joint connection c) Rotational potentiometer connected to first floor level

The detail of the instrumentation set up is given in Appendix B. In summary the instrumentation consisted of:

a) Accelerometers: three accelerometers were installed per each floor, one in the direction of the excitation at the centre of gravity of each floor, and two perpendicular to the movement at the edges of the floor. For the 3-storey model building, three accelerometers were also included at the top of the model building to measure vertical accelerations due to uplifting and rocking at the base.

b) Spring Potentiometers: two spring potentiometers were included per column in the South frame and a pair of them were included in one edge column of the North frame. These potentiometers measured the rocking movement of the column related to the shake-table; one potentiometer was placed at each face of the column to measure the gap opening and the compression in the column.

c) Linear Potentiometers: three linear potentiometers were included at the beam-column interface of each connection at three floor levels for the South frame. For the North frame one connection was monitored. These potentiometers recorded the rocking movement of the beam over the columns registering gap openings, compression in timber and the position of beam neutral axis changes.

d) Rotary potentiometers: one rotary potentiometer was installed per floor to the South frame and one on the fifth level of the North frame, their function was to measure the global floor level displacements. Additionally one rotary potentiometer was connected at the ground floor level to verify the displacement recorded by the shake-table controls.

3.6 Variables under study

A number of modifications to the model building were included to analyse their influence on the response. The different configurations included are summarised below:

a) Amount of mass: the laboratory did not have the capacity of providing all the seismic mass required by similitude, so it was decided to incorporate tests with three levels of mass in order to predict the behaviour for a model with 100% of the mass. The maximum mass available was 78% of the amount necessary for representing the prototype 3-storey building. In order to analyse the influence of the amount of mass the configurations included were 31%, 44% and 78% of the similitude requirements.

b) Level of post-tensioning: the influence of the post-tensioning force was also included in the study. An increase in the post-tensioning force implies a stiffer and stronger system, resulting in a change in the natural period of vibration. To analyse this point, three levels of initial post-tensioning force were included (15kN, 30kN and 45kN per beam corresponding to 1%, 2% and 3% of f'_p respectively). The maximum post-tensioning applied was computed based on the strain limits of the timber during the seismic response. For this it was necessary to consider the strain produced by the initial post-tensioning plus the additional strain due to tendon elongation as the connections open as a result of the maximum deflected shape expected for the model building (2.5% drift on the shake-table).

c) Number of levels: as previously mentioned, a 5-storey model building and a 3-storey model building were tested. The aim was to check whether the dynamic parameters are influenced from the number of connections in the building, i.e. a clear variation in the damping could possibly suggest that some sort of Coulomb type of damping is present as a result of the amount of friction in the system.

d) Inclusion of corbels: even if it is unlikely to construct (or be allowed to design) this kind of buildings without a specific corbel to carry vertical loads at the beam-column joints, it is necessary to know how much influence such an element would have on the response. It is expected that some energy could be dissipated by friction between the bottom of the beam and corbel; additionally the corbel material can influence this friction mechanism. For example, a timber-to-timber contact would be expected to exhibit bigger friction coefficient than a timber-to-steel interface, so the energy dissipation should be bigger in the first case.

Sensitivity analyses of the influence of the mass and level of post-tensioning (lateral stiffness) are important to understand their influence in the damping of the system. A Rayleigh damping model is typically used by engineers in order to uncouple systems with multi-degree of freedom. The damping matrix (C_o) of the system is represented as a function of the mass (M) and the stiffness (K) as expressed by *Equation 3-1*.

$$C_o = a_o \cdot M + a_1 \cdot K \qquad \text{Equation 3-1}$$

Where $\boldsymbol{a_o}$ and $\boldsymbol{a_1}$ are chosen to give the desired fractions of critical damping at two specified frequencies and the variation at all other frequencies follows the variation as shown in *Figure 3-6* .

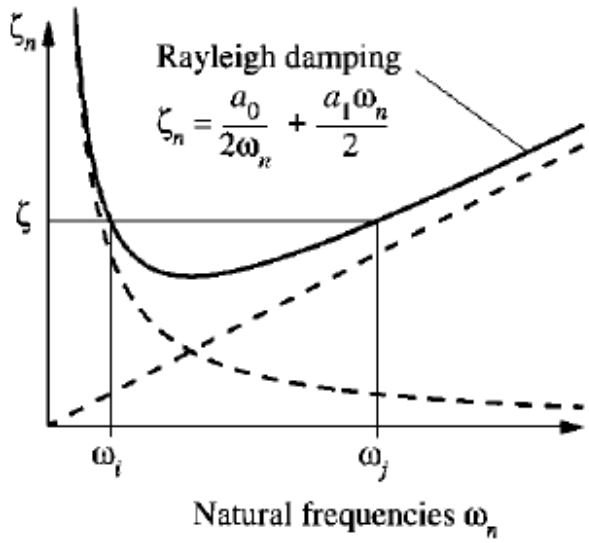

Figure 3-6 Variation of modal damping ratios with natural frequency (Raleigh damping), [Chopra, 1995]

3.7 Experimental program

3.7.1 *Sinusoidal tests*

By testing the structure with sinusoidal displacements it is possible to reach a target maximum displacement (or drift level) in the structure and at the same time compute the natural frequency of the first mode. This is possible by changing amplitudes and frequencies of the exciting function p(t) (Equation 3-2), i.e. creating a sweep of frequencies and looking for the one that produces resonance. As part of this tests campaign, three levels of excitation amplitude (Ao) were included; for each of these levels eleven angular frequencies (ω) were considered.
Worth reminding that the computation of the damping values is one of the main goals of the research. Sinusoidal displacements were applied to the model building for a number of cycles to ensure a pure steady-state response (after the transient response vanished). Then the damping was computed using two methods: 1) the decay of the response, and 2) area-based damping.
More details on the evaluation of damping can be found in Appendix C.

$$p(t) = Ao \cdot \sin(\omega \cdot t) \qquad \text{Equation 3-2}$$

3.7.2 *Earthquake tests*

In order to examine the seismic behaviour of the system, six earthquake records were used to consider a variety of seismic conditions. Every record used was modified (scaled down) to satisfy the maximum capacity of the shake-table (related to a maximum velocity) and similitude conditions. A table with all the results of the seismic cases analysed is included in Appendix D. It is important to realize that the values included in the table have been directly measured using the electronic instrumentation; generally there are small variations for the same record depending on the model building set up (number of floors, mass, post-tensioning levels). These variations could also be due to the interaction between the model buildings and shake-table.

The selection of earthquake record was based on well-known earthquakes that could be scaled by following similitude requirements without exceeding the velocity limits of the shake-table to avoid undesired peaks of acceleration. *Figure 3-7* shows the acceleration and displacement response spectra for the earthquakes record included in this study and imputed to the table. The mean spectral ordinate values are in the figures compared to code-design spectra (NZS1170.5:2005) for Auckland and Wellington cities.

The records were scaled to the New Zealand seismic spectrum for the city of Wellington, with a zone factor Z = 0.4; shallow soil type C; and R = 1 (annual probability of exceedance of 1/500). The suite of earthquakes was scaled for a range of periods around the expected elastic period of the structure (smaller than 1sec.). The characteristics earthquake ground motions used and their spectral values are summarised in
Table 3-4, the characteristics of the scaled ground motions using during shake-table tests are summarised in *Table 3-5*.

Table 3-4 Ground motion records selected

Earthquake Event	Year	Station	M_w	PGA (g)	PGV (mm/s)	PGD (mm)	R (km)
Loma Prieta	1989	Saratoga-W Valley Coll	6.9	0.33	615	364	13.7
Kobe	1995	CEOR Sakai	6.9	0.60	743	199	28.1
Northridge	1994	LA Dam	6.7	0.46	563	487	5.9
C. Mendocino	1992	Rio Dell Overpass-FF	7.0	0.39	439	220	14.3
Parkfield	1966	Cholame S., California	6.2	0.49	761	469	3.5
Sylmar	1994	County Hospital	6.6	0.58	813	204	9.9

Mw: Moment magnitude scale; PGA: Peak Ground Acceleration; PGV: Peak Ground Velocity; PGD: Peak Ground Displacement, R: Recorded distance from the epicentre

Table 3-5 Scaled ground motion applied to shake-table

Earthquake Event	Year	Station	PGA (g)	PGV (mm/s)	PGD (mm)
Loma Prieta	1989	Saratoga-W Valley Coll	0.27	481	326
Kobe	1995	CEOR Sakai	0.38	330	242
Northridge	1994	LA Dam	0.41	546	434
C. Mendocino	1992	Rio Dell Overpass-FF	0.48	531	294
Parkfield	1966	Cholame S., California	0.48	505	304
Sylmar	1994	Sylmar -County Hospital	0.45	449	118

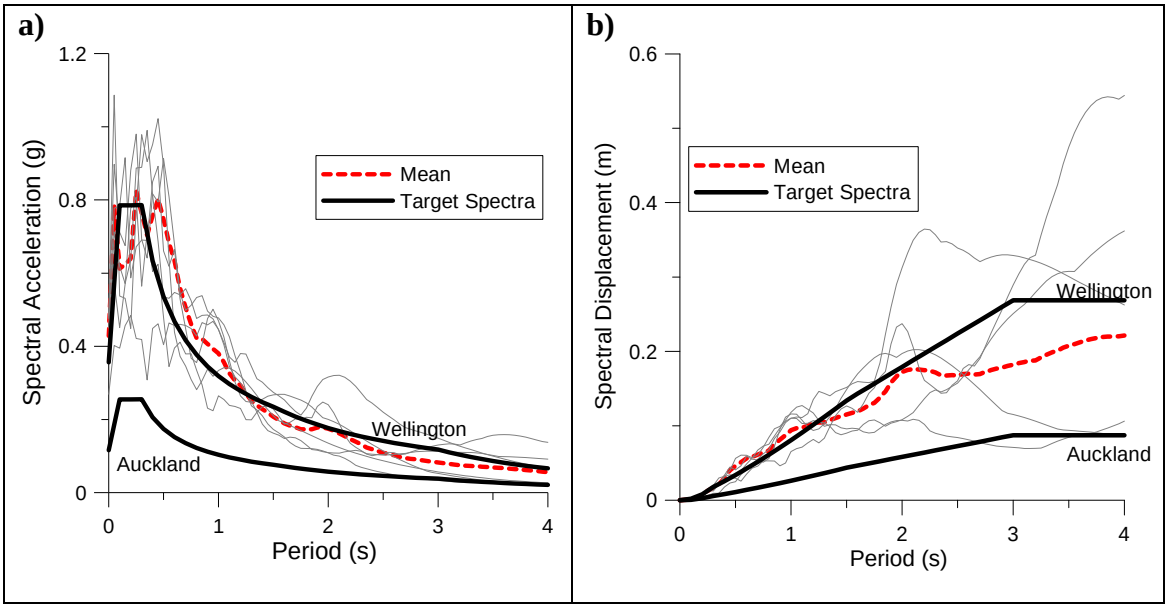

Figure 3-7 Response spectra compared to the NZS1170.5:2005 *design spectra for Wellington and Auckland seismicity: a) Acceleration spectra b) Displacement spectra*

3.8 Experimental response

3.8.1 *Global structural behaviour*

A total of over 300 tests were performed (including sinusoidal tests and recorded ground motions), covering an extended range of imposed accelerations and drifts to the model buildings, simulating seismic solicitations of real and expected seismic events considered as design limits (according to performance-based considerations) for international seismic codes.

The global response of the model buildings demonstrated the capacity of the system to undergo large drifts and resist strong ground movements with minimal damage and no residual deformations.

3.8.2 *Inter-storey drift*

To guarantee an appropriate structural performance of a structure, design codes control the maximum drift allowed during lateral loading, depending on the limit state considered. For Ultimate Limit State (ULS) design, seismic codes usually consider 2.5% as the maximum interstorey drift allowed. Inter-storey drift registered during seismic testing are showed on ***Figure 3-8*** and plotted versus Moment magnitude (M_w) of the seismic records considered and versus their peak ground accelerations (PGA). From these figures it can be seen that for none of the imposed seismic records the structure was subjected to a drift that exceeded the code limits; therefore the maximum deformation design requirement was satisfied. On the other hand, the imposed drifts were of a high magnitude which demonstrates that the model buildings were able to be subjected to large deformations having a very satisfactory performance (better than damage control limit states and closer to fully operational at ULS or 1/500 years event).

a)

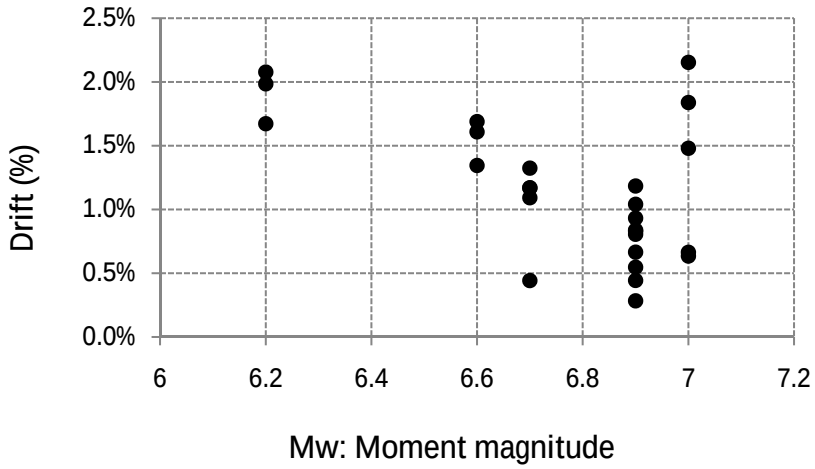

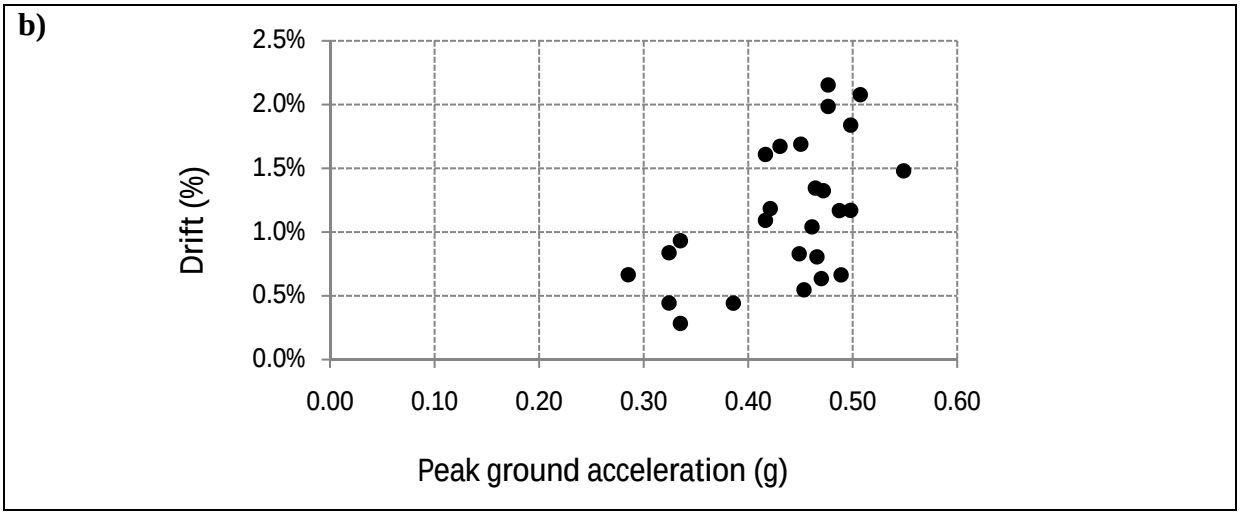

Figure 3-8 Drift reached during seismic testing: a) Drift versus earthquake magnitude b) Drift versus peak ground acceleration

3.8.3 *Horizontal floor accelerations*

Large floor accelerations are likely to happen during earthquake events and these accelerations may generate damage to non-structural components as the ones reported by Kircher [2003; 2006] for the 1994 Northridge earthquake which cost US$9.25 billion. Large floor horizontal accelerations have been recorded in buildings during earthquakes. Such accelerations have been responsible for inertia forces causing damage to services and are the major reason for structural damage and even building collapse [Rodriguez *et al*., 2002]. Therefore, it is necessary to control amplification of the ground accelerations to avoid undesired effects such as damage to non-structural elements.

Data recorded from instrumented multi-storey buildings, except for base-isolated ones, during the Northridge earthquake was analysed and reported by Hall [1995]. The study shows the floor acceleration magnification (FAM) for a range of building construction types and different number of levels. *Figure 3-9* shows the maxima floor acceleration magnification factors obtained as the ratio of the maxima floor horizontal acceleration to the PGA.

Figure 3-10 shows the FAM obtained during the shake-table test for the 3-storey and 5-storey model buildings. It is important to notice that both graphs are directly comparable given that acceleration is kept constant based on the similitude criteria utilized. Hence, there is no appreciable difference in between the FAM that has been recorded in past earthquakes for traditional structures versus the FAM expected for the post-tensioned timber system. Therefore it is possible to conclude that the amplification of ground acceleration expected for post-tensioned timber buildings are in the range of those expected for more traditional types of construction systems.

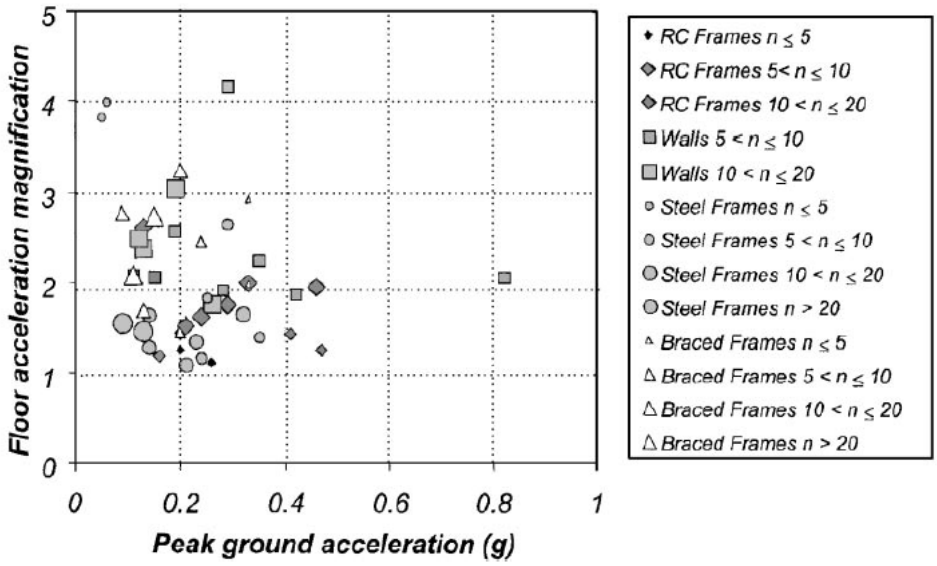

Figure 3-9 Floor acceleration magnification, values obtained from instrumented buildings during Northridge earthquake [Hall, 1995]

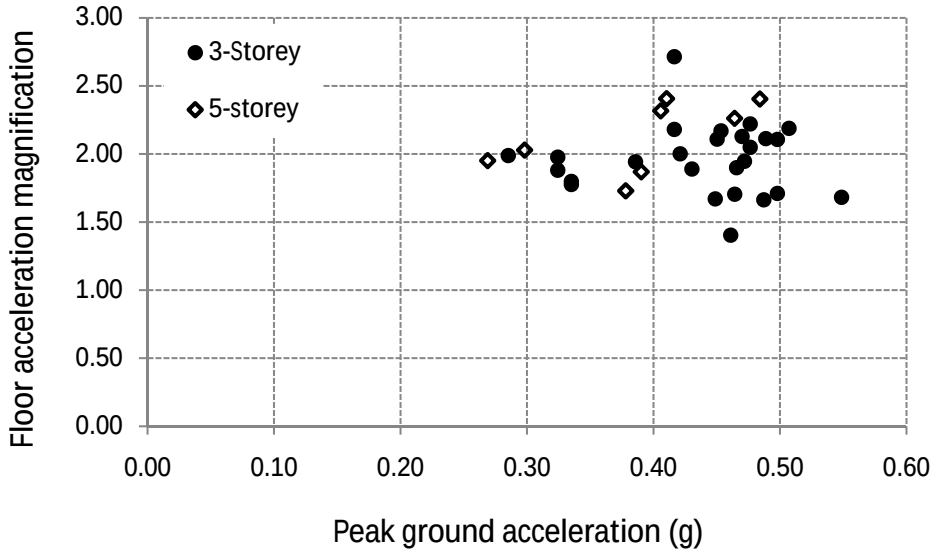

Figure 3-10 Floor acceleration magnification, values obtained from the shake-table tests on post-tensioned timber frame

Finally to illustrate the results obtained from a design code point of view, *Figure 3-11* shows a comparison between the floor acceleration magnifications for the 3-storey model building (including 78% of required mass by similitude) subjected to the earthquake records considered on this research, versus the FAM values given by the New Zealand Standards. From the figure it is possible to see that the design values, given by the New Zealand code, are bigger than the measured values obtained with the shake-table tests, thus on the conservative side.

The NZS 1170.5:2004 estimates the floor acceleration at level i, C_{Hi} as follow:

$$C_{Hi} = 1 + \frac{h_i}{6} \qquad \textit{For all } h_i < 12m \qquad \text{Equation 3-3}$$

$$C_{Hi} = 1 + 10\frac{h_i}{h_n} \qquad \textit{For all } h_i < 0.2h_n \qquad \text{Equation 3-4}$$

$$C_{Hi} = 3.0 \qquad \textit{For all } h_i \geq 0.2h_n \qquad \text{Equation 3-5}$$

Where:

h_i = Height of the floor
h_n = Height from the base of the structure to the uppermost seismic weight or mass

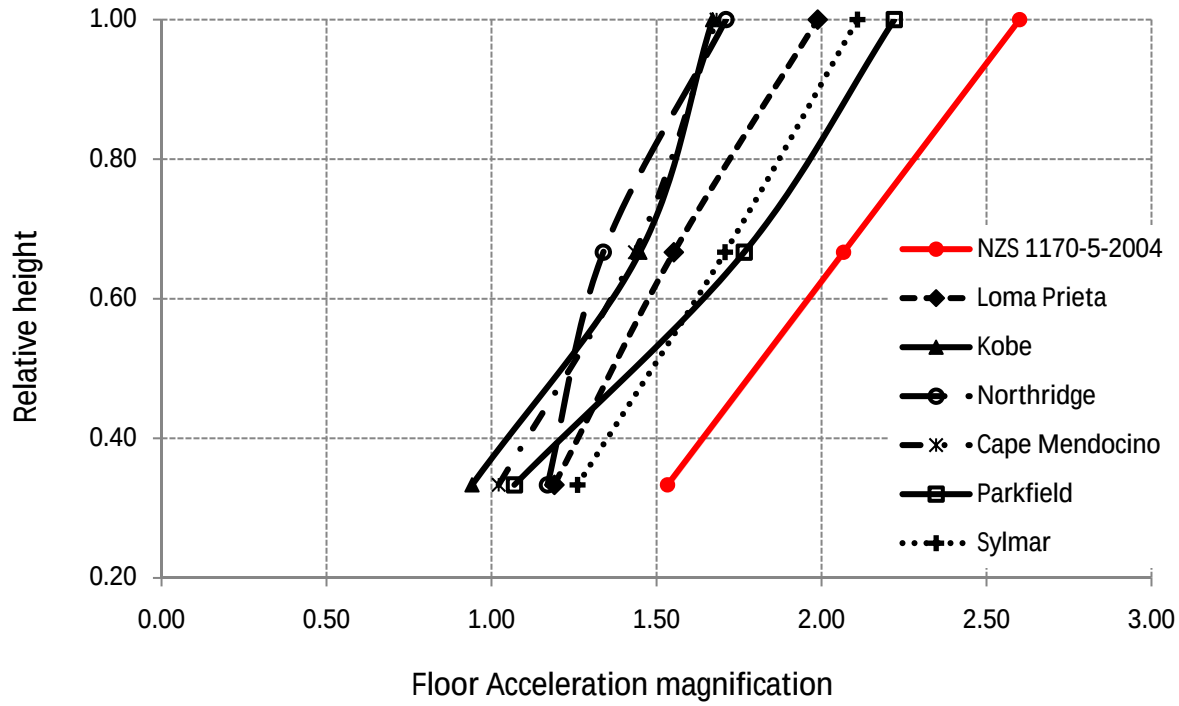

Figure 3-11 Comparison of floor acceleration magnification values obtained for the 3-storey model building versus values given by the New Zealand Standards

3.8.4 *Re-centering action*

The re-centering action has proven to be effective, because only minor residual displacements were obtained after subjecting the structure to high levels of deflections. *Table 3-6* shows the residual absolute floor lateral deflections obtained for some cases analysed.

Table 3-6 Residual absolute lateral global floor deformation after dynamic testing

Test	Maximum Drift (%)	Residual lateral floor deformation (mm)				
		First Storey	Second Storey	Third Storey	Fourth Storey	Fifth Storey
5S-M1-32	1.91	-0.17	-0.14	-0.05	0.38	0.52
5S-M1-62	1.61	0.05	0.11	0.11	0.37	0.19
5S-M1-74	2.13	0.00	-0.09	-0.17	0.00	0.25
5S-M1-85	2.26	0.03	0.08	0.09	0.09	0.16

3.8.5 *Accumulated damage*

As it was expected, a low level of damage was observed. The only damage to be seen was produced at the internal faces of the columns, loaded perpendicular to the grain. Approximately 1.5mm of perpendicular to the grain crushing in columns was recorded. This crushing was probably produced during the sinusoidal tests that went over the 2.5% drift limit. At 2.5% drift the timber strain was in fact expected to be around 90% of the crushing strain, so that increased values of drift produced crushing of the timber in compression. The damage can be observed in *Figure 3-12*.

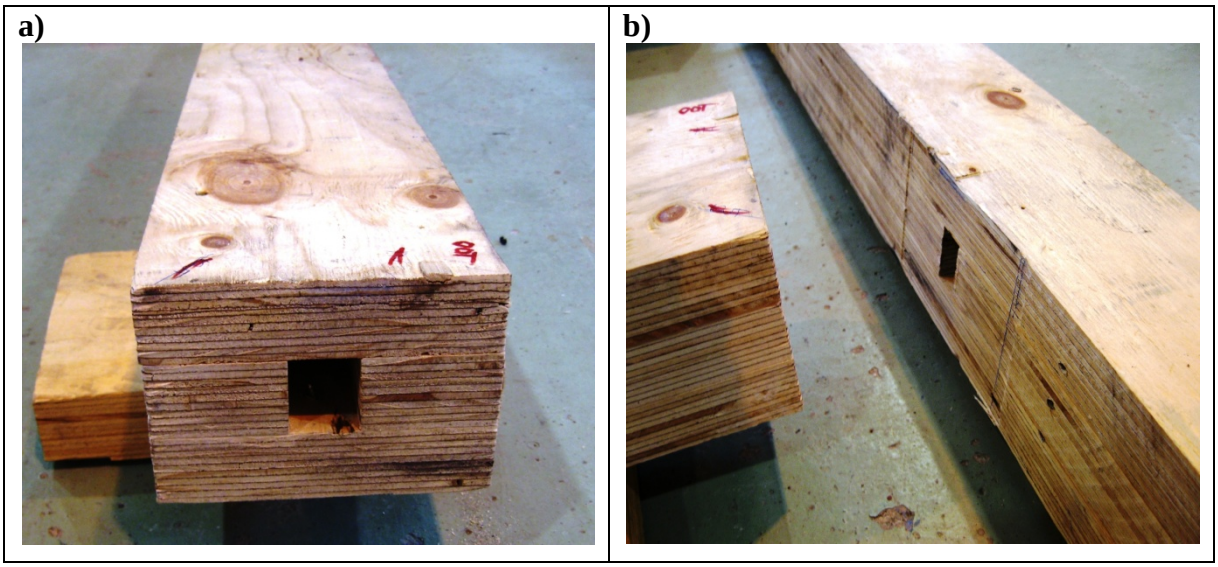

Figure 3-12 Accumulated final damage from dynamic testing: a) Beam (no damage) b) Internal face of column

3.8.6 *Equivalent viscous damping*

Timber has the capacity to undergo large elastic deformations without suffering damage; additionally it has the ability to recover its original shape using part of the strain energy stored in the system, at the same time part of the energy is dissipated generating a source of damping. During time-history analyses an equivalent viscous damping value may be used to represent all the damping of the structure at once. Similarly, for the utilization of a displacement based design, an equivalent elastic (secant stiffness approach) SDOF system is combined with an equivalent viscous damping to reflect the hysteretic damping and the elastic damping. The equivalent viscous damping is defined as the sum of the elastic damping plus the hysteretic damping, and expressed by ***Equation 3-6.*** The hysteretic damping depends on the hysteretic rule that represents the structural system being designed. The elastic damping is defined as the damping not captured by the hysteretic model [Priestley ***et al.***, 2007].

$$\xi_{eq} = \xi_{el} + \xi_{hyst} \qquad \text{Equation 3-6}$$

- Elastic damping (ξ_{el})

There is a lack of dynamic data for the evaluation of the elastic damping of timber systems. Additionally, the existing information corresponds to timber structural systems not directly comparable to post-tensioned timber frames. Foliente [1995] performed ambient vibration tests on light timber frame construction using plywood sheathed shear walls. Foliente obtained a minimum elastic damping value of 3% of the critical damping. The results obtained by Foliente were lately checked by Filiatrault et al. [2002] through the utilization of a DDBD approach, Durham et al. [1998], and Durham et al. [1999] by dynamic testing. For solid timber construction such as post-tensioned timber buildings, the influence on stiffness of cladding and non-structural elements is expected to be smaller than on light timber framing, therefore a smaller value of elastic damping is expected. It has been suggested by Newcombe [2008a] to use 2% of the critical damping as elastic damping for post-tensioned timber frames.

As DDBD uses the secant stiffness matrix rather than elastic (initial) stiffness matrix or tangent stiffness matrix, a correction factor to the elastic damping needs to be applied. The reason is explained in Priestley et al. [2007] where is expressed that a tangent stiffness proportional damping is more appropriate to be used (for design purposes) than the more conventionally adopted initial-stiffness proportional damping. Tangent stiffness properly represents the reduction in damping forces as the structure softens with increasing ductility. Therefore a correction value "κ" has been calibrated and proposed by Grant et al. [2005] as a function of the ductility (***Equation 3-7***), then the equivalent viscous damping is obtained using the Equation 3-8 .Values of κ depending on the hysteretic rule used are shown in ***Figure 3-13***, including a low-dissipative flag-shape rule (FS). Other hysteresis rules represented in the figures are: Elasto Plastic (EPP), Bilinear (BI), Takeda Thin (TT), Takeda Fat (TF), Flag, $\beta = 0.35$ (FS) and Ramberg-Osgood (RO).

$$\kappa = \mu^{\gamma} \qquad \text{Equation 3-7}$$

$$\xi_{eq} = \kappa \cdot \xi_{el} + \xi_{hyst} \qquad \text{Equation 3-8}$$

Where, γ is a constant that depends of the hysteresis rule used *Table 3-7*

Post-tensioned hybrid systems (post-tensioning plus additional energy dissipaters) are better represented by a flag hysteresis shape [Palermo *et al*., 2005], in particular when dealing with frame systems, are expected to reach a relatively small ductility under the design level of earthquake (serviceability limit states criteria tend to govern the design). Hence, the correction factor of the elastic damping contribution for post-tensioned timber is expected to be close to one. Proposed γ values by Newcombe [2008a], are; γ = -0.430 for when tangent stiffness matrix is used and γ = 0.387 for when initial stiffness matrix is used.

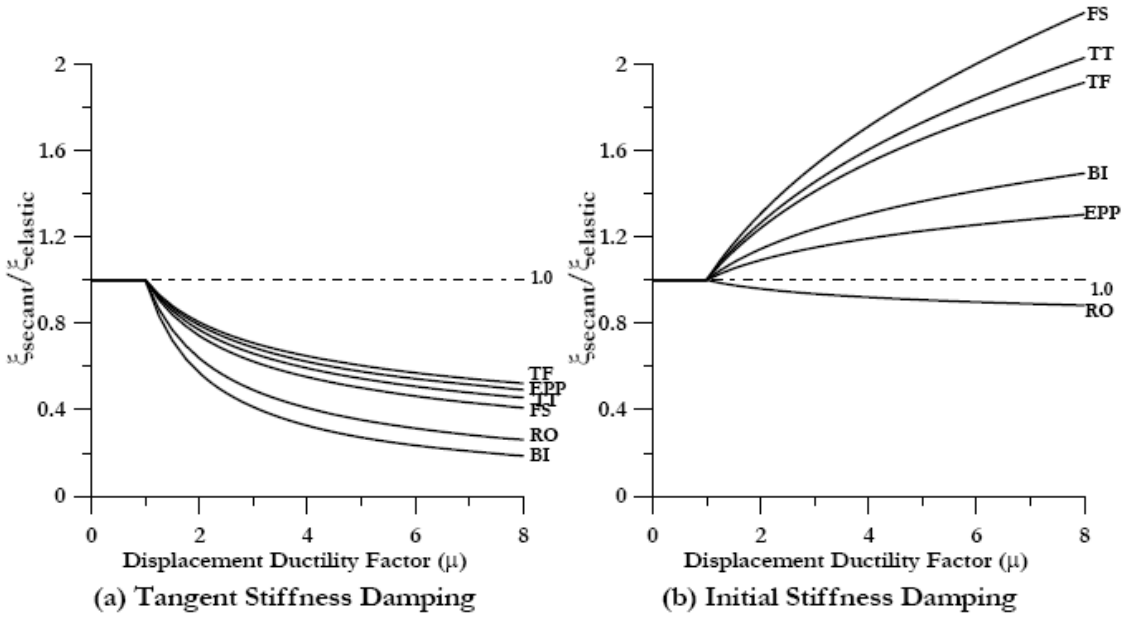

Figure 3-13 Secant stiffness correction coefficient for equivalent viscous damping for different hysteretic rules: a) Related to elastic tangent stiffness damping b) Related to elastic initial stiffness damping [Priestley et al., 2007]

Table 3-7 Secant stiffness correction factors γ for elastic damping [Priestley et al., 2007]

Model	Tangent Stiffness	Initial Stiffness
Elasto Plastic (EPP)	-0.341	0.127
Bilinear (BI)	-0.808	0.193
Takeda Thin (TT)	0.378	0.340
Takeda Fat (TF)	-0.313	0.312
Flag, β = 0.35 (FS)	-0.430	0.387
Ramberg-Osgood (RO)	0.617	-0.060

- Hysteretic damping (ξ_{hyst})

It has been traditionally suggested that the hysteretic component of the equivalent viscous damping can be obtained based on absorbed energy during the inelastic response, Equation 3-9. The original formulation by Jacobsen [1960] was derived through substitute-structure analysis. In such study, the dynamic response of the structures was characterized by the secant stiffness and the hysteretic damping equated from a steady state cyclic response to the peak design displacement.

$$\xi_{\text{hyst}} = \frac{1}{4 \cdot \pi} \cdot \frac{E_D}{E_s} \qquad \text{Equation 3-9}$$

Where, E_D = Total energy dissipated during a complete cycle.
E_S = Equivalent strain energy at the maximum displacement of the cycle.

Many researchers have investigated Jacobsen's approach, especially due to its compatibility with DDBD philosophies. It has been found that area-based damping (Appendix C) gives good results when systems with low-medium level of energy dissipation are analysed, such as a flag hysteresis or the modified Takeda rule. However, area-based damping can significantly overestimate the equivalent damping for systems that possess high energy absorption, such as elasto-plastic or bi-linear rules [Chopra *et al*., 2001].
The recognized errors when using area-based damping have been analysed and correction factors have been proposed. A series of investigations were performed using numerical models to run time-history analyses in order to calibrate area-based damping [Blandon *et al.,* 2005; Dwairi *et al.,* 2004; Grant *et al.,* 2005; Iwan *et al.,* 1979; Judi *et al.,* 2001; Priestley *et al.,* 2005]. Correction values applicable to area-based damping for computing equivalent viscous damping to be used in time-history analysis are shown in ***Figure 3-14*** [Priestley *et al*., 2007]. The correction coefficient is then distinguished depending on the hysteretic rules considered. In the figure the following hysteretic rules are included: Elasto plastic (EPP), Bilinear (BI), Takeda Thin (TT), Takeda Fat (TF), Flag (FS) and Ramberg-Osgood (RO). As previously mentioned the timber hybrid system is better represented by the Flag hysteretic rule (FS.35) which is a thin flag shape.

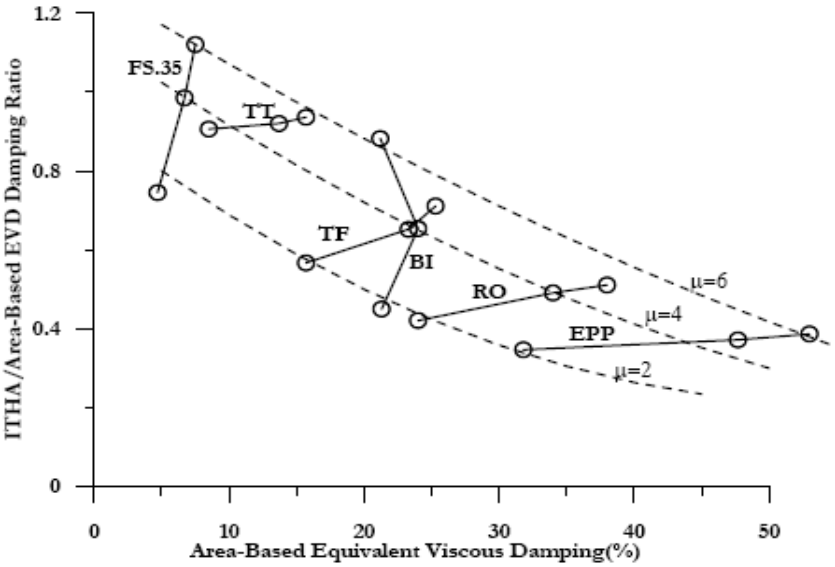

Figure 3-14 Correction coefficient for area-based damping [Priestley et al., 2007]

3.8.7 *Experimental evaluation of equivalent viscous damping for post-tensioned timber frames*

Two approaches were used to evaluate the equivalent viscous damping of post-tensioned timber frame buildings from the experimental dynamic tests. The first method used to compute the damping values was based on the decay in response during free vibration tests. The second method was based on the energy dissipation computed as area-based damping during dynamic testing. Details on these damping evaluation methods are described in Appendix C.

When using the response decay approach, two set of values were obtained depending on whether one-cycle decay or ten-cycle decay were considered. These two set of values show an important difference between them. The reason for this discrepancy in results is the clear influence of the drift level on the damping value (*Figure 3-15*) .One-cycle decay gives a bigger damping value and shows a bigger dispersion than the corresponding obtained using ten-cycle decay. The difference in damping values obtained using one-cycle decay versus the values obtained using ten-cycle decay is enhanced when the lateral drift is increased. For example, the difference in damping values is 1.4% of the critical damping when comparing the mean values of one-cycle decay damping and ten-cycle decay damping at 0.5% drift (ξ = 5.5% considering one-cycle decay and ξ = 4.1% considering ten-cycle decay), when the same comparison is done at 2.5% the difference in damping value is 2.5% of the critical damping (ξ = 7.9% considering one-cycle decay and ξ = 5.4% considering ten-cycle decay).

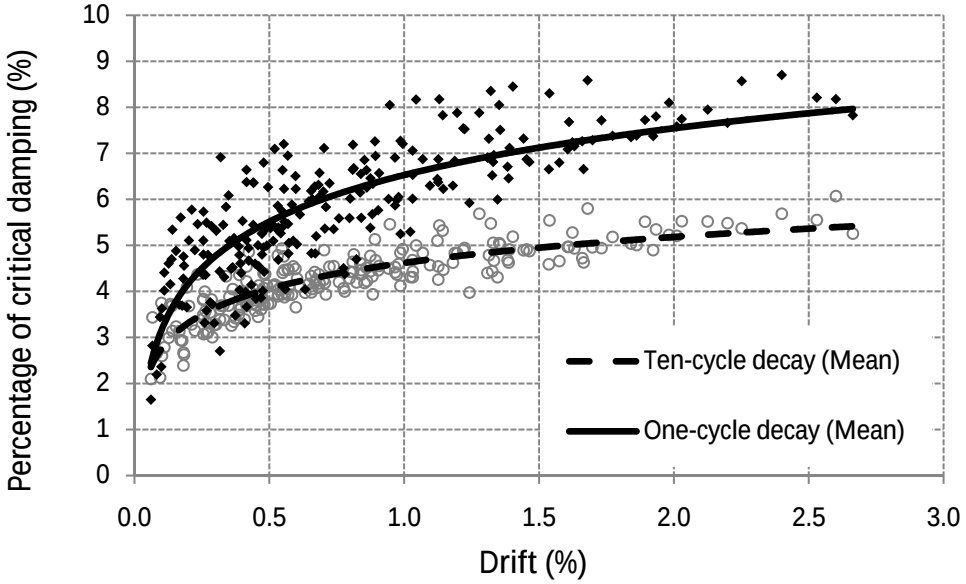

Figure 3-15 Percentage of critical damping versus drift. One-cycle decay compared to ten-cycle decay

For having a different approach to the calculation of an equivalent viscous damping, damping forces were computed from the dynamic tests using RUAUMOKO [Carr, 2008] and plotted versus lateral displacement to compute the dynamic area-based damping. *Figure 3-16* shows a comparison of the dynamic area-based damping values versus the one-cycle decay of response values. It can be observed that for drift values smaller than 1%, area-based damping values are clearly overrated. For small drift levels the hysteresis loops obtained were in general of the *"fat"* type, corresponding to high energy absorption (*Figure 3-17*). In many cases the hysteretic loops obtained had irregular forms due to the difficulty of capturing the cycle behaviour at small lateral drifts. As mentioned, area-based damping overestimates the equivalent viscous damping for "*fat*" hysteretic loops.

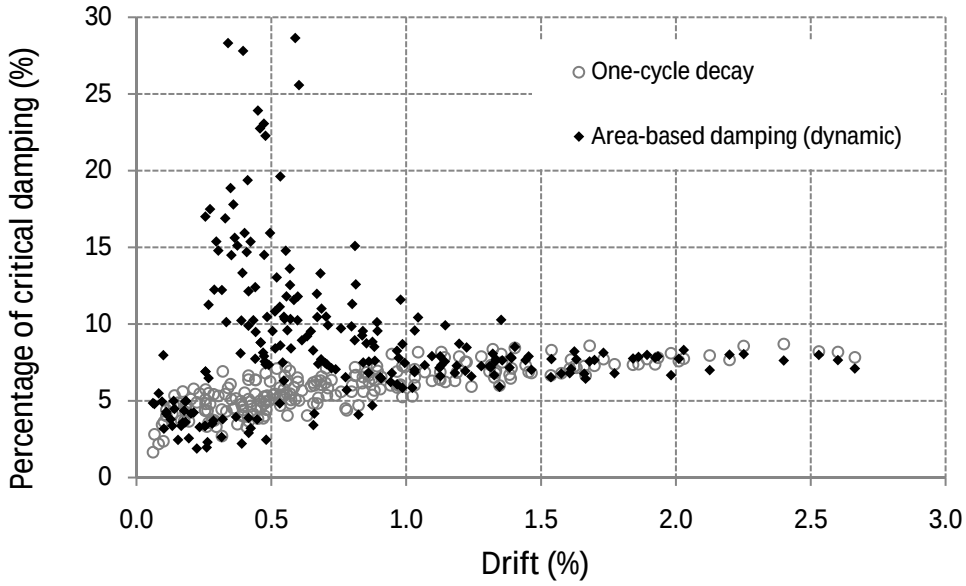

Figure 3-16 Percentage of critical damping versus drift. Area-based damping compared to one-cycle decay damping

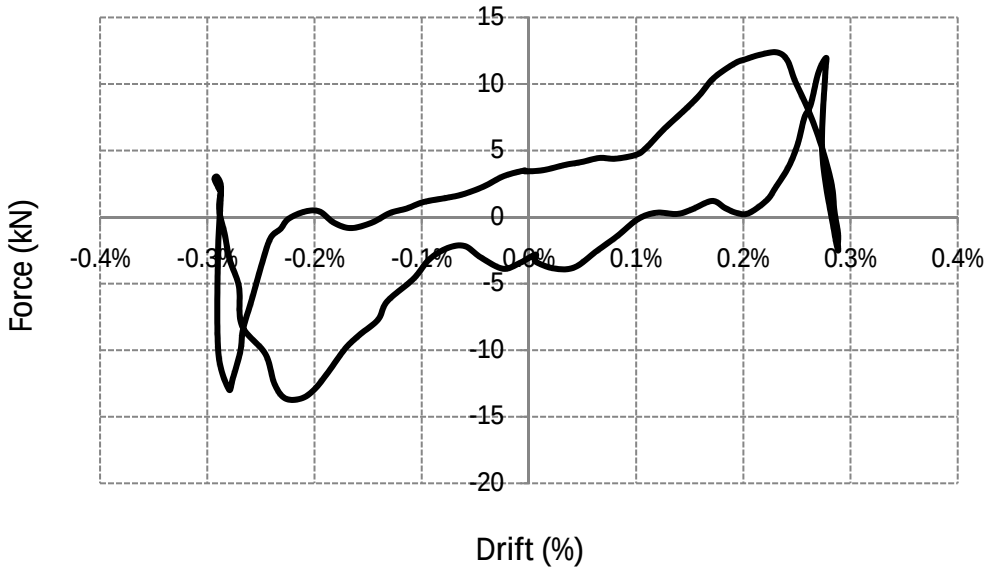

Figure 3-17 Hysteretic loops obtained during dynamic testing. "Fat" loop for small interstorey drift

Upon reaching greater than 1% of inter-storey drift, hysteretic loops become thinner (*Figure 3-18*), and area-based damping and response-decay damping values are similar. The fact that area-based damping and response-decay damping are similar indicates that for post-tensioned timber frame buildings the main source of equivalent viscous damping corresponds to hysteretic damping. Hence, there is a minimal value of elastic damping present during testing.

Additional sources of elastic damping (not considered during the dynamic test performed) are the result of non-structural elements' deformation, soil-structure interaction, foundation compliance, and radiation damping [Priestley *et al.,* 2007].

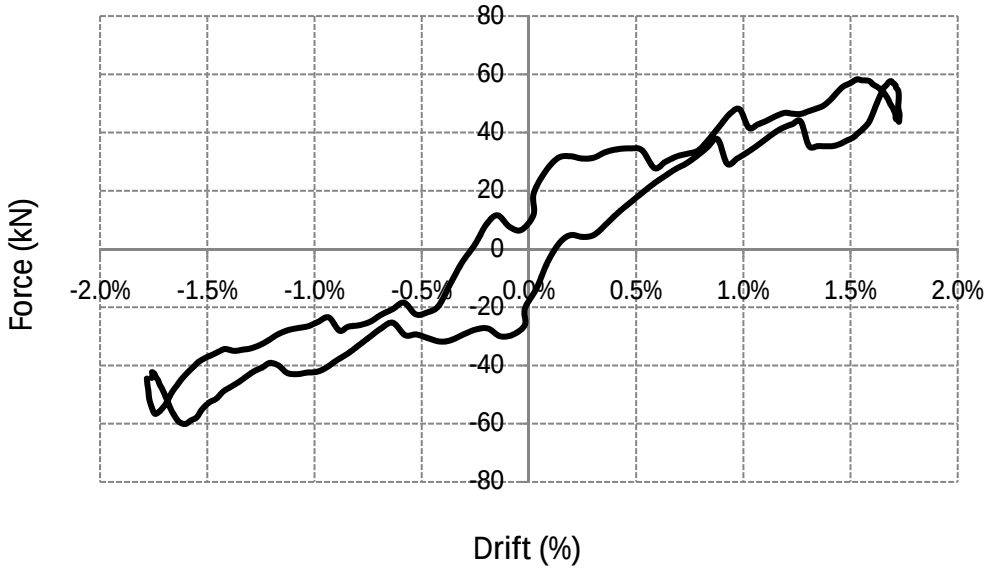

Figure 3-18 Hysteretic loops obtained during dynamic testing. "Thin" loop for high interstorey drift

Zooming-in *Figure 3-16* for the results obtained after 1% of lateral drift (for when area-based damping shows coherent results) it is possible to estimate the amount of elastic damping present in the equivalent viscous damping, this is shown in *Figure 3-19*. Some results are included in *Table 3-8* to quantify the differences using area-based or response-decay approach.

For a small inter-storey drift, 0% to 1%, there is an evident difference between area-based damping and response-decay damping due to the reason explained previously. Clearly, area-based damping overestimates the equivalent damping value. For a higher drift levels, from 1% to 2.7%, the difference between area-based and response-decay damping is reduced. Special interest may be found in the comparison of results for lateral drift that range from 2% to 2.5% due that they are often referred by design codes to be the maximum values allowed for the Ultimate Limit State(ULS) of design. At this range of interstorey drift, the results show that the elastic damping obtained fluctuates in between 0% to 1% of the critical damping.

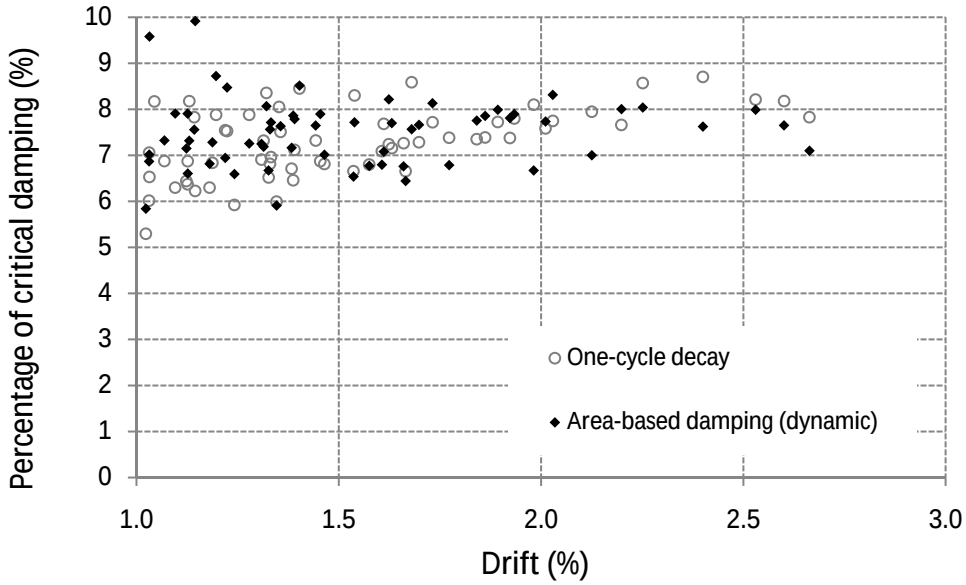

Figure 3-19 Percentage of critical damping versus drift. Zoom-in of area-based damping compared to one-cycle decay damping

Table 3-8 Area-based damping versus response-decay damping

Test (*)	Maximum Drift (%)	Area-based damping (%)	Response-decay damping (%)
3S-M3-03	0.4	15.6	4.5
3S-M3-15	0.6	10.3	4.8
3S-M3-16	0.8	7.5	5.6
3S-M3-27	1.0	7.8	6.0
3S-M3-89	1.5	6.6	6.7
3S-M3-91	2.1	7.2	7.9
3S-M2-40	2.5	8.0	8.2

(*) Tests description included in appendix D.

3.8.8 *Proposed equivalent viscous curve*

The equivalent viscous damping value to be used in DDBD needs to be compatible with the philosophy of the characterization of the structure at maximum displacement. Since the response-decay values obtained with one-cycle decay are related to the maximum displacement achieved when testing, these values seem to be compatible to be used in DDBD. To propose a curve, the mean and the standard deviation for the one-cycle decay damping values were computed. As a result, *Figure 3-20* shows an initial proposed curve for the damping values, corresponding to the mean minus one standard deviation to stay on the conservative side. The figure shows the proposed curved when compared to the response-decay damping (one-cycle and ten-cycle), top figure, and the dynamic area-based damping, bottom figure.

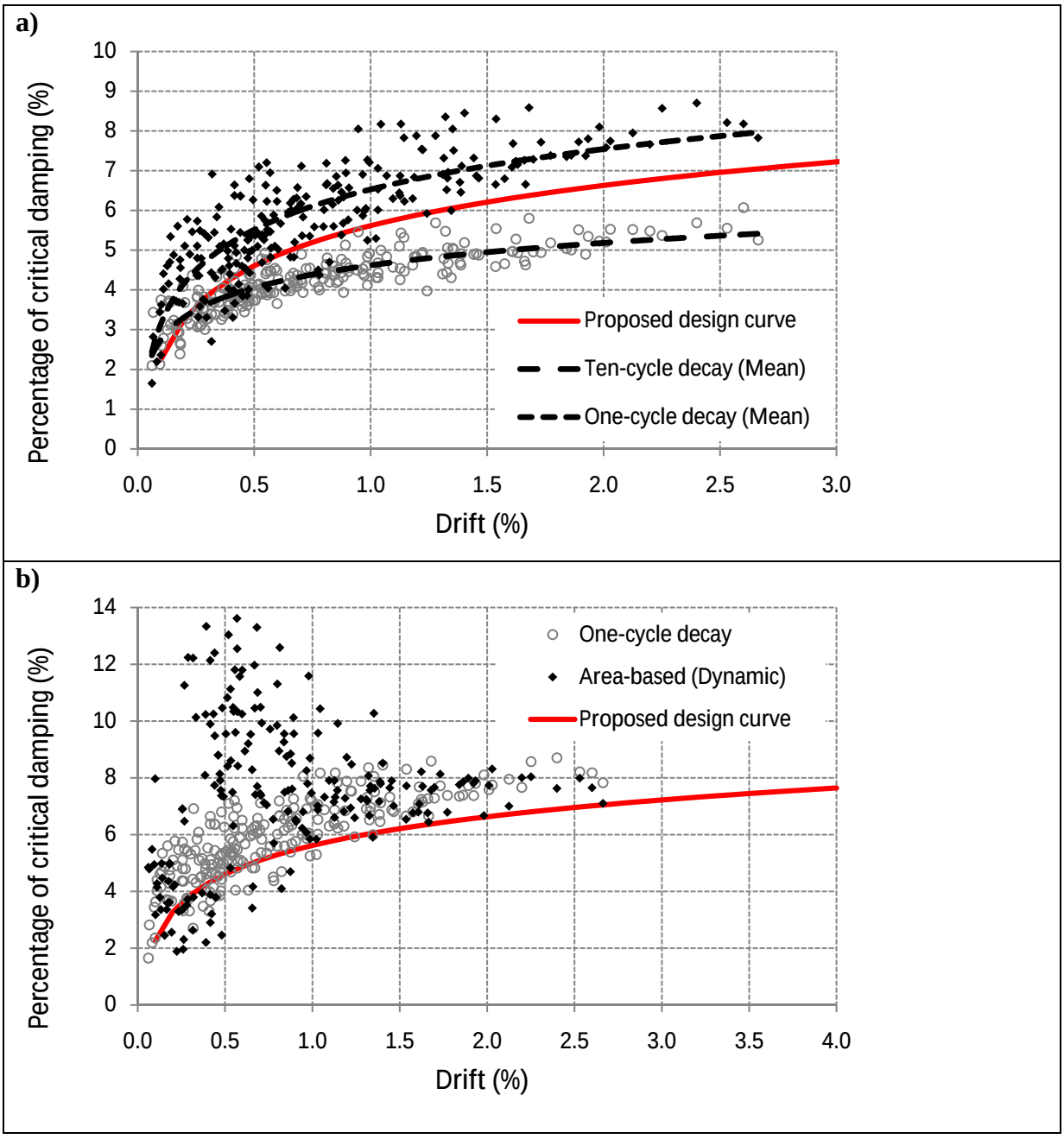

Figure 3-20 a) Proposed damping curve versus response-decay values, one cycle decay and then-cycle decay b) Proposed damping curve versus one cycle decay and area-based dynamic values

The proposed damping-drift relationship and the regression formula is at this stage a simple function of the targeted drift. Even though it is clear that the nature of the damping found is more related to hysteretic damping than others (thus displacement-proportional, more than viscous equivalent), it is recommended that no correction factors are applied. The reason is that the damping values were obtained directly for decay of the response, and were shown to be similar to the area-based values. Additionally, the elastic damping found was minimal, and the correction factor required to be applied to it is close to one because of its flag hysteretic shape nature.

Hence, the equivalent viscous damping for the modelled building (ξ), computed as the mean curve of the one-cycle-decay damping obtained minus one standard deviation is represented by ***Equation 3-10.*** For real post-tensioned timber frame buildings it may be considered to increase the elastic damping value. Conditions no modelled during testing such as: partition walls, cladding, foundations, etc., could be accounted for by adding elastic damping. However, it is recommended that the additional elastic damping value added is limited to 1% of the critical damping to be conservative and consequent with Foliente [1995] who found up to 3% of elastic damping on his research and considering that up to 1.0% of that elastic damping was found to be included by the proposed formula.
Table 3-9 shows the equivalent viscous damping values obtained with the proposed equation for traditionally used design limit states.

$$\xi = 1.46 \cdot Ln(Drift) + 5.62 \qquad \text{Equation 3-10}$$

Table 3-9 Characteristic damping values proposed

Limit state	Drift (%)	ξ (%)
SLS	0.3	3.9
ULS	2.5	7.0
MCE	4.0	7.6

SLS: Serviceability limit state, ULS: Ultimate limit state, MCE: Maximum credible event

For modelling purposes, one option is to develop a numerical model that combines the utilization of the secant stiffness matrix of the structure with a constant equivalent viscous damping. However, it is necessary to understand that the equivalent viscous damping obtained from ***Equation 3-10*** will give accurate results of the response for the drift value targeted and its vicinity. It is expected that for drift values not near the targeted, the response obtained using the numerical model will not represent truly the expected real response due to an overestimation or underestimation of the equivalent viscous damping. To obtain an accurate response during the complete seismic record used, it would be necessary iterations and the use of a variable equivalent viscous damping depending of the drift of the structure. Nevertheless, for design purposes it is necessary to know the correct value of displacements and accelerations at a targeted drift level, which can be obtained with a simple numerical model: A combination of secant stiffness matrix plus a constant equivalent viscous damping computed at the targeted drift level.

3.8.9 *Influence of selected variables on equivalent viscous damping*

From plotting damping values obtained using the response decay approach, it is possible to notice that the amount of damping is greatly influenced by the drift level over other parameters.

For the same drift level the variation of damping obtained is within 1.5%. This variation is analysed for every parameter changed during the test sequence; every analysis is performed using drift versus damping curves due to its predominance.

a) Influence of the number of floors (number of connections)

Fixing all other parameters but the number of storeys, the influence of number of storey levels is analysed. From *Figure 3-21* no clear variation in damping levels is observed once the number of levels is modified, indicating that the number of connections is not an important factor to consider at the moment for determining damping levels.

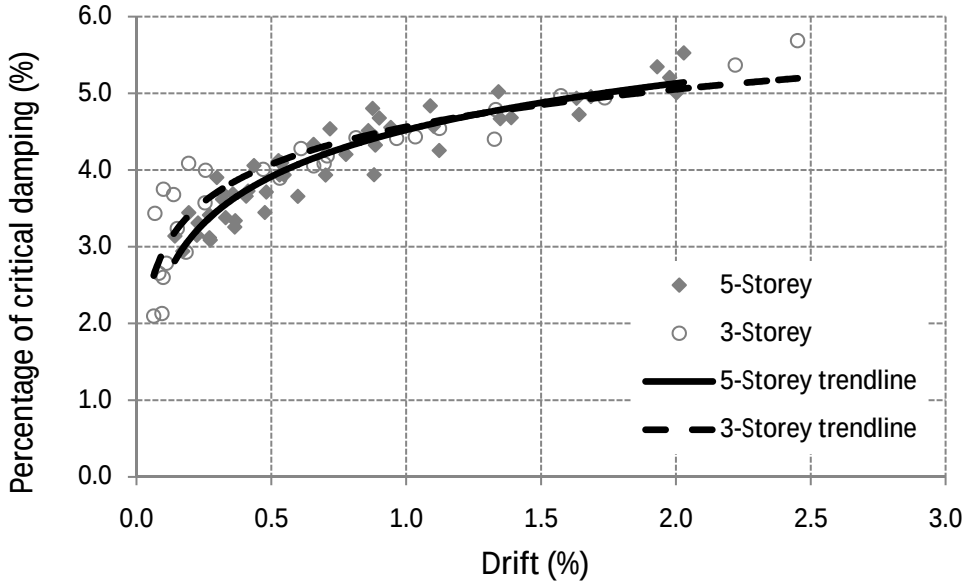

Figure 3-21 Percentage of critical damping versus drift. Comparison of values obtained for 3-storey and 5-storey

b) Influence of the amount of mass

For the 3-storey model building all variable but the amount of mass were fixed. *Figure 3-22* shows the results for this study on mass. There was not a clear influence of the amount of mass included in the model buildings, therefore an estimation of the response including a 100% of the mass required was possible.

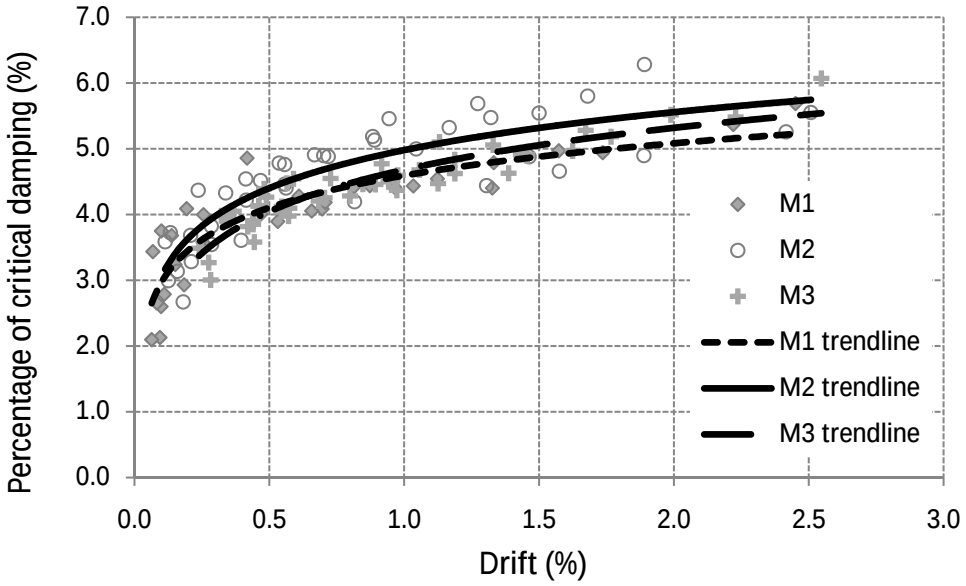

Figure 3-22 Percentage of critical damping versus drift. Comparison of values obtained for the three level of seismic mass considered M1 = 33%, M2 = 44%, and M3 = 78% of required mass by similitude.

c) Influence of amount of post-tensioning forces

Two figures are included to examine the influence of the post-tensioning force on the response. In *Figure 3-23a*, all parameters are fixed but the post-tensioning force for a 5-storey building, in *Figure 3-23b* the same is performed for a 3-storey building. There is not a clear pattern recognizable from the graphs; however both figures show a tendency (trendline) to a smaller damping value for the configuration with 45kN (higher initial post-tensioning, thus higher initial stiffness).

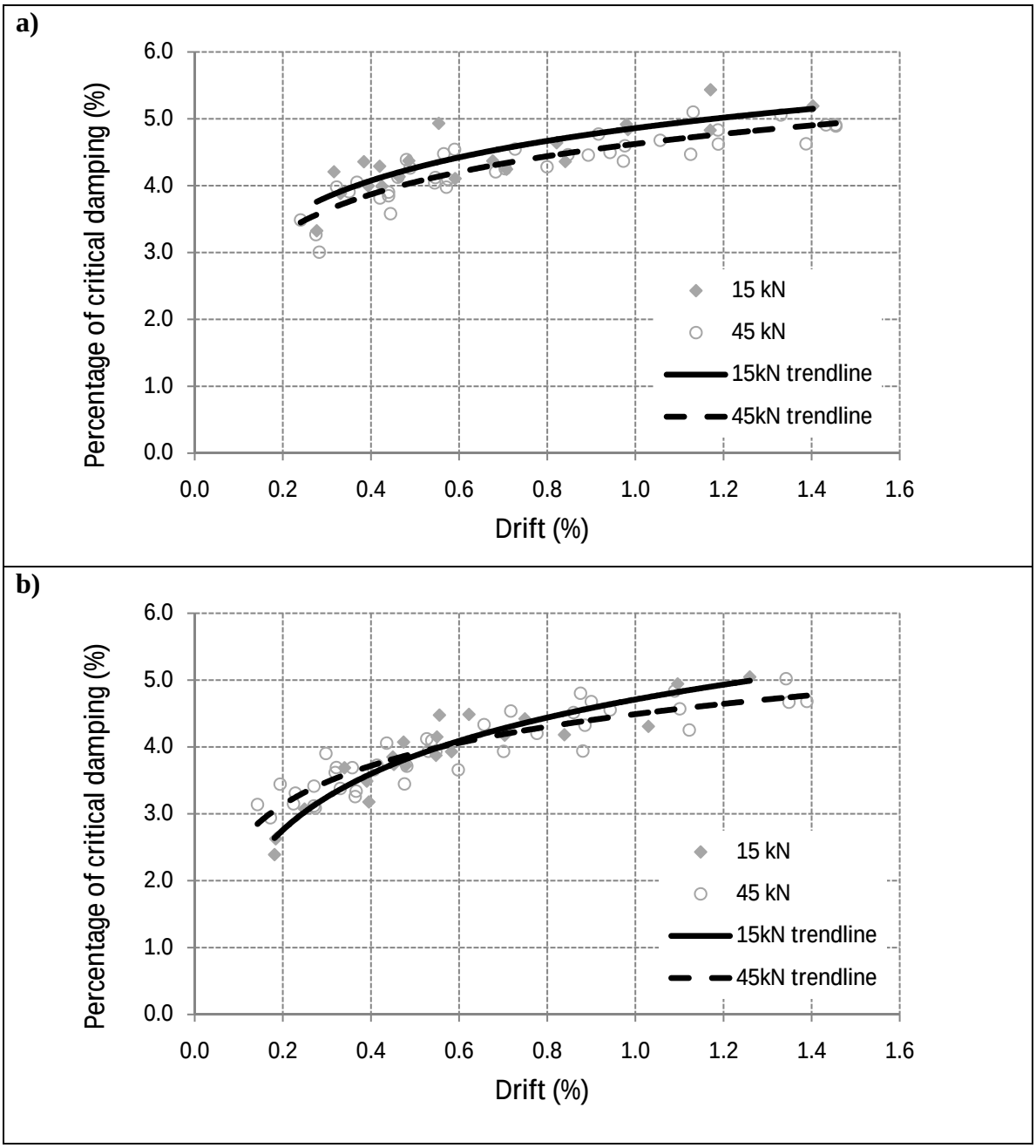

Figure 3-23 Percentage of critical damping versus drift: a) Comparison of values obtained for 15kN of post-tensioning versus 45kN of post-tensioning for the 3-storey model building b) Comparison of values obtained for 15kN of post-tensioning versus 45kN of post-tensioning for the 5-storey model building

d) Influence of corbel

As it was expected, the results (*Figure 3-24*) indicate a reduction of damping for the cases without beam corbels. The figure shows comparison of identical tests but with or without corbels. The maximum difference is around 0.5% of the critical damping. Therefore, part of the damping in the structure is generated by friction/contact between the bottom of the beam and the corbel.

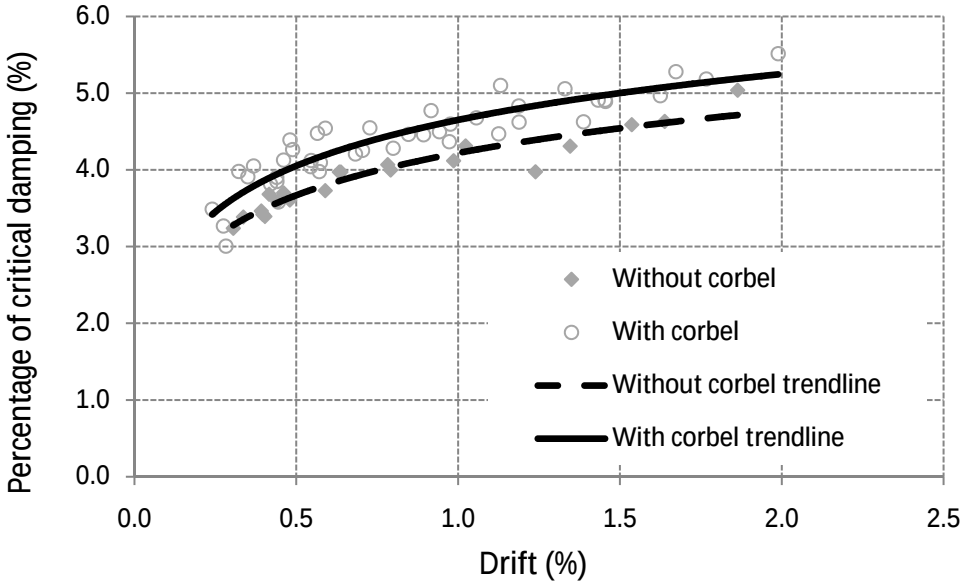

Figure 3-24 Percentage of critical damping versus drift. Comparison of values obtained with and without corbel

3.8.10 *Post-tensioning losses*

The levels of post-tensioning were recorded at the beginning and at the end of each test to compute the average loss of post-tensioning. The results show a minor reduction that seems to be negligible; just four tests have losses bigger than 1% of the initial post-tensioning with a maximum recorded loss of 2.4%. *Figure 3-25* shows the variation of post-tensioning forces for storeys one and five during the first 85 tests. First tests considered a post-tensioning force of 15kN, in test Nº22 the post-tensioning force was increased and targeted to approximately 30kN, finally at test Nº38 the post-tensioning force was increased to reach approximately 45kN. Exact values can be found in the Appendix E.

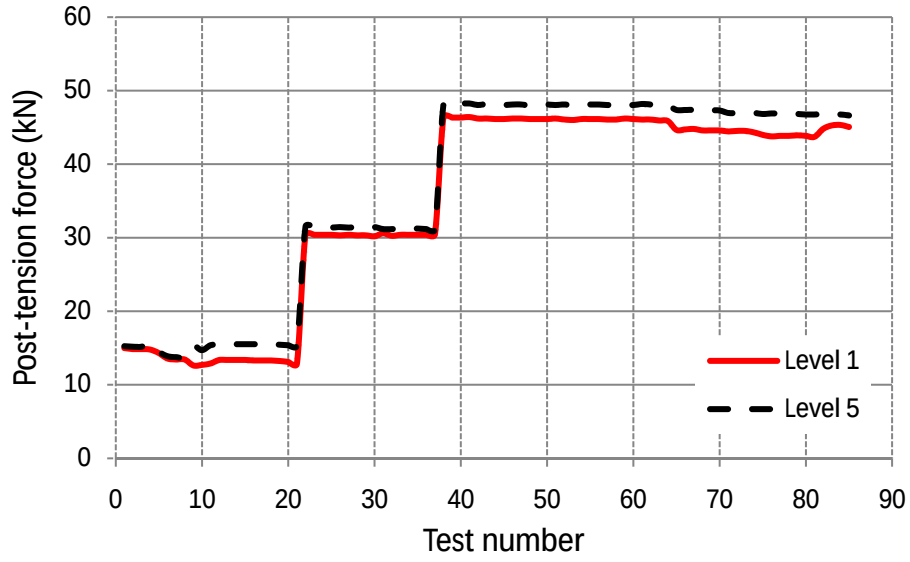

Figure 3-25 Loss of post-tensioning for first 85 tests

3.8.11 *Gap opening*

The maximum gap opening obtained at the beam-column connection (at 2.2% drift) was 2mm measured at the top (or bottom) of the beam of the first floor level. For bottoms of columns the maximum gap opening was 2.5mm measured at the outside of the column. ***Table 3-10*** shows beam rotations, column rotations and maximum gap opening measured at the top (or bottom) of the first floor beams for three levels of inter-storey drift. It is necessary to mention that maximum beam gap openings were recorded (as expected) at first floor level, beam gap opening reduces at a higher floor level. For 2.5mm of gap opening (10mm at real scale) dissipater devices attached to the structure might not be very effective; therefore, to make them work properly it is necessary to design the connection for reaching a greater gap opening or to reduce the unbonded length (to the extreme of using internally bonded, epoxied, rebars as in the original hybrid configuration [Palermo ***et al.***, 2005]) or to locate them in a configuration (e.g. diagonal haunch; external to the section with additional level arm) such that their maximum deformation demand can be amplified.

Analysis shows that the rotation (gap opening) of first level beams and the rotations at the bottom of the column are similar to the drift of the structure. One reason for this is the difference between beam and column capacity (M_n = 20kNm) versus connection capacity (M_c = 2.3kNm at 2% drift). This indicates that most of the deflections come from the connection (gap opening) rather than from the elastic deformation of the beams and columns. The fact that beams and columns suffer small deformations for an imposed lateral drift implies that in general they remain in the elastic range, i.e. the timber strain remains elastic. However, the system itself is non-linear elastic due to the gap-opening of interfaces that produces the non-linearity.

Table 3-10 Beams and columns rotation

5-storey Test	Drift (%)			Beam rotation (%)			Base column rotation (%)	Max. beam gap opening (mm)
	First floor	Third floor	Fifth floor	First floor	Third floor	Fifth floor		
5S-M1-30	1.40	1.20	0.61	1.05	0.86	0.28	1.42	1.31
5S-M1-77	1.04	0.85	0.44	0.92	0.59	0.18	1.02	0.99
5S-M1-85	2.27	1.95	0.94	2.12	1.49	0.46	2.46	2.07

3-storey Test	Drift (%)			Beam rotation (%)			Bottom column rotation (%)	Max. gap opening (mm)
	First floor	Second floor	Third floor	First floor	Second floor	Third floor		
3S-M3-56	1.00	1.04	0.91	1.88	1.00	0.40	1.07	1.03
3S-M3-67	1.58	1.49	1.07	1.48	1.18	0.86	1.82	0.98
3S-M3-91	2.26	2.18	1.72	2.13	1.86	1.33	2.59	1.52

3.9 Conclusions

- The construction process for post-tensioned timber frames stands out because of the simplicity, level of tolerances achieved, and rapid erection.

- Extensive experimental results have proven low levels of damage and significant re-centering capacity as a result of using post-tensioned connections, including:
    - Small permanent compressive deformations (around 1.5mm at maximum drift levels) were observed at the internal faces of the columns.
    - Frame re-centering was effective.
    - Residual global lateral deformations at floor levels were less than 1mm.

- Amplification of ground/table acceleration at the floor level is in the range of those expected for more traditional types of construction systems.

- Damping levels were highly influenced by drift levels; the relation between these two parameters follows a logarithmic shape. At SLS and ULS displacements, 3.9% and 7.0% of the critical damping were obtained, respectively.

- A damping-drift relationship formula as a function of the targeted drift was proposed. It was recommended that no correction factors are applied to the values obtained using the equation. The values obtained using the proposed formula may be applied as a total equivalent viscous damping during time-history-analysis.

- Additional sources (not considered during dynamic testing) of elastic damping may be added to the value computed using the proposed formula. The additional elastic damping has to be limited to 1% of the critical damping.

- The mass did not appear to influence elastic damping. For three levels of mass, there was not a clear effect on the elastic damping obtained experimentally. Further investigation is required to verify this for a higher proportion of seismic mass.

- The number of connections did not influence the elastic damping.

- The level of post-tensioning had a minor influence on the maximum drift demand. The damping values were in general smaller for higher levels of post-tensioning forces, as expected. However, the data did not indicate a consistent trend.

- Timber corbels increased the level of damping of the structure up to 0.5% (from 3.0% to 3.5% and from 5.0% to 5.5%). This damping was the result of friction between corbel and beam, and should not be relied upon in seismic design.

Chapter Four: **QUASI-STATIC TESTING OF A POST-TENSIONED TIMBER FRAME**

4.1 Introduction

This chapter presents the experimental response of one 1:4 scale post-tensioned three-storey timber frame. The frame was tested under uni-directional quasi-static cyclic loading. The aim of this test was to compute the static properties of the frame, in particular the full quasi-static hysteretic behaviour of the frame, including the initial stiffness vs. drift relationship for the three post-tensioning forces used during the shake-table test. A characterisation of the static response of the frame is fundamental for comparison to the dynamic response.

The experimental testing indicates that a) the frame was able to undergo large deformations, up 4.5% drift, with minimal damage; b) stiffness degradation and loss of post-tensioning were negligible until the selected design drift limit (2.5%) and; c) stiffness degradation and loss of post-tensioning occurred after 2.5% drift as expected in the frame design.

4.2 General frame description

The frame is one of the same used during the shake-table tests. Given that the accumulated damage after the dynamic testing was minimal, it was decided to reuse the same beams and columns. To avoid any minimal influence from the previous damage, the three least damaged of the six columns used during dynamic tests were reused, and the damaged face was placed against anchorage plates. The maximum damage from dynamic test was around 1.5mm of timber crushing on column faces at the connections to beams.

The global dimensions of the model building are; 1.5m wide and 2.4m height, representing a 3-storey building. The inter-story height is 800mm. Material used as well as cross sections are the same used during the dynamic testing. Refer to Chapter three for details. Test set up is shown in *Figure 4-1*.

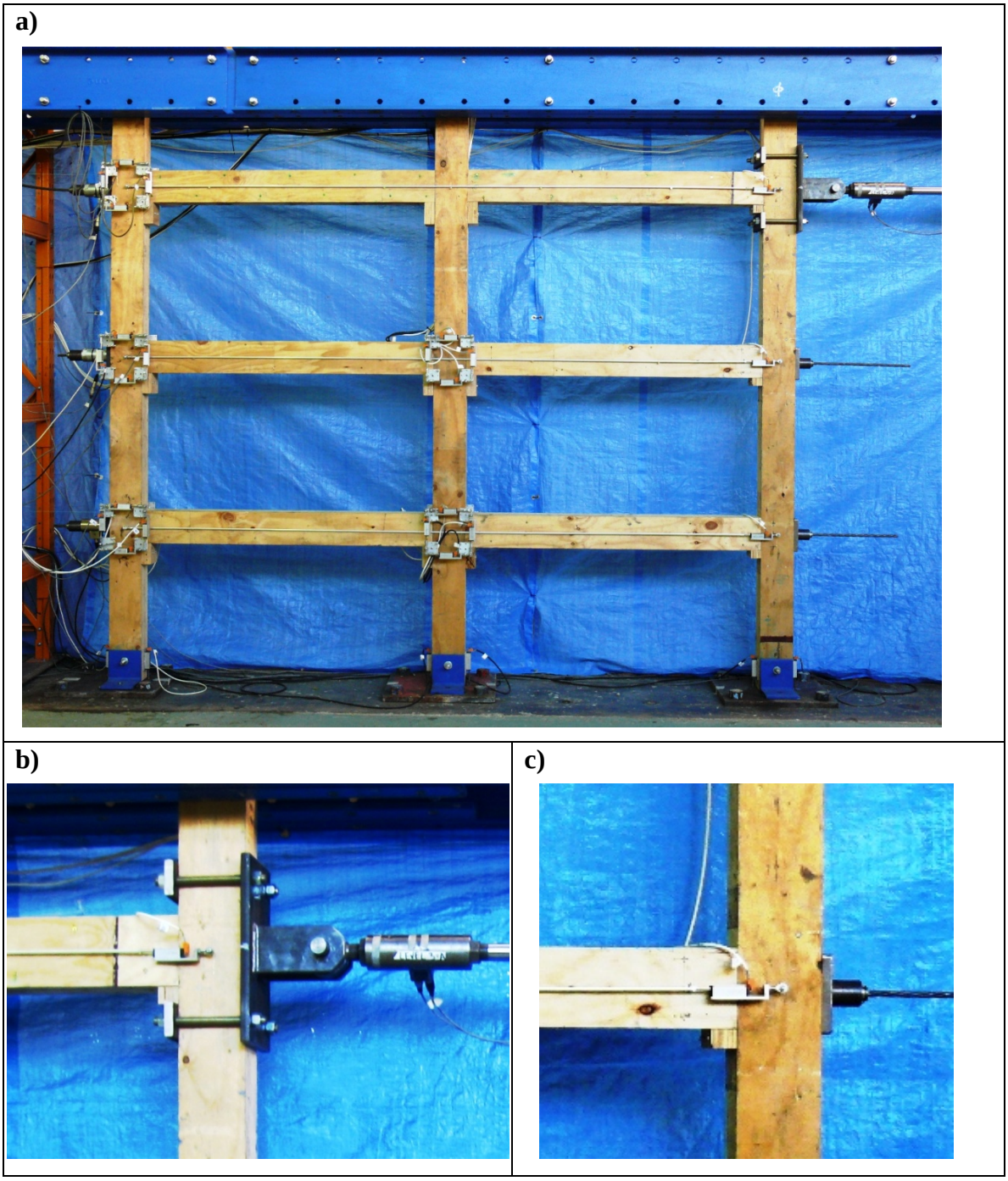

Figure 4-1 Quasi-Static test: a) 3-storey frame b) Hydraulic ram connection to frame c) Typical beam-column connection

4.3 Testing set-up

The testing arrangement is illustrated in *Figure 4-2*. The 3-storey frame was tested uni-directionally. A target displacement for the third level was applied using a hydraulic jack connected to that level. Two reaction frames were included to maintain straightness during the test. Two steel beams were placed at the top of the frame allowing for in-plane movement while restraining it from out of the plane movements during testing. The whole set-up was bolted down to a strong concrete floor.

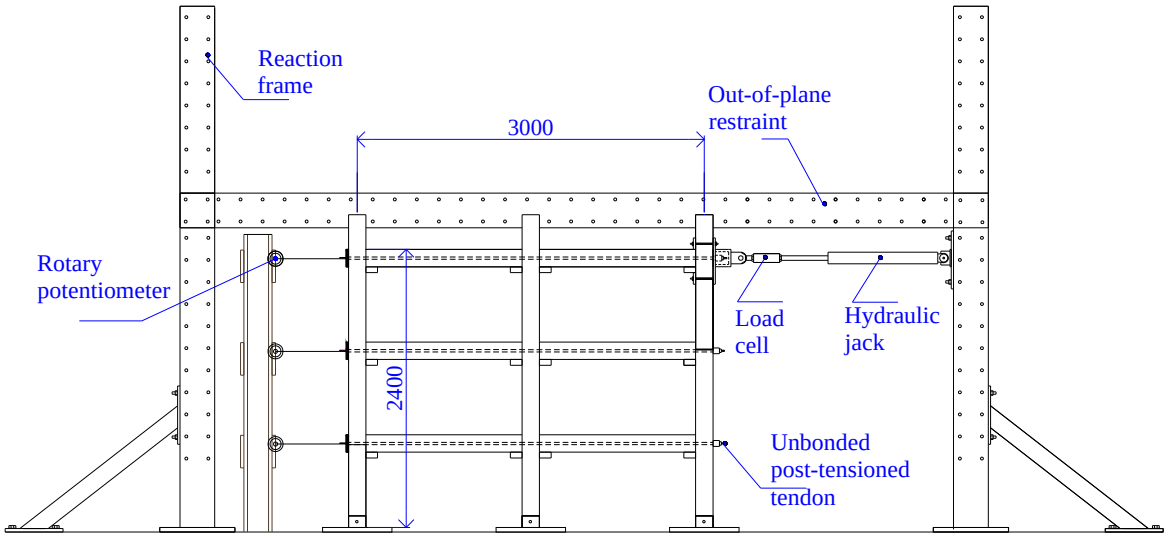

Figure 4-2 Quasi-static testing arrangement

4.4 Testing instrumentation

A summary of the instrumentation and their function is listed here, while a detailed instrumentation scheme is included on Appendix F:

(a) Measuring applied load

To measure the required load for obtaining the desired displacement, a 150kN load cell was connected directly between the hydraulic jack and the post-tensioned frame (*Figure 4-2*).

(b) Measuring lateral displacements

Lateral displacements were measured by one rotary potentiometer per level (*Figure 4-3d*). One side of the rotary potentiometer was fixed to the frame and the other side was fixed to an independent frame.

(c) Measuring tendon loads

150kN load cells were installed at the end of each tendon between the anchorage plate and the anchoring collet.

(d) Measuring gap openings and beams & columns rotation

30mm linear potentiometers were installed at both faces of beam-column connections, arranged on one side in a square form (*Figure 4-3a*) and for the other side in a cross shape (*Figure 4-3b*), in order to check values measured. Gap opening at the bottom of the column and rotation were recorded using two 50mm linear potentiometers connected to the side of the column (*Figure 4-3c*).

(e) Measuring frame elongation

50mm linear potentiometers were connected to both external columns in order to measure the relative frame elongation.

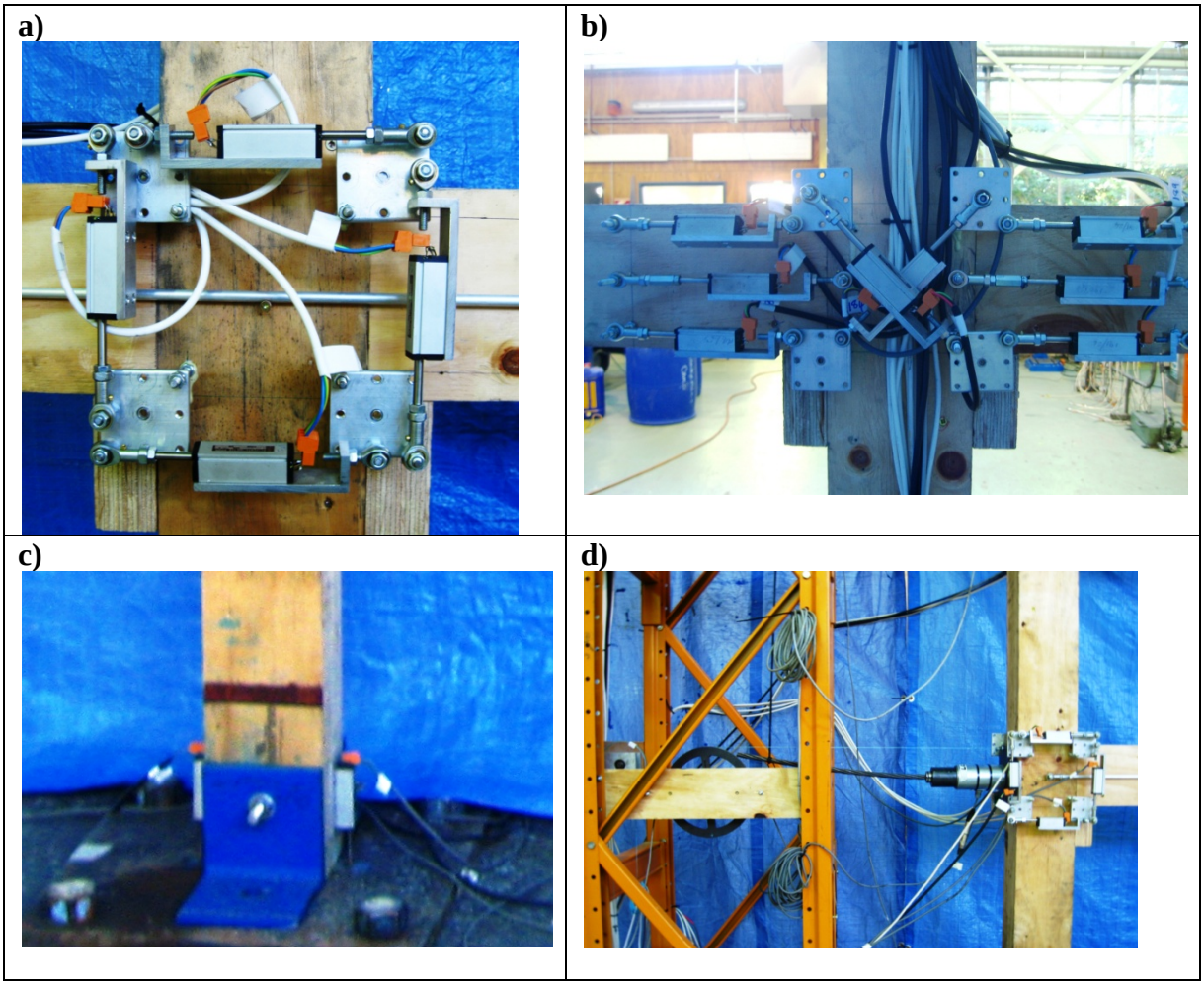

Figure 4-3 Quasi-static test instrumentation: a) Beam-column joint (North) b) Beam-column joint (South) c) Bottom column d) Rotary potentiometer

4.5 Experimental program

The building was subjected to uni-directional back-and-forward, quasi-static motions. Displacement-controlled reverse cyclic loading was applied to the structure (on the top column at the level of the top storey) using hydraulic actuators and steel reaction frames. The quasi-static experimental protocol was implemented to subject the structure to increments of 0.25% drift up to a maximum of 4.5% drift, which represents a value over the Maximum Credible Event (MCE) defined by seismic codes. The testing protocol is illustrated in *Figure 4-4*. The speed of application of the deformations was controlled to ensure that no dynamic effects occurred.

In total 3 tests were performed:

i. ***Test Nº1:*** post-tensioning force of 17kN per floor level, drift maximum of around 1%.
ii. ***Test Nº2:*** post-tensioning force of 29kN per floor level, drift maximum of around 1%.
iii. ***Test Nº3:*** post-tensioning force of 44kN per floor level, drift maximum of around 4.5%.

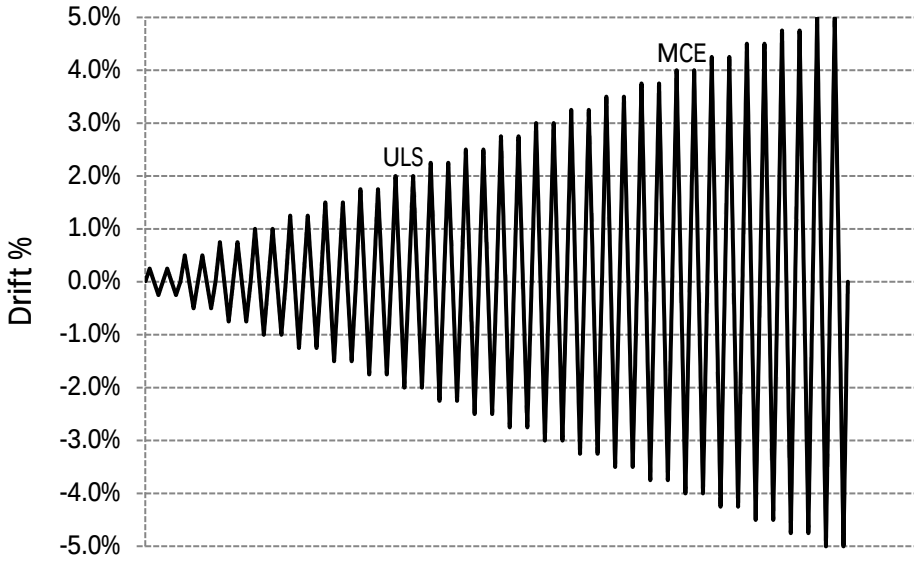

Figure 4-4 Quasi-static testing protocol

4.6 Damage observation

Up to drifts of 2.5%, there was no visual damage to the building. The timber surrounding all beam-column connections remained elastic. Up to drifts of 4.5%, the damage was still not visible from the outside (*Figure 4-5c*), however, after dissembling the frame it was possible to observe damage accumulated in the internal face of the columns (beam-column connection). The damage was a consequence of the timber being loaded perpendicular to the grain over its crushing limit. The maximum total damage corresponds to 2mm of compression (*Figure 4-5d*). The entirety of rest of the structure did not suffer any damage.

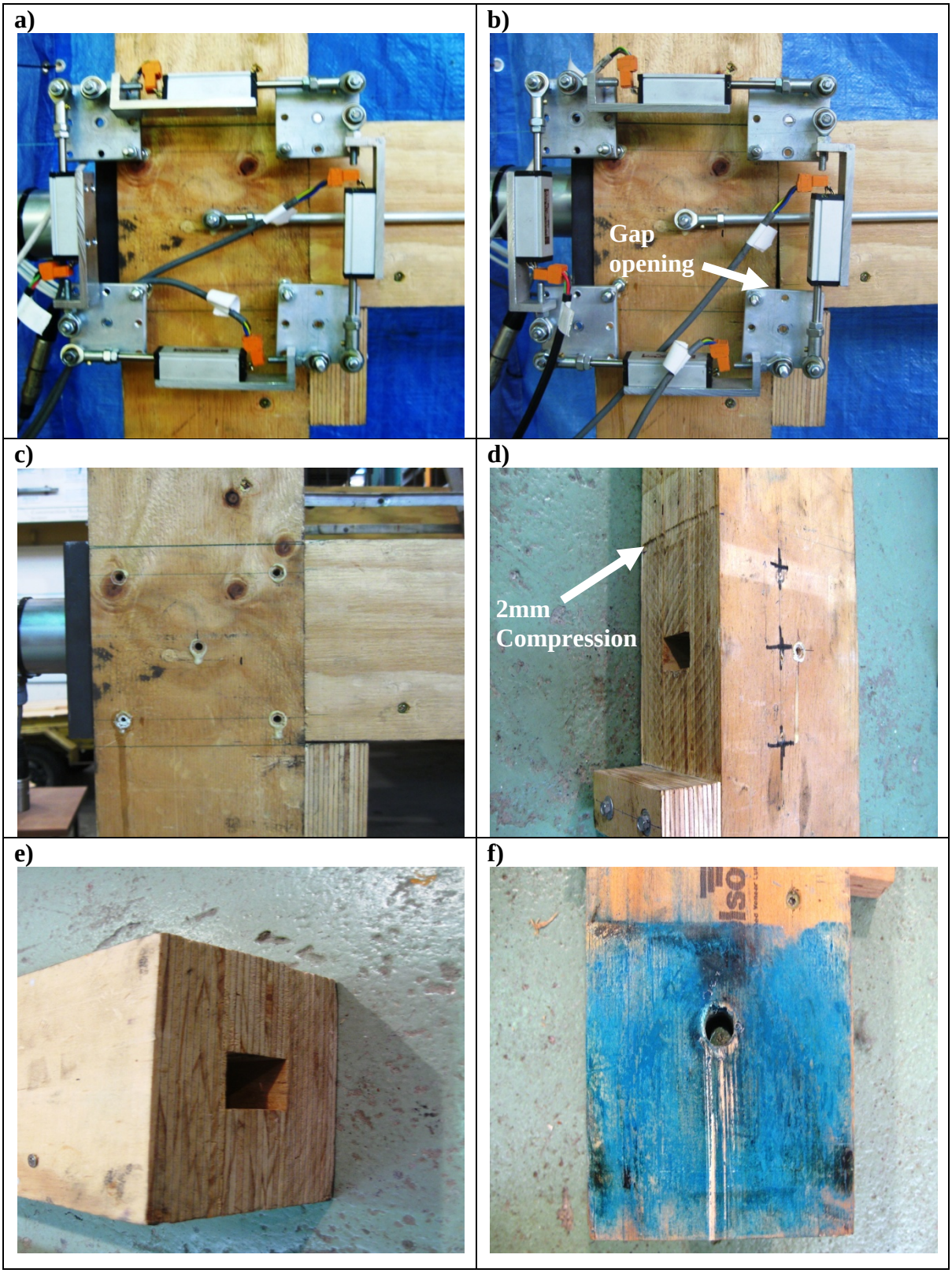

Figure 4-5 Quasi-static test, damage: a) Initial beam-column conditions b) Gap opening at 4.5% drift c) Final beam-column conditions d) Final accumulated damage at column e) Final conditions of beams (no damage) f) Final conditions of pin column connections (no damage)

4.7 Frame response

In general, the frame response was optimal, large deformations were applied to the frame with minimal loss of post-tensioning force, lateral stiffness, or load carrying capacity.
Observing the hysteresis loops for Test Nº1 and Test Nº2 (*Figure 4-6a*), it is possible to see thin loops and an elastic response of the frame until 1% of drift, i.e. there are no indications of loss in strength. The experimental Test Nº3 (*Figure 4-6b*) shows the same thin and stable hysteresis loops up to around 2.5% of drift. After 2.5% of drift, decay in lateral strength is observed, however this decay does not seem to be significant considering the level of drift achieved. Snapshots of 0.0%, 1.0%, 2.0% and 4.0% of lateral drift are shown in *Figure 4-7*.

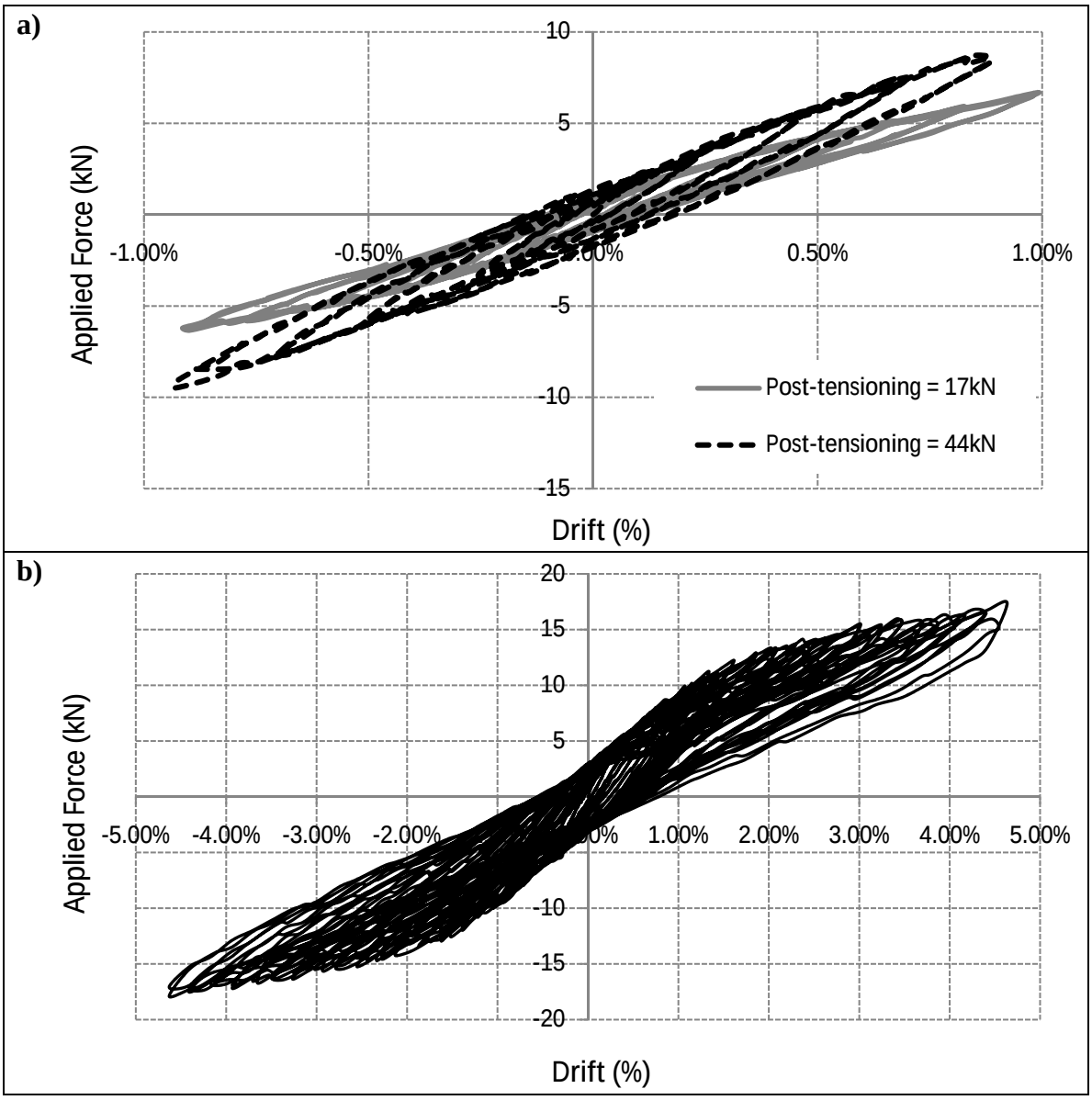

Figure 4-6 Quasi-static test, frame stiffness: a) Frame hysteresis Test Nº1 and Test Nº2 b) Frame hysteresis Test Nº 3

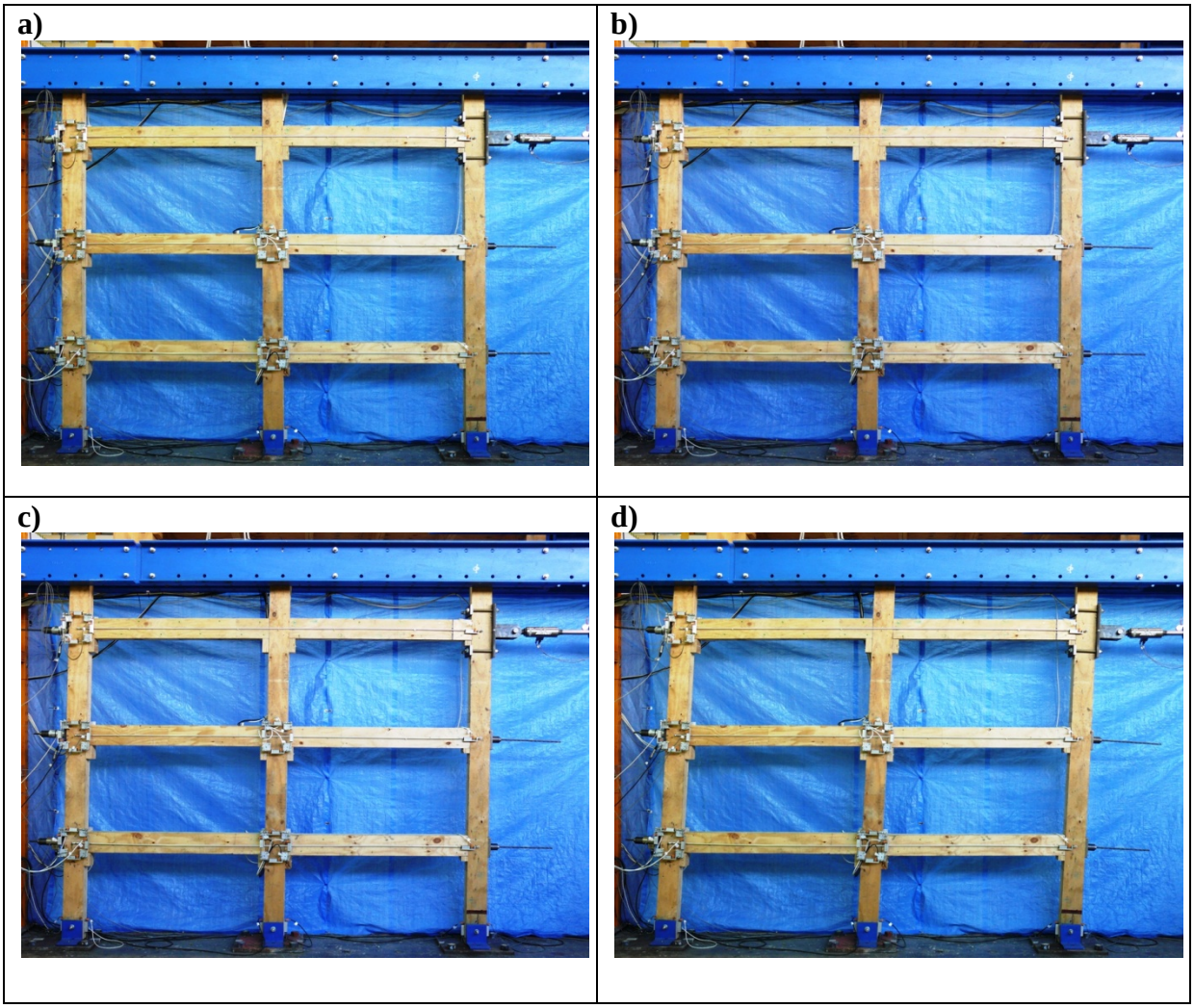

Figure 4-7 Snapshots during quasi-static test: a) 0.0% lateral drift b) 1.0% lateral drift c) 2.0% lateral drift b) 4.0% lateral drift

4.8 Frame stiffness

The lateral stiffness of the frame was calculated following testing. *Figure 4-8a,* shows the result of applying a drift level, and increasing the post-tensioning force. *Figure 4-8b* shows the decrease in lateral tangent stiffness for an increase in drift. Thus, secant stiffness increases with an increase of the post-tensioning force and decreases with an increase of the drift level.

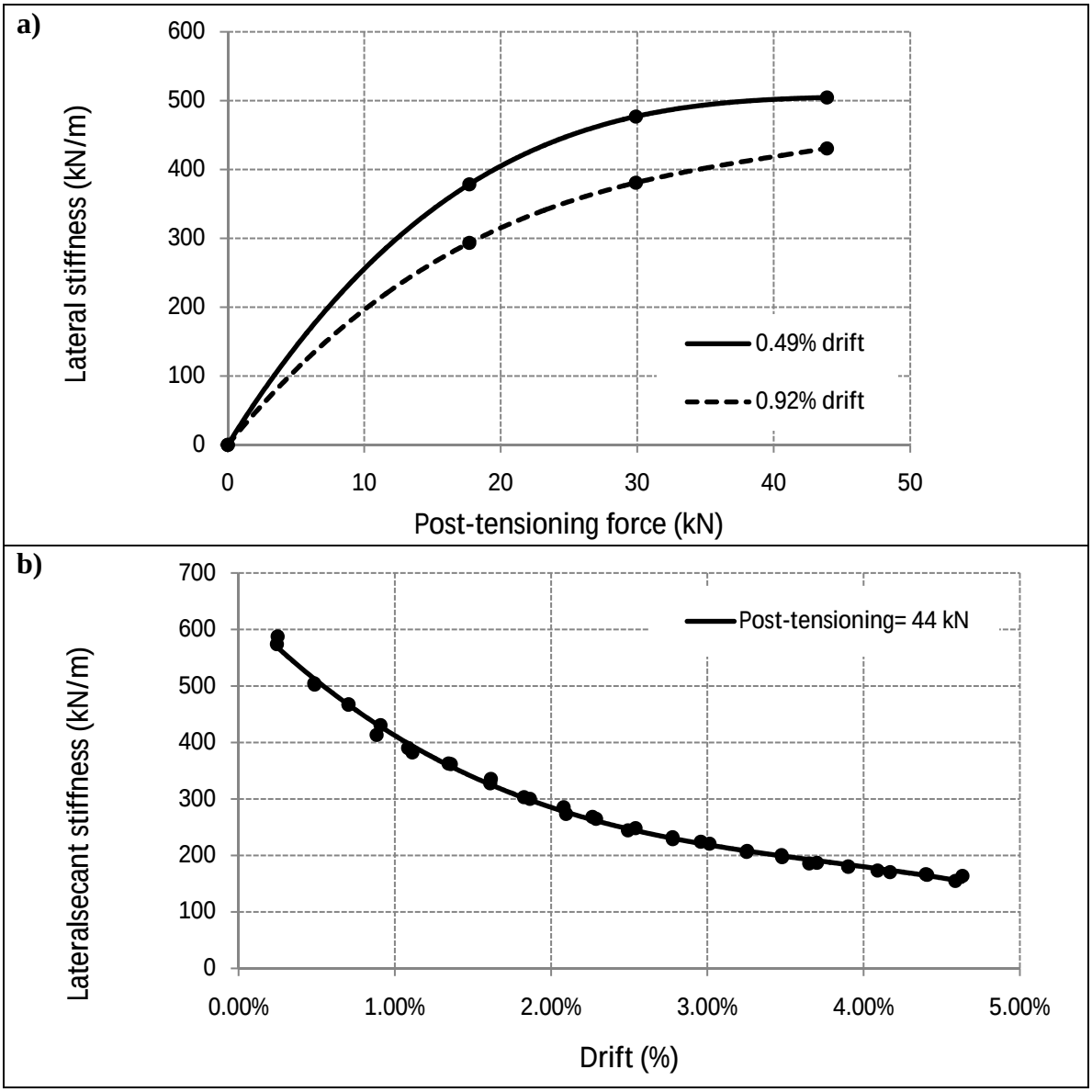

Figure 4-8 Quasi-static test: a) Influence of post-tensioning force on frame lateral stiffness b) Influence of drift in frame lateral secant stiffness

4.9 Post-tensioning forces

When discussing post-tensioning systems, it is always important to consider the loss of post-tensioning forces and the maximum force achieved for tendons. It is noted that for Test Nº1 and Test Nº2 (*Figure 4-9a, and Figure 4-9b*), there was not a significant loss of post-tensioning forces; for Test Nº1, the loss of post-tensioning forces was zero, and a reduction of 1% of the initial post-tensioning was registered in Test Nº2.
The experimental results from Test Nº3 (*Figure 4-9c*) indicate a noticeable loss in post-tensioning. At the end of the test losses of approximately 7% of the initial post-tensioning occurred.

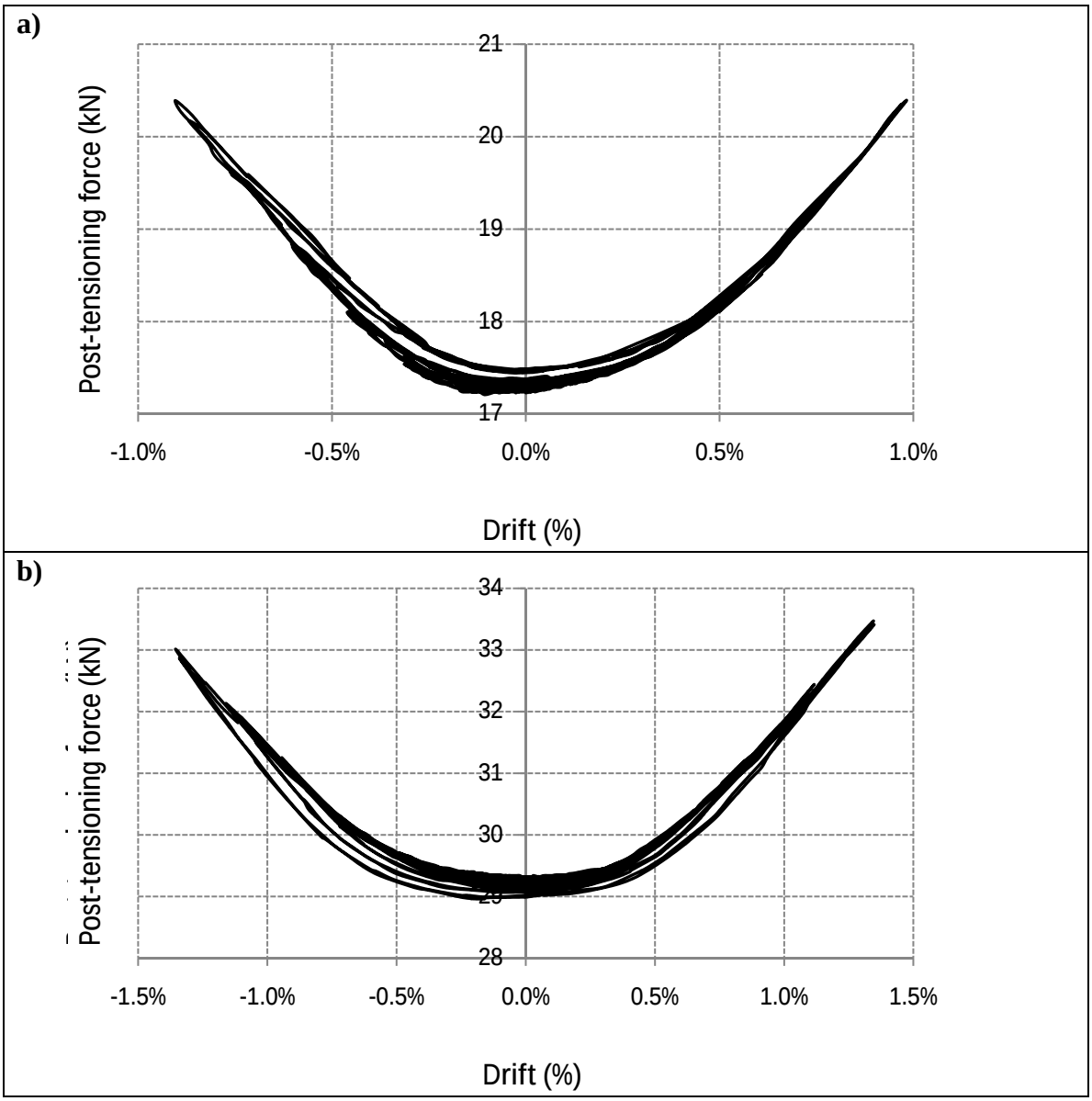

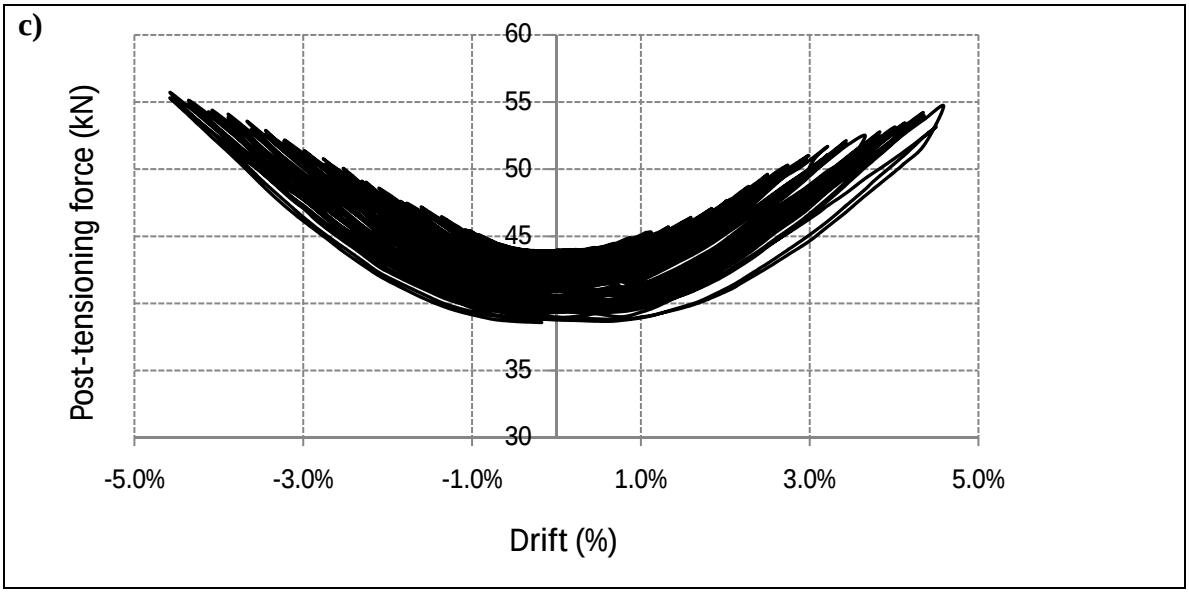

Figure 4-9 Post-tensioning forces versus drift: a) Test Nº1 b) Test Nº2 c) Test Nº3

To analyse the loss of post-tensioning forces in a visual way two graphs are included here. *Figure 4-10*a shows the loss of post-tensioning forces measured at the end of every loading cycle for the three tests performed. Observe that for drifts smaller than 2.5%, there is a minimal reduction in the tendon force. After 2.5% of drift, as in Test Nº3, a consistent decay in post-tensioning force is apparent.

The loss of post-tensioning is related with the crushing of timber perpendicular to the grain in the beam-column connection, and to the consequent relaxation of steel tendons. As explained in the design of the model buildings, 2.5% drift combined with 45kN of post-tensioning was the value fixed as a limit for crushing of the timber, therefore, once this point is reached, permanent damage in beam-column connections was expected which is the trigger for loss of post-tensioning and frame lateral resistance.

Additionally, as mentioned previously, the maximum tendon force needs to be monitored to compute safety factors. *Figure 4-10b* illustrates the maximum post-tensioning force achieved during every loading cycle. The graph indicates that at 4.6% drift an increase of 26% of the original post-tensioning force was reached, this means the value increased from 44kN to 55.3kN, this last value was the maximum post-tensioning force.
Considering that the yielding force for the tendons is 151kN, a safety factor of S.F = 2.7 was maintained. Current design practice for a post-tensioned structures (NZ3101:2006) allow to reach level of tensioning close to the yielding (90% of f_{py}) at ULS drift level.

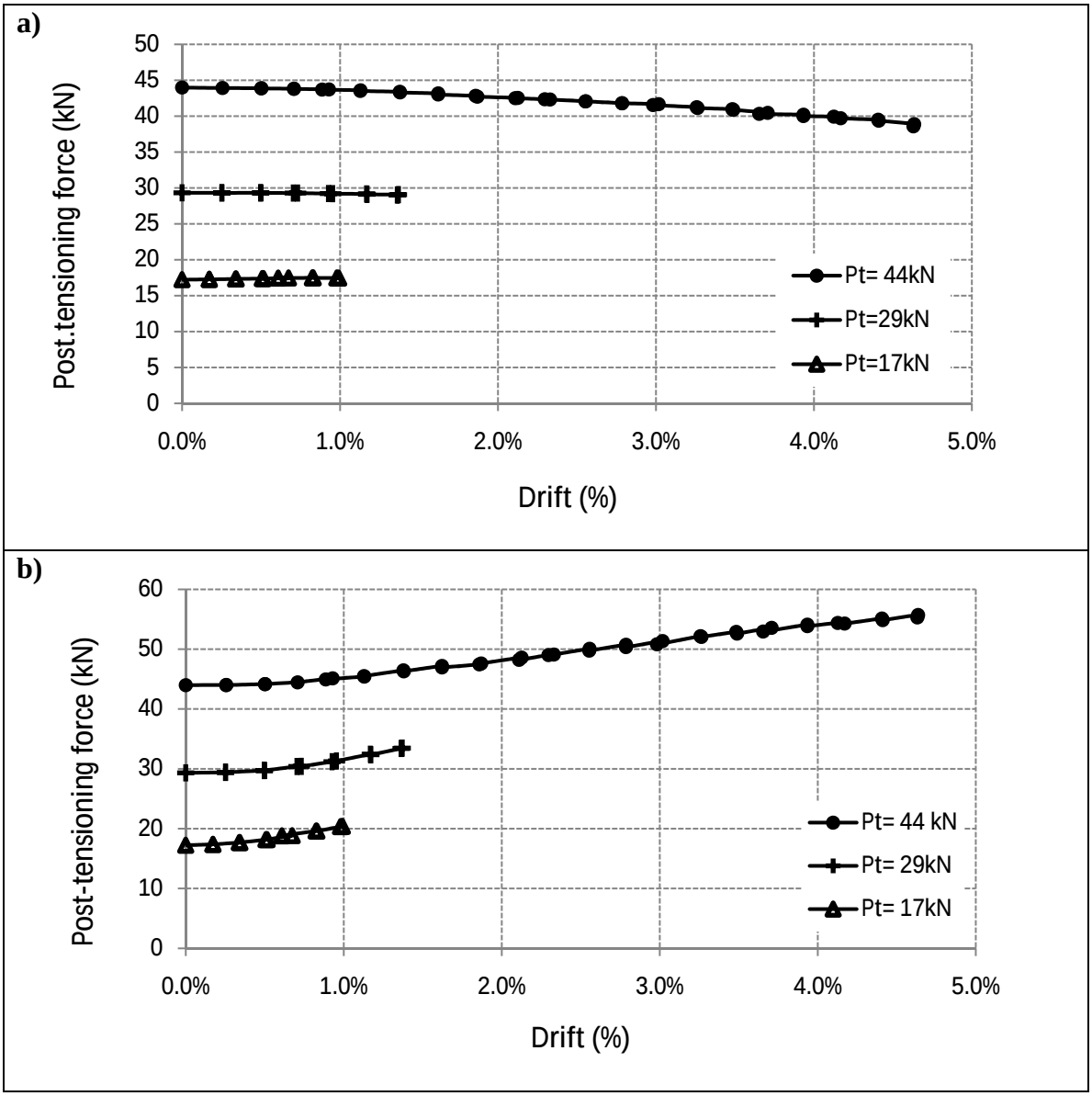

Figure 4-10 Post-tensioning force: a) Decrease on post-tensioning force at the end of each loading cycle b) Maximum post-tensioning force during each loading cycle

4.10 Gap opening

The gap opening achieved is vital in the case of adding external mild steel rods as additional dissipater devices. A minimum gap is necessary to accomplish the desired effects as increase in strength and energy dissipation. Even when past subassemblies tests of beam-column connections have proven mild dissipater bars would be effective, Iqbal et al. [2010], recent experimental tests of scaled buildings by Newcombe et al. [2010b], have shown that the effectiveness of the mild bars is reduced due to the elastic deformation of the frame itself (beams and columns), i.e. the activation of the dissipaters can happen at a high level of drift (around 1%, depending on geometry and design conditions).

As a consequence of delayed activation of dissipaters, the increase of strength of the frame and the energy dissipation is low, in particular at service limit states; this is the limit that usually controls the design. Considering that the benefits of adding external dissipaters depend highly of the configuration/solution adopted the cost/effectiveness of adding them needs to be evaluated for each particular case.

The maximum gap opening reached measured at the top of the beam, at 4.6% drift, was 3.3mm (*Figure 4-11*). At service loads (1% drift), the gap opening recorded was around 1mm which is in a real scale 4mm (frame is 1:4 scale). This low value of gap opening would require careful design of external dissipaters to be activated, thus implying low unbonded length and different configuration.

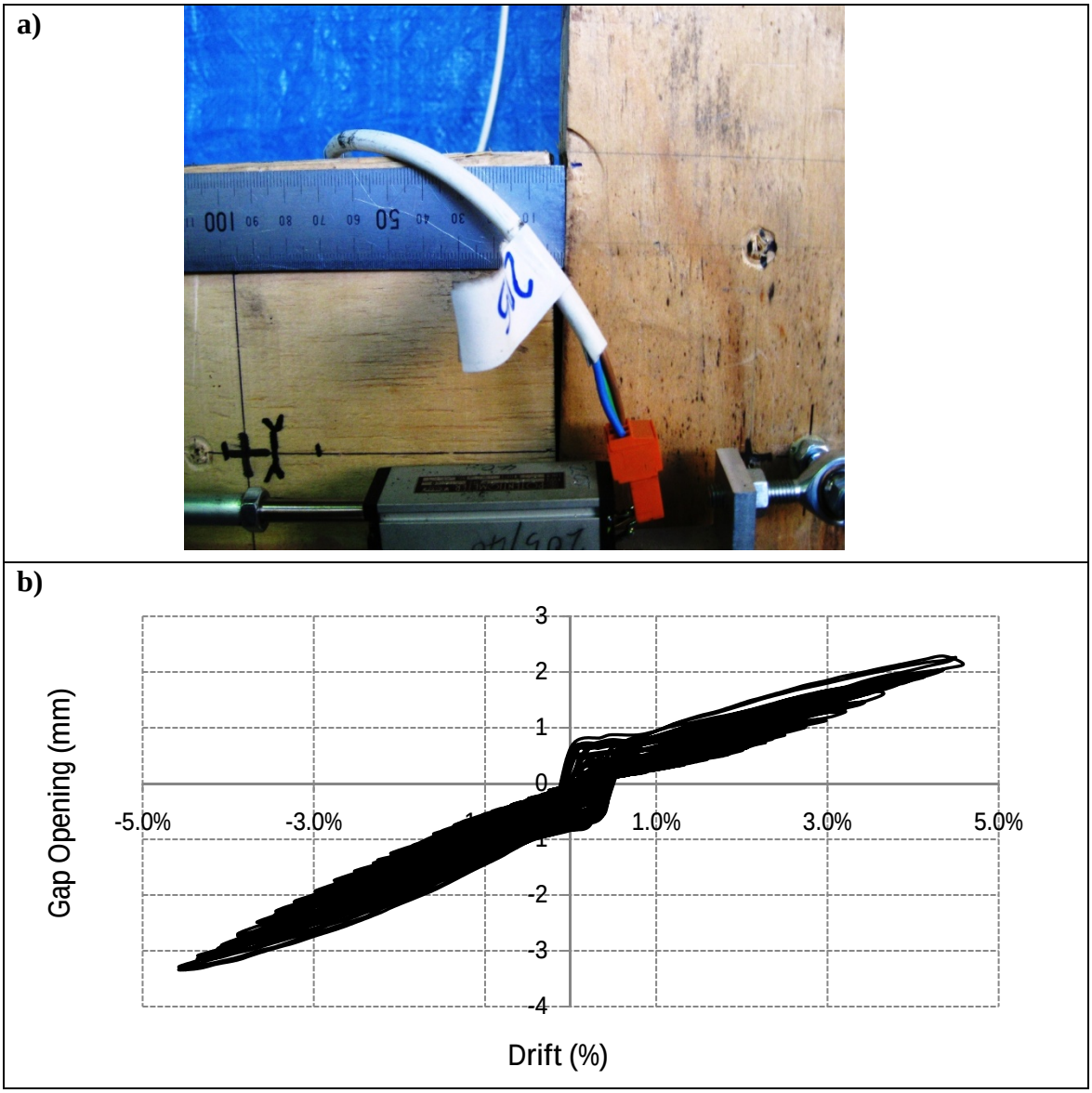

Figure 4-11 Quasi-static test: a) Gap opening at 4.6% drift, test 3 b) Gap opening versus drift, Test Nº3

4.11 Frame elongation

Geometric beam elongation has been a concern for frame systems (*Figure 4-12*). An important beam elongation could generate excessive cracks in the floor slabs. Unbonded post-tensioned concrete frames have also been part of this concern; researchers have investigated effective connections to take into account the displacement incompatibilities between the lateral resisting system and the floor [Amaris *et al.*, 2008].
However, given the inherent flexibility of the system post-tensioned timber buildings have demonstrated a good control over slab cracking, being even smaller than the ones obtained using equivalent concrete systems, Newcombe et al. [2010c]. For a given level of drift, and equal geometric conditions, in fact, the gap opening is lower in a post-tensioned timber frame than in a post-tensioned concrete frame.
To find more information about slabs solutions developed to be used for post-tensioned timber systems the reader is referred to Yeoh et al. [2008], for information about slabs effects on dynamic response of post-tensioned timber buildings refer to Newcombe et al. [2009].

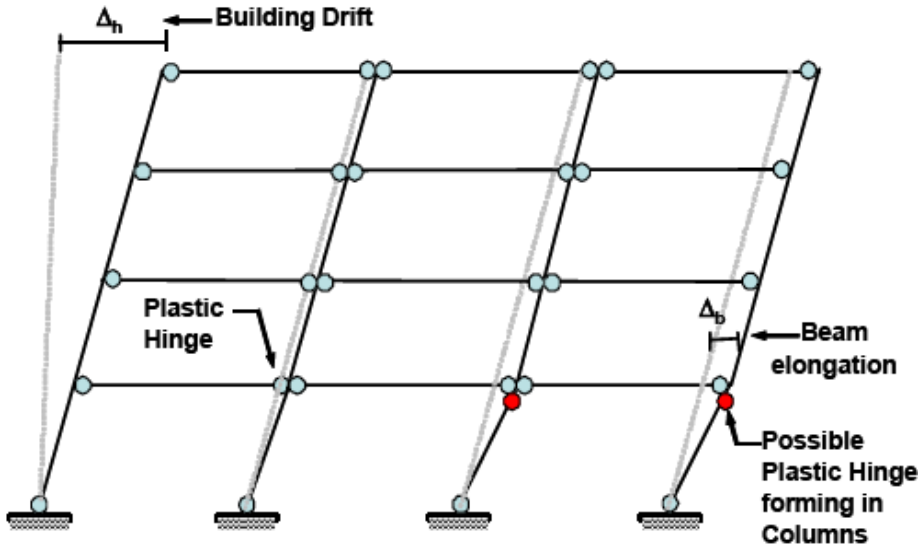

Figure 4-12 Frame elongation [Amaris et al., 2008]

Figure 4-13 shows the frame elongation registered during test Nº3, the total frame elongation at 2.5% drift (ULS) was 1.4mm, 5.6mm in real scale, representing an average of 0.46mm/m of slab cracking meaning that this value is not difficult to accommodate by cracking of the slab. Therefore a minimal damage (cracking) is expected to happen to the slab even for ULS.

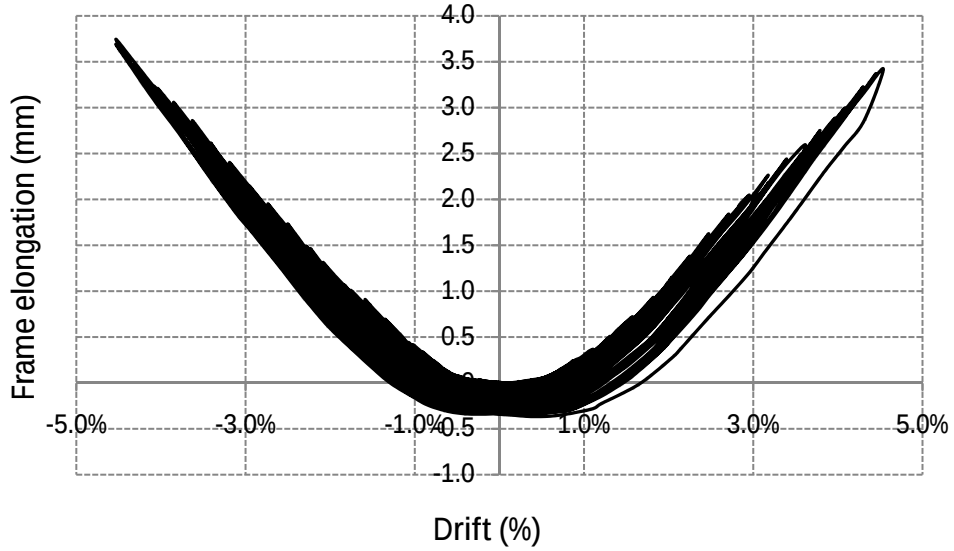

Figure 4-13 Quasi-static test. Frame elongation versus drift, Test Nº3

4.12 Area-based quasi-static damping

The damping associated with the cyclic quasi-static testing of the frame is evaluated using the traditional area-based equivalent viscous damping relationship used by Jacobsen [1960].
From the experimental results obtained in Test Nº3, the equivalent viscous damping associated with force applied versus drift was computed. *Figure 4-14a* shows hysteresis loops for four levels of drift, in general these loops are "thin". *Figure 4-14b*, shows the values obtained for quasi-static computed damping. As the drift level increases, the damping decreases, in part due to loss of lateral strength of the frame.

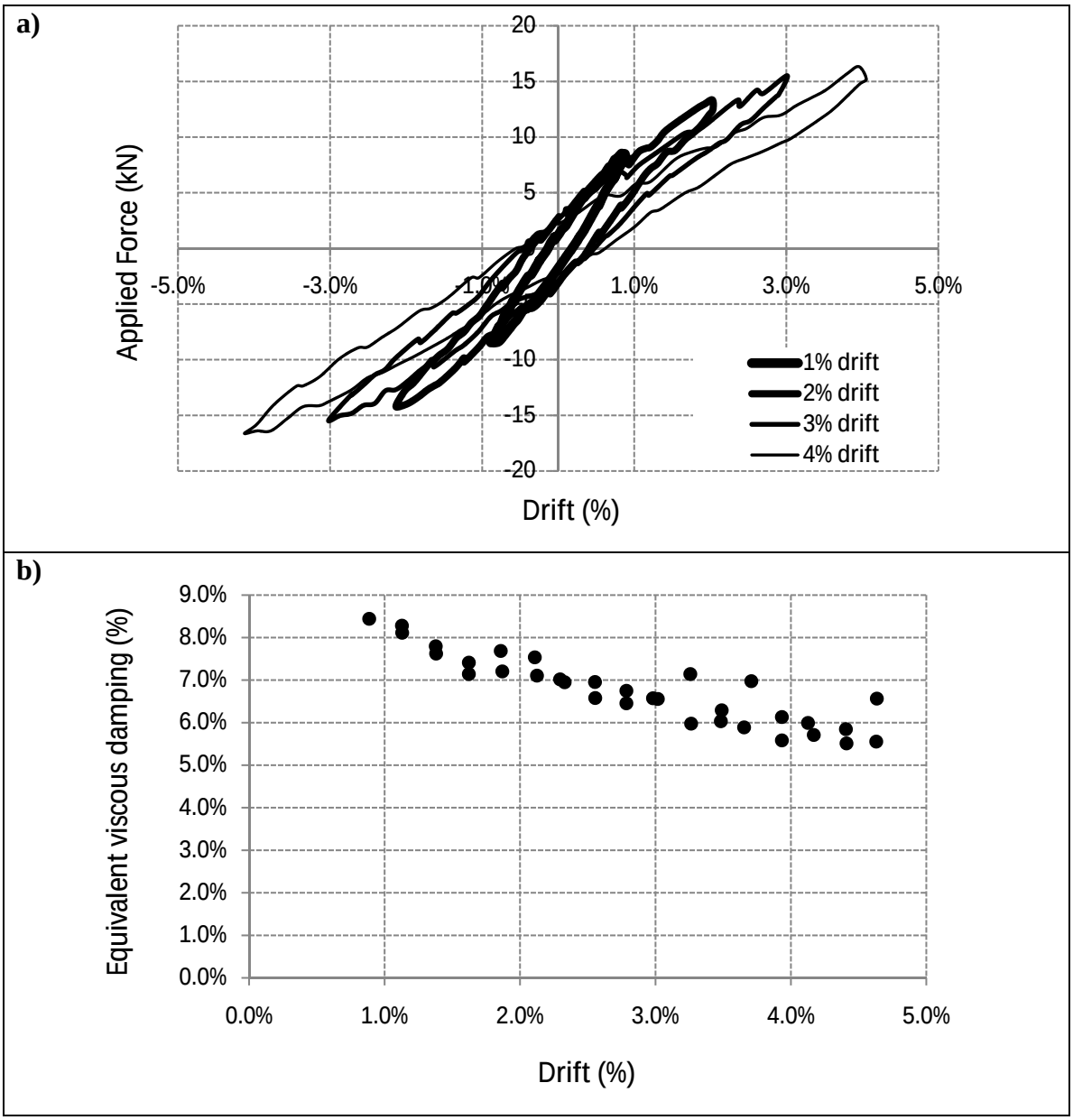

Figure 4-14 Quasi-static test, area-base damping: a) Hysteresis curves for 1%, 2%, 3%, and 4% drift b) Area-based damping versus drift

The quasi-static area-based damping obtained is compared to the damping obtained in Chapter three. Therefore, plotted on *Figure 4-15* is; area-based damping obtained during quasi-static testing, area-based damping obtained through dynamic testing, and one-cycle decay damping obtained with dynamic testing. Hence, quasi-static damping seems to be in good agreement with dynamic damping.

It is noticeable that the quasi-static hysteretic damping computed is smaller than the dynamic hysteretic damping. This difference fluctuates in between 0.5% to 1.5% of the critical damping. It could be many reasons for this difference, velocity dependent damping (viscous damping) and Coulomb damping may be some of them. Velocity dependent damping is expected to be close to zero during quasi-static testing due to the low speed of lateral deformation applied to the frame.

On the other hand, Coulomb damping which absorbs energy with friction also depends of velocity but it also depends of the normal axial force (N), as expressed on *Equation 4-1* . It was shown in Chapter three that approximately 0.5% of de equivalent viscous damping obtained was friction between bottom of beams and corbels. Particularly during the quasi-static tests performed, this source of Coulomb damping was not present due to the lack of axial loads (additional to self-weight) transferred from beams to corbels. Therefore, the viscous damping present during dynamic tests could be estimated as 0% to 1% of the critical damping.

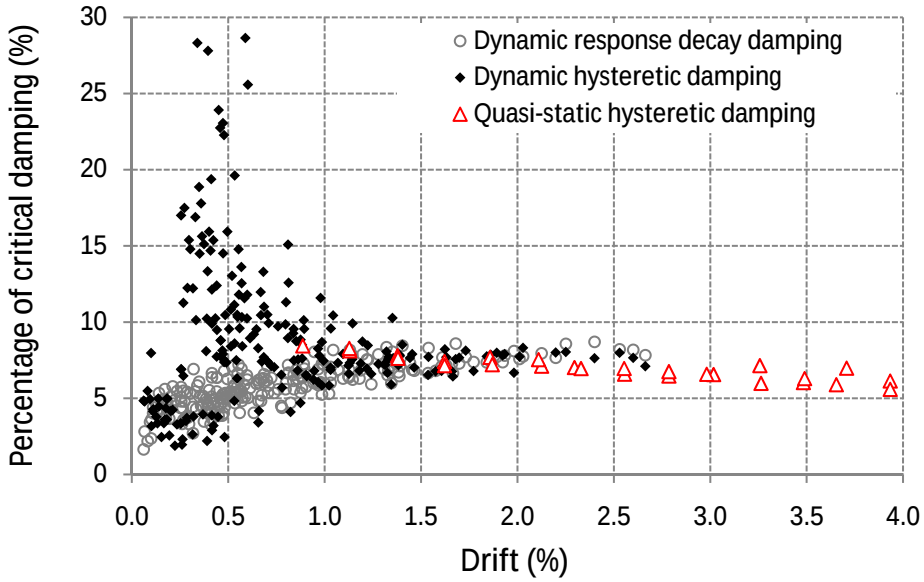

Figure 4-15 Quasi-static damping compared to dynamic damping

$$F_s = \mu_s \cdot N$$ Equation 4-1

$$F_k = \mu_k \cdot N$$

Where,

F_s = Force for static friction
F_k = Force for kinetic friction
μ_s = Coefficient of static friction
μ_k = Coefficient of kinetic friction

Zooming in the previous figure it is possible to observe with better details the difference between Quasi-static damping and dynamic damping.

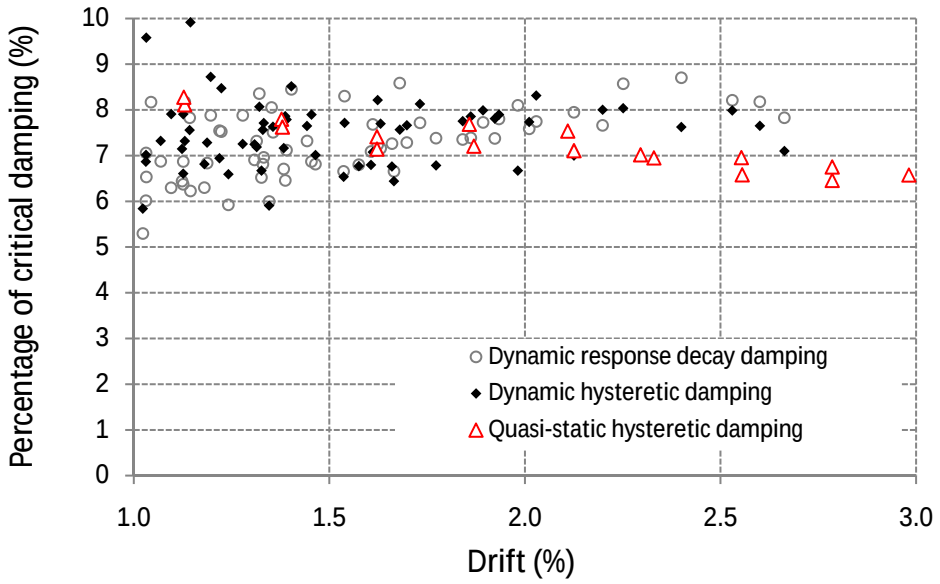

Figure 4-16 Quasi-static damping compared to dynamic damping

Observing *Figure 4-15* it is possible to realize that quasi-static hysteretic damping values show no further increase after 2.5% inter-storey drift, instead it shows a slight decrease. Consequently, it has been decided to provide a plateau to the proposed design curve at 1.8% of drift, resulting in no increase of damping values over 6.5% of the critical damping. *Figure 4-17* shows the modified proposed design curve compared to response-decay damping values. *Figure 4-18* shows the modified design curve compared to area-based dynamic damping, area-based quasi-static damping and response-decay damping.

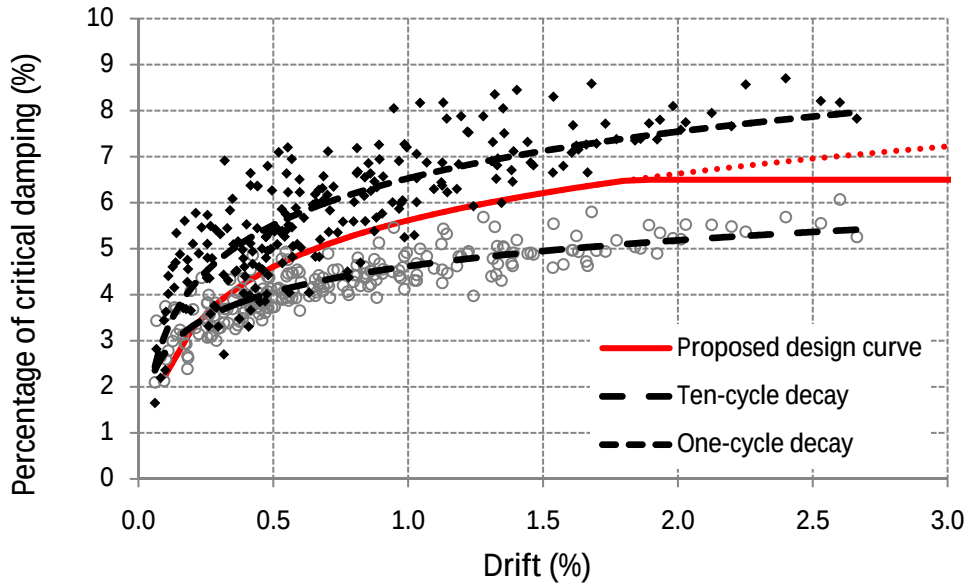

Figure 4-17 Proposed damping design curve compared to response decay damping values

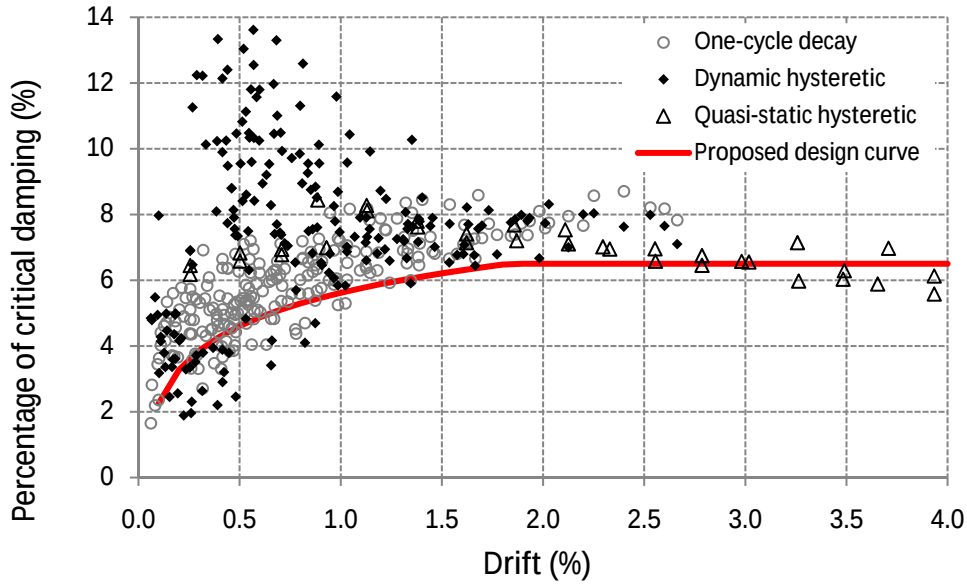

Figure 4-18 Proposed damping design curve compared to response decay damping values

Hence, the formulation presented in Chapter three is modified by *Equation 4-2*. Values proposed to use for the most common used design limit states are shown in *Table 4-1*.

$$\xi = \min(6.5\,;\ 1.46 \cdot Ln(Drift) + 5.62\,) \qquad \text{Equation 4-2}$$

Table 4-1 Final characteristics damping values proposed

Limit state	Drift (%)	ξ (%)
SLS	0.3	3.9
ULS	2.5	6.5
MCE	4.0	6.5

SLS: Serviceability limit state, ULS: Ultimate limit state, MCE: Maximum credible event

4.13 Conclusions

- Low levels of damage were verified using quasi-static testing of a single post-tensioned three-storey timber frame. Two millimetres of timber crushing at column faces in contact with beams was all the damage achieved after taking the post-tensioned timber frame to 4.5% of inter-storey drift.

- Frame lateral stiffness reduces in a parabolic manner once the drift level is increased. A larger amount of post-tensioning force results in higher lateral stiffness being achieved.

- Post-tensioning losses due lateral loading were minimal until crushing of timber perpendicular to the grain occurred (column face in contact with beam). Once crushing started, the post-tensioning losses began to increase. Only 4% of the initial post-tensioning force was lost when the frame was laterally displaced up to 2.5% drift. A total of 11% of the initial post-tensioning force was lost when the frame was laterally displaced up to 4.5% drift.

- Gap openings recorded do not appear to be large enough to properly activate external energy dissipaters in the form of axially load mild steel. To generate benefits of adding external dissipater devices, a greater gap opening or a different design (lower unbonded length) or configuration (diagonal haunch, steel angle) will be required.

- Frame elongation was very small, corresponding to 0.46mm/m at real scale, a value easily accommodated with minimal slab cracking.

- Area-based quasi-static damping proved to be in good agreement with damping values obtained during dynamic testing. Differences were attributable to velocity dependent damping and Coulomb damping.

- Quasi-static damping values obtained suggested the incorporation of a maximum damping value of 6.5% of critical damping to the proposed design damping curve.

Chapter Five: **MAIN CONTRIBUTORS TO THE INTER-STOREY DRIFT**

5.1 Introduction

This chapter explains the main contributors to the inter-storey drift (θ_d) and summarizes current methods to obtain their value. The four main contributors to inter-storey drift are; the connection rotation at the face of the column (θ_{con}), the joint-panel shear deformation (θ_j), and the rotations due to the flexure and shear deformation of the beam (θ_b) and column (θ_c).
Connection rotation has been predicted for precast concrete, utilising the Monolithic Beam Analogy (MBA) [Pampanin ***et al***., 2001; NZS3101:2006], recently adjusted to the particular timber conditions [Newcombe ***et al***., 2008]. The joint flexibility has been studied through analytical models and compared with experimental results. Beam and column rotations are computed using traditional approaches. A modified monolithic beam analogy is first presented and then incorporated with joint and member flexibility to account for all the main contributors to the frame drift.

5.2 Contributors to frame drift

5.2.1 *Monolithic beam analogy – Connection rotation (θ_{con})*

During the PRESSS (PREcast Seismic Structural System) program [Priestley ***et al***., 1999] a moment-rotation prediction was developed for precast concrete and called Monolithic Beam Analogy (MBA) [Pampanin ***et al***., 2001]. This analogy establishes a relationship between a monolithic concrete member developing a traditional plastic hinge and a rocking connection using unbonded post-tensioning. In the case of a monolithic member, the reinforcement is bonded to the concrete to ensure strain compatibility, and then during member deformation cracks are distributed along the length of the element. In the case of rocking connections, a single opening would occur. This opening could be considered as a crack, and an infinite curvature develops at the interface, resulting in a situation where Bernoulli's plane sections remain plane hypothesis is no longer valid. Thus, moment-curvature analysis is not applicable and a moment-rotation analysis is instead required. The adopted solution, instead of using section strain compatibility, uses member strain compatibility.

The original MBA focused on the plastic rotation domain of the response, and allow to derive a relationship between material strain (εc) and imposed curvature (θ_{imp}), as expressed in *Equation 5-1.*

$$\varepsilon_c = \left[\frac{\theta_{imp} \cdot L_{cant}}{\left(L_{cant} - \frac{L_p}{2}\right) \cdot L_p} + \phi_y\right] \cdot c$$

Equation 5-1

Where,
L_{cant} = Length of a cantilever (or shear span)
L_p = Plastic hinge length
c = Neutral axis depth
$ø_y$ = Yield curvature

The MBA formulation is based on three boundary conditions obtaining a moment-rotation relationship, the key points are explained below.

a) Decompression point: the initial post-tensioning force generates a uniform compression strain on the cross section; decompression occurs when an imposed deformation results in tension strain equal to the initial compression strain, then the outermost fibre reaches zero strain. This point is characterized by a fast reduction of the stiffness as a result of a geometric non-linearity due to the change of the position of the neutral axis, and it can be observed as a bi-linear behaviour similar to the yielding point of a traditional connection. At the decompression point the neutral axis depth is located at the edge of the section.

b) Yielding point: for hybrid systems, the yielding point is given by yielding of the mild steel reinforcement. For pure post-tensioned systems an equivalent "yielding" would occur when timber reaches its crushing strain in compression. In both cases, at this point the stiffness reduces slightly while strength continues to increase due to the elongation of the prestressed reinforcement from the continued opening of the gap at the base of the wall.

c) Ultimate point: two scenarios could be defined as possible ultimate point. The first one corresponds to excessive compressive strain on the column (beam-column connection), producing a column fracture. The second possibility is yielding of the tendons. Post-tensioning tendons are brittle with minimal ductile capacity, thus, a sudden fail could be the result of excessive deformation.

Recently, the MBA was extended by Palermo [2004] to refine the pre-yielding behaviour (after decompression point). The Modified Monolithic Beam Analogy formulated by Palermo [2004] is illustrated and summarized below.

For $\mathbf{0 \le \theta \le \theta_{dec}}$

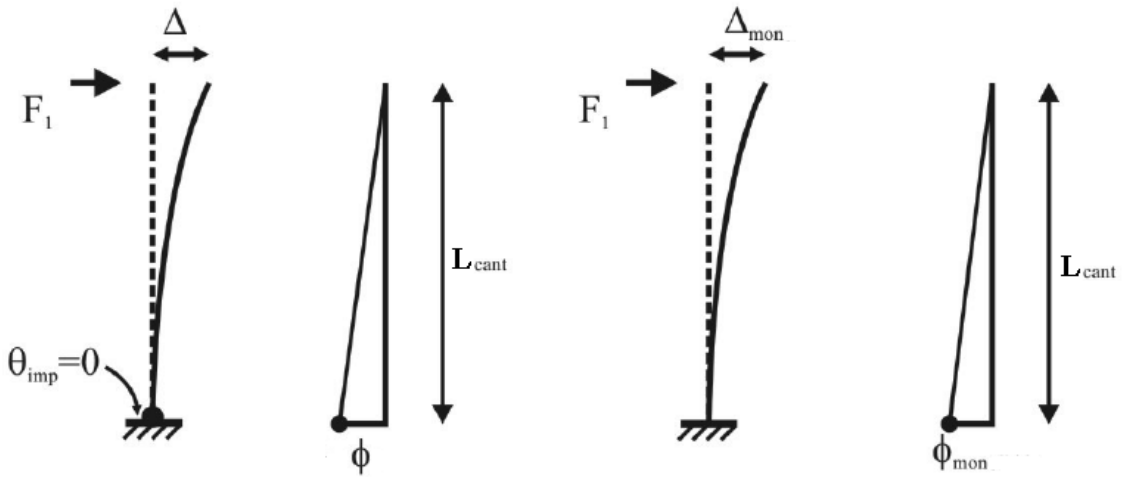

Figure 5-1 Monolithic beam Analogy for a rotation smaller than the decompression point (Modified from Marriot, D. 2009)

Before the decompression point there is no gap opening and strain compatibility is still valid, then applying the moment-area method, it is possible to compute the lateral displacement Δ :

$$\Delta = \phi \cdot \frac{L^2{}_{cant}}{3}$$ Equation 5-2

For $\boldsymbol{\theta_{dec} \le \theta \le \theta_y}$

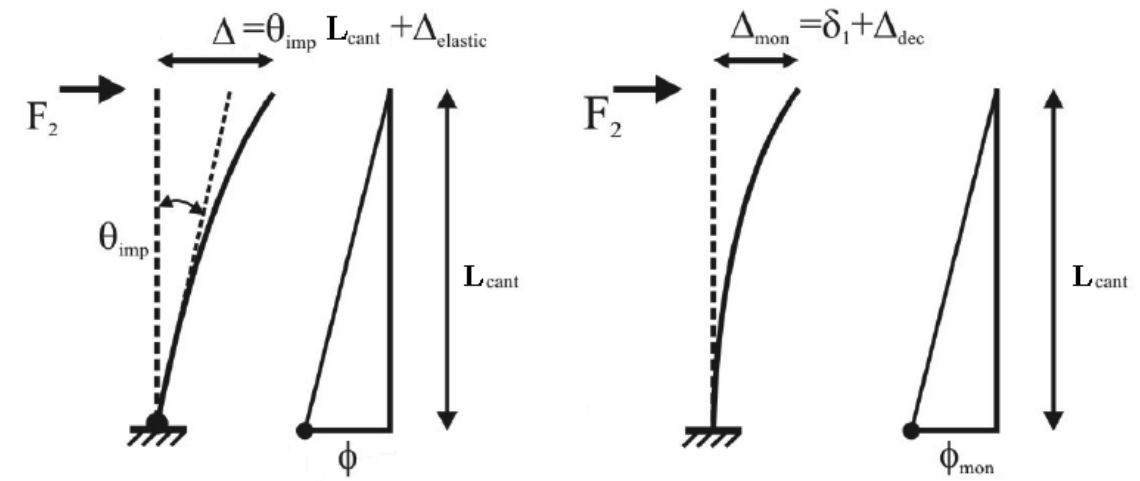

Figure 5-2 Monolithic beam Analogy for a rotation between decompression point and yield point (Modified from Marriot, D. 2009)

After the decompression point and previous to reach the yielding point, the displacement of the monolithic element is given by

$$\Delta_{mon} = \phi_{mon} \cdot \frac{L^2{}_{cant}}{3}$$ Equation 5-3

For the rocking connection the total lateral displacement is given by:

$$\Delta = \theta_{imp} \cdot L_{cant} + \phi_{dec} \cdot \frac{L^2{}_{cant}}{3}$$ Equation 5-4

Where for a rectangular section, ϕ_{dec} is given by:

$$\phi_{dec} = \frac{2 \cdot T_{pt}}{b \cdot h \cdot E}$$ Equation 5-5

The analogy then establishes an equivalence of displacements for both systems:

$$\Delta_{mon} = \Delta$$ Equation 5-6

Then, combining the previous equations:

$$\phi = 3 \cdot \frac{\theta_{imp}}{L_{cant}} + \phi_{dec}$$ Equation 5-7

Hence, the expected compression strain in the timber is:

$$\varepsilon_c = \left(3 \cdot \frac{\theta_{imp}}{L_{cant}} + \phi_{dec}\right) \cdot c$$ Equation 5-8

For $\boldsymbol{\theta_y \leq \theta \leq \theta_u}$

The final region includes compression strains greater than the yielding strain; the displacement for the rocking connection is expressed as before, meanwhile the displacement for the monolithic element includes elastic and inelastic contributions

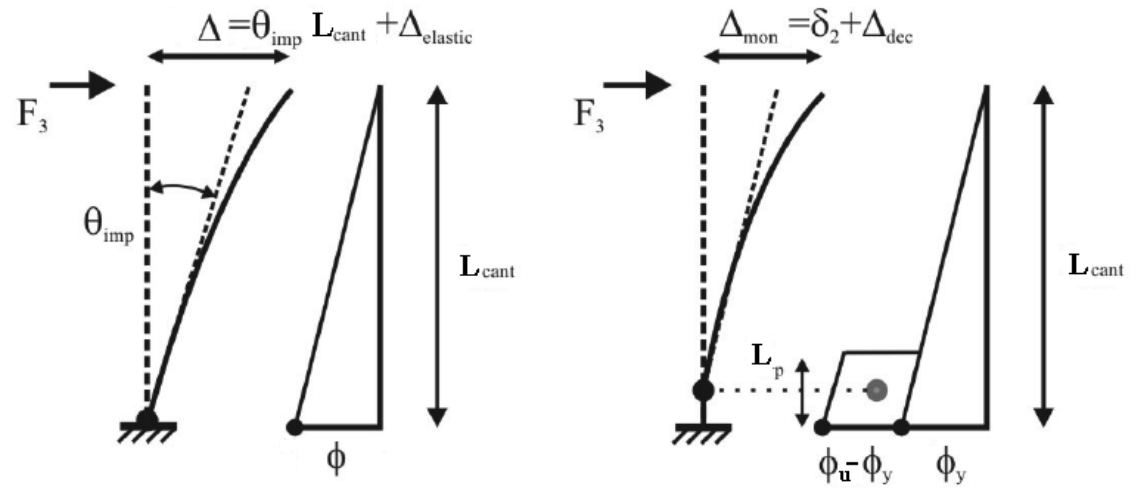

Figure 5-3 Monolithic beam Analogy for a rotation between yield point and ultimate point (Modified from Marriot, D. 2009)

$$\Delta_{mon} = \Delta_y + \Delta_p = \Delta$$ Equation 5-9

$$\Delta = \phi_y \cdot \frac{L^2{}_{cant}}{3} + \left(\phi_u - \phi_y\right) \cdot L_p \cdot \left(L_{cant} - \frac{L_p}{2}\right)$$ Equation 5-10

Combining the previous equations, the equivalent curvature is given by:

$$\phi = \left[\frac{\theta_{imp} \cdot L_{cant} - \frac{\left(\phi_y - \phi_{dec}\right) \cdot L_p}{3}}{\left(L_{cant} - \frac{L_p}{2}\right) \cdot L_p} + \phi_y\right]$$ Equation 5-11

Therefore, the equivalent strain is:

$$\varepsilon_c = \left[\frac{3 \cdot \frac{\theta_{imp}}{L_{cant}} - \left(\phi_y - \phi_{dec}\right)}{\frac{3 \cdot L_p}{L_{cant}} \cdot \left(1 - \frac{L_p}{2 \cdot L_{cant}}\right)} + \phi_y\right] \cdot c$$ Equation 5-12

The extension of this method to post-tensioned rocking timber connections requires some adjustments to account for the stress-strain material properties, bond characteristics and in general orthotropic behaviour (parallel vs. perpendicular to grain loading); more recently Newcombe et al. [2008c] suggested the parallel to the grain modulus of elasticity for the computation of ϕ_{dec} and the use of an "effective connection elastic modulus" to compute the stress at the extreme fibre. The effective connection elastic modulus values were calibrated on available experimental results. Further work is on-going in this area to further refine based on mechanically-based model, the prediction of the connection behaviour.

The proposed values are:

$$f_t = E_{con} \cdot \varepsilon_t \qquad \text{Equation 5-13}$$

$E_{con} = 0.55 \cdot E_{para}$ For timber to timber interface connections

$E_{con} = 0.1 \cdot E_{para}$ For timber to concrete/steel interface connections

Where:

f_t = Timber stress
ε_t = Timber strain
E_{para} = Mean parallel to grain elastic modulus of the timber

The previous formulation presented is used to compute moment-rotation response of the post-tensioned timber connection. The design method includes computing the other three components of the allowed drift and then calculating the rotation and moment design parameters for the connection. The detailed design method is presented in Chapter eight.

5.2.2 *Moment-rotation of joint-panel zone – joint-panel deformation* (θ_j)

The second point to consider in modelling post-tensioned timber structures is the effect of the elastic joint-panel deformation (***Figure 5-4***). Low values of bending modulus (E) and shear elastic modulus (G) in comparison with concrete, makes the understanding of the phenomenon important. In addition to low modulus values, joint-panel deformation in post-tensioned systems is expected to be greater than traditional systems due to large horizontal joint shear forces induced by the axial force from the post-tensioned tendons. Previous research [Newcombe, 2008a] demonstrated that the deformation in the joint-panel zone of post-tensioned systems may make an important contribution to inter-storey drift, depending on connection detailing. This significant contribution of joint-panel deformation is particularly important at service limit states that usually control the design of timber structures. An investigation and calibration of values to use for modelling was performed by Cusiel [2009], who also included some methods to improve the stiffness of the joint-panel zone. For more detailing refer to Cusiel et al. [2010] and Newcombe et al. [2010e]. A summary of these research projects is illustrated and presented below.

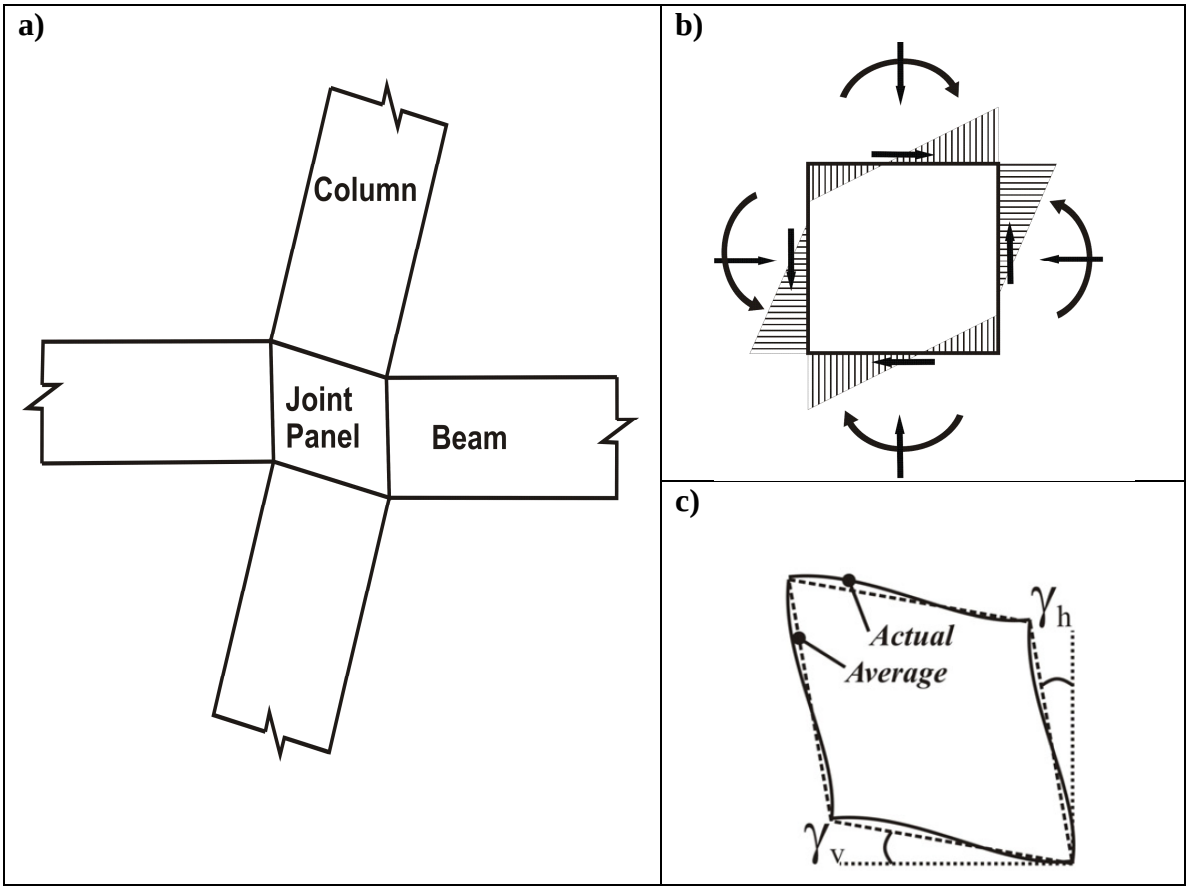

Figure 5-4 Joint-panel deformation: a) Pure shear deformation of joint-panel b) Applied actions and stress resultants for an internal beam-column joint c) Approximation to actual joint-panel deformation

The rotation of the joint-panel zone due to rotation γ is given by:

$$\theta_j = \gamma_t \cdot \left(1 - \frac{h_c}{L_b} - \frac{h_b}{H}\right)$$ Equation 5-14

Where γ_t composed by a horizontal and a vertical component as showed in ***Figure 5-4***:

$$\gamma_t = \gamma_h + \gamma_v$$ Equation 5-15

$$\gamma_h = \frac{1}{G \cdot A_{sh} \cdot h_b} \cdot \int_0^{h_b} V_{jh} \cdot dy = \frac{\bar{V}_{jh}}{G \cdot A_{sh}}$$ Equation 5-16

$$\gamma_v = \frac{1}{G \cdot A_{sv} \cdot h_c} \cdot \int_0^{h_c} V_{jv} \cdot dx = \frac{\bar{V}_{jv}}{G \cdot A_{sv}}$$ Equation 5-17

As previously mentioned, analytical theory has been compared with experimental tests performed by Cusiel [2009], *Figure 5-5* shows the agreement obtained. It can be observed that the joint stiffness is well predicted by the analytical results shown by the red line, in this case for a post-tensioned only beam-column connection.

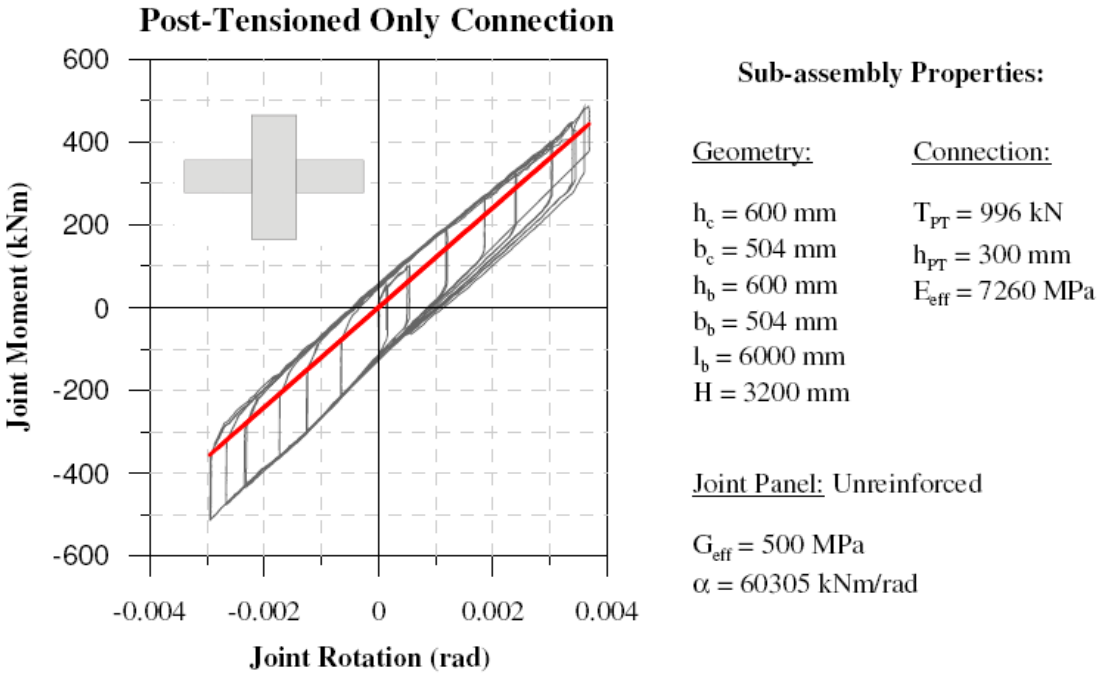

Figure 5-5 Joint-panel deformation, comparison of analytical (red line) and experimental results Cusiel [2009]

5.2.3 *Beam* (θ_b) *and column* (θ_c) *rotations*

Finally, the elastic rotation of beam and columns can be obtained using the stiffness theory:

$$\theta_b = \frac{M_{cl}}{E_t \cdot I_b} \cdot \left(\frac{L_b - h_c}{L_b}\right)\left[\frac{(L_b - h_c)}{6} + \frac{E_t}{G} \cdot \frac{{h_b}^2}{4 \cdot (L_b - h_c)}\right] \qquad \text{Equation 5-18}$$

$$\theta_c = \frac{M_{cl}}{E_t \cdot I_c} \cdot \left(\frac{H}{6} + \frac{E_t}{G} \cdot \frac{{h_c}^2}{4 \cdot H}\right) \qquad \text{Equation 5-19}$$

Once the main contributors to the frame deformation have been identified, the inter-storey drift is determined using Equation 5-20:

$$\theta_d = \theta_{con} + \theta_j + \theta_b + \theta_c \qquad \text{Equation 5-20}$$

5.3 Examples

Illustrative examples are included. A typical beam section (*Figure 5-6*) is analysed to compare contributions of each one of the components over four beam configurations. The beam and column dimensions selected are 500mm wide and 600mm height. For the example a strand area (post-tensioning tendons) A_{pt} = 990mm^2 inside beams and through columns is included, the tendons are considered to be at the centre of the beam. Bay length used is 6m and inter-storey drift 3.2m. Timber properties are included in *Table 3-1*. Post-tensioning strand properties are showed in *Table 3-2*.

Two level of post-tensioning force are considered on the analysis, being these 40% and 70% of the strand yielding force (f_{py}). The inclusion of steel armouring is also analysed; then the cases with and without reinforcing steel plates are included. Hence, the analysed cases are:

Case 1: beam without steel armouring and initial post-tensioning at 40% f_{py}
Case 2: beam without steel armouring and initial post-tensioning at 70% f_{py}
Case 3: beam with steel armouring and initial post-tensioning at 40% f_{py}
Case 4: beam with steel armouring and initial post-tensioning at 70% f_{py}

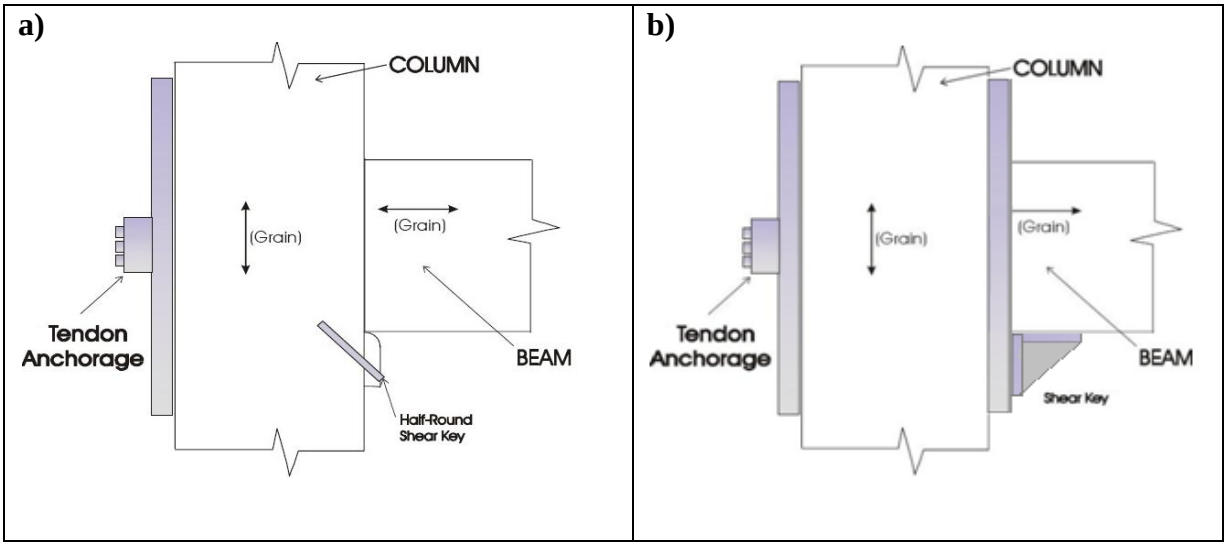

Figure 5-6 Beam-column configuration: a) Connection without steel armouring b) Connection with steel armouring (Modified from Newcombe, M. 2008a)

In order to analyse the contribution of the four components to the total inter-storey drift, some information related to design is included. Firstly the moment capacity is plotted, for the four analysed cases, as a function of the drift (*Figure 5-7*). From studying the figure it is possible to highlight three important facts:

a) For a same beam-column joint configuration, the increase of post-tensioning force does not affect initial connection stiffness. Only once decompression point is reached (gap is opened), the beam with a higher level of post-tensioning force shows a greater stiffness and therefore an increased moment capacity.

b) Configurations that include column armouring present a greater stiffness and moment capacity than ones without it. The reason is the increase of effective Young's modulus of the connection.

c) Beam-column interface moment capacity increases at higher levels of lateral drift as a consequence of an enhancement of tension of the tendons.

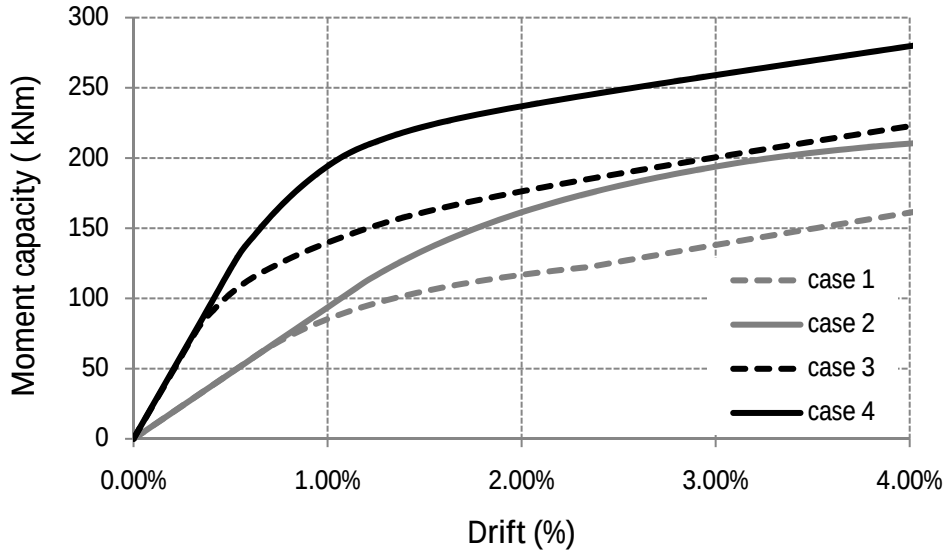

Figure 5-7 Drift versus moment capacity for the considered cases

Another important point to take into consideration during design is the timber strain at the connection zone (beam-column contact area), as explained previously this is an important area due to high levels of compression perpendicular to the column face. Damage is expected to happen after the crushing stress is exceeded at the face of the column; the damage will lead to an increase of post-tensioning losses and a decrease in lateral stiffness of the system. *Figure 5-8* shows the timber strain at the column face in contact with the beam for the four included cases, clearly when a higher level of initial post-tensioning force is applied to the section, timber strain is greater. Timber strain constantly rises with an increase of inter-storey drift. Including column armouring reduces timber strain due to an increase of effective Young's modulus of the connection and to an increased area of contact at the beam-column interface.

Figure 5-9 shows the comparison of contribution to inter-storey drift, for cases with and without steel armouring. For the case that does not include armouring, there is an obvious predominance of connection rotation over other components. When steel armouring is included there is a more homogenous contribution to drift of each of the components until the decompression point is reached. At the beginning of the gap opening a pronounced drop in beam, column, and joint contributions to inter-storey drift is noticed.
Hence, for configurations that include armouring, SLS may be controlled by other component rather connection rotation. For analysed cases, specific values have been included in *Table 5-1*. From this table, it is clear that there is a small influence of post-tensioning force over the contributions to drift.

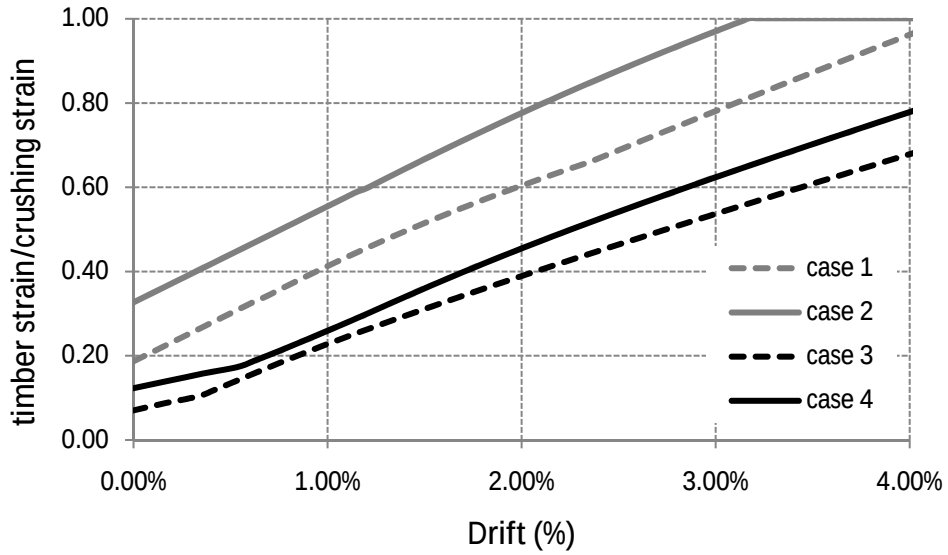

Figure 5-8 Drift versus normalized timber strain for the considered cases

Table 5-1 Contribution of the four components to inter-storey drift, comparison of cases

Case 1	beam	column	joint	connection
SLS	11.0%	8.4%	11.6%	69.0%
ULS	5.9%	4.5%	6.3%	83.3%
MCE	4.7%	3.7%	4.9%	86.7%
Case 2	beam	column	joint	connection
SLS	11.0%	8.4%	11.6%	69.0%
ULS	8.5%	6.4%	8.9%	76.2%
MCE	6.2%	4.7%	6.5%	82.6%
Case 3	beam	column	joint	connection
SLS	27.9%	21.2%	29.3%	21.6%
ULS	8.9%	6.8%	9.3%	75.0%
MCE	6.5%	5.0%	6.9%	81.6%
Case 4	beam	column	joint	connection
SLS	28.4%	21.6%	29.9%	20.1%
ULS	11.6%	8.9%	12.2%	67.3%
MCE	8.2%	6.2%	8.6%	77.0%

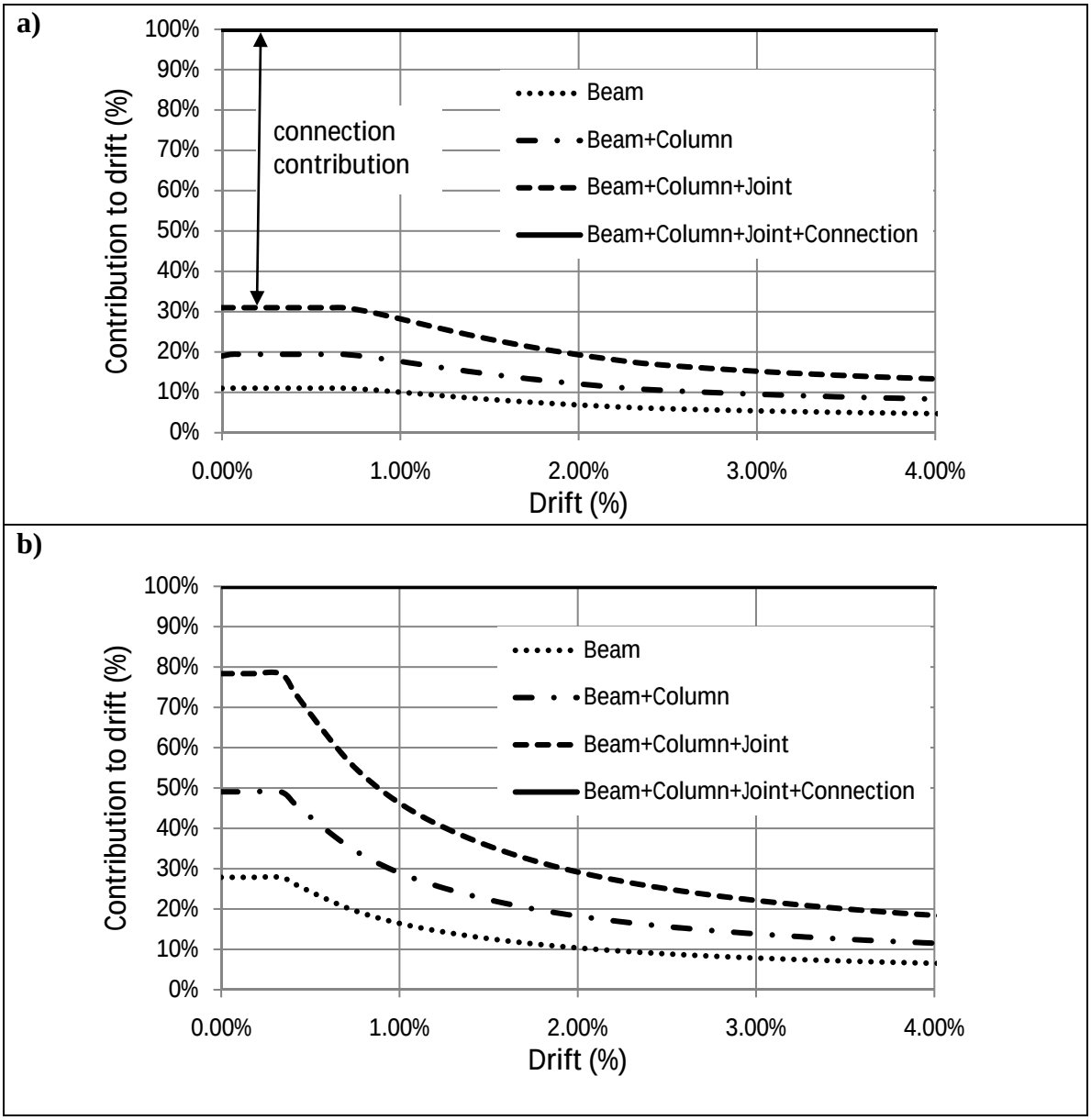

Figure 5-9 Contribution to inter-storey drift of each component: a) Case without column armouring b) Case with column armouring

5.4 Conclusions

- There are four main contributors to inter-storey drift; connection rotation, joint-panel shear deformation, beam rotation, and column rotation.

- When the post-tensioning force is increased, the initial stiffness (to the decompression point) of the connection does not change. Furthermore, there is negligible influence of the amount on post-tensioning force over the contribution to inter-storey drift of the mentioned four components.

- The main contributor to predicted drift depends of the beam-column-configuration as well as the level of drift in question. For the analysed cases the biggest contribution to drift was provided by the gap opening (connection) which is what is expected in the design to activate the rocking mechanism. Exceptions were the cases with steel armouring at SLS, for small deformations the main contributor to drift was the result of joint-panel deformation.

Chapter Six: **MODELLING MONOTONIC AND DYNAMIC RESPONSE OF POST-TENSIONED TIMBER FRAMES**

6.1 Introduction

This chapter presents modelling techniques used for post-tensioned systems. These techniques are based on the use of lumped plasticity to concentrate the inelastic behaviour of the members in chosen points represented by springs. A rotational-spring model and multi-spring model are presented first, and then the models are used to predict an envelope of the force-displacement curves obtained during quasi-static testing. A combination of a non-linear elastic spring model with the equivalent viscous damping values proposed (dynamic tests, Chapter three) is implemented and compared to shake-table results.
Finally, inelastic spring models are considered. Hysteretic behaviour is calibrated to match quasi-static testing and then used for modelling dynamic tests to be compared versus shake-table results.
The numerical study indicates that a simple rotational-spring model with non-linear elastic behaviour in combination with the equivalent viscous damping values proposed is the simplest way to obtain an accurate approximation of the dynamic behaviour of post-tensioned-only timber buildings.

6.2 Spring models

Spring models are traditionally used to represent the non-linear behaviour of post-tensioned systems. The accuracy of this kind of model for predicting the response of rocking systems has been proven and validated against several experimental test results [Pampanin *et al.,* 2001; Spieth *et al.,* 2004; Palermo *et al.,* 2005a; Palermo *et al.,* 2005b].
The model buildings were modelled using RUAUMOKO [Carr, 2008], a finite element, non-linear dynamic computer program. A general representation of the model used is shown in *Figure 6-1*. Beams and columns were represented by elastic Giberson elements, the joint-panel zone was represented by a zero-length rotational linear-elastic spring combined with rigid links, and a beam-column rocking interface was represented by a zero-length rotational-spring or multi-spring (axial springs) as indicated in *Figure 6-2*.

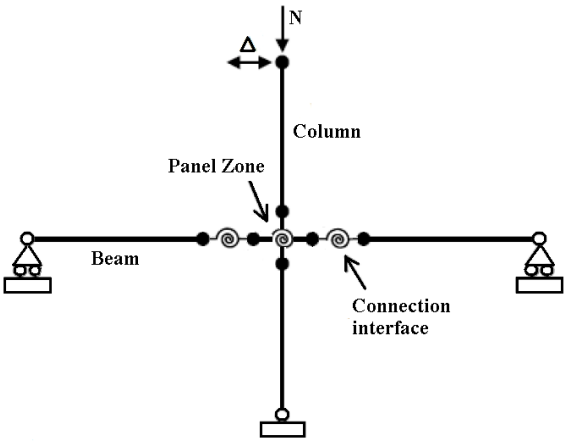

Figure 6-1 General post-tensioning frame modelling [Palermo et al., 2005b]

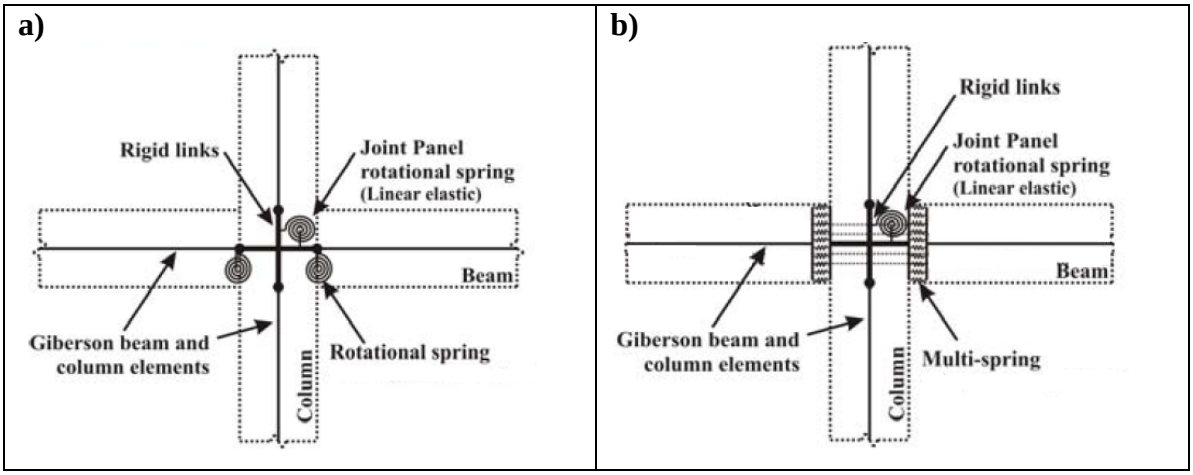

Figure 6-2 a) Rotational-spring modelling b) Multi-spring modelling [Newcombe, 2010d]

As mentioned, two approaches for modelling beam-column rocking interfaces are included; a) Rotational-spring (RS) and b) Multi-spring (MS). Both methods combined with elastic and inelastic hysteresis rules were used for comparing numerical models versus shake-table test results and quasi-static test results.

When using a spring for representing the connection interface, the moment-rotation curve needs to equal the moment-rotation curve of the rocking connection as indicated in Chapter five, Monolithic Beam Analogy [Pampanin *et al*., 2001] is used to predict the connection rocking behaviour. In the case of using multi-springs, they need to be calibrated to match the predicted response.

6.3 Calibration of connection rotation to non-linear elastic hysteresis rules

Once the moment-rotation curve that represents the beam-column rocking connection has been obtained analytically, the difficulty and accuracy of the representation/calibration of the elastic behaviour varies depending on the spring model used. In the case of using rotational-springs, a simple multi-linear hysteresis representation as shown in *Figure 6-3* can be used. Multi-linear hysteresis provides a good approximation (red-slashed line) of the original analytical curve as illustrated in *Figure 6-4* through *Figure 6-6* for the three different post-tensioning forces used during experimental testing.

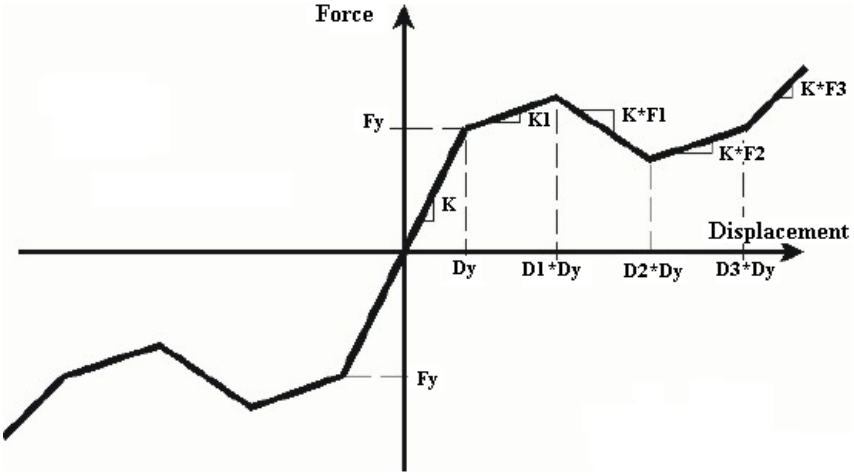

Figure 6-3 Multi-linear-elastic hysteresis rule

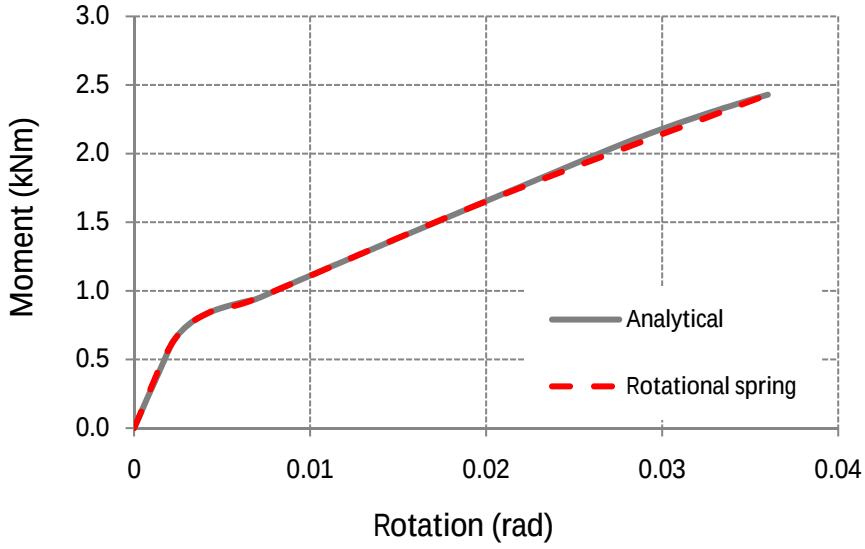

Figure 6-4 Non-linear elastic (NLE) rotational-spring calibration to analytical moment-rotation curve, post-tensioning force Pt =15kN

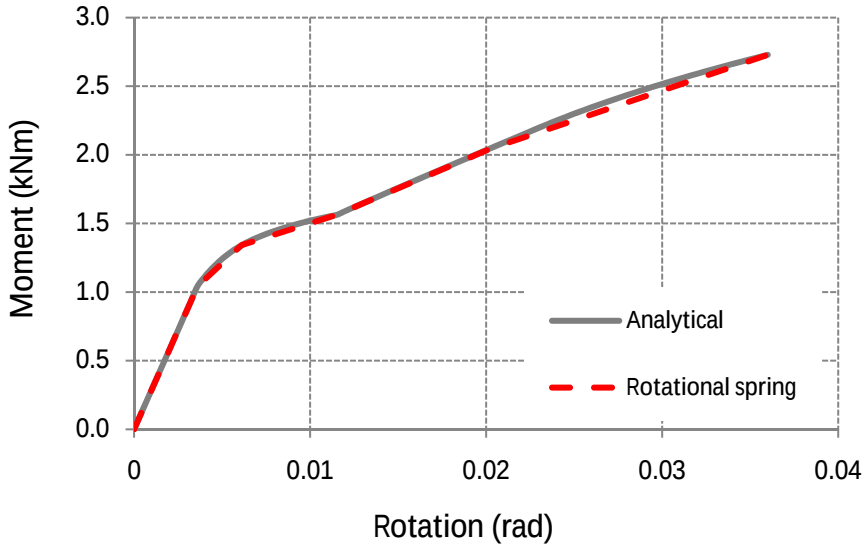

Figure 6-5 Non-linear elastic rotational-spring calibration to analytical moment-rotation curve, post-tensioning force Pt = 30kN

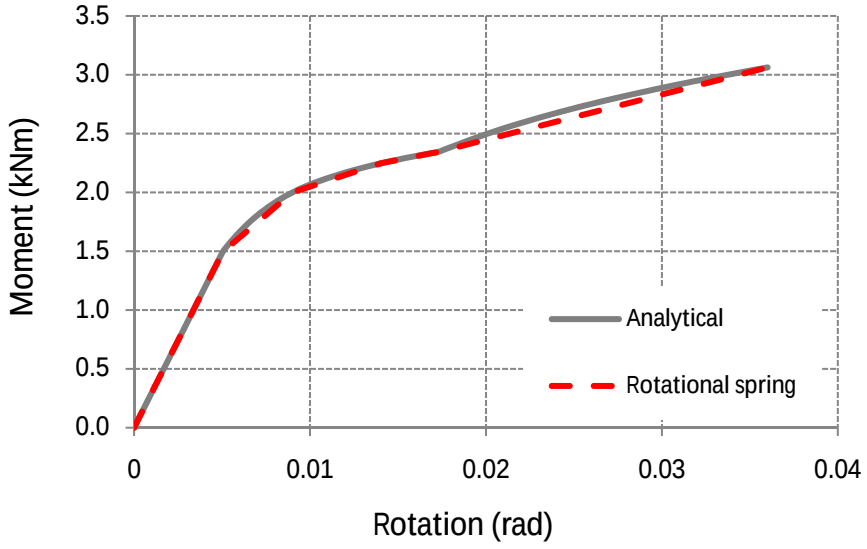

Figure 6-6 Non-linear elastic rotational-spring calibration to analytical moment-rotation curve, post-tensioning force Pt = 45kN

When using multi-springs, which in principle can provide a more details information on the interface rocking behaviour, the model requires calibration on the experimental or more refined numerical results. The main difficulty of the MS focuses on the estimation of the axial stiffness of the springs (*Equation 6-1*).

$$K_s = \frac{A_g \cdot E_{eff}}{L_s}$$ Equation 6-1

Where A_g the cross section area of the beam is, E_{eff} is the effective Young's modulus of the connection, and L_s is the length of the spring which is unknown. A trial and error method needs to be used in order to obtain admissible accuracy between the predicted moment-rotation curve and that obtained using a multi-spring element. The calibrated curves, for the three levels of post-tensioning forces included, are shown below (*Figure 6-7* to *Figure 6-9*). When using a multi-spring model for a post-tensioning force of 30kN (*Figure 6-8*) it can be observed that an over-estimation of the moment force occurs. This overestimation will have some consequences that will be highlighted when a quasi-static test is analysed.

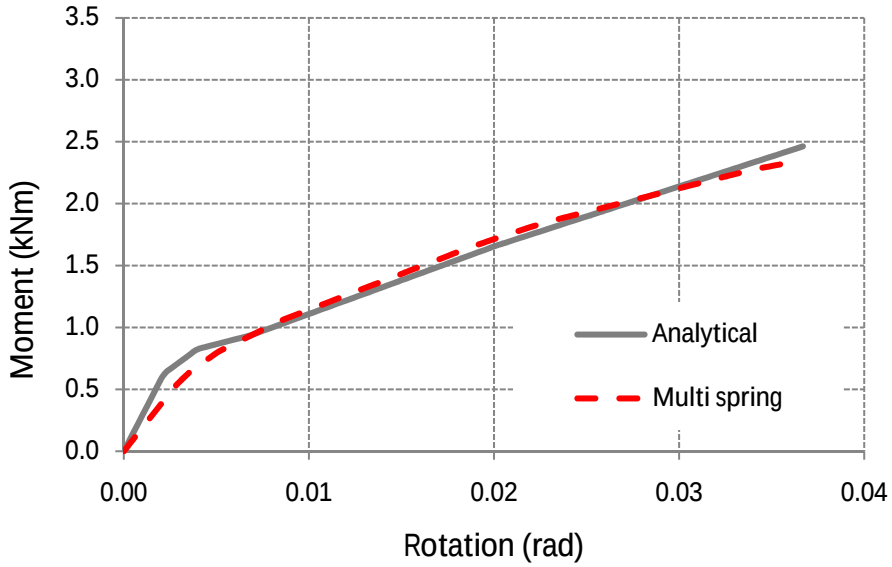

Figure 6-7 Multi-spring model (axial elastic springs) calibration to analytical moment-rotation curve, post-tensioning force Pt = 15kN

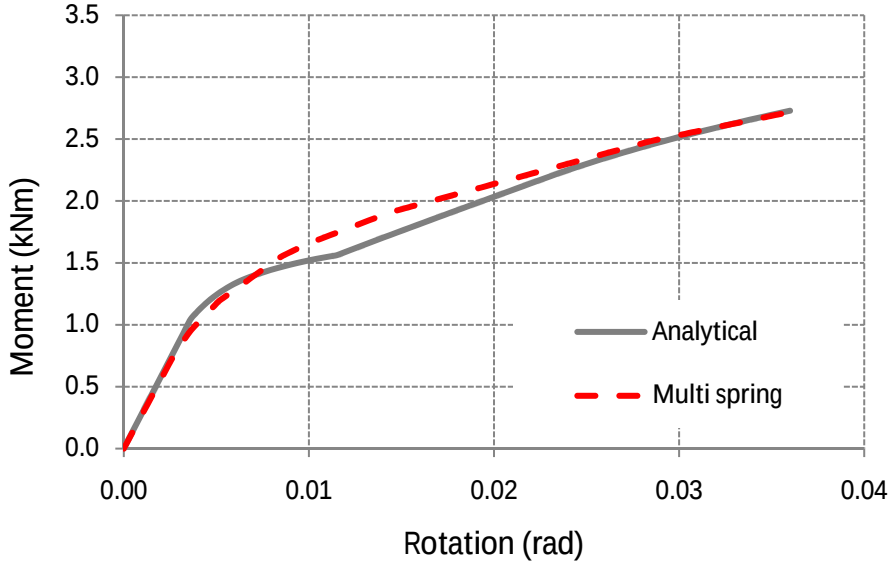

Figure 6-8 Multi-spring model (axial elastic spring) calibration to analytical moment-rotation curve, post-tensioning force Pt = 30kN

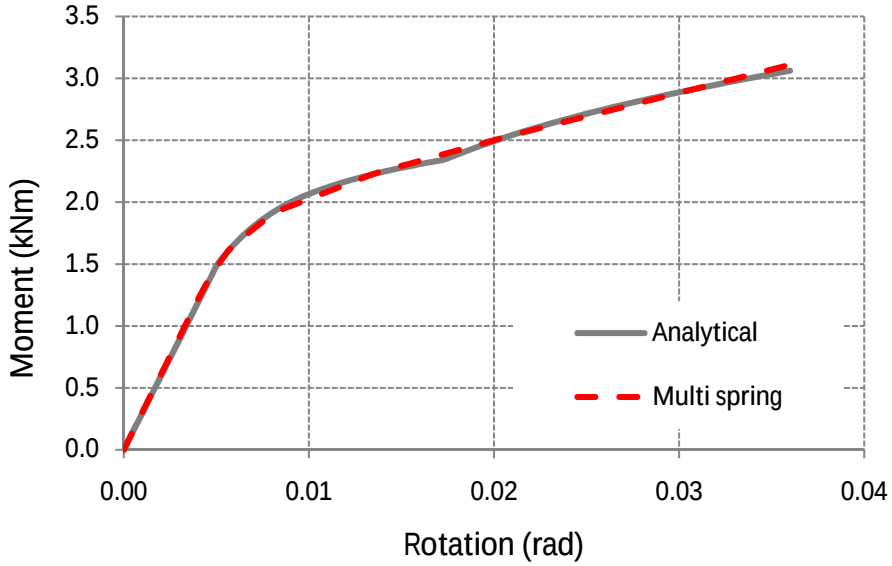

Figure 6-9 Multi-spring model (axial elastic springs) calibration to analytical moment-rotation curve, post-tensioning force Pt = 45kN

6.3.1 *Numerical models using non-linear elastic rotational-spring elements compared to quasi-static experimental tests*

Numerical models were developed using non-linear elastic rotational-spring elements for representing the moment-rotation relationship of the beam-column interface. The Moment-rotation curve was calibrated using a multi-linear elastic hysteresis loop. Numerical models were used in order to predict an envelope curve (applied force versus inter-storey drift) of the quasi-static tests presented in Chapter four. Results are shown in *Figure 6-10* through *Figure 6-12*. In general, a good agreement was achieved for the three tests presented below. It is possible to observe that initial stiffness was well predicted as well as the non-linear behaviour.

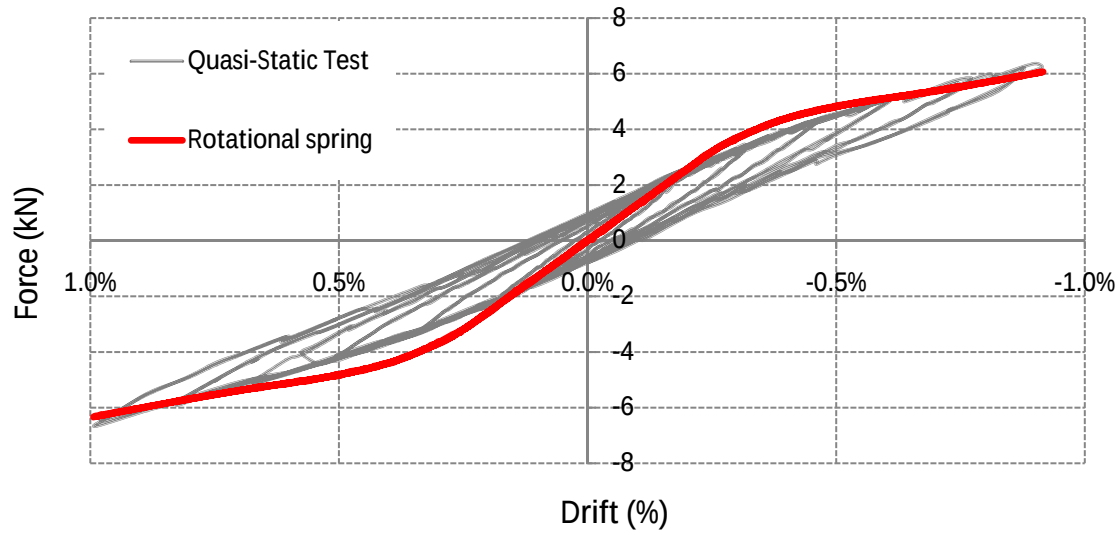

Figure 6-10 Quasi-static Test N°1 versus rotational-spring model using a multi-linear-elastic hysteresis rule

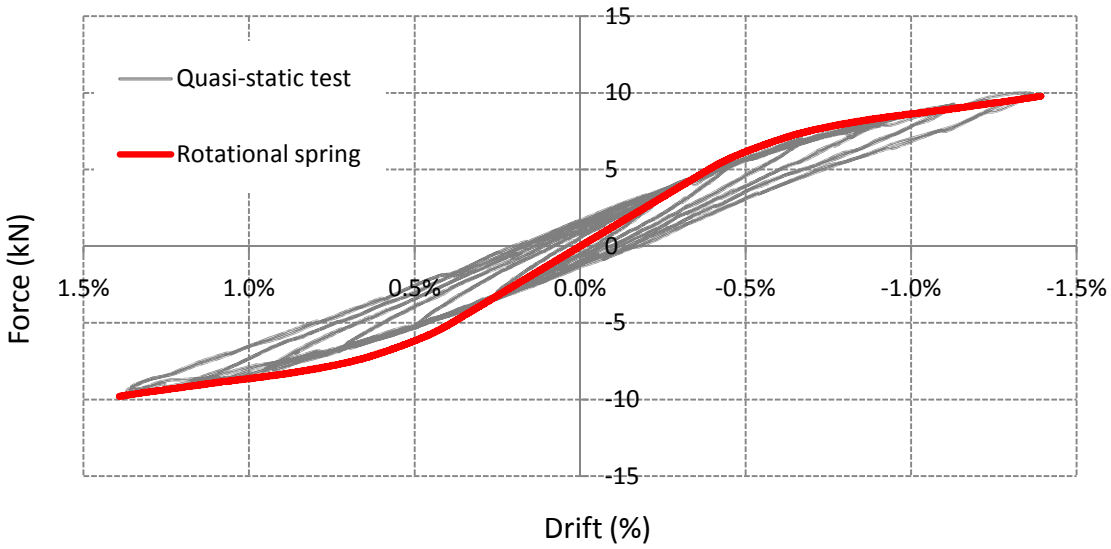

Figure 6-11 Quasi-static test N°2 versus rotational-spring model using a multi-linear-elastic hysteresis rule

In the case of Test N°3, corresponding to a post-tensioning force of 45kN per beam, it is possible to appreciate that after 2.5% drift the prediction curve over-estimates the required force applied and consequently, the stiffness. The reason is that the model building was designed to enter into the inelastic range at 2.5% of inter-storey drift, i.e. perpendicular crushing of the grain in the beam-column interface was expected to occur at this drift limit. As a consequence of timber crushing, an increase in post-tensioning losses occurred, and the lateral strength of the frame was smaller than expected. The non-linear elastic model used does not consider crushing of timber or loss of post-tensioning forces. To visualize the influence of the post-tensioning force over the lateral stiffness of the frame, an additional curve is added in *Figure 6-12*, this curve was obtained using the same model but with a post-tensioning force of 37kN, corresponding to the final post-tensioning force recorded on beams after completion of the test.

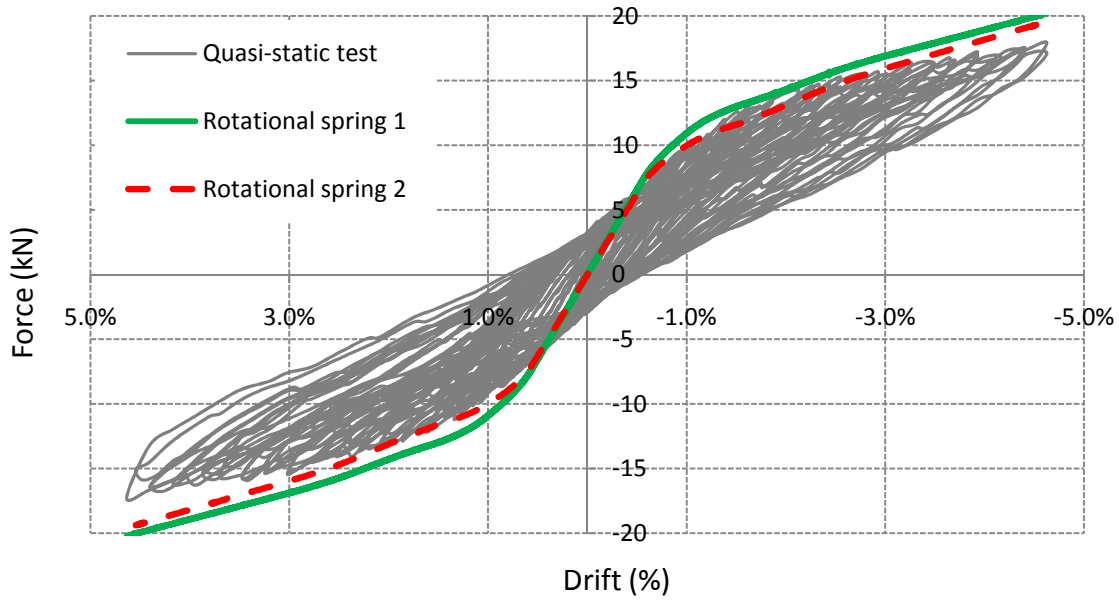

Figure 6-12 Quasi-static test N°3 versus rotational-spring model using a multi-linear-elastic hysteresis rule

6.3.2 *Numerical models using multi-spring elements compared to quasi-static experimental tests*

In the same way previously described for non-linear elastic rotational-springs, multi-springs with elastic behaviour were implemented in the numerical model to measure their accuracy predicting the frame response when it is subjected to a quasi-static test.
Obtained results are shown in *Figure 6-13* through *Figure 6-15*. Multi-spring models proved to be able to predict precisely the measured quasi-static behaviour. However, given that multi-spring models were more difficult to calibrate, an inaccurate calibration of the moment-rotation curvature of the joint (*Figure 6-8*) was reflected in the global behaviour. For Test Nº2 (*Figure 6-14*) the curve was slightly over-predicted by the model.

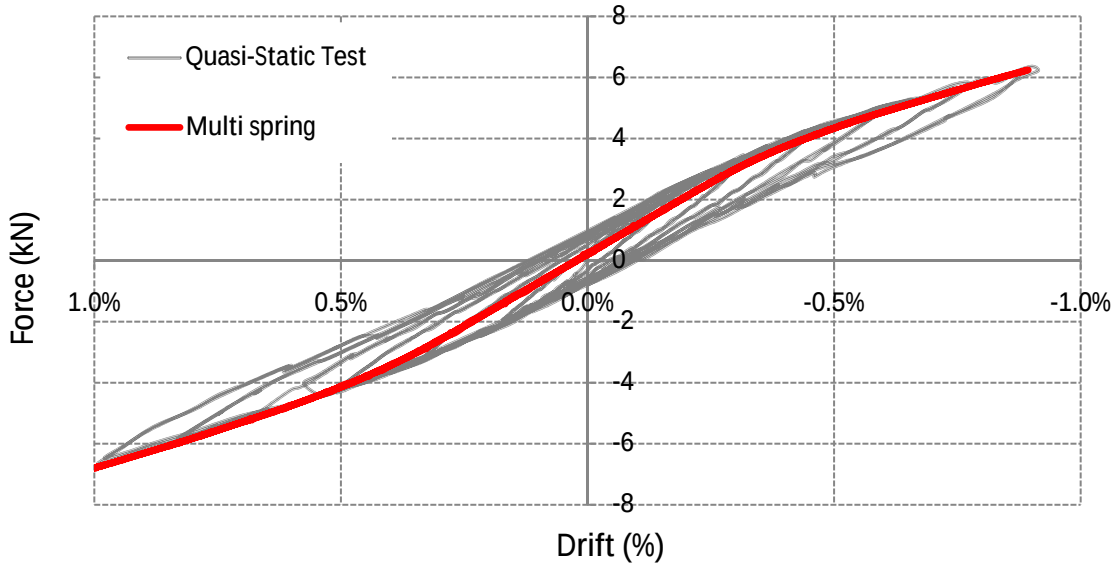

Figure 6-13 Quasi-static Test Nº1 versus multi-spring model using a multi-linear-elastic hysteresis rule

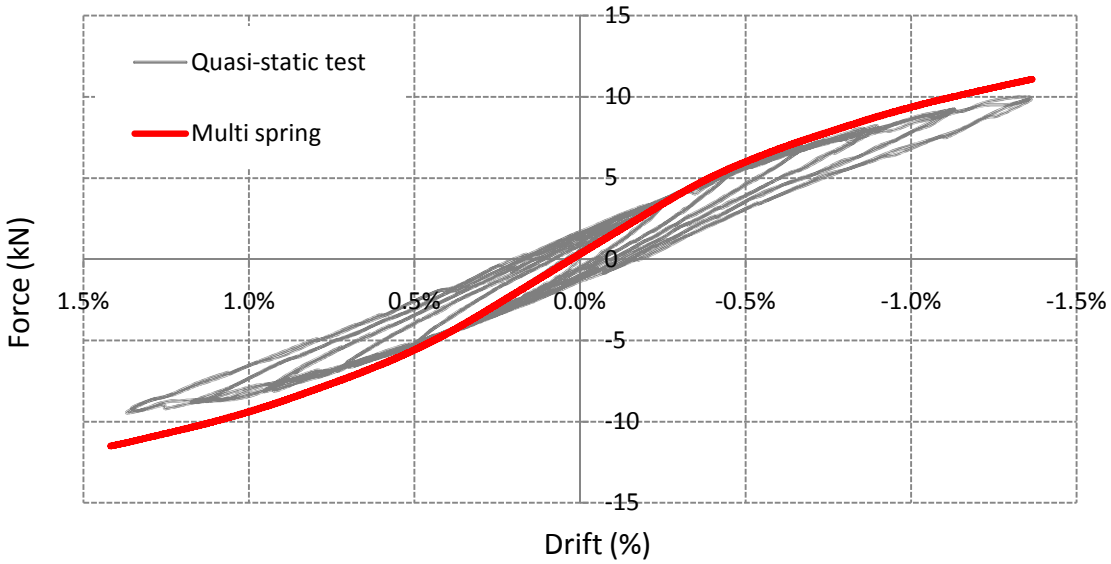

Figure 6-14 Quasi-static Test N°2 versus multi-spring model using a multi-linear-elastic hysteresis rule

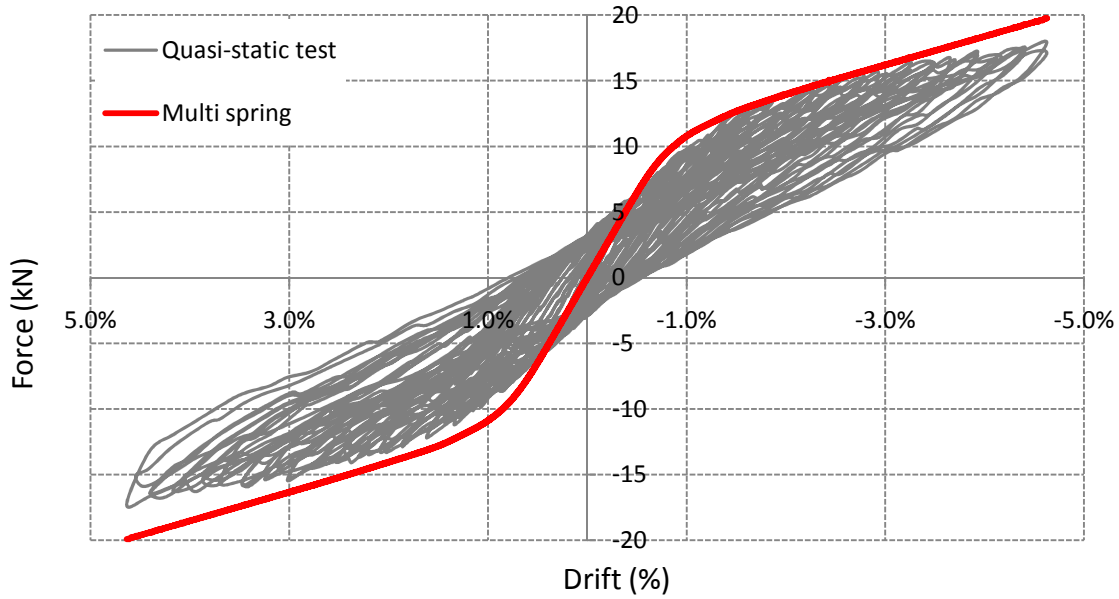

Figure 6-15 Quasi-static Test N°3 versus multi-spring model using a multi-linear-elastic hysteresis rule

6.3.3 *Numerical elastic models comparison to dynamic experimental tests*

In Chapter three equivalent viscous damping values were computed for the over 300 sinusoidal tests performed on the shake-table. It was shown that values obtained depend on the number of cycles used to compute them. This is because damping was proved to be mainly dependent on the drift level. Additionally, good agreement of values computed with one-decay cycle and values computed using area-based damping was shown giving enough proof to propose an equation to compute the equivalent viscous damping of post-tensioned timber frame buildings. To test the proposed formula, numerical models were developed and a constant equivalent viscous damping value was added in order to compare versus dynamic results obtained with shake-table tests. Equivalent viscous values were directly obtained from *Equation 4-2* selected at maximum expected drift level (already knew from dynamic tests).

Both rotational-spring models and multi-spring models using non-linear elastic hysteresis are able to sufficiently represent the building stiffness-drift relationship (e.g. tangent stiffness behaviour). Providing non-linear elastic-spring models with an equivalent viscous damping, which represents all the energy dissipated by the structure, will make possible a better prediction of the dynamic behaviour of post–tensioned timber buildings.

Nonlinear time-history analyses were performed on the five-storey and three-storey model buildings using RUAUMOKO [Carr, 2008]. The following analyses presented combine the use of non-linear elastic-spring models with a constant equivalent damping obtained from the proposed formula. During the time-history analysis tests, a Rayleigh damping model was used with a tangent-stiffness-proportional damping matrix.

Top floor displacement and top floor accelerations obtained during shake-table tests are compared with those obtained using numerical models. Time-history analyses, corresponding to the Cape Mendocino earthquake, performed for 5-storey model buildings are shown in *Figure 6-16* and *Figure 6-17*. In the same way, modelled dynamic comparison is performed for the 3-storey model building. The results confirmed that it is possible to model the dynamic response of post-tensioned timber frames with an acceptable level of accuracy using the equivalent damping values proposed.

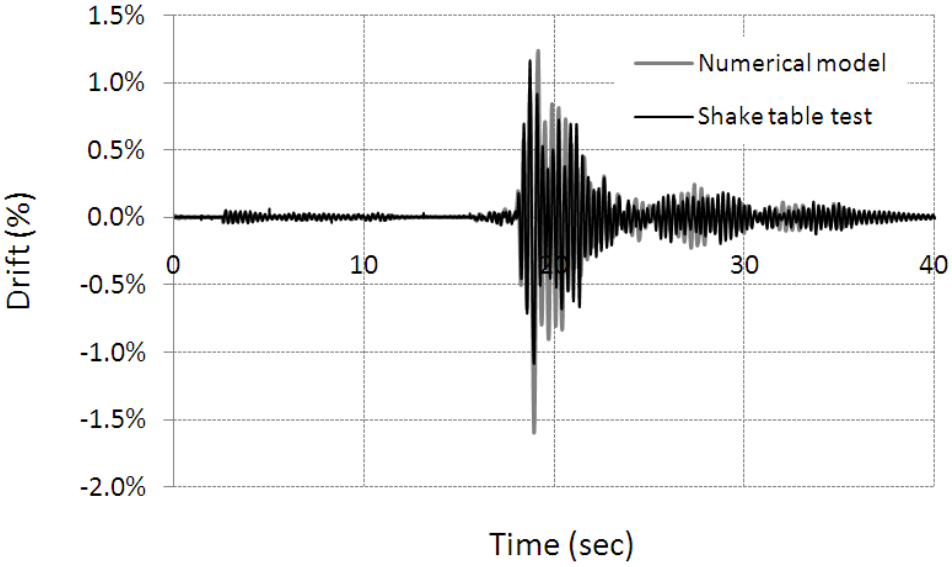

Figure 6-16 Top floor displacement for a 5-storey model building during Cape Mendocino earthquake. Shake-table test versus numerical model

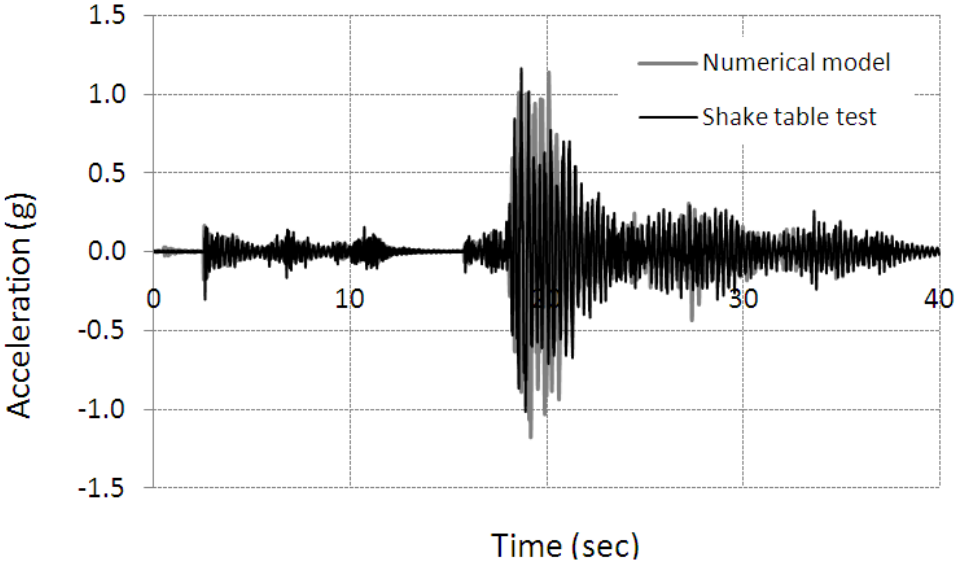

Figure 6-17 Top floor acceleration for a 3-storey model building during Cape Mendocino earthquake. Shake-table test versus numerical model

When analysing *Figure 6-18*, it is clear that the use of a constant equivalent viscous damping independent of the level of drift is not going to produce an exact match between both curves. This is because of damping being a function of drift level, however for design proposes where the maximum drift values are required, the numerical model supplied with the equivalent viscous damping is able to predict accurately maximum displacements and maximum floor accelerations (*Figure 6-19*).

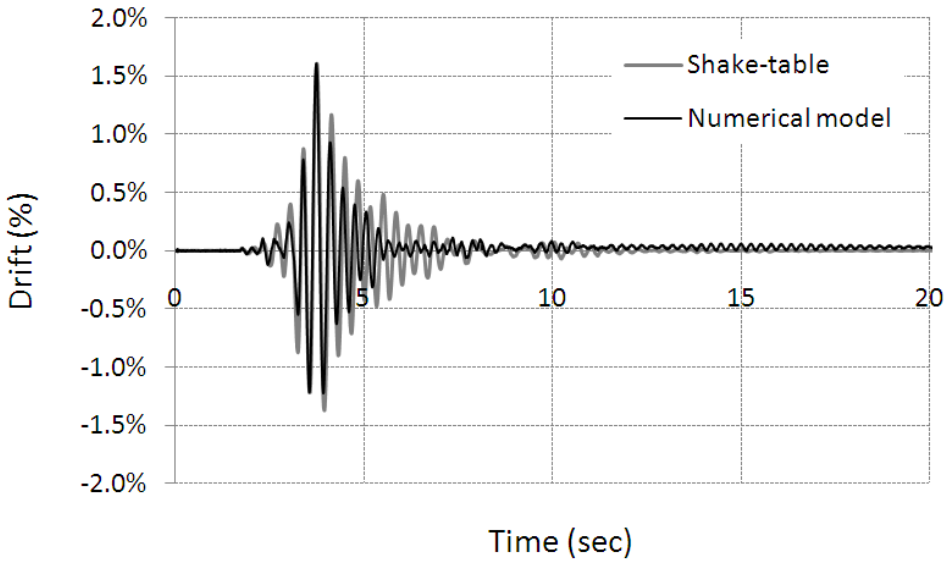

Figure 6-18 Top floor displacement for a 3-storey model building during Parkfield earthquake. Shake-table test versus numerical model

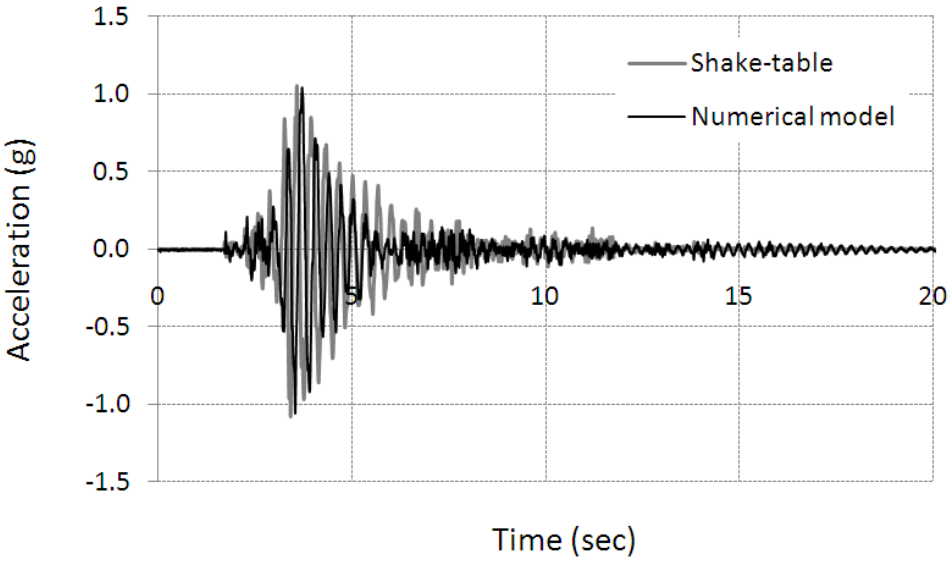

Figure 6-19 Top floor acceleration for a 3-storey model building during Parkfield earthquake. Shake-table test versus numerical model

Time-history analyses were performed using non-linear elastic rotational-springs and multi-springs, incorporating a constant equivalent viscous damping (computed at maximum drift level expected). The following graphs show the main results, floor displacements and floor accelerations, obtained for each one of the seismic records performed. As indicated, results of modelling using the equivalent viscous damping proposed are conservative, in particular regarding displacements. 5-storey results are shown from *Figure 6-20* to *Figure 6-24*, and 3-storey results are shown from *Figure 6-25* to *Figure 6-31*.

Legend description for the comparison of non-linear elastic numerical models (plus added damping) to dynamic tests for the figures below

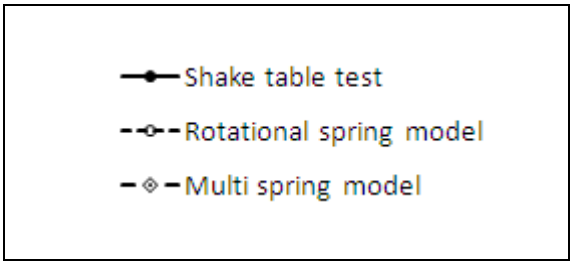

i. 5-Storey tests:

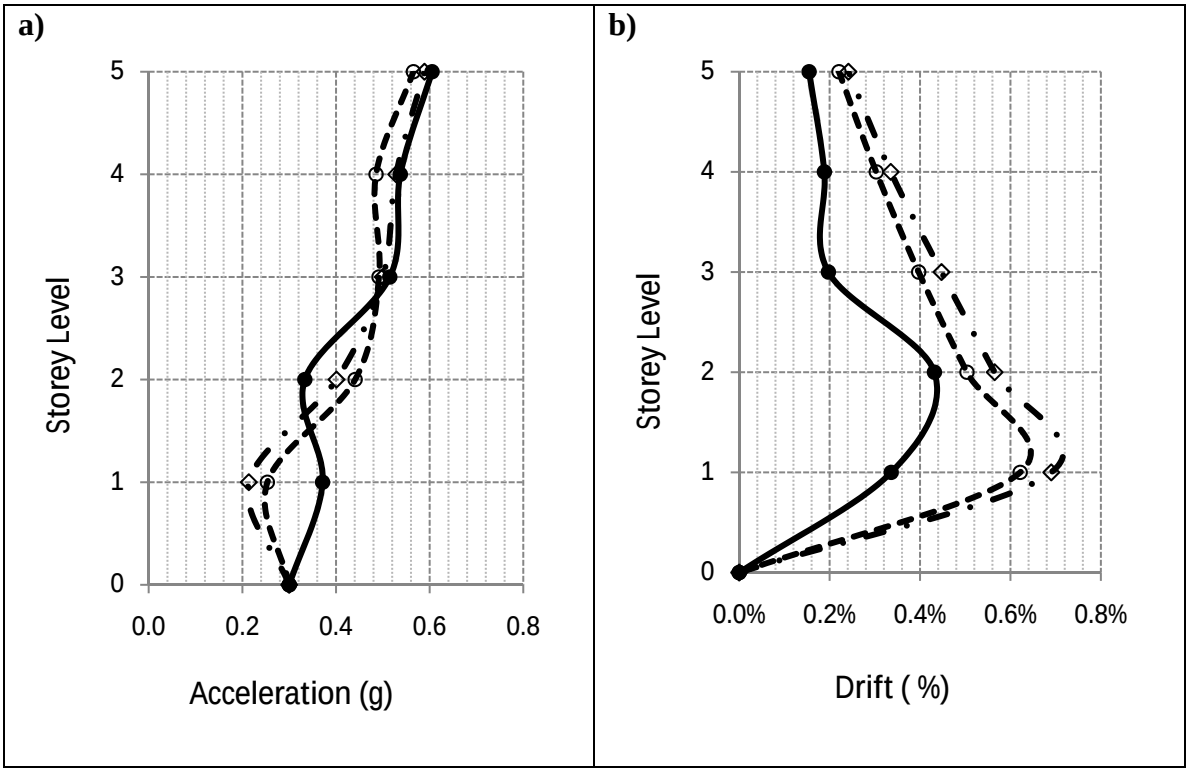

Figure 6-20 Shake-table test versus numerical elastic models, Loma Prieta Earthquake, 5-storey building: a) Floor accelerations b) Inter-storey drift

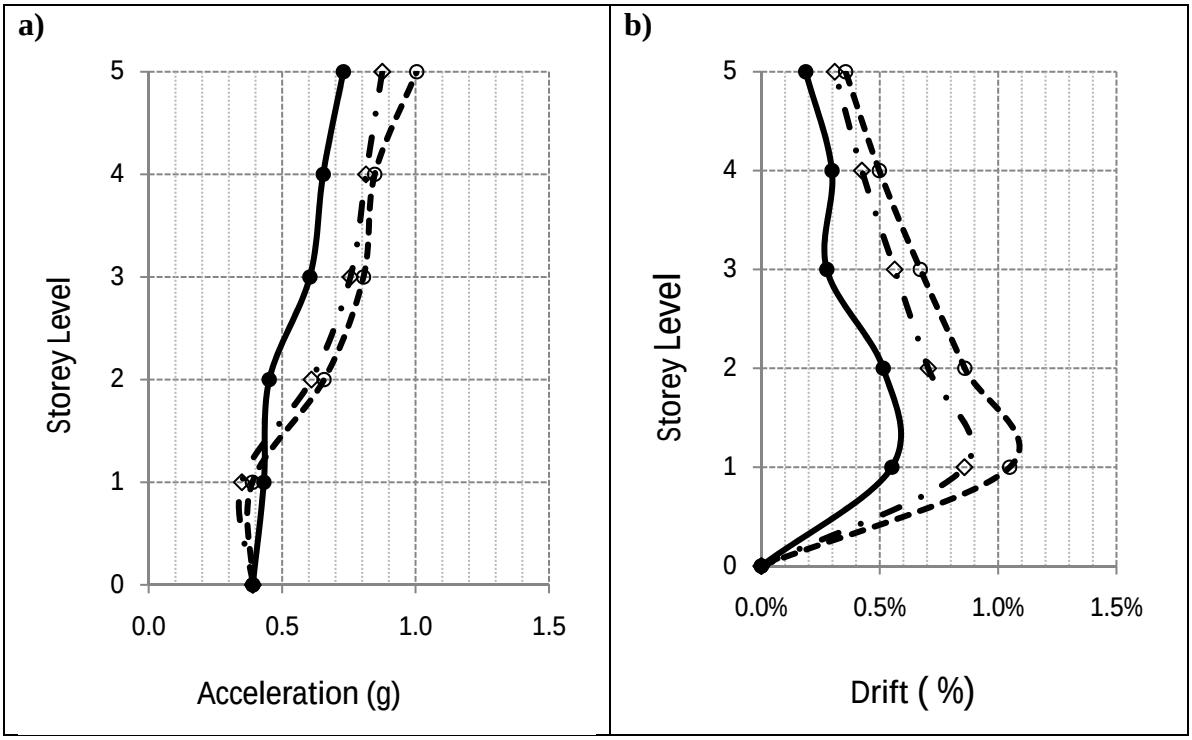

Figure 6-21 Shake-table test versus numerical elastic models, Kobe Earthquake, 5-storey building: a) Floor accelerations b) Inter-storey drift

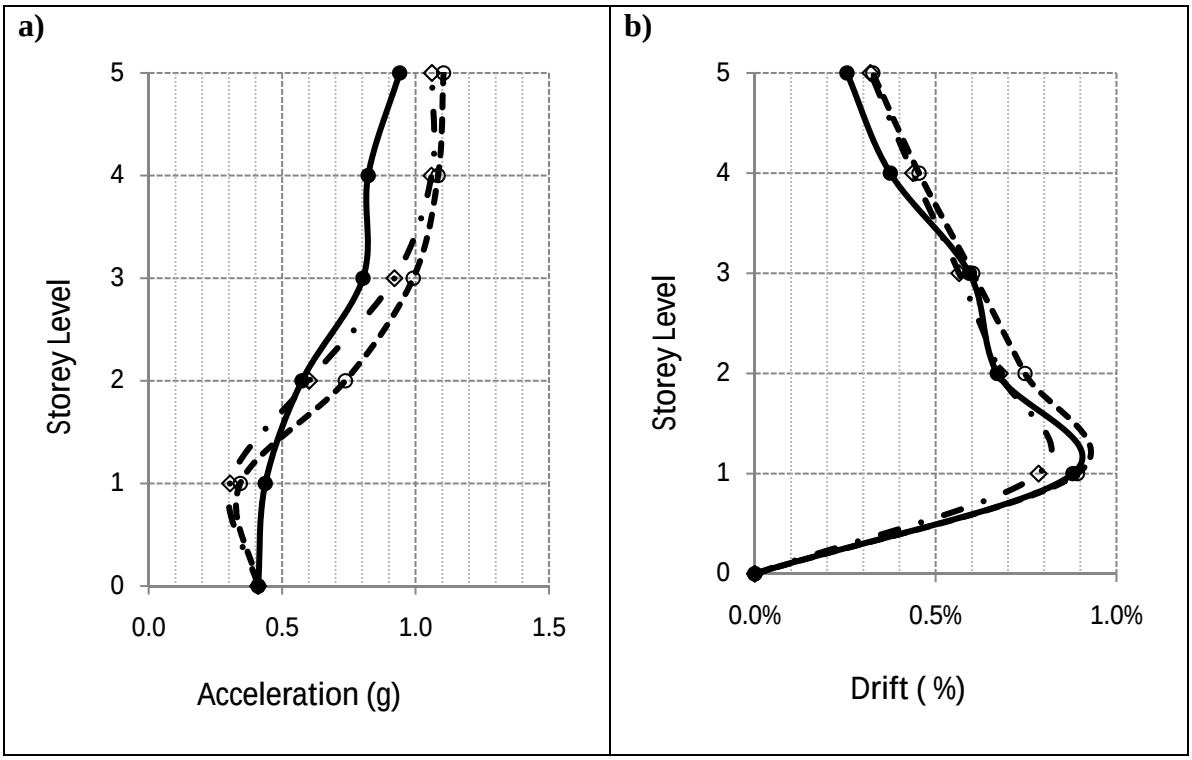

Figure 6-22 Shake-table test versus numerical elastic models, Northridge Earthquake, 5-storey building: a) Floor accelerations b) Inter-storey drift

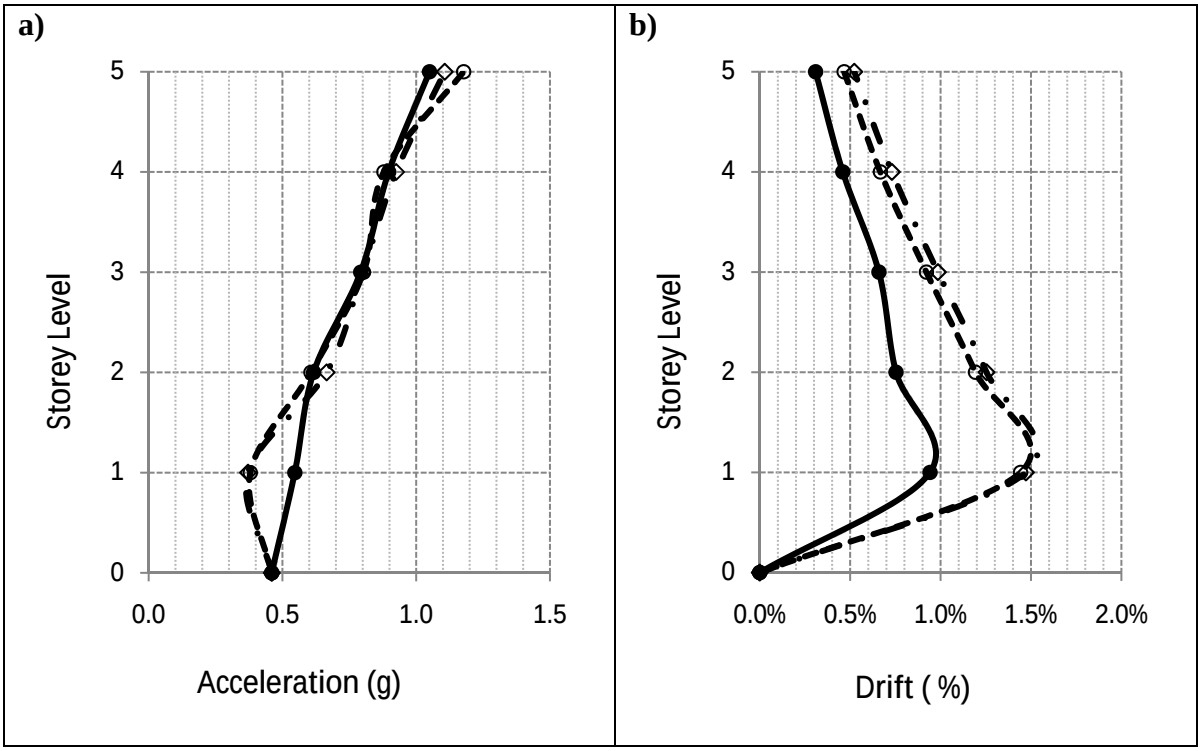

Figure 6-23 Shake-table test versus numerical elastic models, Cape Mendocino Earthquake, 5-storey building: a) Floor accelerations b) Inter-storey drift

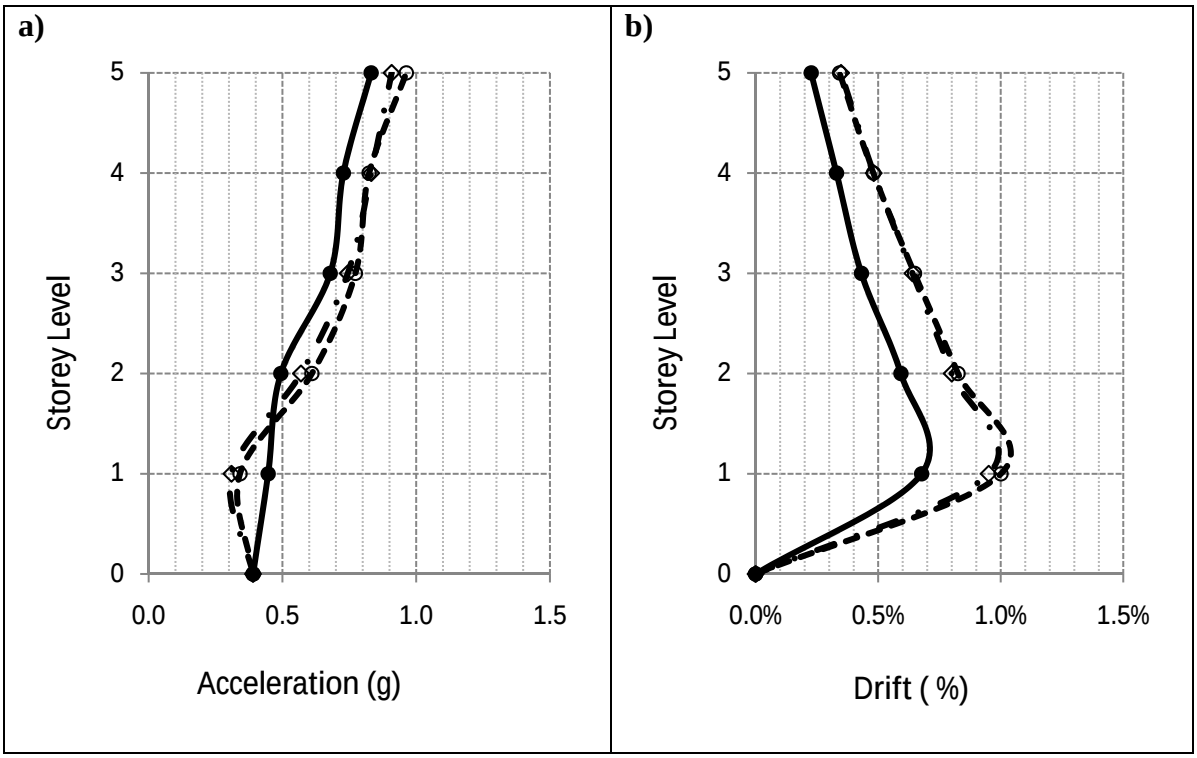

Figure 6-24 Shake-table test versus numerical elastic models, average of all seismic tests performed on the 5-storey model building: a) Floor accelerations b) Inter-storey drift

ii. 3-Storey tests:

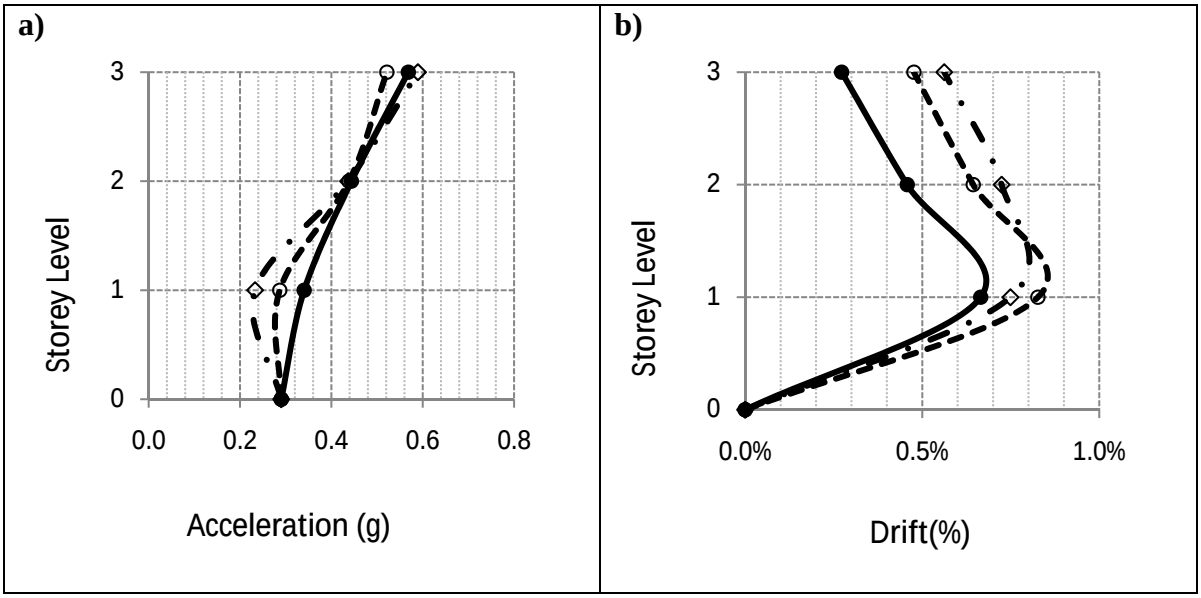

Figure 6-25 Shake-table test versus numerical elastic models, Loma Prieta Earthquake, 3-storey building: a) Floor accelerations b) Inter-storey drift

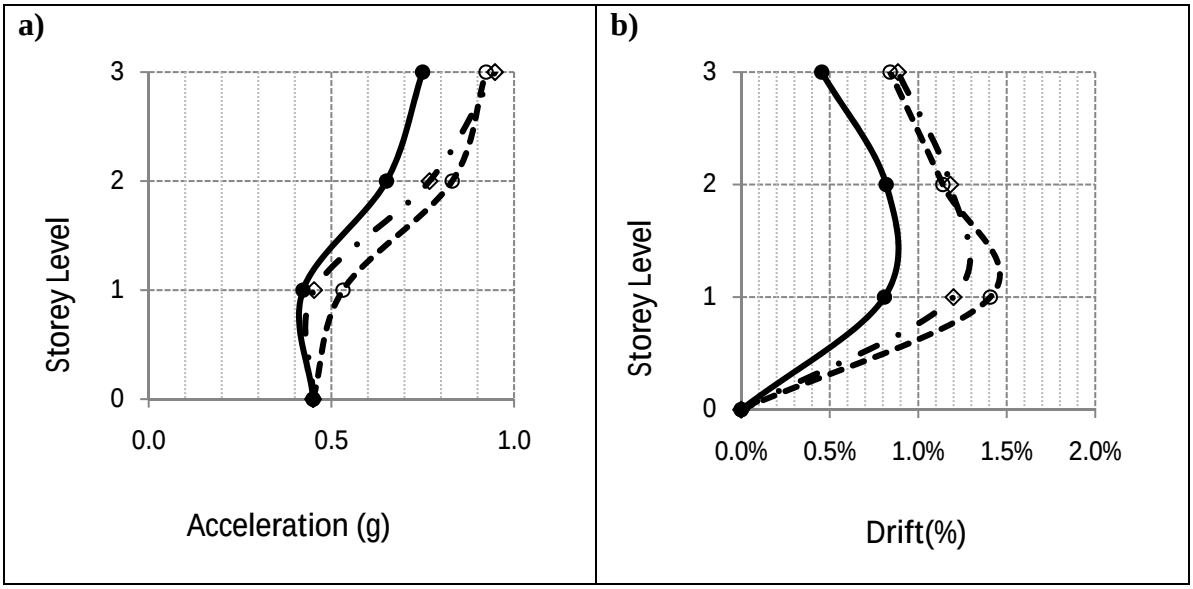

Figure 6-26 Shake-table test versus numerical elastic models, Kobe Earthquake, 3-storey building: a) Floor accelerations b) Inter-storey drift

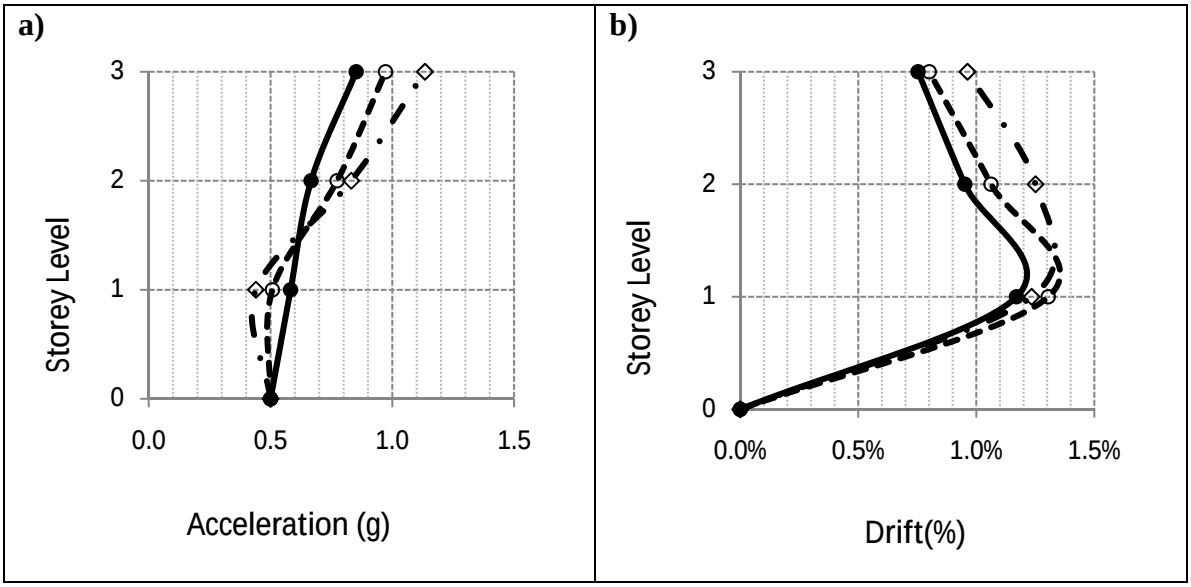

Figure 6-27 Shake-table test versus numerical elastic models, Northridge Earthquake, 3-storey building: a) Floor accelerations b) Inter-storey drift

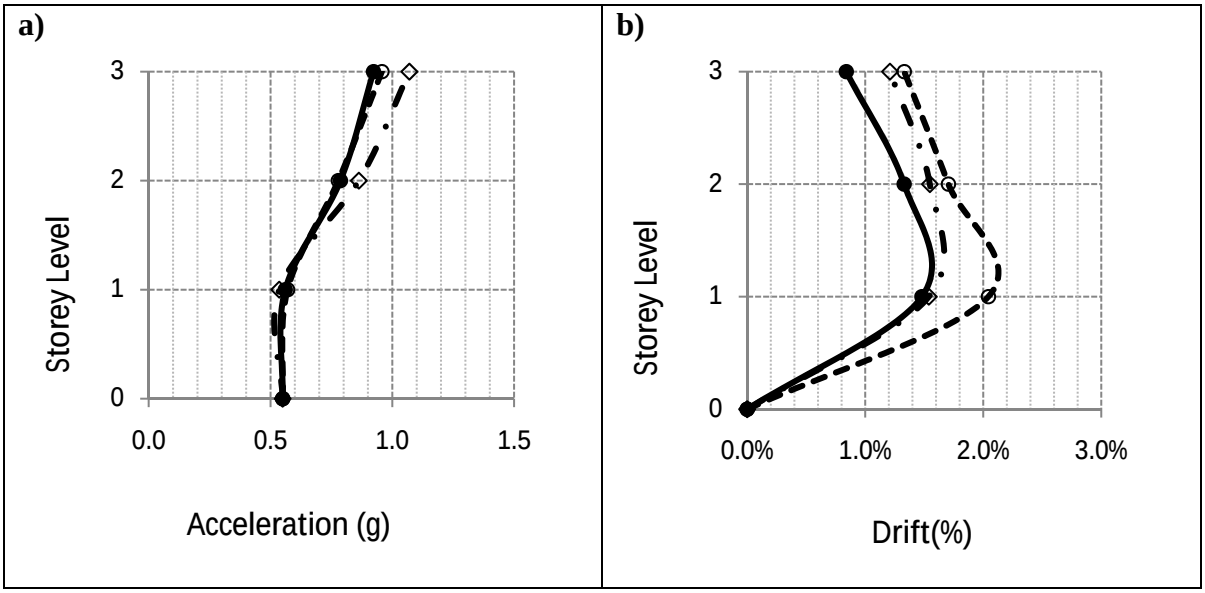

Figure 6-28 Shake-table test versus numerical elastic models, Cape Mendocino Earthquake, 3-storey building: a) Floor accelerations b) Inter-storey drift

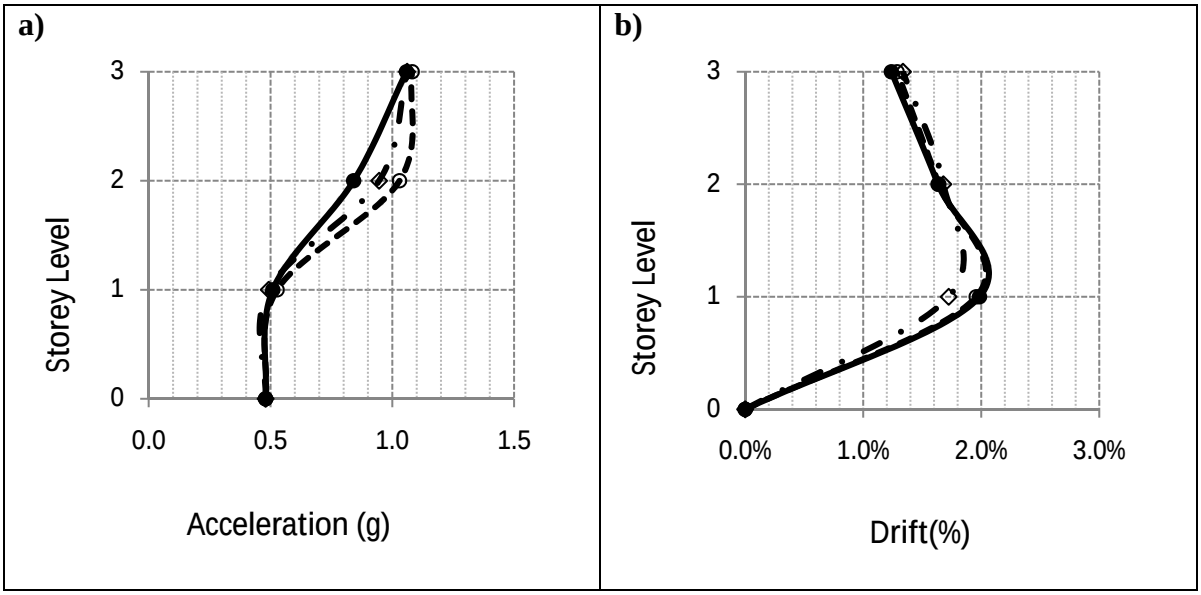

Figure 6-29 Shake-table test versus numerical elastic models, Parkfield Earthquake, 3-storey building: a) Floor accelerations b) Inter-storey drift

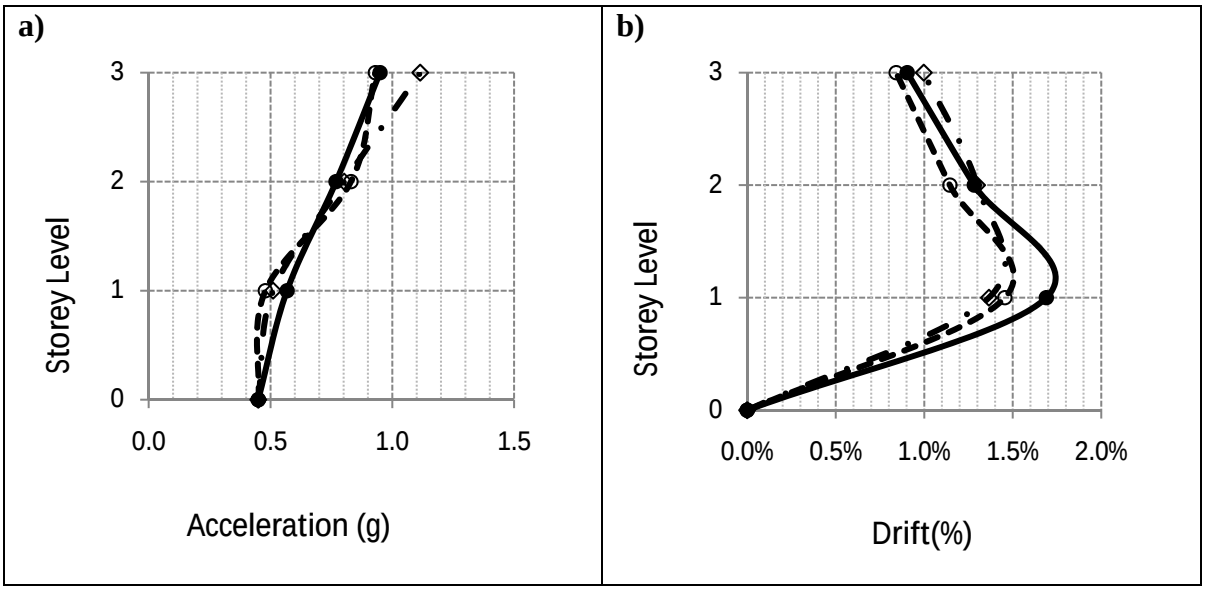

Figure 6-30 Shake-table test versus numerical elastic models, Sylmar Earthquake, 3-storey building: a) Floor accelerations b) Inter-storey drift

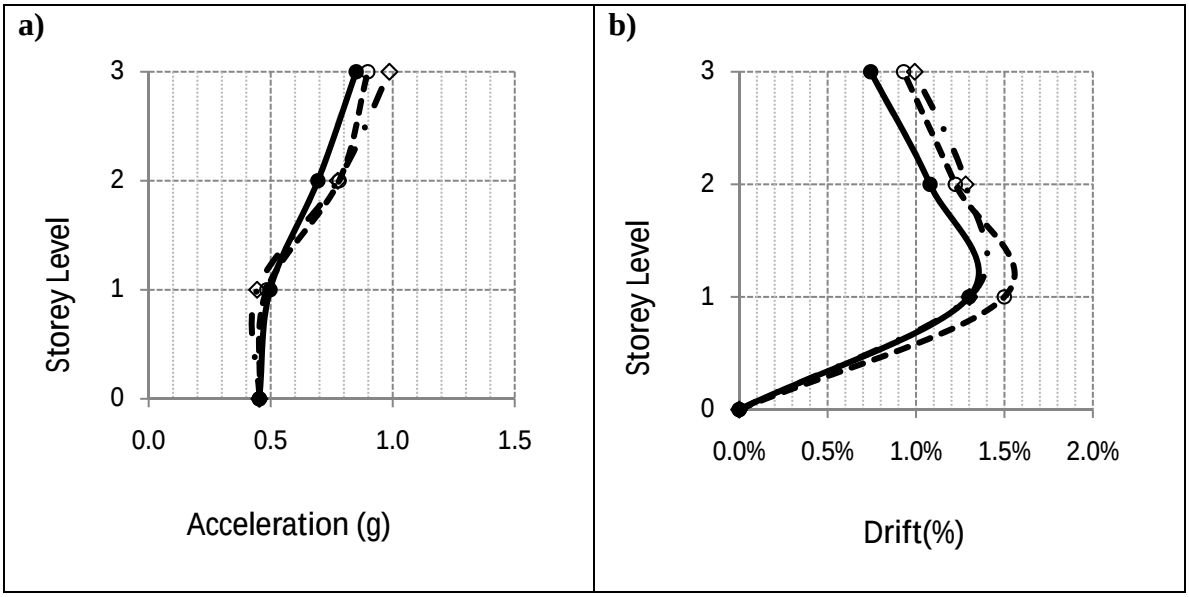

Figure 6-31 Shake-table test versus numerical elastic models, average of all seismic tests performed to the 3-storey model building: a) Floor accelerations b) Inter-storey drift

6.4 Calibration of model buildings force-drift cycle to bi-linear hysteresis rule

Another simple method for modelling the seismic response is described here. This method consists of the calibration of the spring models, considering a bi-linear inelastic hysteresis rule, (*Figure 6-32*) in order to more accurately match the cyclic behaviour obtained during quasi-static testing.
It is worth noting that a more appropriate hysteresis loop would be represented by a flag-shape hysteresis including the same amount of hysteretic damping observed in the experimental tests. However, in order to simplify the modelling process and allow for the use of standard hysteresis loop available to practicing engineers in any commercial software a bilinear (or elasto-plastic with hardening) hysteresis has been selected for this exercise.

The idea is to assess the numerical model accuracy when the same amount of energy dissipated during quasi-static tests is included in a dynamic model. In other words, since it was shown that most of the energy dissipated by post-tensioned timber frames is hysteretic, the connections are supplied with non-linear behaviour in order to create the hysteresis. Therefore, all the dissipation of energy is concentrated in the non-linear behaviour of the modelled connections.

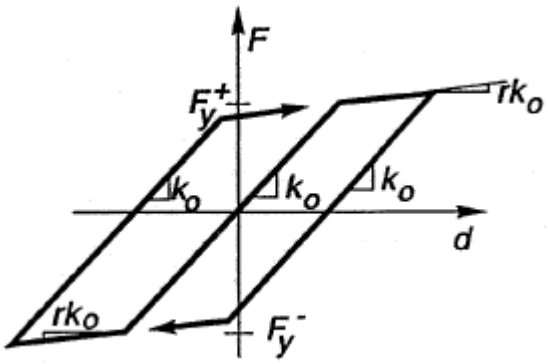

Figure 6-32 Bi-linear inelastic hysteresis rule

6.4.1 *Numerical models using inelastic-rotational-springs compared to quasi-static experimental tests*

The calibration of the rotational-springs, using a bi-linear inelastic hysteretic rule, to match quasi-static tests was a tedious and highly time-consuming process. Moreover, the obtained force-drift curve was possible to be calibrated only for a specific drift. The numerical models were calibrated to match the envelope of the force-drift cycles; therefore, initial stiffness and internal loops did not represent in a proper manner the experimental results.

Calibrations for the three quasi-static tests are presented below (*Figures 6-33, 6-34 and 6-35*). *Figure 6-34* shows the calibration for the second test. An internal loop is included in order to illustrate that even when at a certain level of drift the model is calibrated, at smaller or greater drift levels, the model does not provide good results. In this particular case, stiffness seems to be appropriate, but the dissipated energy is not. Hence, when the calibration is done for a certain level of drift, the loops at lower drift levels have inaccurate values of stiffness and energy dissipation.

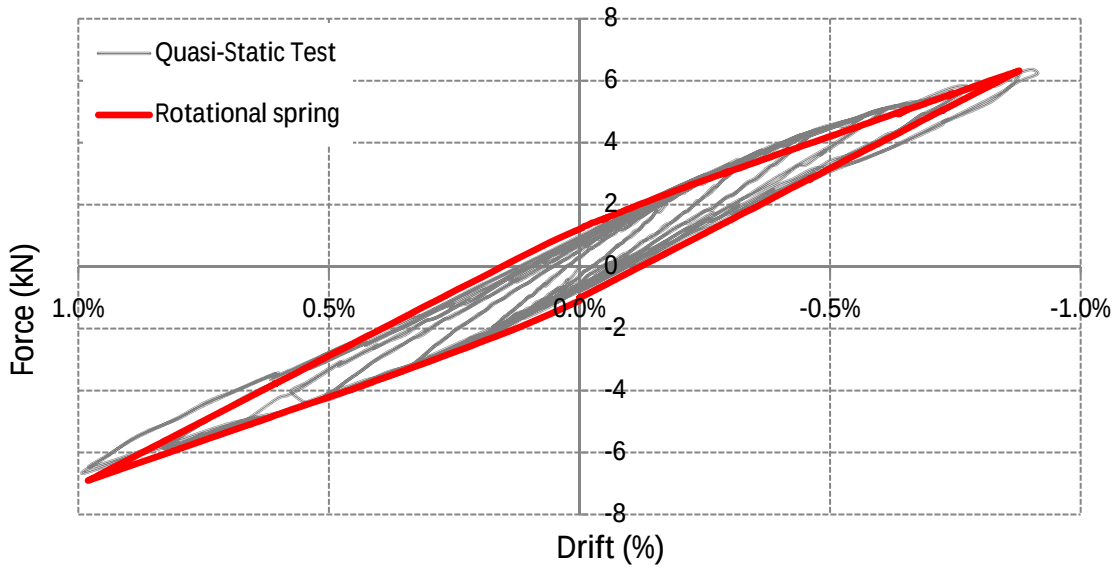

Figure 6-33 Quasi-static Test N°1 versus rotational-spring model using a bilinear inelastic hysteresis rule

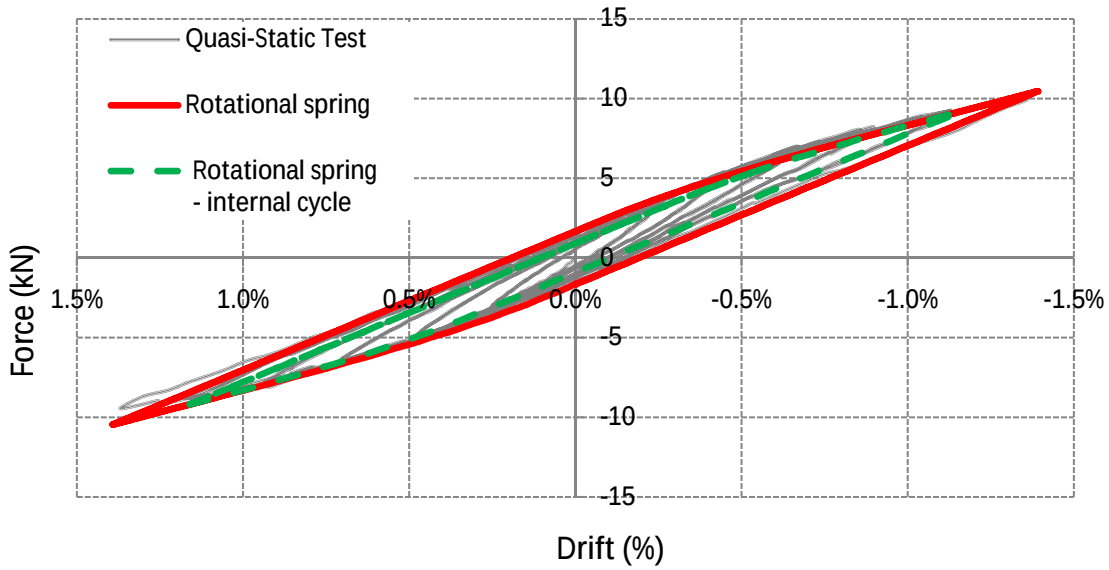

Figure 6-34 Quasi-static Test N°2 versus rotational-spring model using a bilinear inelastic hysteresis rule

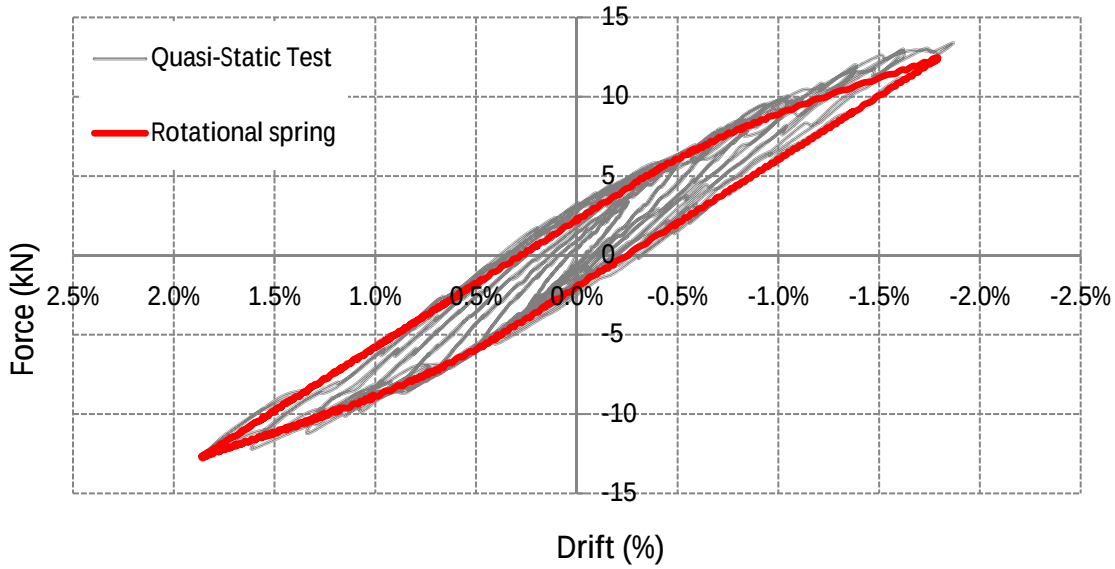

Figure 6-35 Quasi-static Test N°3 versus rotational-spring model using a bilinear inelastic hysteresis rule

6.4.2 *Numerical models using inelastic-multi-spring comparison to quasi-static experimental tests*

The previous calibration exercise was also performed using an inelastic-multi-spring model combined with a bi-linear hysteretic rule (*Figures 6-36, 6-37 and 6-38*). In this case, calibration was even more difficult than using inelastic-rotational-springs and more time consuming. Similar to previous results, the calibrated model was only effective for a specific selected drift level and in this case internal loops were even less accurate (*Figure 6-37*). Thus, energy dissipated, for smaller drifts than those targeted during calibration, was less than the test data, producing over-predictions of the dynamic response.

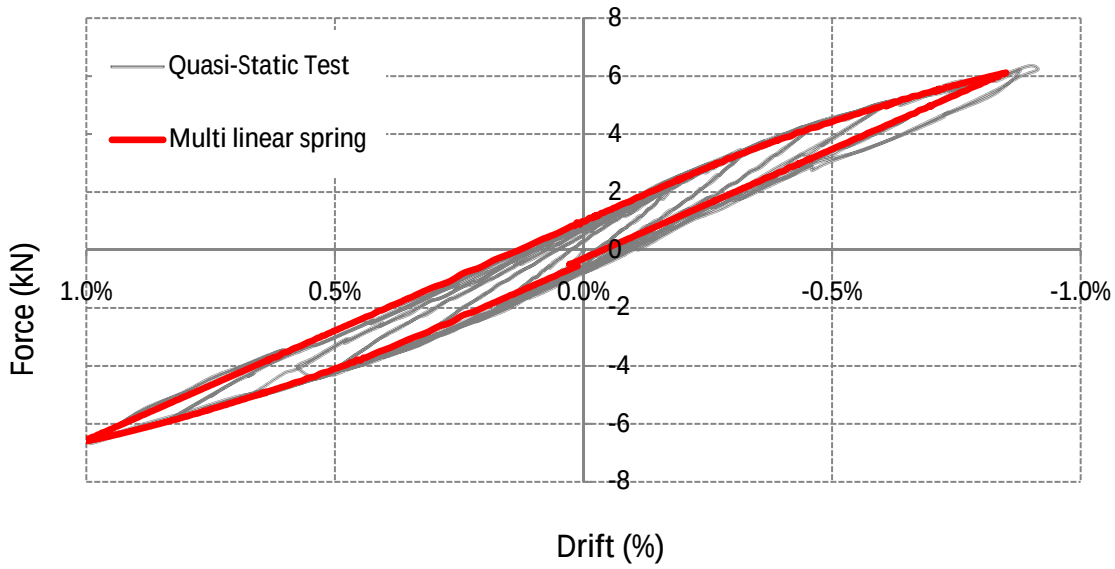

Figure 6-36 Quasi-static Test N°1 versus multi-spring model using a bilinear inelastic hysteresis rule

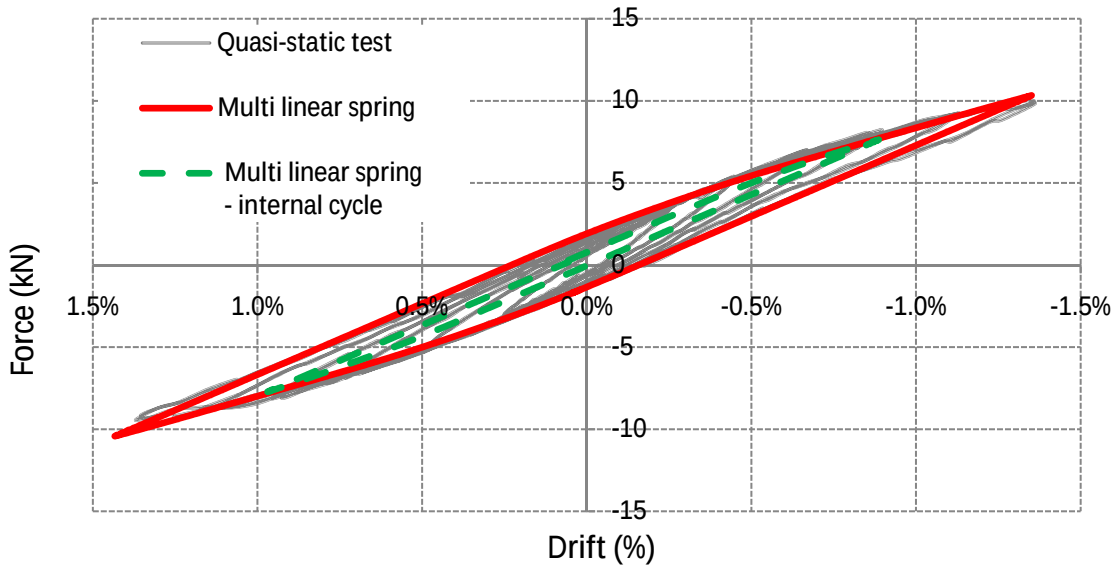

Figure 6-37 Quasi-static Test N°2 versus multi-spring model using a bilinear inelastic hysteresis rule

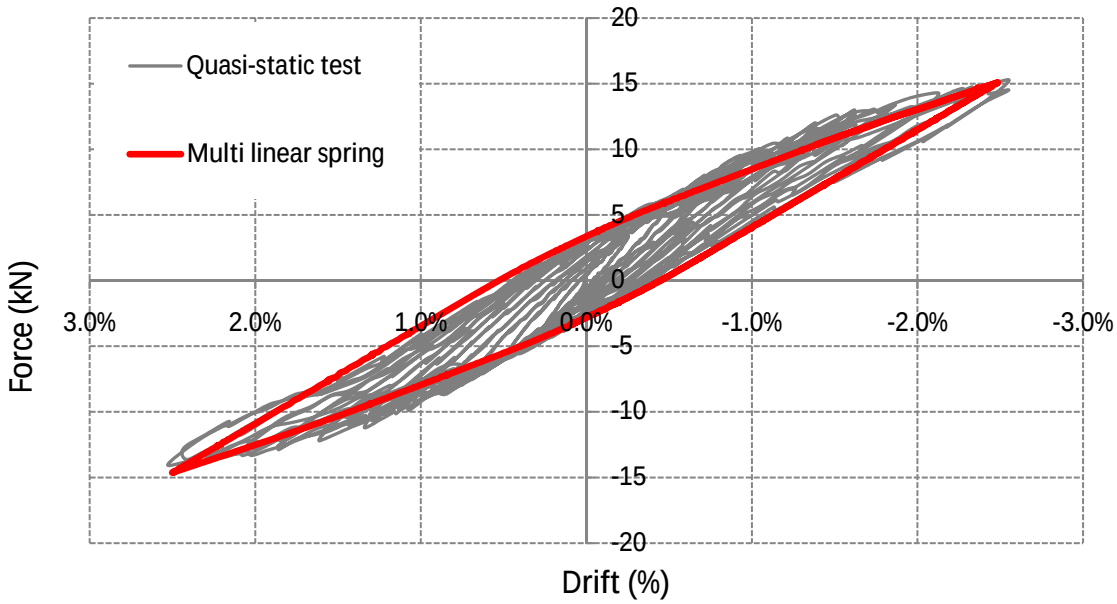

Figure 6-38 Quasi-static Test N°3 versus multi-spring model using a bilinear inelastic hysteresis rule

6.4.3 *Numerical inelastic model comparisons with dynamic experimental tests*

Inelastic spring models can be properly calibrated for a particular drift value, but it seems to be inaccurate for drift levels different than those targeted. The following results compare earthquake tests that reached 1% drift, versus numerical models calibrated for that specific drift level.

In spite of the complexity of the model, difficult calibration and the fact that the model could only be calibrated for a particular drift level, the results obtained were still less accurate than results obtained using a simple elastic-spring model plus an equivalent viscous damping. The comparisons of the values obtained using the three mentioned numerical model are included below. 3-storey results are shown from *Figure 6-39 to Figure 6-41*. 5-storey test comparison is not included considering that the level of accuracy obtained is similar to the 3-storey results.

Legend description for the comparison of inelastic numerical models with dynamic tests.

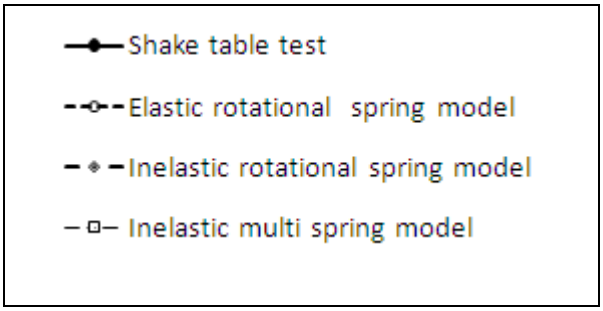

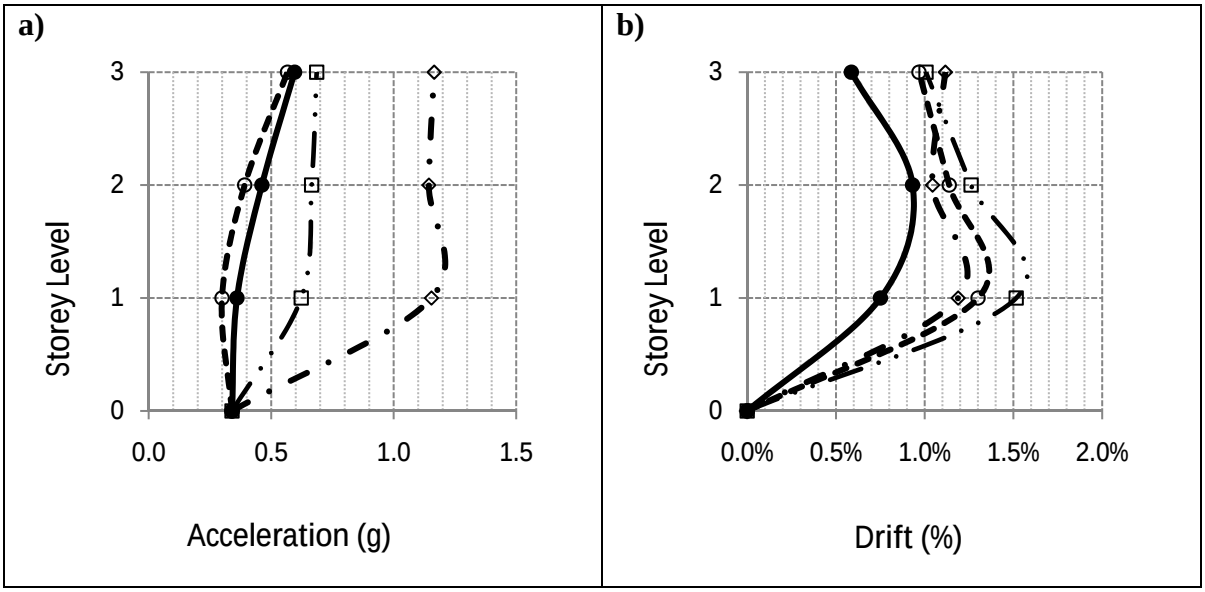

Figure 6-39 Shake-table test versus numerical inelastic models, Loma Prieta Earthquake, 3-storey building: a) Floor accelerations b) Inter-storey drifts

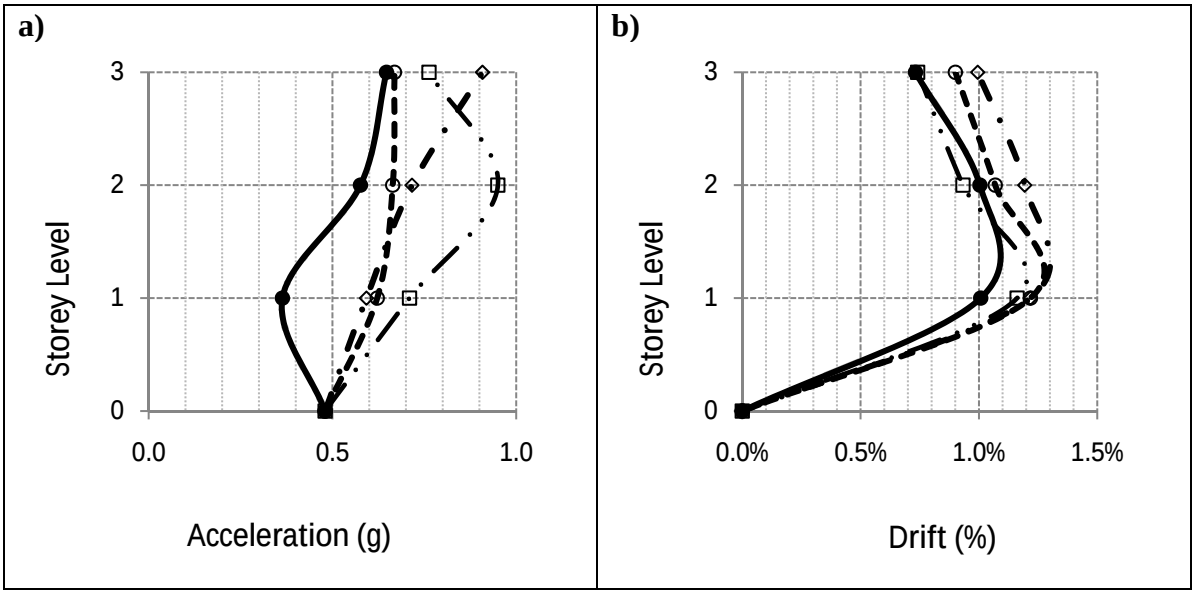

Figure 6-40 Shake-table test versus numerical inelastic models, Kobe Earthquake, 3-storey building: a) Floor accelerations b) Inter-storey drifts

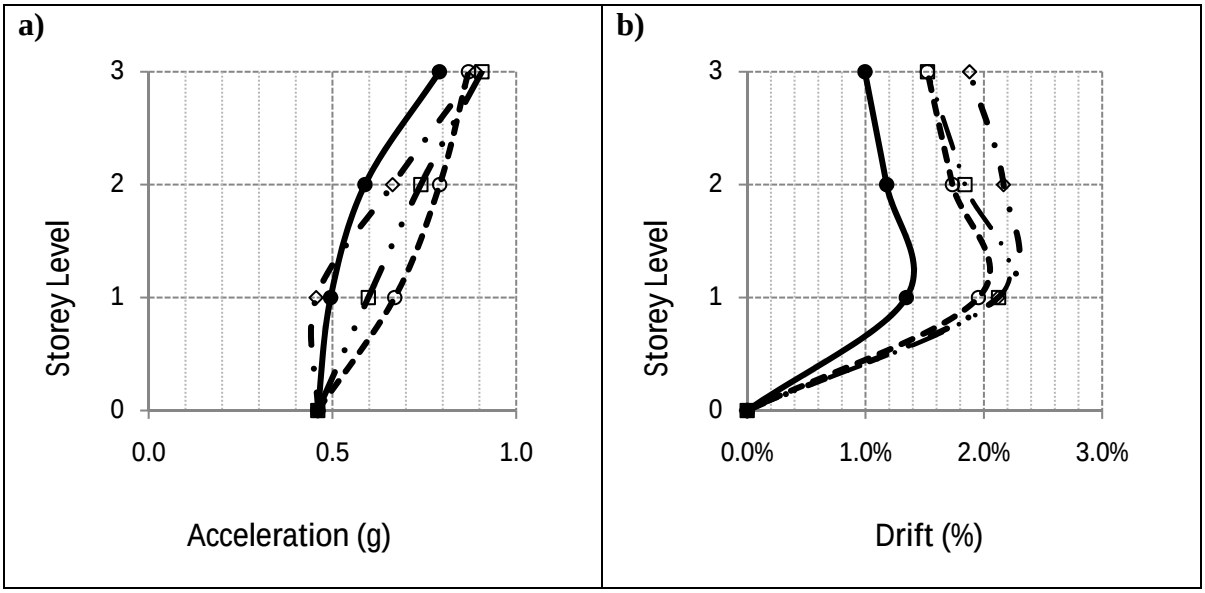

Figure 6-41 Shake-table test versus numerical inelastic models, Sylmar Earthquake, 3-storey building: a) Floor accelerations b) Inter-storey drifts

6.5 Conclusions

- The non-linear elastic rotational-spring or multi-spring (axial elastic springs) models are able to accurately predict initial stiffness and envelope of force-displacement curves obtained during quasi-static tests.

- Such rotational-spring and multi-spring models complemented with an equivalent viscous damping value, proposed in Chapter three, provided a good estimation of the dynamic behaviour of the tested post-tensioned timber frame buildings.

- Inelastic-rotational-spring models and inelastic-multi-spring models calibrated using a simplified bilinear hysteresis loop to match quasi-static response at a determined drift level did not provide better results than elastic models. Additionally, the inelastic calibration was much more time consuming than the one based on non-linear elastic models.

- The simplest model solution, using a non-linear elastic-rotational-spring model complemented with an equivalent viscous damping value, gave the best prediction of the dynamic response of multi-storey post-tensioned timber structures.

Chapter Seven: **SENSITIVITY ANALYSIS OF MODELLING AND FRAME CONFIGURATION**

7.1 Introduction

There are several different options available in the literature and in particular within the RUAUMOKO [Carr, 2008] analysis program for modelling damping. At the same time, the stiffness matrix could be considered as the initial, secant or tangent stiffness, depending on the particular approach to the problem.

At the time of designing a post-tensioned timber frame, there are some decisions that may influence the dynamic response and therefore the geometry and cost of the structure.
The aim of this chapter is to provide guidelines for the possible impact as a result of utilising one way to model the structure over another, and at the same time to quantify the impact of engineer options during design.

Firstly the Rayleigh damping model is analysed with the three mentioned options of stiffness matrices, and then the influence on the responses of post-tensioning force, beam-column joint stiffness, and column armouring are examined.

7.2 Influence of damping models and stiffness matrix

Structural damping is traditionally modelled by the Rayleigh approach (***Figure 7-1***). Rayleigh proportional damping uses a combination of mass matrix and stiffness matrix to generate a damping matrix. The main reason for selecting this approach is the uncoupling of the vibration modes and therefore a small computational cost. Additionally, damping values can be specified at two frequencies given the orthogonality property of the mode shapes of free-vibration. Rayleigh damping may be modelled proportionally to the initial stiffness matrix (Ko) or to the tangent stiffness matrix (Kt). The limitations of using an initial stiffness matrix has been questioned [***Priestley et al.***, 2007] because once non-linear behaviour starts on the structure an elastic stiffness matrix is not adequate to be used. The use of tangent stiffness matrix has also been questioned [***Priestley et al.***, 2007]. When the structure goes to the inelastic range, the tangent stiffness will be reduced and therefore damping values will decrease what it opposite to the expected increase in damping levels from elastic to an inelastic state. For the purpose of comparison, this study considered the use of a Rayleigh model using an initial stiffness matrix, a tangent stiffness matrix and a secant stiffness matrix.

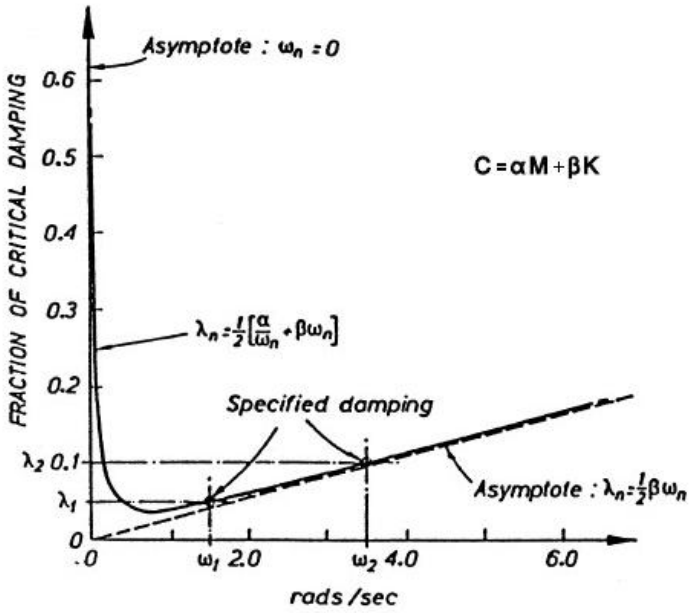

Figure 7-1 Rayleigh damping model in RUAUMOKO *[Carr, 2008]*

Time-history analyses were performed for the considered earthquake records. For each one, computer models were run considering an initial stiffness matrix, a tangent stiffness matrix, and a secant stiffness matrix to be used with a Rayleigh damping model.
The same value of constant equivalent viscous damping was considered for each model. It could be argued that different values of equivalent viscous damping should be used depending of the stiffness matrix considered, however the aim of the exercise was to have a direct comparison of the stiffness matrix influence in the response.
Since the numerical results obtained were independent of the seismic record used, the Cape Mendocino record was considered in order to better explain the results.

The selection of stiffness matrix used did not affect the seismic response. *Figure 7-2* shows in parts a) and b) the accelerations and drifts obtained for the original modelled building, (31% mass required by similitude and 45kN of post-tensioning force), and no difference was obtained by using the three stiffness matrices. *Figure 7-2* c) and d) show accelerations and drifts for a case where mass has been increased four times in order to enforce a greater inter-storey drift, and only a negligible difference was observed in accelerations, meanwhile drift levels showed no change. *Figure 7-3* a) and b) consider also four times the mass but with 15kN and 80kN of post-tensioning force, respectively, only for the case that used 15kN there was a small difference when comparing accelerations.

The explanation can be inferred observing *Figure 7-7* and *Figure 7-8* where it is possible to see that non-linear behaviour of the structure starts at greater drift levels as a consequence of a design choice. Additionally, after the non-linear behaviour occurs, the reduction in lateral stiffness is not significant. Hence, when non-linear behaviour occurs at an earlier stage, the chances of having a different response increase. As an illustration, minor response differences were obtained for a post-tensioning force of 15kN. No response changes were obtained when a post-tensioning force of 80kN was used; this is due to non-linear behaviour occurring later for a greater post-tensioning force.

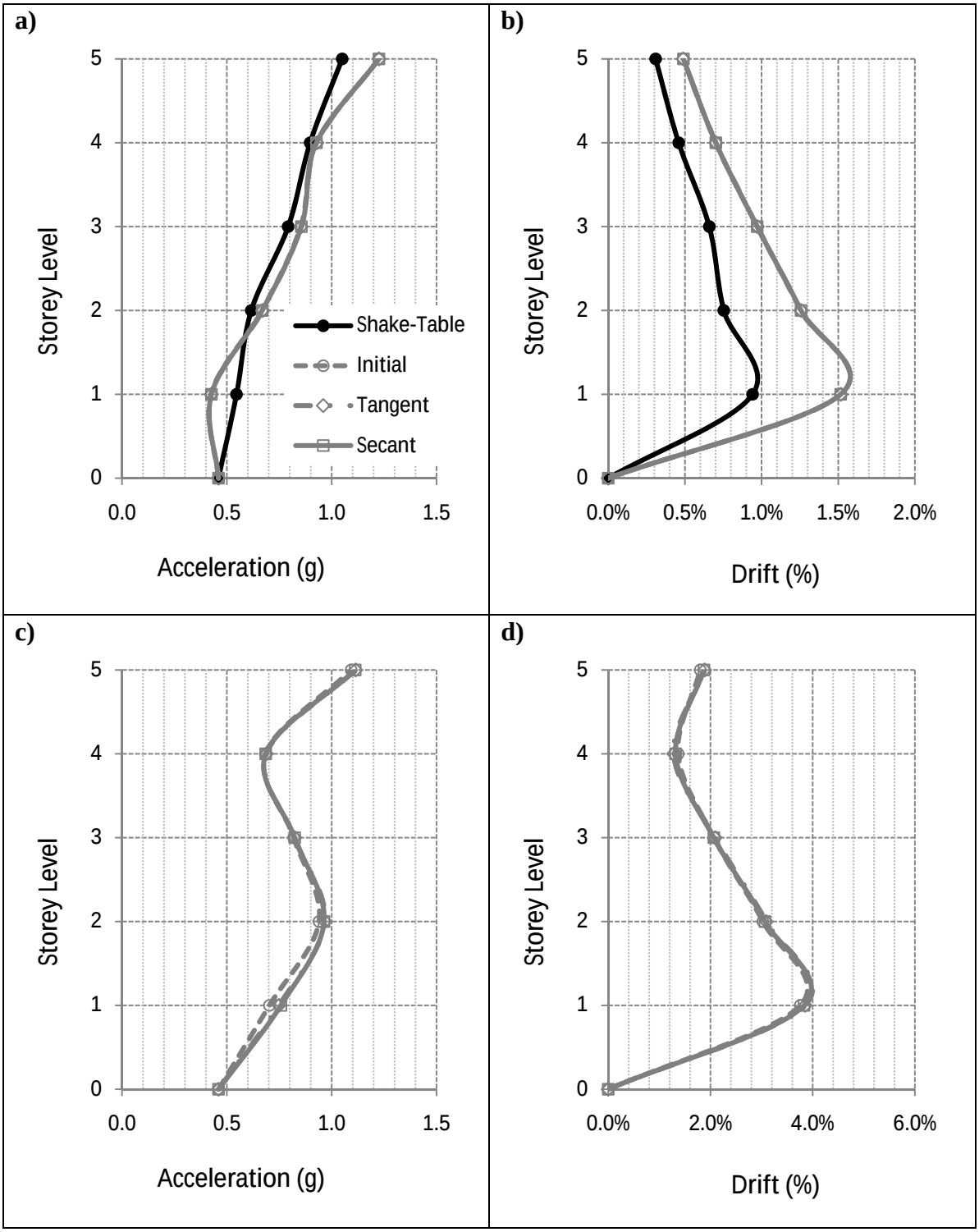

Figure 7-2 5-storey model building, Cape Mendocino earthquake, stiffness matrix comparison: a) Original model building, acceleration b) Original model building, drift c) Four times the mass, acceleration d) Four times the mass, drift

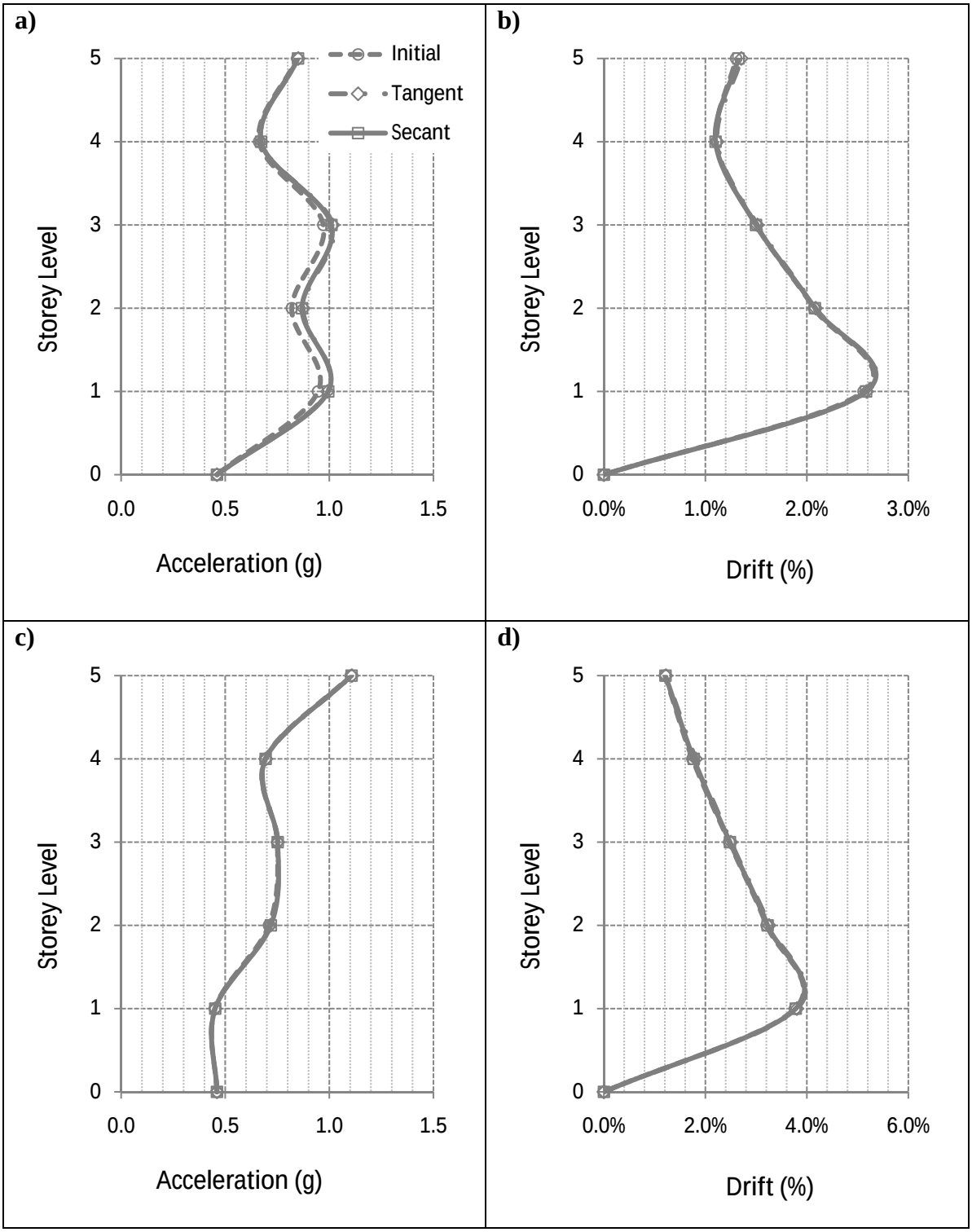

Figure 7-3 5-storey model building, Cape Mendocino earthquake, stiffness matrix comparison: a) Four times the mass, 15kN post-tensioning force , acceleration b) Four times the mass, 15kN post-tensioning force, drift c) Four times the mass, 80kN post-tensioning force , acceleration d) Four times the mass, 80kN post-tensioning force, drift

7.3 Post-tensioning force

The influence of the post-tensioning force in the beam-column connection on the overall response is studied. For this, five levels of post-tensioning force were applied to the model buildings, for 3-storey and 5-storey configurations. The section considered was the same used for the model buildings (See Chapter 3). The impact of the post-tensioning force on the lateral stiffness was analysed through push-over tests, and then a comparison of secant stiffness was carried out. In particular the secant stiffness at 2.5% of drift was examined as this is the value typically used during DDBD.

In a first stage, the post-tensioning force impact is considered at the connection level, i.e. the moment-rotation capacity of the connection was computed for 15kN, 30kN, 45kN, 60kN, and 80kN of post-tensioning, *Figure 7-4* shows the results. The plot is characterized for a clear increase of the moment capacity of the connection and a delay in the occurrence of the non-linearity part of the curve. This non-linearity denotes the starting of the gap opening; therefore, there is a reduction of the stiffness as a consequence of the relocation of the neutral axis. *Table 7-1* shows the connection moment capacity at 2.5% drift for the beam sections used for the model buildings; more realistic section moment capacities can be found in Chapter eight.

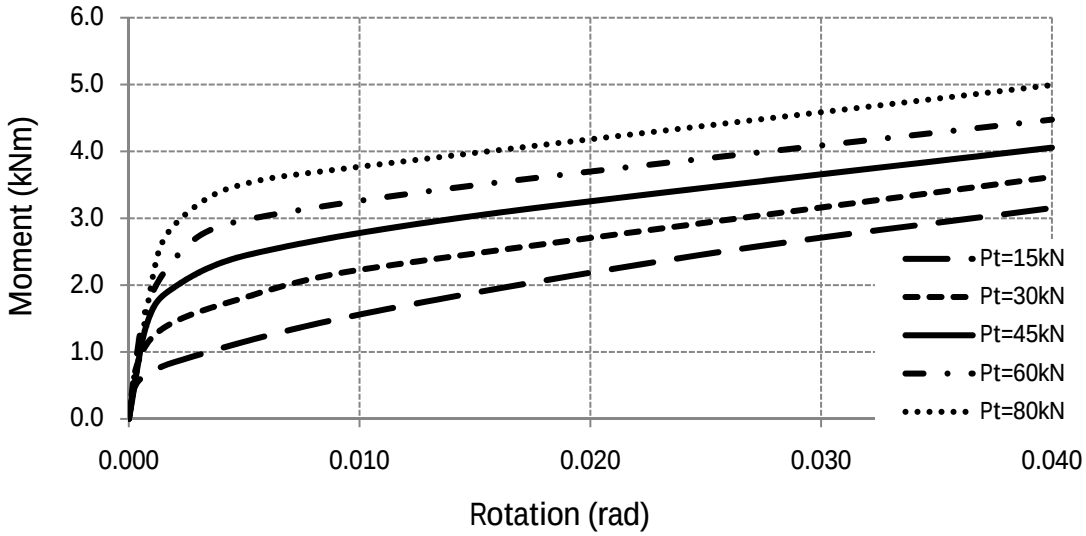

Figure 7-4 Connection moment-rotation curves as a function of post-tensioning force

At the same time, the expected levels of timber strain at the column face in contact with beams are included. The importance of knowing the timber strain value of design limits lies in having an idea of the expected damage, such as the crashing of timber loaded perpendicular to the grain. The occurrence of timber crushing will lead to a loss of post-tensioning force, stiffness, and moment capacity.
Another important point to consider is the gap opening achieved at a determined drift level which is inversely proportional to the post-tensioning force applied. In the case of the incorporation of energy dissipaters (mild steel bars), a greater gap opening would generate a larger amount of energy dissipation.

Table 7-1 Connection moment capacity and timber strain as a function of post-tensioning force

Post-tensioning Force (kN)	Connection moment capacity at Drift = 2.5% (kNm)	Timber strain/Yielding strain at Drift = 2.5%
15	1.55	0.65
30	2.02	0.82
45	2.44	0.98
60	2.97	1.16
80	3.48	1.40

Global responses of the considered model buildings are included. Time-history analyses were performed on both building configurations (3-storey and 5-storey height) varying the post-tensioning force on frames. From previous analyses, the initial-elastic period (T_e) of the model building is expected to be around 0.3 sec. Elastic displacement response spectra (*Figure 7-5*) and Acceleration response Spectra (*Figure 7-6*) of the Parkfield earthquake are included to have an idea of expected lateral displacements and floor accelerations.
Inter-storey drift and floor accelerations obtained during the study of the post-tensioning force influence are plotted in *Figure 7-9* for the 3-storey modelled building, and in *Figure 7-10* for the 5-storey modelled building.

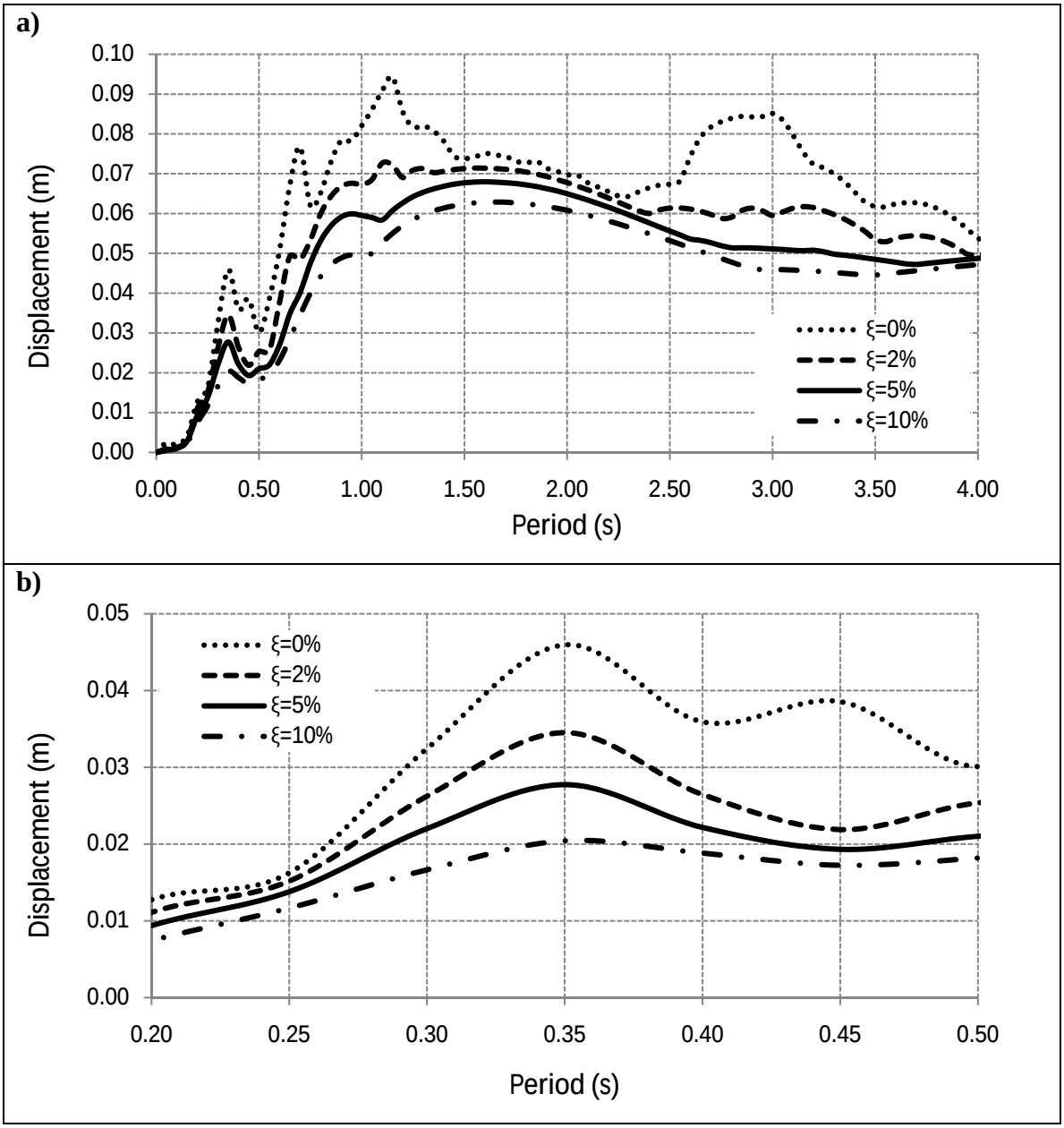

Figure 7-5 Elastic Displacement response spectra for Parkfield earthquake: a) Full range of natural periods b) Zoom-in of the interested range of natural periods

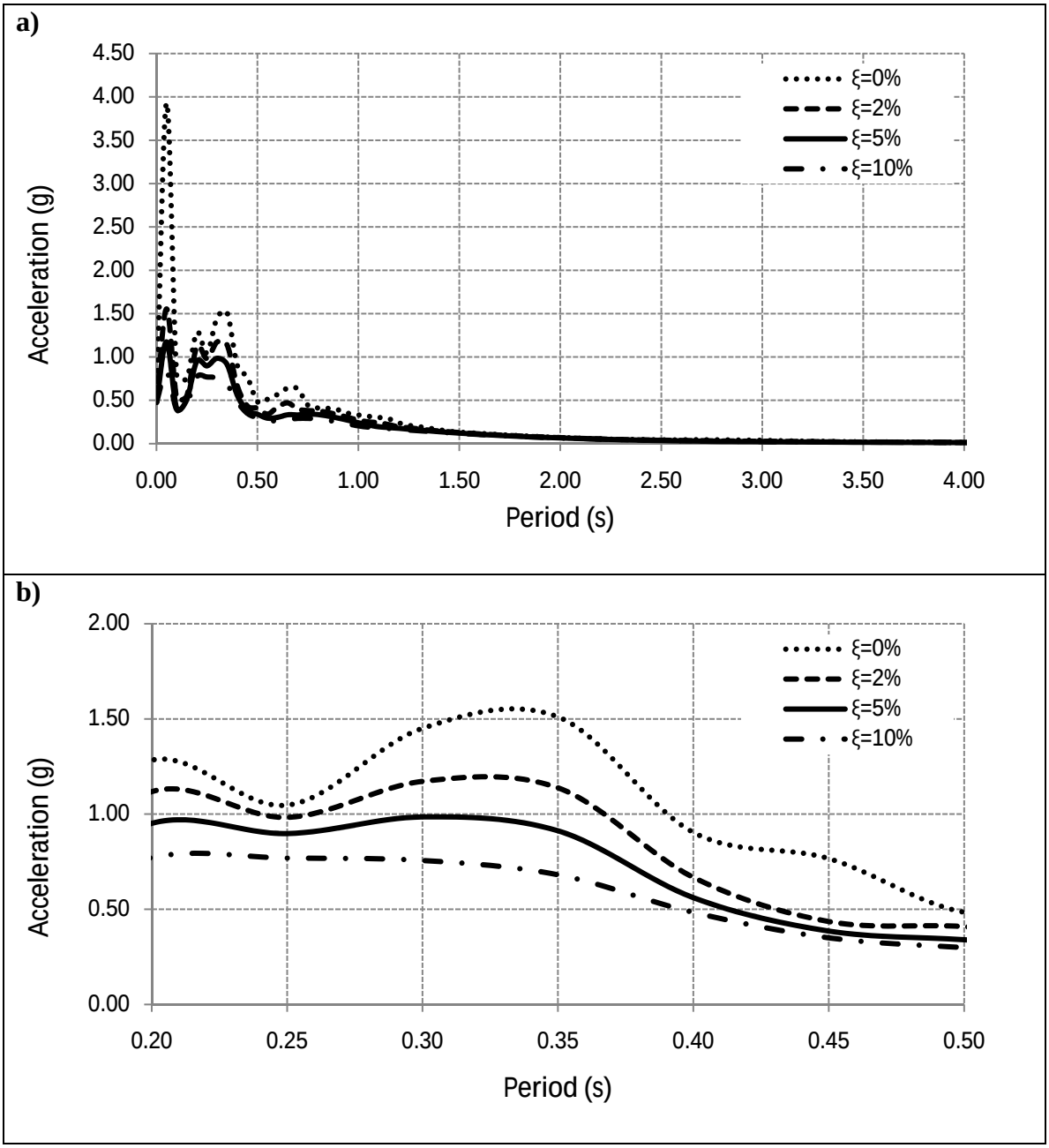

Figure 7-6 Elastic Acceleration response spectra for Parkfield earthquake: a) Full range of natural periods b) Zoom-in of the interested range of natural periods

Before carrying on with the time-history analysis, the influence of the post-tensioning force on the lateral stiffness was studied. Hence, push-over analyses were performed. *Figure 7-7* shows the curves obtained for one 3-storey frame and one 5-storey frame. Initial lateral stiffness in both cases was independent of post-tensioning force, the difference begins at the moment when the first decompression point is reached on one beam-column connection, then the gap opens and the non-linear behaviour starts.

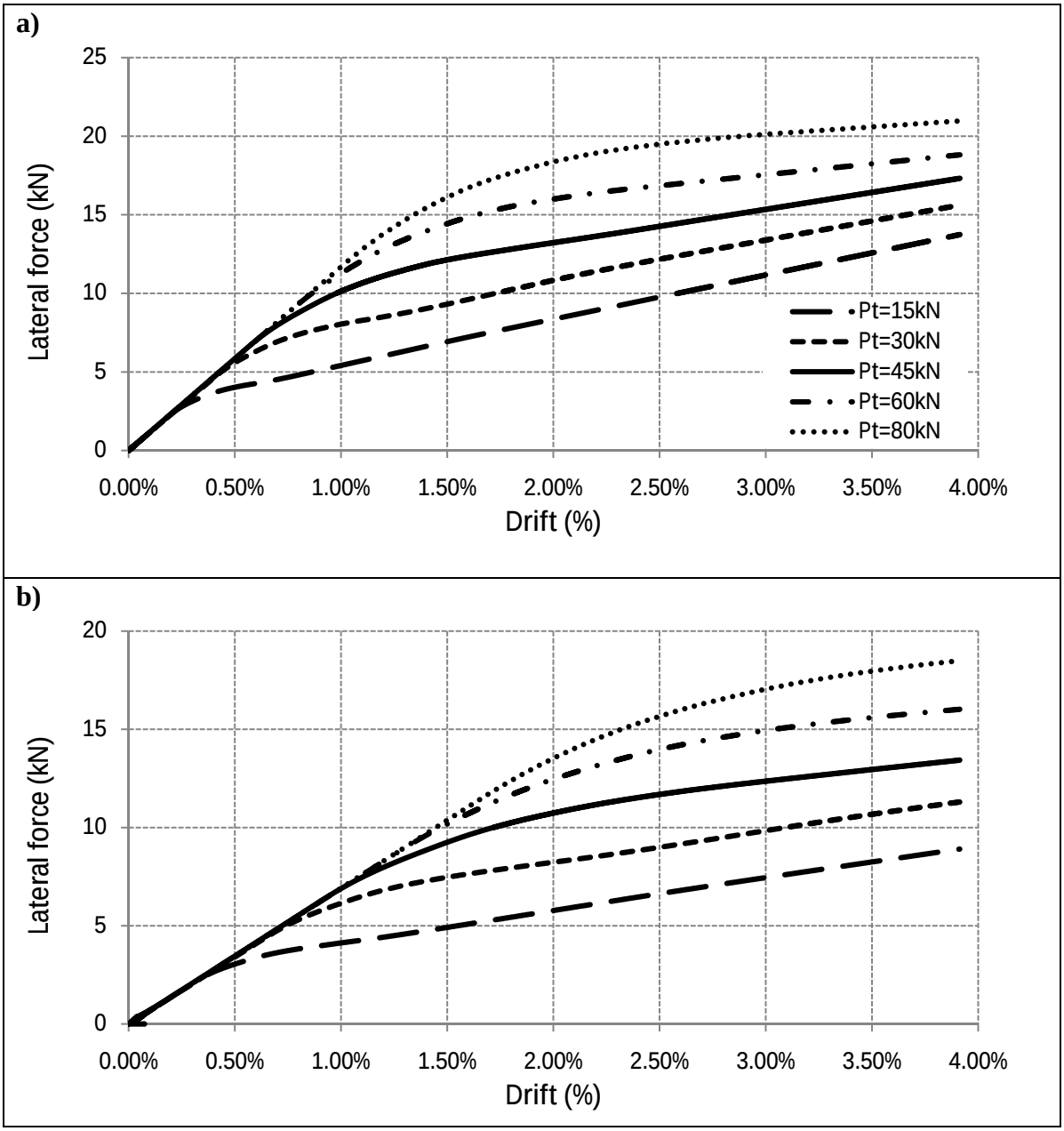

Figure 7-7 a) Push-over analysis of 3-storey post-tensioned timber frame b) Push-over analysis of 5-storey post-tensioned timber frame

The secant stiffness is also plotted (*Figure 7-8*), essentially to quantify the values that would be used in case of structure being designed based on DDBD, where secant stiffness is used to characterize the equivalent single-degree of freedom model at maximum displacement response. Significant differences on secant stiffness are observed for the 3-storey level frame depending on the post-tensioning force used. The difference is even greater for the 5-storey building.

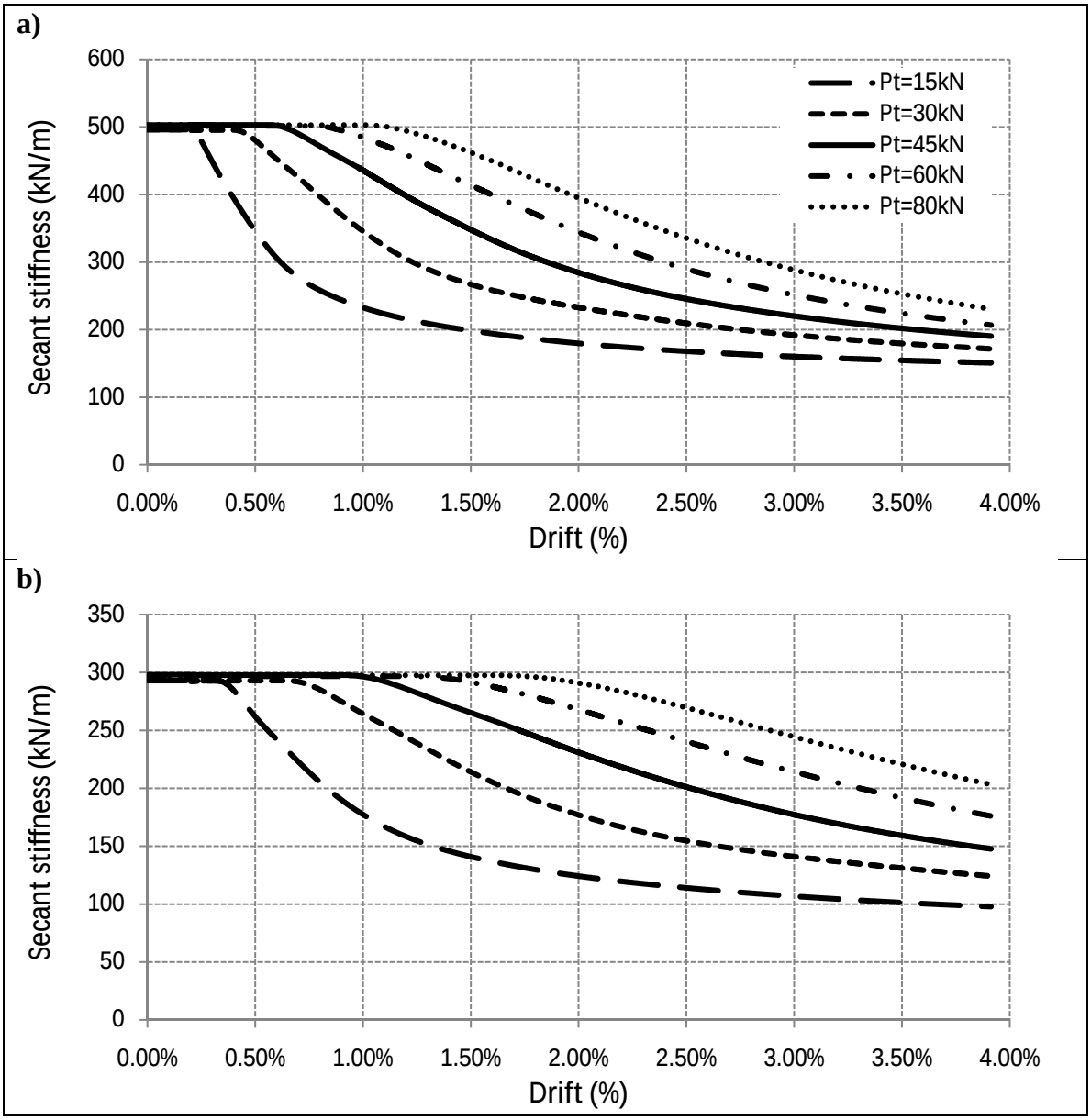

Figure 7-8 Influence of post-tensioning force: a) Secant stiffness of 3-storey post-tensioned timber frame b) Secant stiffness of 5-storey post-tensioned timber frame

Time-history analyses were carried out for four of the seismic records considered, varying the post-tensioning force applied on frames. In the case of the 3-storey model building the case analyzed corresponds to a 45kN of post-tensioning force in beams and 78% of the mass required by similitude. The 5-storey model building considers 45kN of post-tensioning force and 31% of the mass required by similitude. Results are illustrated in ***Figure 7-9*** and ***Figure 7-10***. In general the amount of post-tensioning force had little influence on floor accelerations or inter-storey drifts, the explanation for this can be found in the displacement spectra and acceleration spectra previously shown (***Figure 7-5*** and ***Figure 7-6***), where it is possible to realise that for the range of a natural period of the analysed model building, a large variation of displacements or accelerations is not likely to happen. However, for structures where a change in the natural period could imply a significant variation of floor accelerations or inter-storey drift, the study of the optimal post-tensioning force applied is worthy of investigation. In the case of the mentioned spectrum, structures with a natural period around one second or three seconds may be sensitive to changes in lateral stiffness.

Even when large variations of seismic response were not expected, they occurred as shown in ***Figure 7-10*** where an important increase of acceleration was obtained in the case of using a post-tensioning force of 15kN, in the same way the increase of inter-storey drift was around 40%.

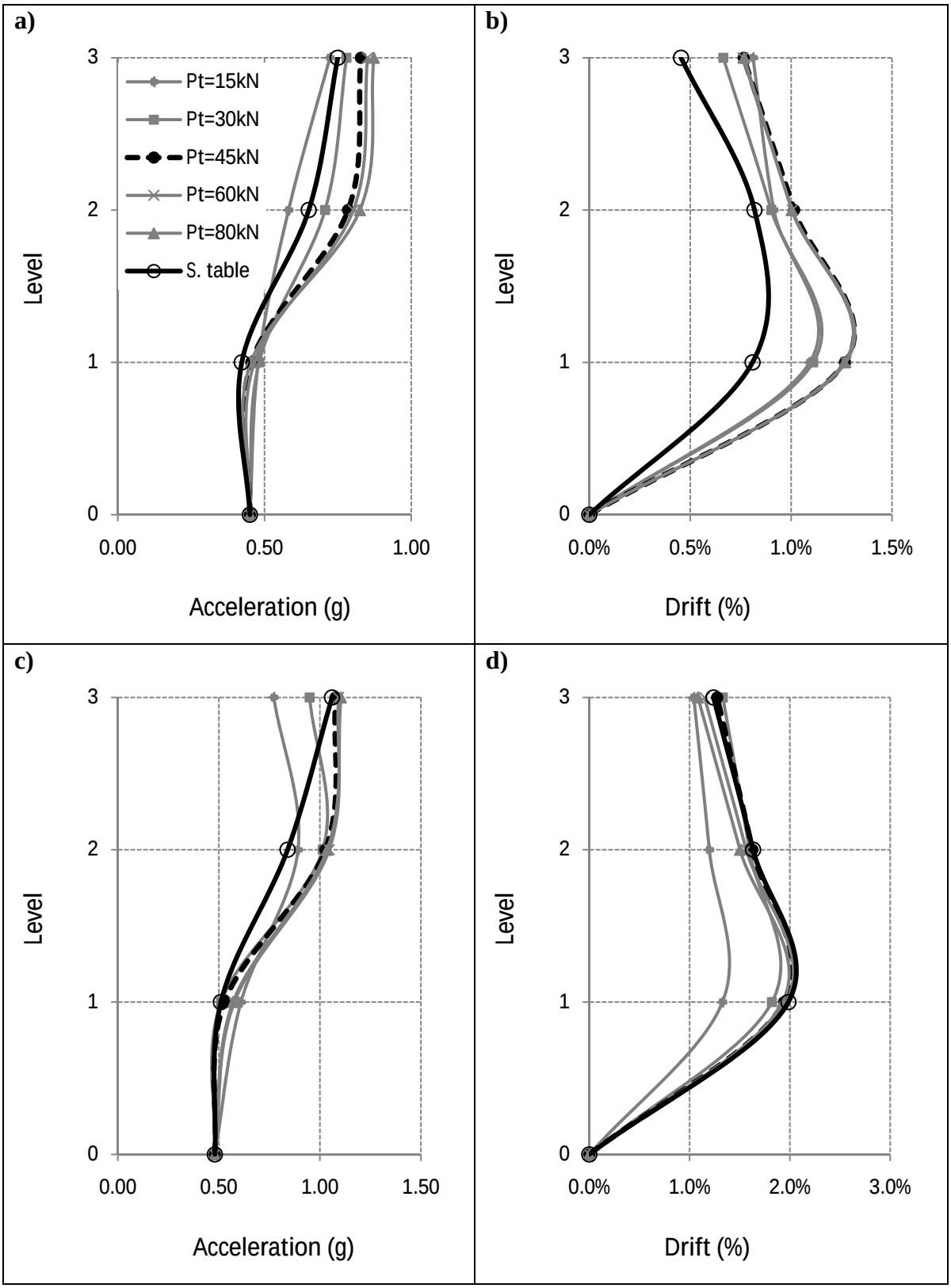

Figure 7-9 3-storey model building: a) Kobe earthquake, floor accelerations b) Kobe earthquake, inter-storey drift c) Parkfield earthquake, floor accelerations d) Parkfield earthquake, inter-storey drift

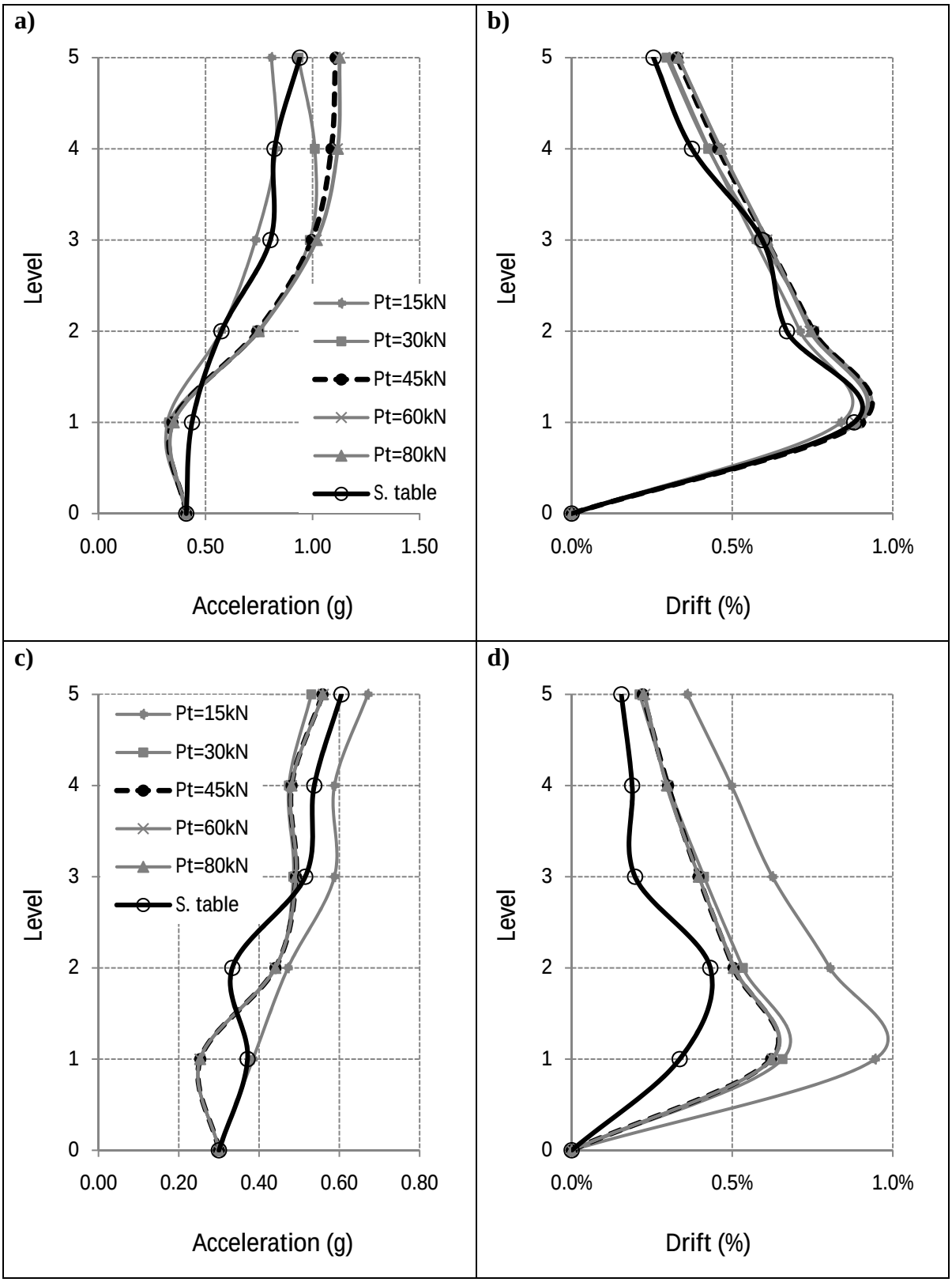

Figure 7-10 5-storey model building, post-tensioning force influence: a) Northridge earthquake, floor accelerations b) Northridge earthquake, inter-storey drift c) Loma Prieta earthquake, floor accelerations d) Loma Prieta earthquake, inter-storey drift

7.4 Beam-column joint stiffness

Previous investigations have indicated that joint flexibility plays an important role during design of post-tensioned timber frames. In some cases, especially during service limit states a large percentage of total frame deformation occurs at beam-column joints, thus controlling the design. As a consequence, different ways of stiffening up the panel zone have been proposed. However, the joint-panel flexibility may not be a big influence in some cases when it is stiff enough and then the connection (beam-column rocking interface) could be the main contributor to lateral drift.

Constituent contributions of each one of the components to the inter-storey drift for the modelled buildings can be seen in *Figure 7-11*. Even when this analysis depends highly on beam and column geometry and post-tensioning force among others, in most cases the joint-panel rotation is not as relevant as it was initially assumed to be.
In particular for the illustrated case (beam-column configuration used for model buildings with 45kN of post-tensioning force applied) the biggest contribution comes from connection rotation. To be more specific *Figure 7-11b* shows the contributions at typical design limit states, where it is possible to see that the contribution of the joint-panel rotation at the service limit state is around 13%, similar to beam and column contributions (11% and 9% respectively) and much smaller than connection contribution (67%). At the ultimate limit state (ULS), the contribution to the total deformation of joint-panel zone becomes even less important. At the ULS, the percentages are; joint-panel 8%, beam 7%, column 5%, and connection 80%.

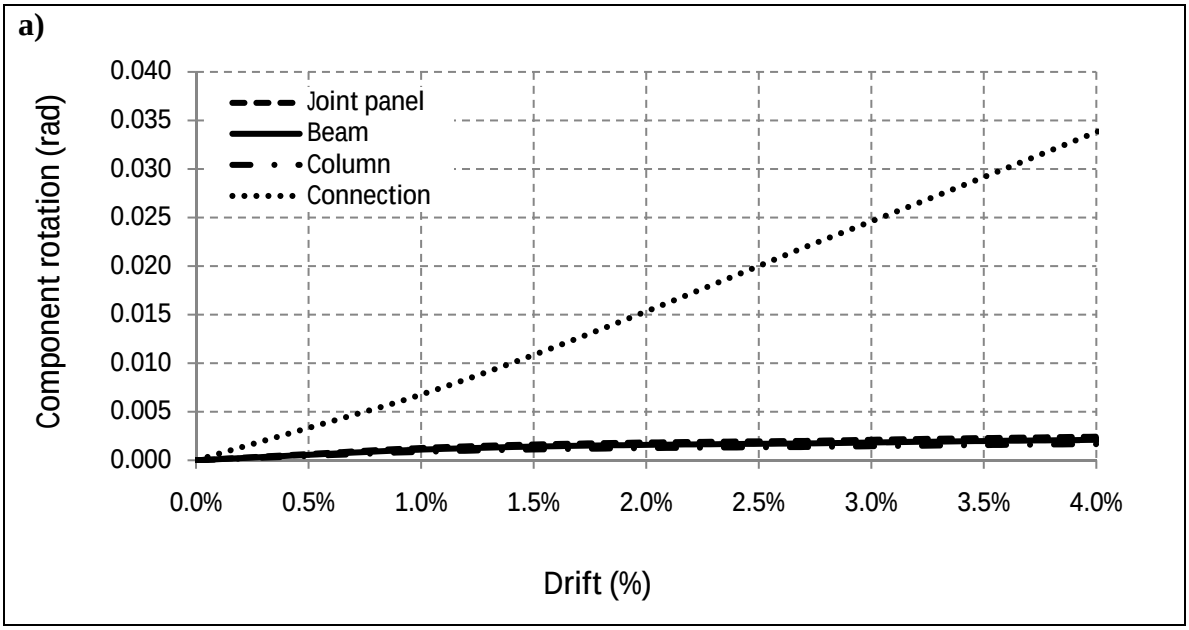

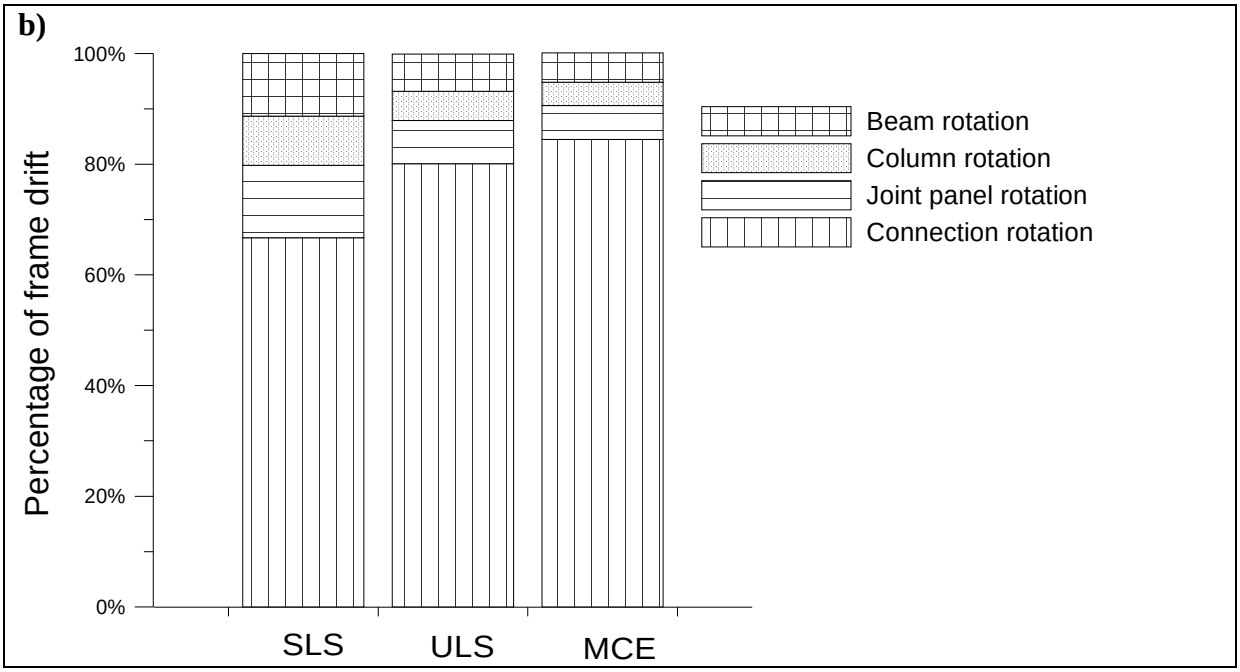

Figure 7-11 Contributions to inter-storey drift: a) Contributions up to 4% of lateral drift b) Contributions at design drift limits

As mentioned, it was believed that the joint-panel stiffness is an important contributor to the frame deformation, especially at SLS. Hence, some attempts of stiffening up the area have been done. Cusiel [2009], analysed different ways to stiffen up the joint-panel zone, being the simplest way to do it through the utilization of screws, and the most complex using an external steel jacketing as the ”bow-tie” [Cattanach *et al*., 2008] steel armouring which has been successfully applied to post-tensioned concrete structures (*Figure 7-12*).

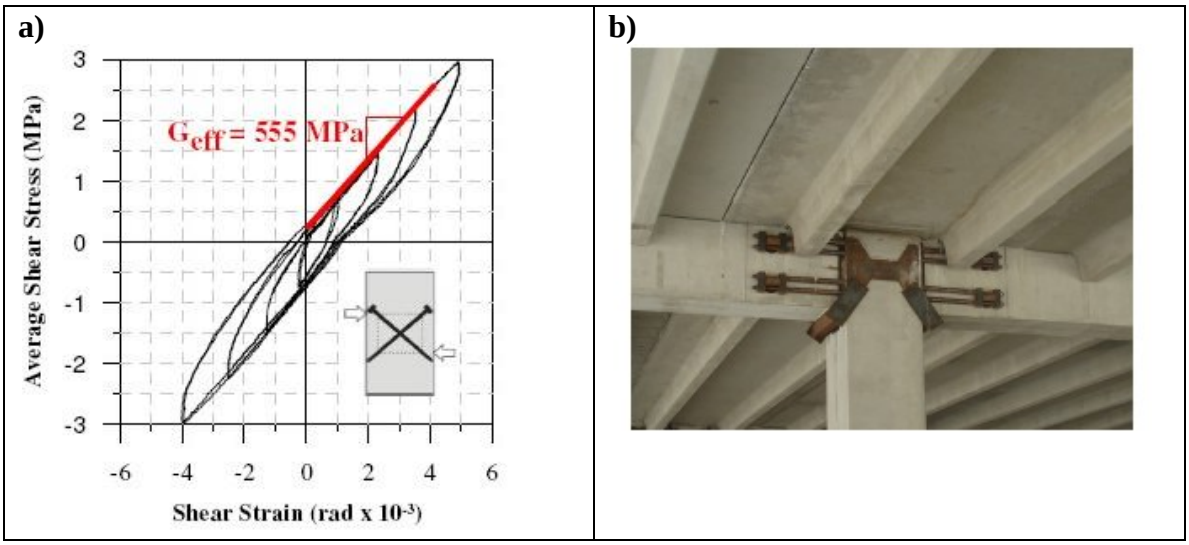

Figure 7-12 Joint-panel reinforcement: a) Using screws [Cusiel 2009] b) Using “bow-tie” solution [Cattanach et al., 2008]

From experimental testing it was proven that the maximum increase of joint stiffness, using screws, was around 25%. On the other hand, a "bow tie" or similar armouring solution is expected to increase the joint stiffness up to 11 times [Cusiel 2009].

Numerical models were developed for the model building to study the effect of increasing joint stiffness. Dynamic tests were performed using time-history analysis considering a maximum increase of joint stiffness up to 8 times. Firstly, push-over analyses were performed to compute the increase in lateral stiffness of the considered modelled buildings. *Figure 7-13* shows that even when joint stiffness is increased up to 8 times, there is not a considerable increase in lateral stiffness of the complete frame. The lateral stiffness of the 3-storey model increased from 503kN/m to 523kN/m, and was not expected to have an influence on the joint stiffness or dynamic response. The time-history analyses were performed and the results have verified the mentioned expectations (*Figure 7-14*).

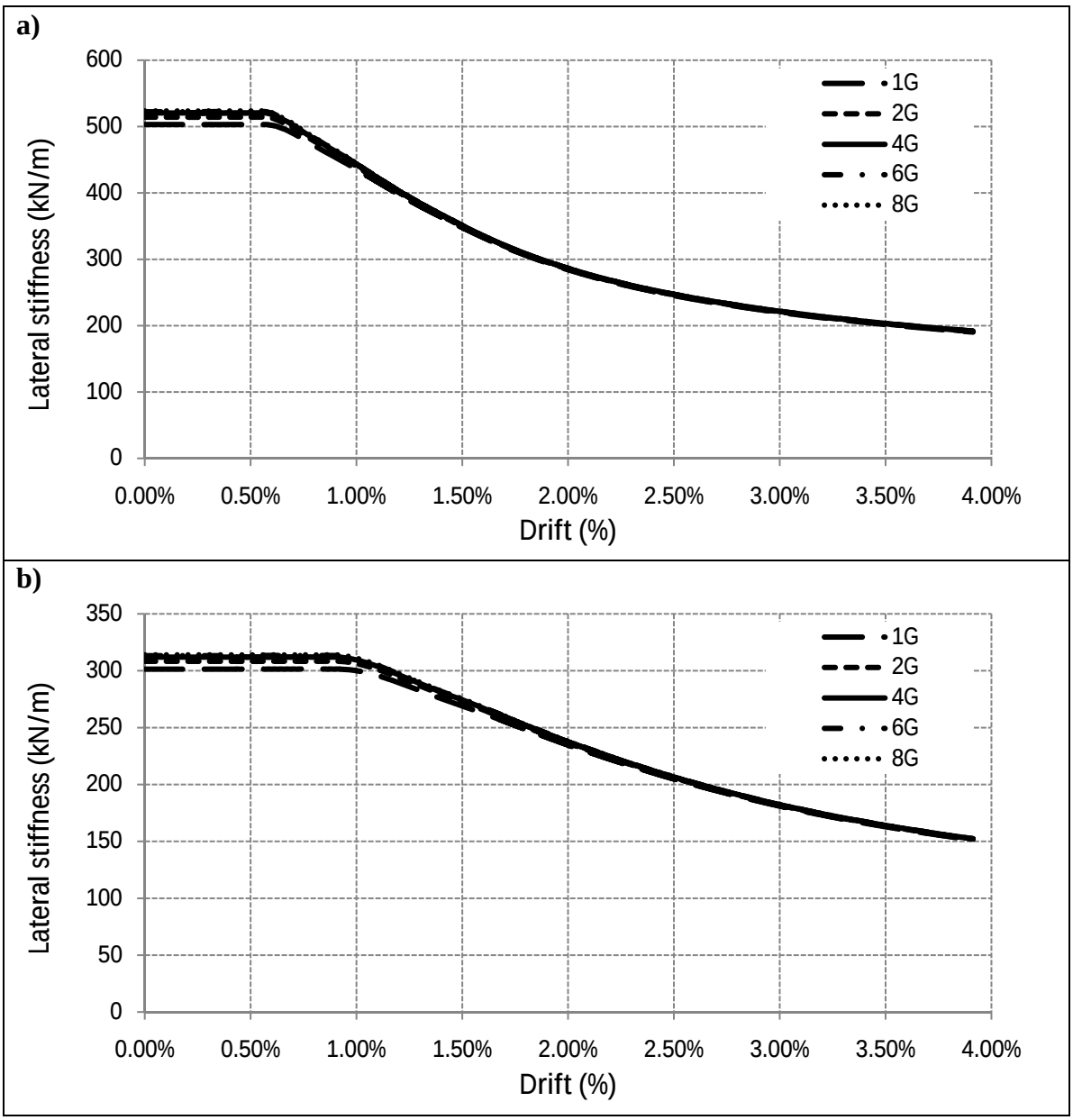

Figure 7-13 Influence of joint stiffness: a) Secant stiffness of 3-storey post-tensioned timber frame b) Secant stiffness of 5-storey post-tensioned timber frame

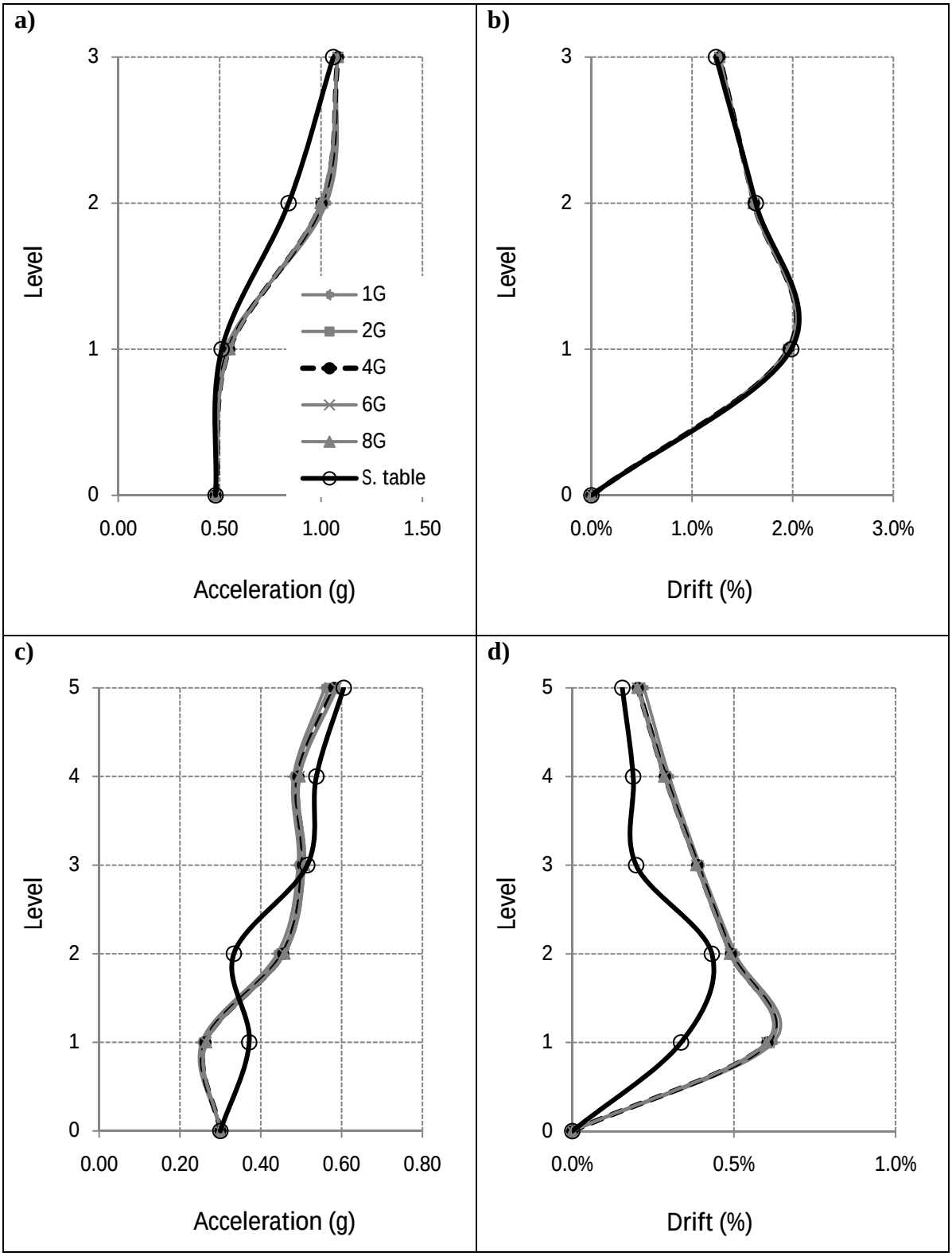

Figure 7-14 Influence of joint stiffness using time-history analyses: a) 3-storey model, Kobe earthquake, floor accelerations b) 3-storey model, Kobe earthquake, inter-storey drift c) 5-storey model, Loma Prieta earthquake, floor accelerations d) 5-storey model, Loma Prieta earthquake, inter-storey drift

7.5 End of column armouring

The final study consisted of analysing the modification of the response when an end-plate (steel armouring) is included, as the one shown in *Figure 7-15*. As concluded by Newcombe [2008a], the inclusion of steel armouring increases the effective stiffness of the beam-column connection. The numerical moment-rotation curve shown in *Figure 7-16* is for the beam used on model buildings. It is clear that armouring can result in a significant increase of the connection stiffness and connection moment capacity.
Another important effect of adding steel armouring is the reduction of the timber strain, at the beam-column interface, as a consequence of stress redistribution and greater effective Young's modulus.

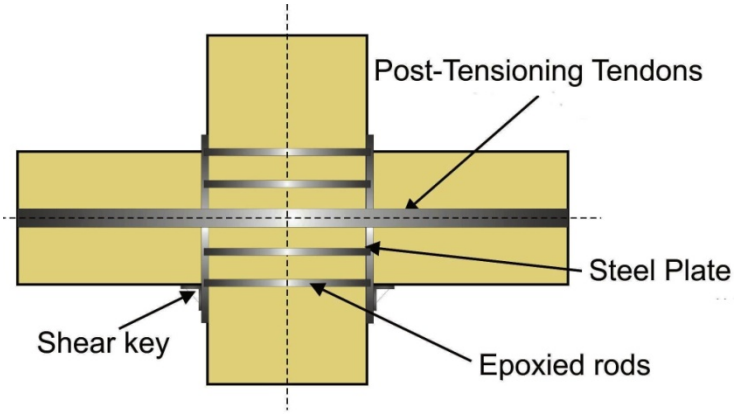

Figure 7-15 Beam-column connection with column armouring (Courtesy of M. Newcombe)

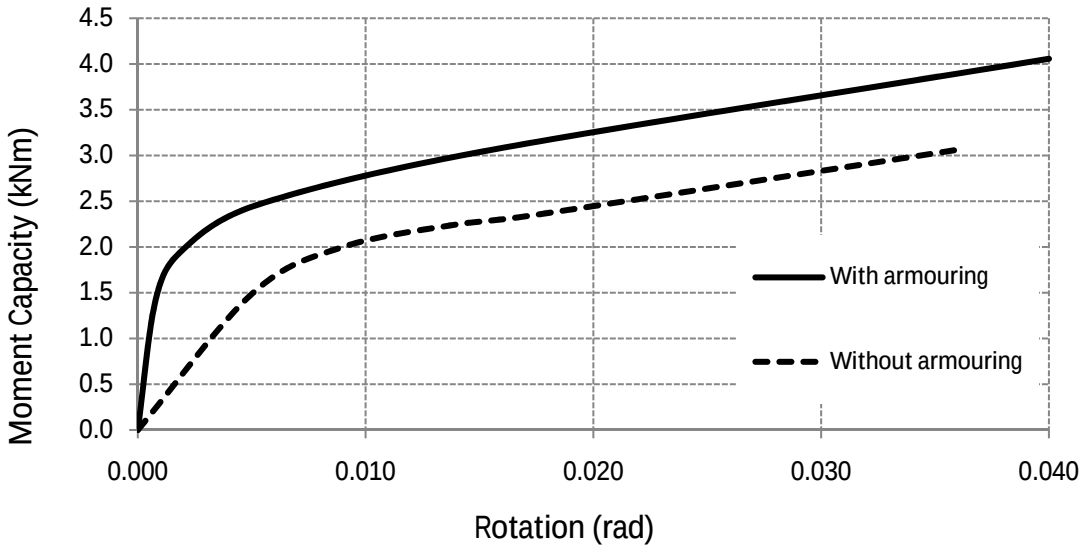

Figure 7-16 Moment-rotation comparison of beam end with and without steel armouring

Table 7-2 shows the increase in moment capacity, at 2.5% drift, afforded once steel armouring is considered. Timber strain values are included which can be directly compared with the ones in *Table 7-1* to understand the strain reduction for cases considering steel armouring is illustrated.

Table 7-2 Connection moment capacity and timber strain as a function of post-tensioning force, beam-column joint includes steel armouring

Post-tensioning force (kN)	Without steel armouring		With steel armouring		Increase of moment capacity (%)
	Connection moment capacity at drift = 2.5% (kNm)	Timber strain/Yielding strain at drift = 2.5%	Connection moment capacity at drift = 2.5%	Timber strain/Yielding strain at drift = 2.5%	
15	1.55	0.65	2.08	0.414	34
30	2.02	0.82	2.60	0.492	29
45	2.44	0.98	3.16	0.562	30
60	2.97	1.16	3.99	0.630	34
80	3.48	1.40	4.90	0.711	40

The inclusion of steel armouring also affects the contribution of the four main components to inter-storey drift. *Figure 7-17* shows the contributions, and it is possible to realise that at SLS the joint-panel rotation is the greatest contributor, providing 32% of the total deformation. However, at ULS and MCE, the connection rotation is the largest contributor to frame deformation.

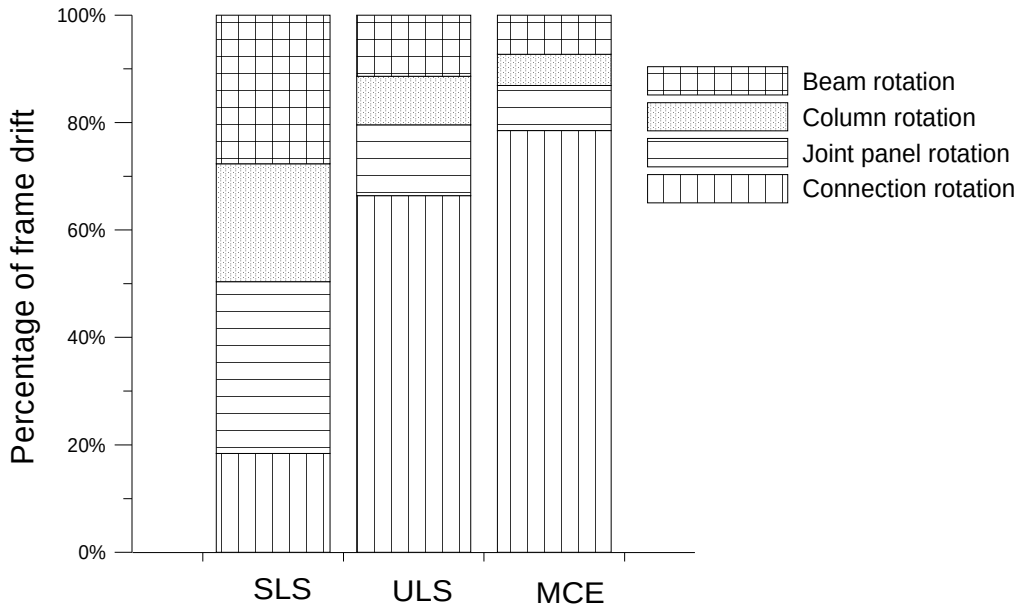

Figure 7-17 Contributions to inter-storey drift considering column armouring

As before, push-over analyses were performed on the 3-storey, and 5-storey modelled buildings, and secant stiffness was computed for both cases. *Figure 7-18* shows the comparison of secant stiffness with and without column armouring. *Table 7-3* shows particular values of initial stiffness (Ko) and secant stiffness (Ks) at 2.5% drift. Clearly there is an important increase of initial stiffness, 120% for both cases considered. Beam gap opening occurs earlier in cases with armouring, i.e. at smaller drift levels. Once the decompression point is reached there is a drop in the lateral stiffness of the frame which implies that at 2.5% drift, the increase of tangent stiffness (when column armouring is considered) is reduced to 30%.

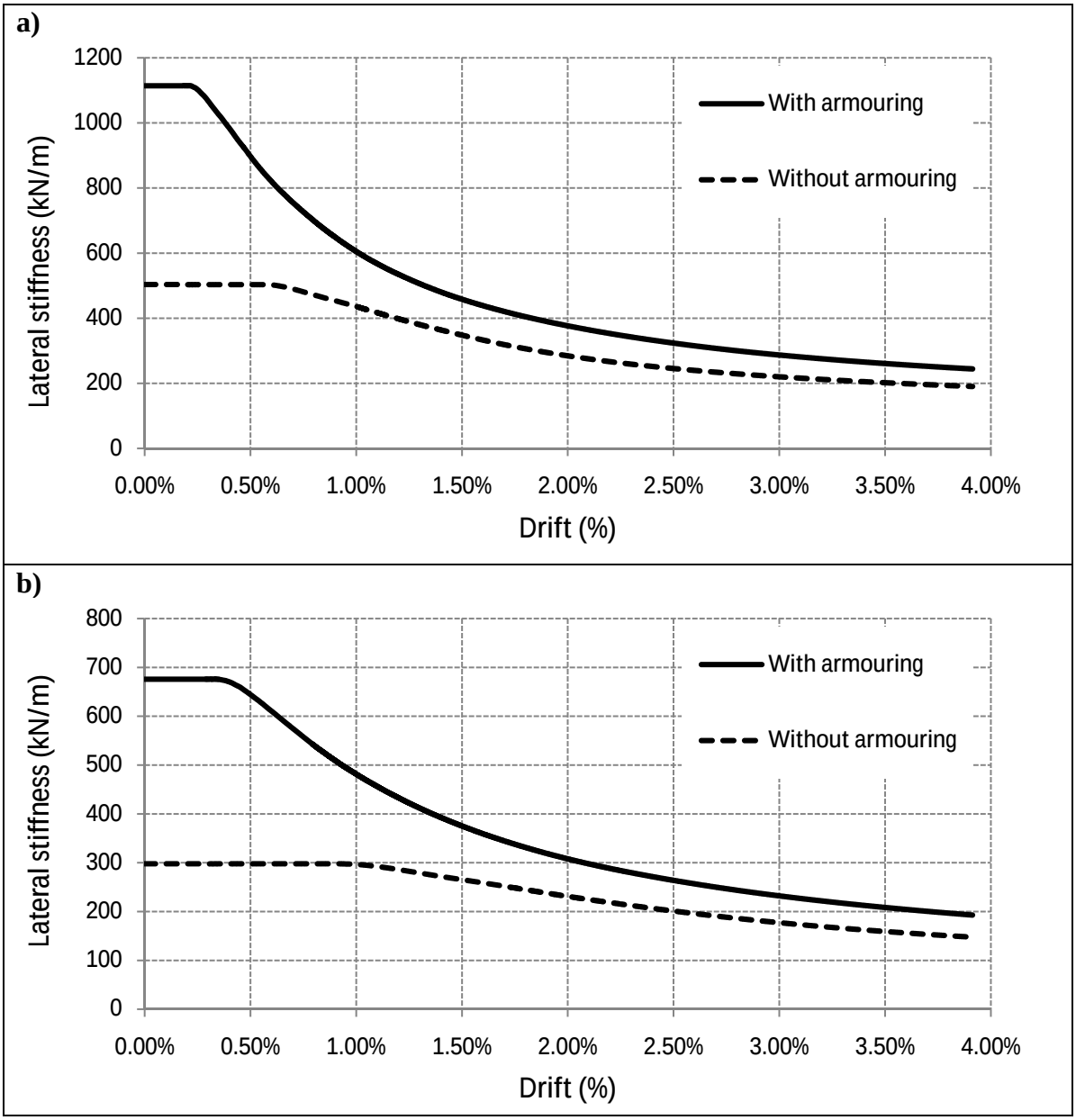

Figure 7-18 Influence of column armouring: a) Secant stiffness of 3-storey post-tensioned timber frame b) Secant stiffness of 5-storey post-tensioned timber frame

Table 7-3 Connection moment capacity and timber strain as a function of post-tensioning force

	Number of levels	Without armouring	With armouring	Increase of stiffness (%)
Initial stiffness: Ko (kN/m)	3	503	1114	121
	5	298	676	126
Secant stiffness at 2.5%: Ks (kN/m)	3	246	324	32
	5	201	264	31

A change in lateral stiffness may imply a change in the dynamic behaviour of the structure and this change could be positive or negative depending on the specific seismic conditions and the design of the structure. ***Figure 7-19*** and ***Figure 7-20*** show the results obtained for the 3-storey and 5- storey modelled building after being subjected to time-history tests of the considered seismic records. For most of the studied cases, the inclusion of column armouring produced a beneficial effect, reducing floor accelerations and inter-storey drifts.
Table 7-4 includes base-shear force and overturning moments for the four considered seismic records. The Loma Prieta earthquake was the only one where the inclusion of column armouring produced a negative effect. Base shear was increased to 45% and overturning moment was increased to 33%. Therefore, it is important to consider that the inclusion of column armouring might not be beneficial; hence every particular case needs to be analysed by the design engineer who has to consider or not the use of steel armouring.

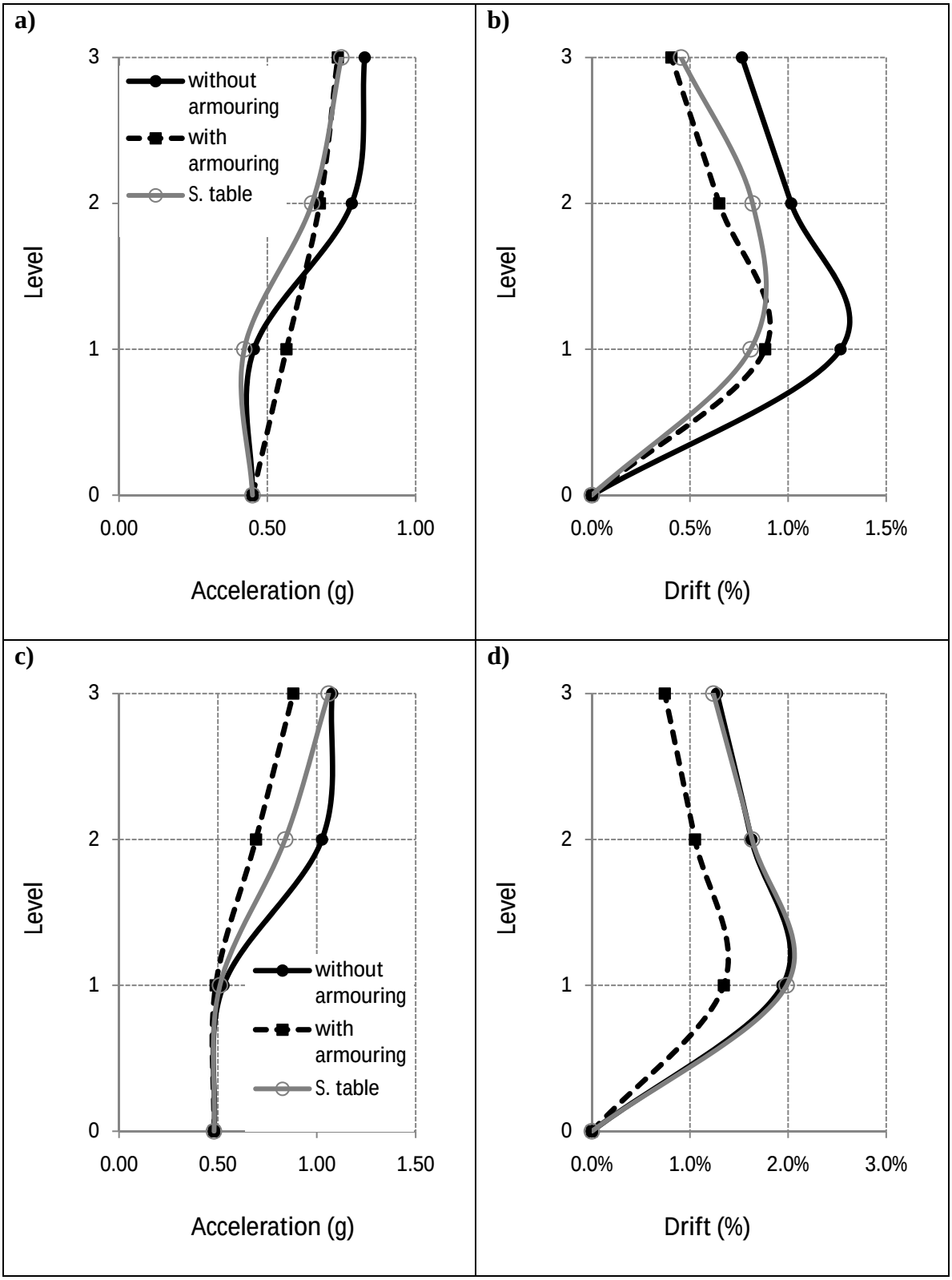

Figure 7-19 3-storey model building, influence of column armouring: a) Kobe earthquake, floor accelerations b) Kobe earthquake, inter-storey drift c) Parkfield earthquake, floor accelerations d) Parkfield earthquake, inter-storey drift

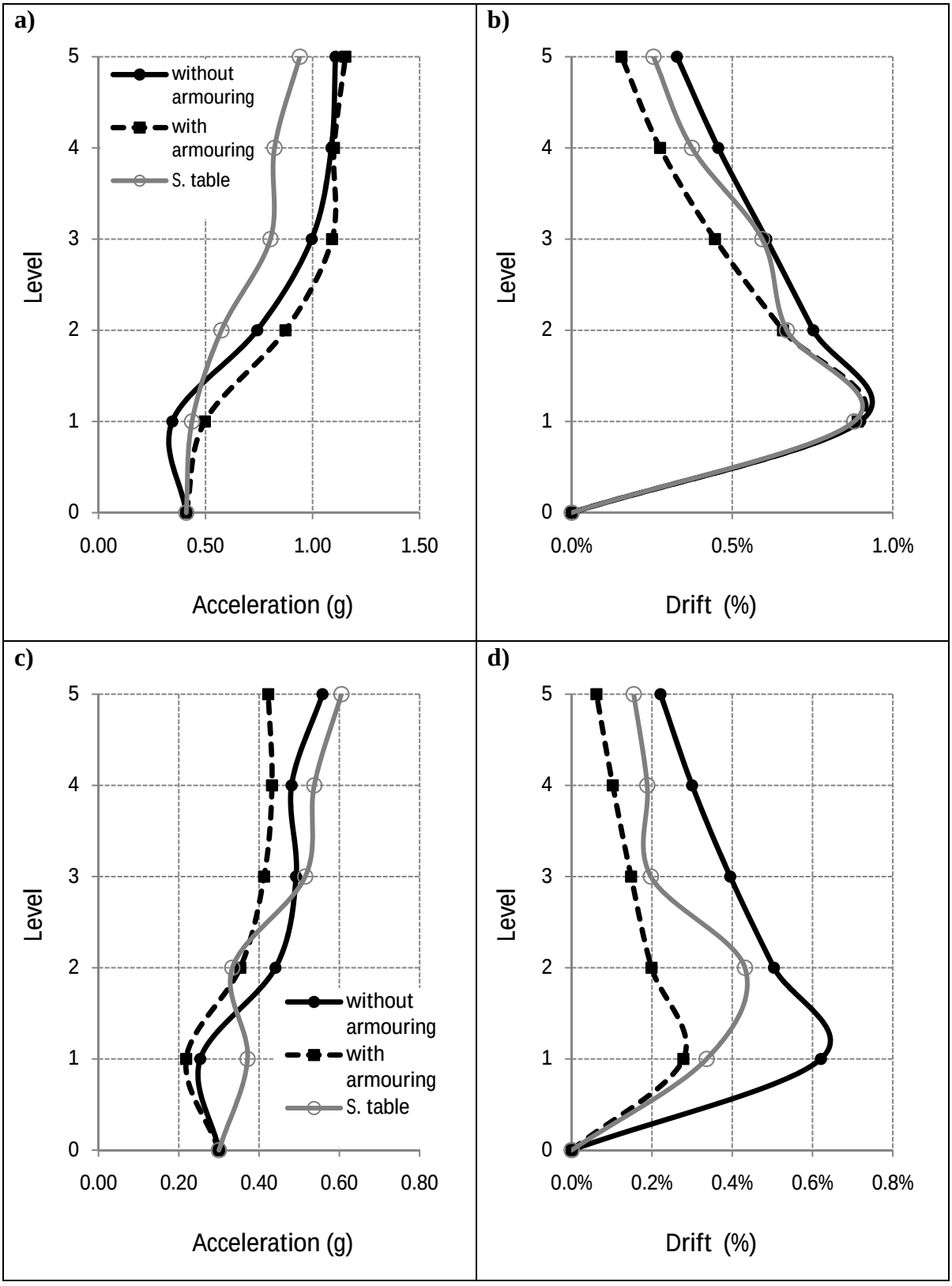

Figure 7-20 5-storey model building, influence of column armouring: a) Northridge earthquake, floor accelerations b) Northridge earthquake, inter-storey drift c) Loma Prieta earthquake, floor accelerations d) Loma Prieta earthquake, inter-storey drift

Table 7-4 Connection moment capacity and timber strain as a function of post-tensioning force

		Base shear (kN)		Overturning moment (kNm)	
Seismic record	Nº Levels	Without armouring	With armouring	Without armouring	With armouring
Kobe	3	13.1	13.7	24.8	24.4
Parkfield	3	17.0	15.5	31.4	28.7
Loma Prieta	5	9.2	13.4	27.3	36.4
Northridge	5	6.9	5.9	19.0	15.8

7.6 Conclusions

- Different stiffness matrix formulations resulted in a negligent difference on dynamic response for the model building. This may not be the case for buildings which initial, secant, and tangent stiffness matrix are considerably different between them. Secant stiffness matrix is the most appropriate to combine with the equivalent viscous damping values proposed since they were computed at a targeted drift level.

- The initial lateral stiffness of the frame is independent of the post-tensioning force until de decompression point. After the decompression point, a variation of post-tensioning force leads to a change of the lateral stiffness of the structure. A minor change of lateral stiffness may lead to a change of dynamic response, therefore a design recommendation is to analyse post-tensioning effects on building earthquake behaviour.

- The joint-panel stiffness may be crucial at low levels of drift, in particular at SLS controlling the design. In some cases the joint-panel stiffness is not the main contributor to lateral deflections. For the case of study, increasing the joint-panel stiffness did not give a significant increase of lateral stiffness of the complete frame. Hence, there was no change on the dynamic response.

- The inclusion of column armouring clearly increases the initial lateral frame stiffness. The increase of initial secant stiffness for the analysed case was around 120%. Once the decompression point is reached, the increase of the lateral stiffness starts to reduce drastically. At ULS limit, the increase of lateral stiffness due to armouring was computed as 30%.

Chapter Eight: **POST-TENSIONED TIMBER FRAME ANALYSIS AND DESIGN**

8.1 Introduction

This chapter illustrates the methodology used during the design of the modelled post-tensioned timber buildings and the applicability to two case studies using realistic geometries and loadings.
The design of a 3-storey post-tensioned timber frame building and a 5-storey post-tensioned timber frame building were performed using the combination of DDBD [Priestley *et al.*, 2007] and the monolithic beam analogy [Pampanin *et al.*, 2001] in its revised version [Palermo, 2004]. Both buildings were subjected to seismic motions using an inelastic time-history analysis via the finite element modelling program RUAUMOKO [Carr, 2008].

8.2 General building descriptions

Two building geometries were considered, both frame types with 6 bays and 3-storey or 5-storey height, respectively. The seismic masses were computed based on the prototype building presented in Chapter three; therefore realistic values were considered (Table 8-1). Same loads were used for all floor levels, including roof.
Both buildings included post-tensioning in beams only with no additional source of energy dissipation, i.e. columns are not post-tensioned and mild-steel bars or additional non-prestressed and damping reinforcement are not used.
For simplicity, the beam and column geometries were consistent and maintained throughout the height of the structures. Frame elevations are shown in *Figure 8-1*.

Table 8-1 Seismic loads for frames

Dead load: D	2.92 kN/m^2
Live load: Q	3.00 kN/m^2
Seismic load	3.82 kN/m^2

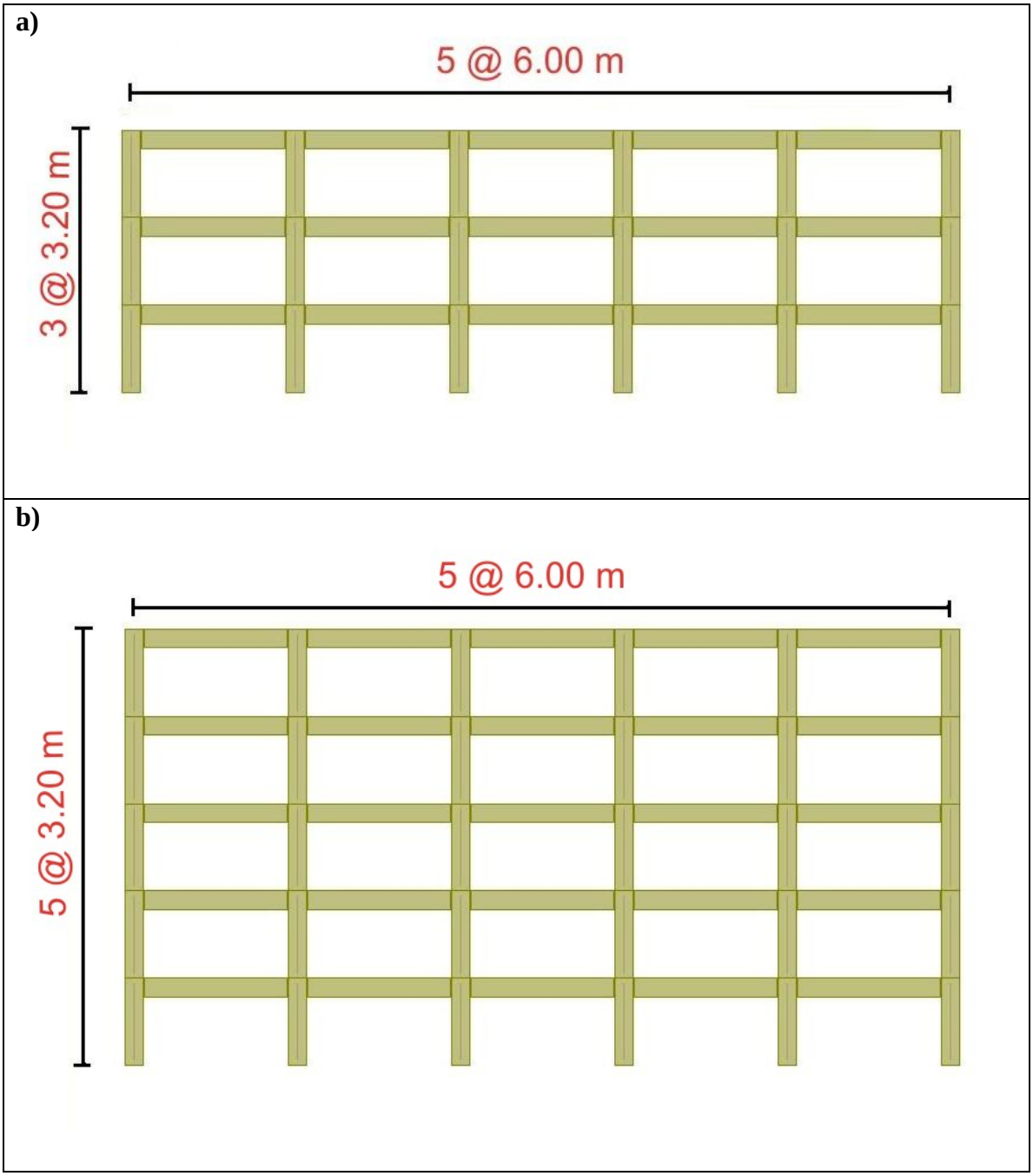

Figure 8-1 Elevation view of buildings considered: a) 3-storey building b) 5-storey building

8.3 Design parameters

Structural designs were performed according to New Zealand Standards; in particular the seismic analyses were based on specifications provided in NZS1170.5:2004. A 2.5% lateral drift limitation was used to represent Ultimate Limit Design corresponding to an annual probability of exceedance of 1/500.
The same records and seismic parameters used in Chapter three were considered and they are repeated for simplicity. The records were scaled to the New Zealand seismic spectrum for the city of Wellington, zone factor Z = 0.4; shallow soil type C; and R = 1. The suite of earthquakes was scaled for a range of periods around the expected elastic period of the structure. The earthquake spectral curves are shown in *Figure 8-2*.

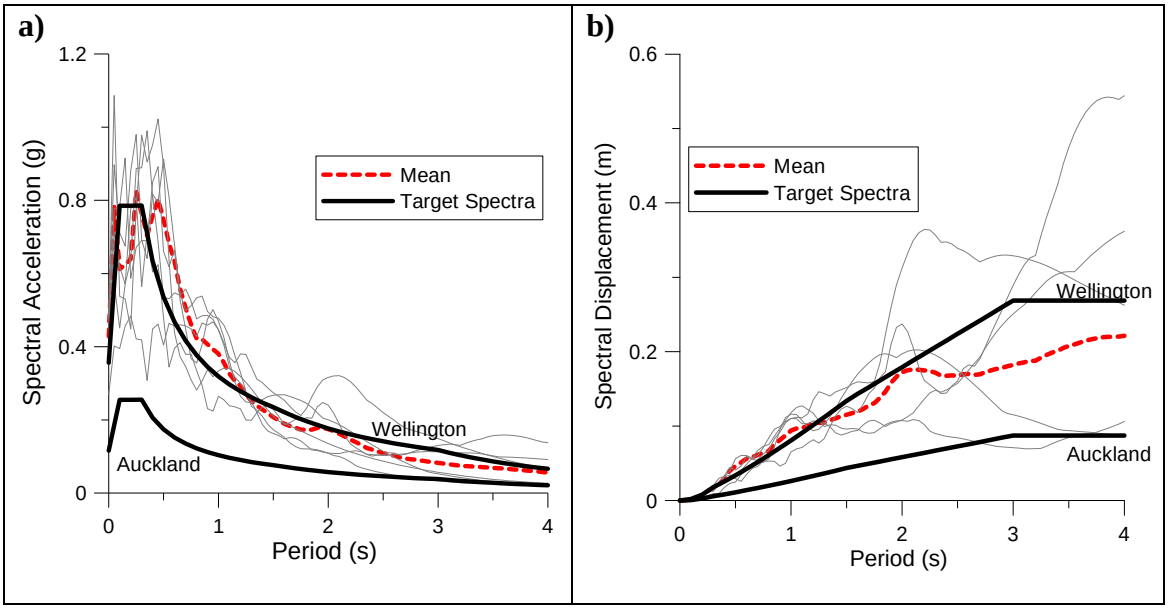

Figure 8-2 Scaled ground motion inputs: a) Acceleration spectra b) Displacement spectra

8.4 Determination of design forces

The design process was basically a combination of Direct Displacement-Based Design [Priestley *et al.*, 2007] and the Revised Monolithic Beam Analogy [Palermo, 2004]. DDBD was used to compute equivalent forces acting over the structure to satisfy an expected deflected shape, and then RMBA was used to analyse, in detail, the moment-rotation relationship of the connection [Newcombe *et al.*,2008b], allowing the calculation of moment capacity for a given rotation (drift). The design process is outlined in the following steps:

Step 1: Select drift design.

Design codes usually impose a critical design drift (θ_d) depending on the design limit state considered; with the most commonly used being Serviceability Limit State (SLS) and Ultimate Limit State (ULS). For ULS θ_d = 2.5% is specified by New Zealand Standards.

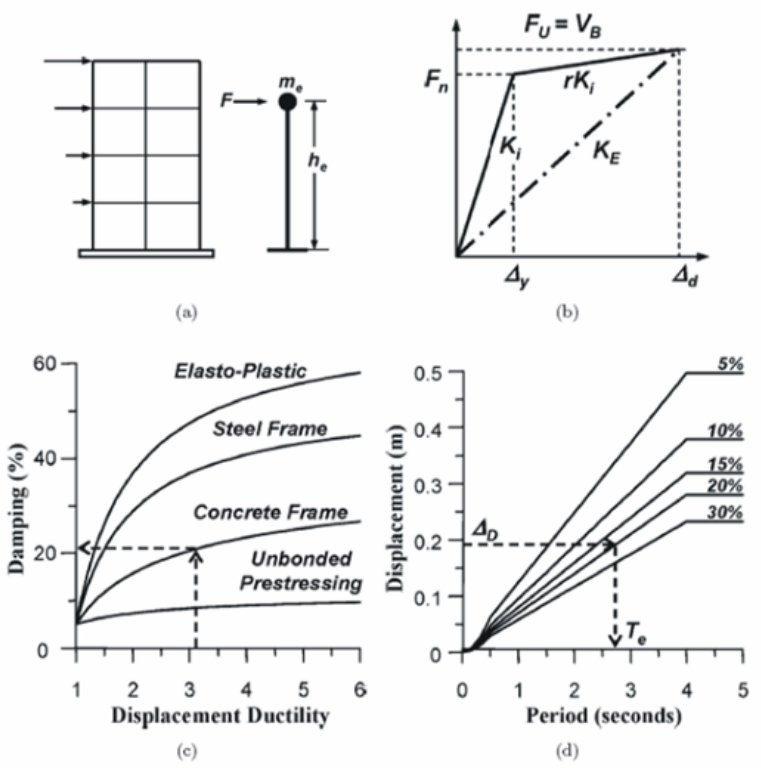

Figure 8-3 Fundamental principles of Direct Displacement-Based Design [Priestley et al., 2007]: a) SDOF representation of structural frame b) Definition of the effective stiffness: K_E c) Equivalent viscous damping versus ductility curves d) Design displacement spectra as a function of damping

Step 2: Compute DDBD parameters for an equivalent single degree of freedom system.

Once the design drift has been defined, the critical displacement is computed as:

$$\Delta_c = \theta_d \cdot H_1 \qquad \text{Equation 8-1}$$

The displacement profile of the frame is calculated:

For n<4

$$\delta_i = \left(\frac{H_i}{H_n}\right) \quad \text{Equation 8-2}$$

For n>4

$$\delta_i = \left(\frac{H_i}{H_n}\right) \cdot \left(1 - \frac{H_i}{4 \cdot H_n}\right) \quad \text{Equation 8-3}$$

n: Floor number
H_i: Height of the level i

Then the floor displacement at each level:

$$\Delta_i = \delta_i \left(\frac{\Delta_c}{\delta_1}\right) \quad \text{Equation 8-4}$$

The peak design displacement:

$$\Delta_d = \sum_{i=1}^{n} \left(m_i \cdot {\Delta_i}^2\right) \Big/ \sum_{i=1}^{n} (m_i \cdot \Delta_i) \quad \text{Equation 8-5}$$

m_i: Mass at the level i

The effective height:

$$h_e = \sum_{i=1}^{n} (m_i \cdot \Delta_i \cdot H_i) \Big/ \sum_{i=1}^{n} (m_i \cdot \Delta_i) \quad \text{Equation 8-6}$$

The effective mass:

$$m_e = \sum_{i=1}^{n} (m_i \cdot \Delta_i) \Big/ \Delta_d \quad \text{Equation 8-7}$$

Step 3: Determine equivalent viscous damping.

As mentioned previously, the existing information suggested a value of $\xi = 2\%$ of critical damping to be used during time-history analysis as the only source of damping. However, in Chapter three it was demonstrated that a greater value could be used. Thus, for post-tensioned timber frame buildings $\xi = 6.5\%$ is recommended to be used as an equivalent viscous damping at 2.5% of interstorey drift.

One benefit of knowing directly the equivalent viscous damping value is that the requirement of computing the displacement ductility can be avoided. This ductility is needed in order to obtain a damping value as illustrated in ***Figure 8-3c***. Besides, the available guides on DDBD regarding unbonded prestressing systems are for precast concrete frames, not necessarily representing the behaviour of post-tensioned timber structures.

Step 4: Determine effective period and effective stiffness.

Once computed the peak displacement design and selecting the appropriate displacement spectrum, the effective period is determined as shown in ***Figure 8-3d*** depending of the damping expressed as a percentage, this displacement needs to be adjusted to the value of damping of the system. For this, the formula used is the proposed in the revision 2003 of the Eurocode (EC8):

$$\Delta_{T,\xi} = \Delta_{T,5} \cdot \left(\frac{0.1}{0.05 + \xi_{eq}} \right)^{0.5} \qquad \text{Equation 8-8}$$

$\Delta_{T,\xi}$: Scaled displacement for the equivalent damping associated to the structure analyzed
$\Delta_{T,5}$: Displacement obtained from the displacement spectrum using 5% of damping
ξ_{eq}: Equivalent damping

This modification is mainly due to the spectrum values which were computed for a damping of 5% of the critical. When the analyzed structure has a damping value different than 5% the formula is applied as a correction.

The effective stiffness is computed as follows:

$$K_e = 4 \cdot \pi^2 \cdot \frac{m_e}{{T_e}^2} \qquad \text{Equation 8-9}$$

Step 5: Compute design forces.

The base shear is computed as:

$$V_B = K_e \cdot \Delta_d \qquad \text{Equation 8-10}$$

Then, the seismic force is distributed to each floor level accounting for higher mode effect by applying 10% of the base shear force at the roof level:

$$F_i = V_t + \frac{0.9 \cdot V_B \cdot (m_i \cdot \Delta_i)}{\sum_{i=1}^{n}(m_i \cdot \Delta_i)} \qquad \text{Equation 8-11}$$

$V_t = 0.1 \cdot V_B$ For roof level and $V_t = 0$ for other levels

Design forces in beams and columns are then determined based on an equilibrium approach. The detailed process can be found in Priestley et al. [2007], however a summary of the main assumptions are listed below:

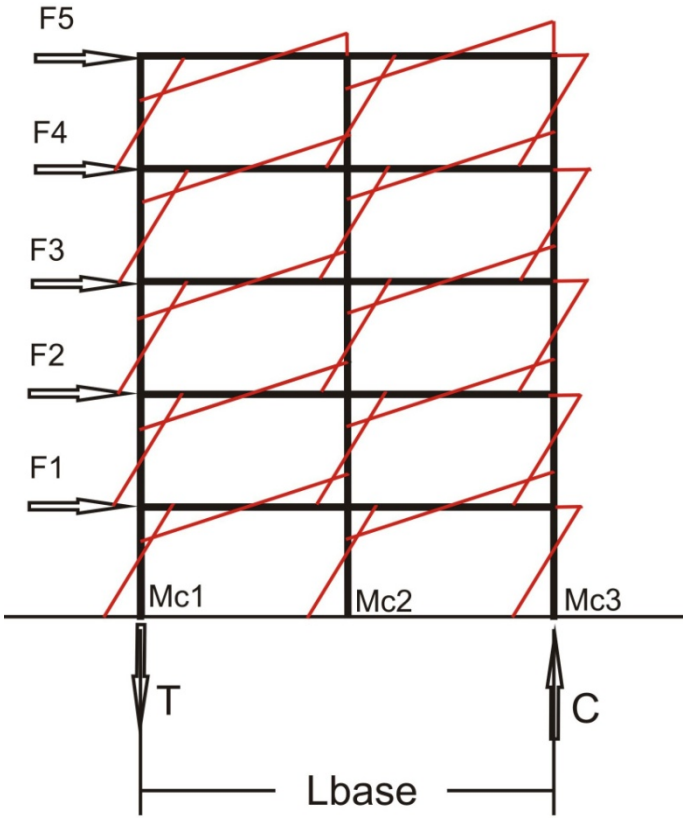

Figure 8-4 Seismic moments from DDBD lateral forces

- Moments capacities at the column bases of the structure may be chosen by the designer, with the condition that the resulting moments on the structure are in equilibrium with the applied forces. The selection of this moment capacity needs to consider the design criterion that does not allow a soft story mechanism. In particular, for the analysed buildings a moment capacity equal to zero was selected to represent base-pined conditions.

- Given the symmetry of shear forces induced in beams by seismic forces, seismic induced tension (T) and compression (C) axial forces are considered only at the external columns of the frames (***Figure 8-4***).

- Seismic and gravity moments on beams are not combined, as proposed by Priestley et al. [2007]; beam design is based on seismic moments only. When combining gravity and seismic forces during design, structural members may be stronger than expected, increasing lateral strength. An enhanced lateral strength will be reflected on a decrease in the overall displacement ductility demand; this approach is considered to avoid over-prediction of ductility demand. Besides, the addition of seismic and gravity moments increases the required section strength and reduces the response drift levels below the target values.

- Moment demands on the columns above and below each floor are supposed to be equal. In the same way, design forces on beams of a given floor are also equal. Therefore, beam geometry is the same at a specific floor level. In particular, for the analysed buildings, beam and column geometries are kept constant for the complete building.

Once the base shear has been determined from DDBD principles, the design process continues as summarized in the steps below:

i. Compute the Total Overturning Moment (OTM)

$$OTM = \sum F_i \cdot H_i \qquad \text{Equation 8-12}$$

ii. Compute seismic induced tension and compression axial forces

$$OTM = \sum Mc_j + T \cdot L_{base} \qquad \text{Equation 8-13}$$

where, Mc_j , are the base columns moments or the j column. Therefore:

$$T = \left(OTM - \sum Mc_j\right) / L_{base} \qquad \text{Equation 8-14}$$

iii. Determine the storey shear forces:

$$V_{s,i} = \sum_{k=i}^{n} F_k \qquad \text{Equation 8-15}$$

Meaning that to obtain the shear force at one level, it is required to add all forces applied from that level up to the roof level.

iv. Compute shear force on beams:

$$V_{Bi} = T \cdot \frac{V_{s,i}}{\sum_{k=i}^{n} V_{s,i}} \qquad \text{Equation 8-16}$$

v. Compute design forces for columns by simple forces equilibrium

8.5 Determination of sections capacities

To determine section capacities, traditional design methods are used. To determine connection capacity, the process outlined in *Figure 8-5* needs to be followed.

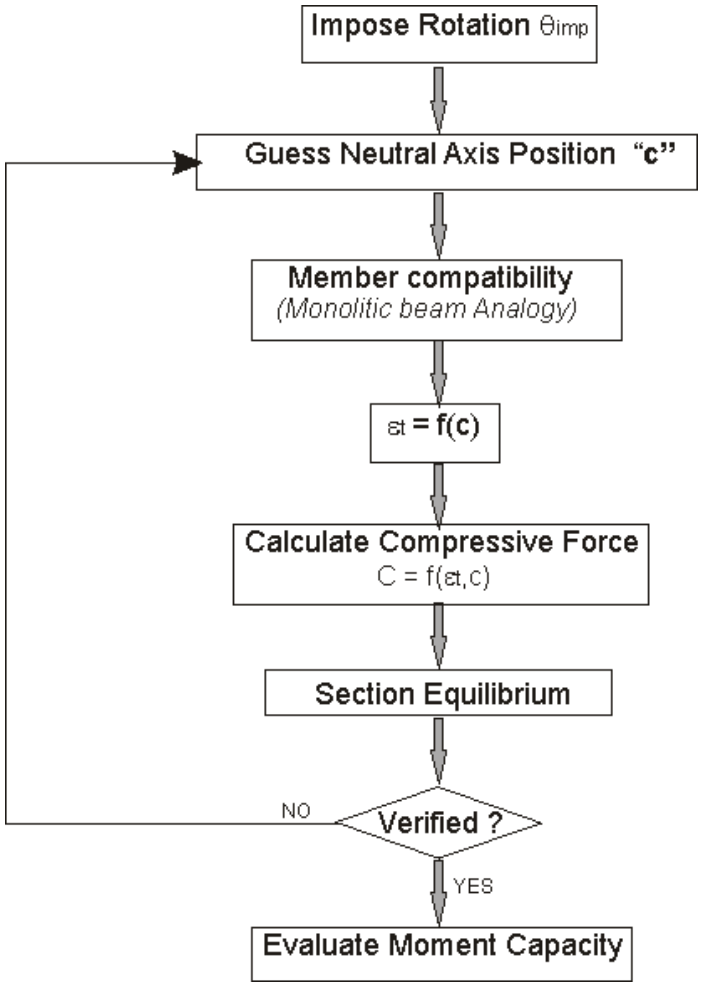

Figure 8-5 Evaluation of connection moment capacity [Pampanin et al., 2001]

Where θ_{imp} corresponds to the connection rotation in radians. As explained in Chapter five, θ_{con} is one of the four components of the total drift of the structure (***Equation 8-17***). Then, it is required to compute the contributions to the design drift of each one of the components in order to compute the connection moment capacity at that drift level.

$$\theta_D = \theta_{con} + \theta_j + \theta_b + \theta_c \qquad \text{Equation 8-17}$$

8.6 Design of cases of study

The 3-storey building and the 5-storey building were designed following the process previously summarized. The configuration and geometry used during the design are shown in *Figure 8-6*.
Both buildings were analysed considering two values of equivalent viscous damping. First, the current ξ = 2% value was used, then a value computed with the proposed formula at 2.5% of inter-storey drift was applied, i.e. ξ = 6.5% of critical damping.

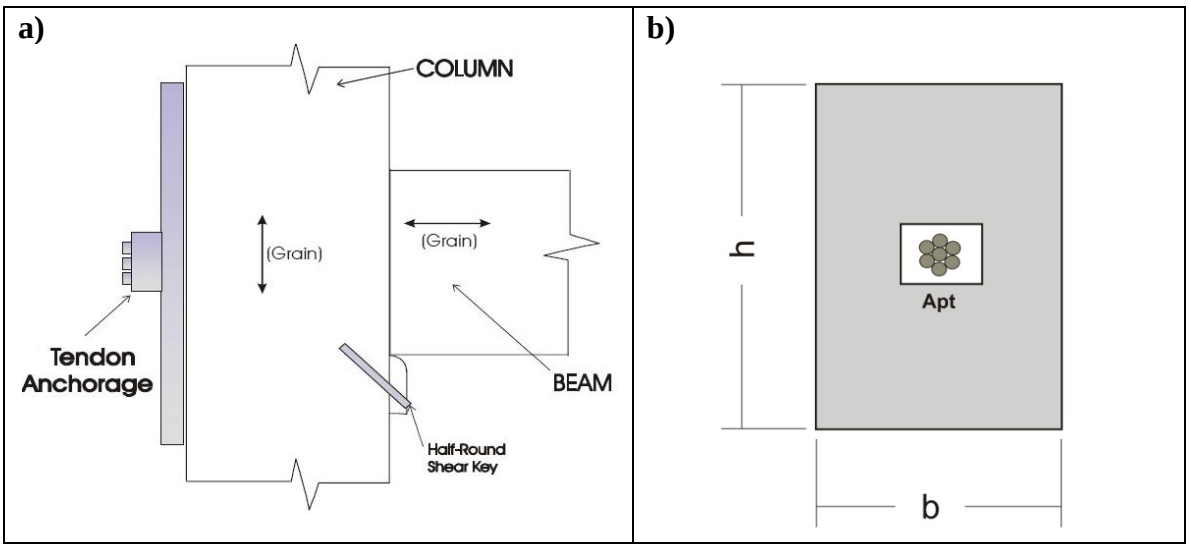

Figure 8-6 a) Beam-column configuration (Courtesy of M. Newcombe) b) Beam cross section

In *Table 8-2* it is possible to recognize an important difference in design forces when ξ = 2% or ξ = 6.5% is used. In particular, for both buildings when ξ = 2% is used, the beam design moment is around 64% greater than the moment obtained when ξ = 6.5% is applied. The overestimation of design forces will be reflected in the size and reinforcement of beams and columns required.

Table 8-2 Design values for a 3-storey building and a 5-storey building

Parameter	3-Storey building		5-Storey building	
	ξ = 2%	ξ = 6.5%	ξ = 2%	ξ = 6.5%
Effective period: T_e (sec)	1.78	2.28	2.29	2.94
Effective stiffness: K_e (kN/m)	2248	1370	2271	1381
Base shear: V_B (kN)	420	256	546	332
Seismic coefficient: C_d (g)	0.20	0.12	0.16	0.11
Overturning moment: M_o (kNm)	3223	1964	6485	4540
First floor beam moment: M_b(kNm)	134.3	81.8	174.6	106.1

As previously mentioned, it is important to quantify the contributions to the design drift of each one of the rotational components in order to compute the connection moment capacity at that specific deformation. To initialise the design process, θ_{imp} is required. In previous design guides [Newcombe, 2008a], it has been indicated that 50% of the total drift of the structure could be assigned to the connection rotation to compute an estimated value of the moment capacity of the connection. However, the deformation of the connection depends strongly on the connection stiffness, beam and column geometry, and post-tensioning force applied, among others. A wrong assumption of the contribution of the connection rotation to the total drift may lead to an unconservative design. To illustrate the importance of computing properly the contribution of each deformation component, a detailed analysis for a 500mm wide by 600mm deep beam has been included (A_{pt} = 990mm^2). *Figure 8-7* shows the contribution of each one of the components to the total drift. For this particular beam, there is a dominant contribution of the connection rotation over other components. Contribution to drift of joint-panel, beam and column are similar.

Figure 8-8 shows the percentage of contribution for three design limit states. In the case of Ultimate Limit State, the contribution of the connection rotation to the total structure drift is around 80%. In this particular case, computing the moment capacity assuming 50% of the total rotation occurs in the connection implies an underestimation of the connection moment capacity of around 10%, which is on the conservative side. This difference is basically due to an underestimation of the gap opening, what implies a lower tendon force and a greater neutral axis depth.

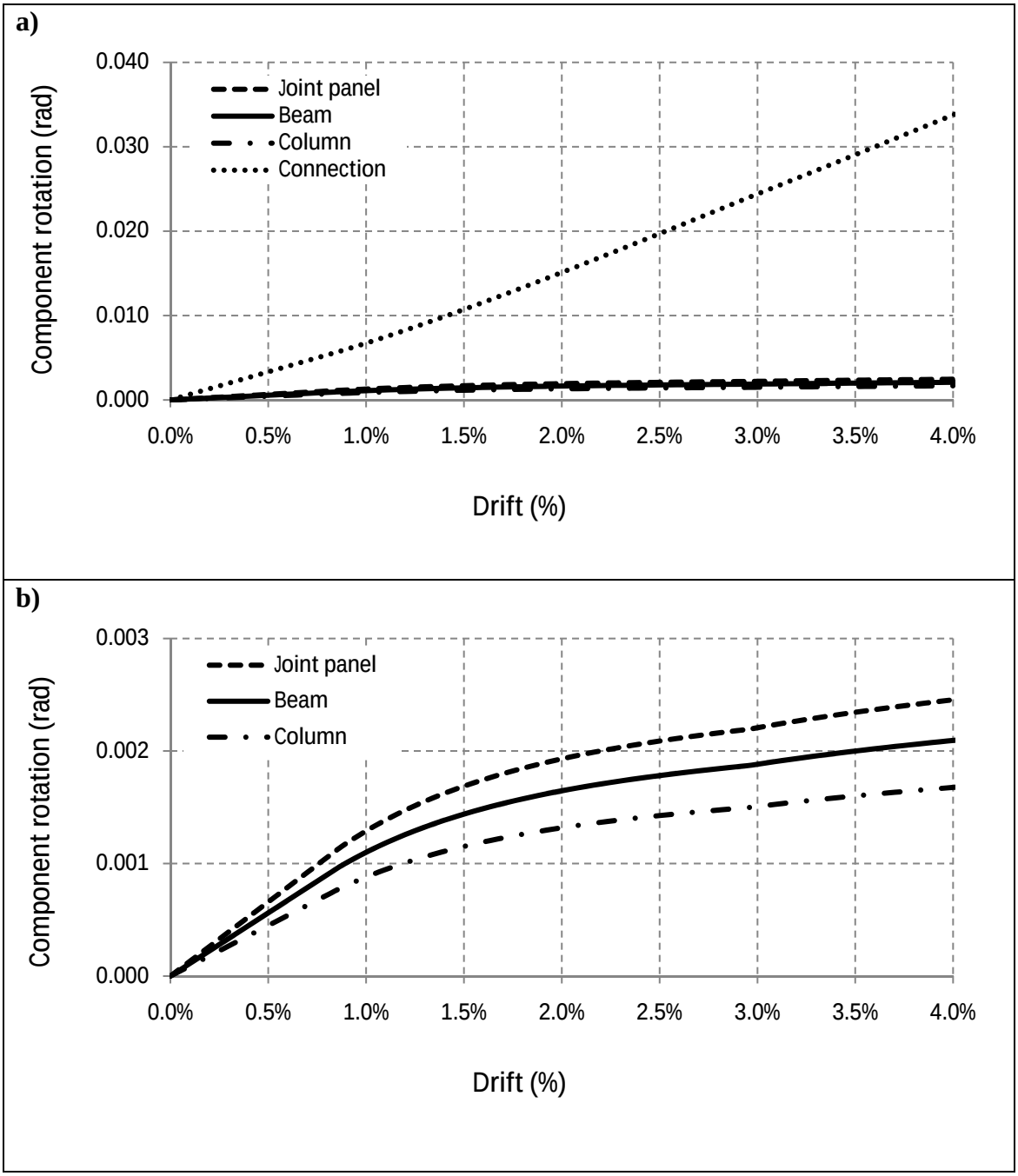

Figure 8-7 Contributions to drift of each one of the components

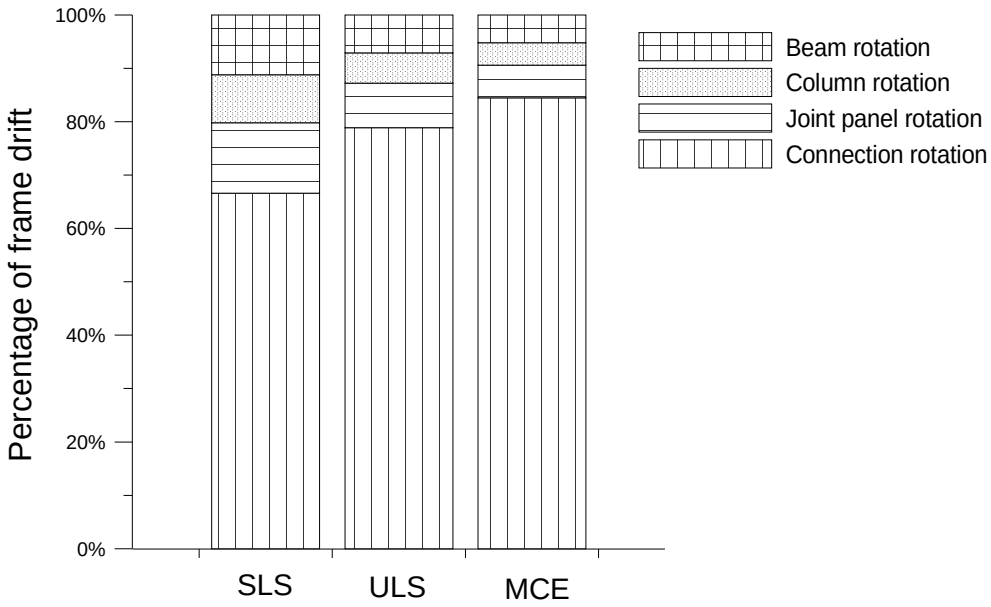

Figure 8-8 Contributions to drift of each one of the components at design limit states

The design was carried out considering the correct connection rotation, and the design parameters used are summarized in *Table 3-1* and *Table 3-2*.
For all beams, 60% of initial post-tensioning force was considered, additionally it was decided to keep members in the elastic range until 2.5% drift, i.e. timber strain (at the column face of beam-column connections) was checked to be close to the crushing strain at ultimate limit state (*Figure 8-9*). The previous consideration is a design choice, if timber crushing is allowed to happen at ULS, it would have an impact on component contribution to drift. Besides, timber crushing may lead to a loss in post-tensioning force, affecting system lateral stiffness and moment capacity of members; hence it needs to be considered during design.

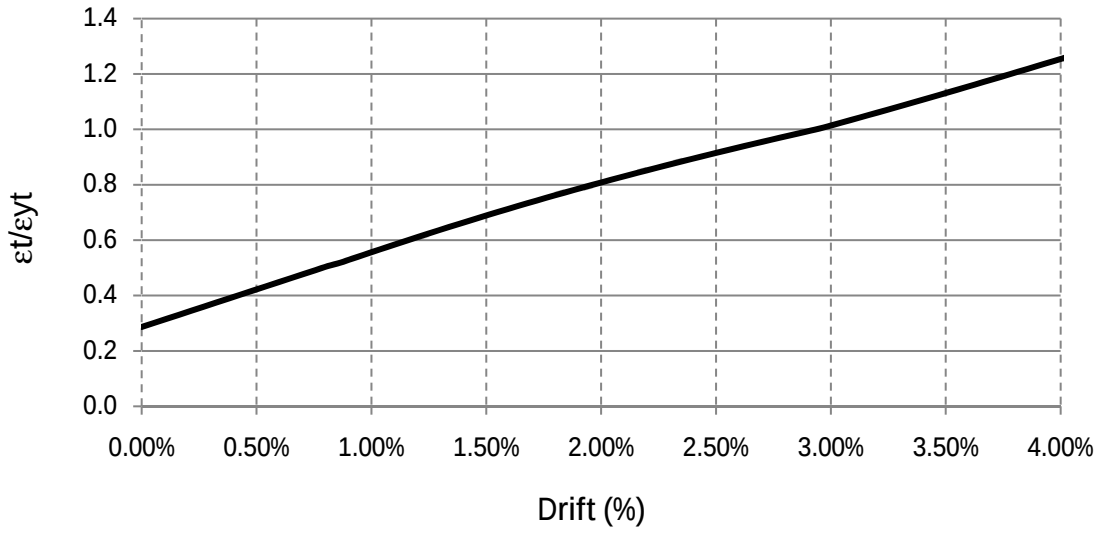

Figure 8-9 Normalized timber strain versus drift

Required section sizes and connection moment capacities are shown in *Table 8-3*. Design was performed according to New Zealand Standards: NZS4357:1995, NZS3603:1999, NZS1170:2004, and supported with Buchanan [2008]. As it was expected, the use of equivalent viscous damping, ξ = 2% of critical, produced an increase in the required size of beams and columns in some cases.

Table 8-3 Required beam and column sections for a 3-storey building and a 5-storey building

3-storey building		ξ = 2%	ξ = 6.5%
Beam depth	h_b (mm)	600	500
Beam width	b_b (mm)	500	400
Post-tensioning area	A_{pt} (mm^2)	990	990
Connection moment capacity at 2.5% drift	øMn (kNm)	165	101
Column depth	h_c (mm)	600	500
Column width	b_c (mm)	500	400
5-storey building		ξ = 2%	ξ = 6.5%
Beam depth	h_b (mm)	700	600
Beam width	b_b (mm)	500	500
Post-tensioning area	A_{pt} (mm^2)	990	990
Connection moment capacity at 2.5% drift	øMn (kNm)	211	165
Column depth	h_c (mm)	700	600
Column width	b_c (mm)	500	500

8.7 Modelling parameters

As before, the time-history analyses were performed using the finite element modelling program RUAUMOKO [Carr, 2008]. The numerical models considered the use of a constant equivalent viscous damping and the use of the secant stiffness matrix. It was decided to use a non-linear elastic rotational-spring modelling approach (*Figure 8-10*) since it has been proven to provide good results (see Chapter six). Therefore rotational-springs were calibrated to represent the analytical moment-rotation curve. *Figure 8-11* shows the moment-rotation curve for the 600mm deep beams defined in *Table 8-3*.

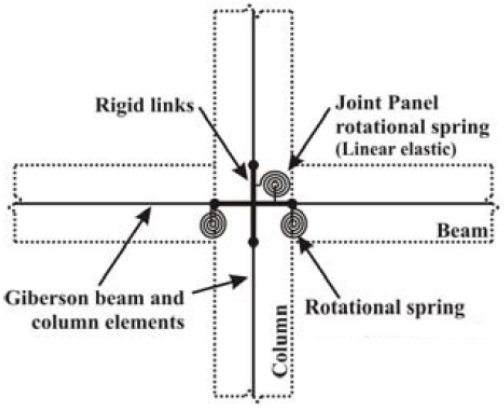

Figure 8-10 Rotational-spring modelling [Newcombe, 2010d]

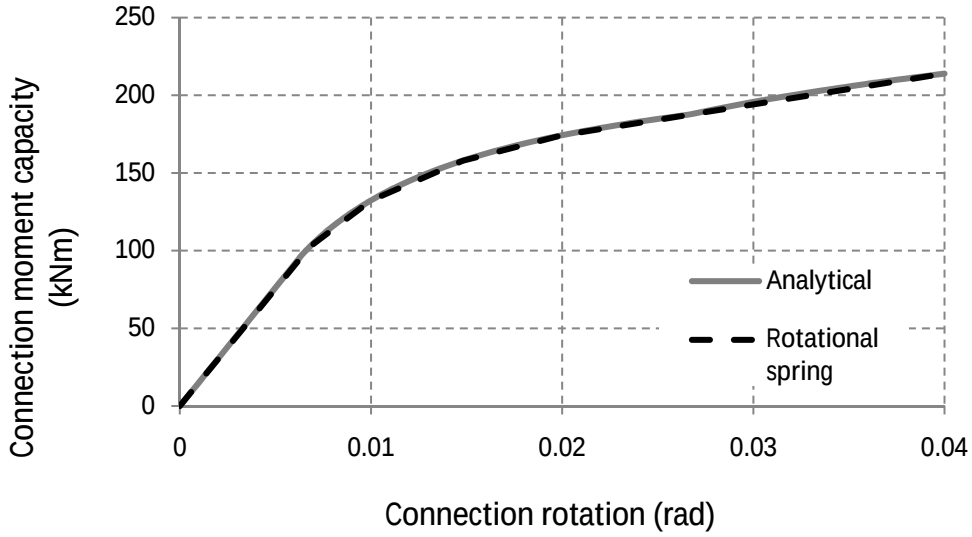

Figure 8-11 Elastic-rotational-spring calibration to analytical moment-rotation curve

At this point it is important to mention limitations related to the use of a rotational-spring based model. One of them is the incapability to model the effects of beam elongation. Beam elongation is an effect mainly localized on first floors of buildings.

The increase of beam length (or bay) produces an increase in shear and moment demand on columns as well as an increase in the demand over the flooring system and a significant increase of beam axial forces, with the most important effect being the strength demand increase on beams.

This increase of expected beam strength could produce an inversion of the hierarchy of strength between beams and columns, meaning that the desired strong-column, weak-beam mechanism may not happen. Effects of beam elongation on concrete structures have been analysed by Peng et al. [2006], which showed that the increase of beam elongation on concrete buildings has to be considered during analysis and modelling, as a significant increase of beam strength was obtained. The strength enhancement reached by Peng was around 25% over the moment capacity computed considering over-strength factors ($ø_o$ = 1.25). On the other hand, Newcombe et al. [2010c] have shown that beam elongation is not a problem for post-tensioned timber buildings. Newcombe's results show that not only there is not a significant increase of force demand on columns or an increase of beam capacity, but there is also an important reduction in slab cracking in comparison to equivalent concrete structures. The reason is that for a given rotation, the elongation induced by a gap opening at the connection for a post-tensioned timber system is smaller than the elongation obtained in a concrete system. Therefore, the exclusion of beam elongation effects during post-tensioned timber building loading have only a minor influence on final results.

8.8 Numerical results

Time-history analyses were performed to the 3-storey and 5-storey buildings of the example using a unique member size to directly compare the influence of the equivalent viscous damping selected. The seismic records included were the same mentioned in Chapter three. The numerical response obtained for each one of the considered seismic records was compared to the results obtained using DDBD approach. The average of the dynamic response for the earthquakes considered is also included. Results are discussed below:

i. Lateral displacement and drift

In general, for the analysed cases, it is possible to say that the lateral displacements obtained are in the range of the values expected. Additionally, as expected, an important difference in lateral displacement was obtained depending on the value of equivalent viscous damping used. Independent of the damping value used, the displacement profile obtained using DDBD for 3-storey and 5-storey buildings were similar to the average of values computed using time-history analysis. DDBD seems to provide a conservative design. Lateral displacements and drifts are presented in ***Figure 8-12*** and ***Figure 8-13*** for 3-storey and 5-storey analyses, respectively.

ii. Floor acceleration and acceleration amplification

The equivalent viscous damping value used had a small influence on floor acceleration, there were not large differences between values obtained using ξ = 2% or ξ = 6.5%. For the 3-storey building, the maximum acceleration amplification (floor acceleration over ground acceleration) was 2.7 for ξ = 2% and 2.1 for ξ = 6.5%. Similarly, for the 5-storey building the maximum acceleration amplifications obtained were 2.2 times the base acceleration for ξ = 2% and 1.9 times the base acceleration for ξ = 6.5%. Peak floor accelerations and acceleration amplifications achieved are shown in ***Figure 8-14*** and ***Figure 8-15*** for 3-storey and 5-storey analyses, respectively.

iii. Base shear and overturning moment

In the case of base shear and overturning moment, the difference on values obtained using an equivalent viscous damping ξ = 2% or ξ = 6.5% becomes significant. In the case of the 3-storey buildings there was an increase of 30% on base shear and overturning moment when the smaller damping value was used. Similarly, for the 5-storey building the increase was 22% and 29% respectively. The use of DDBD in this case also seems to be accurate in order to compute design forces over the structure. Base shear and overturning moment for the analysed cases are displayed in ***Figure 8-16*** and ***Figure 8-17*** for 3-storey and 5-storey analyses, respectively.

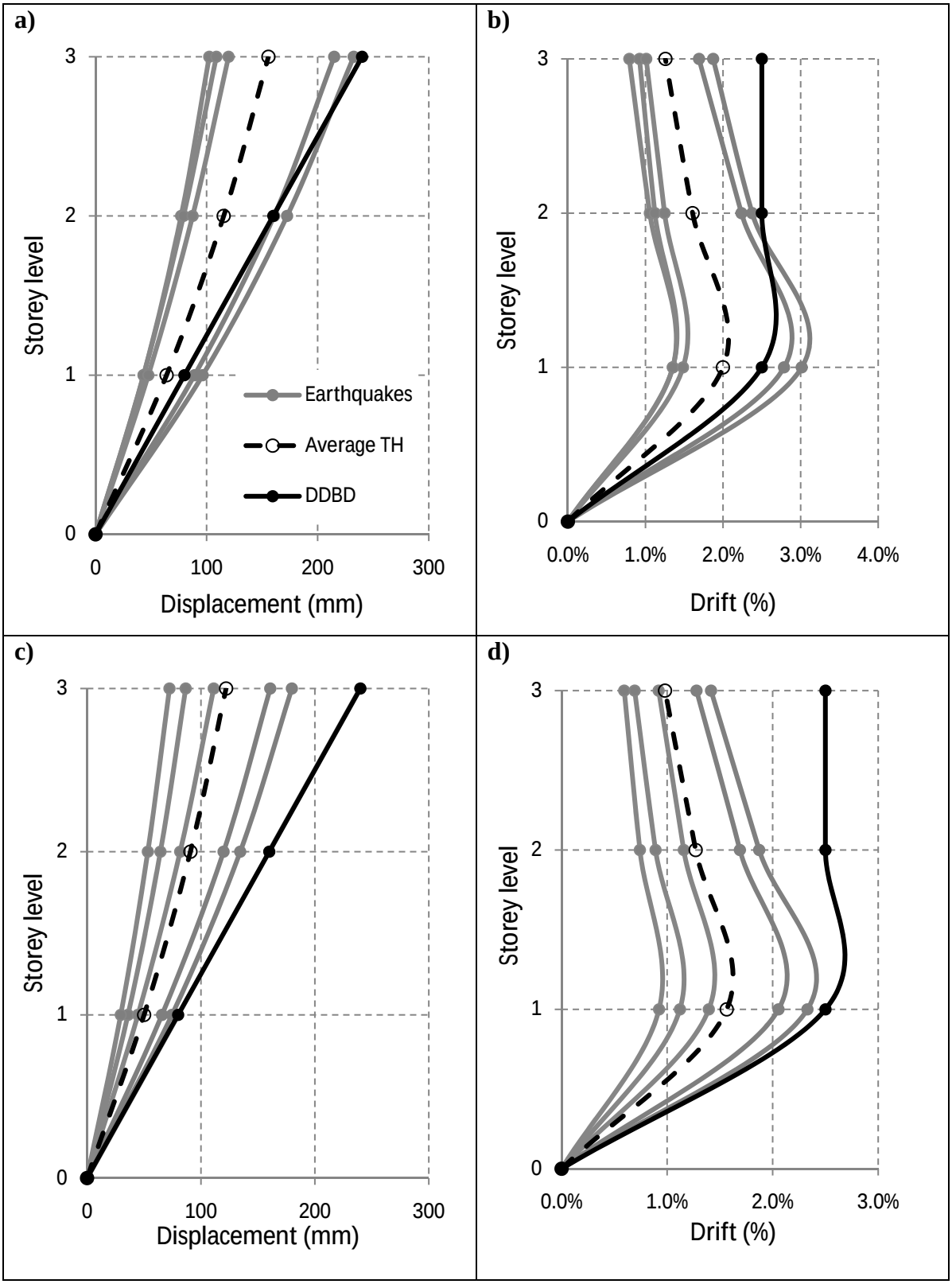

Figure 8-12 Time-history analyses compared to DDBD, 3-storey building: a) Floor displacement ξ = 2% b) Inter-storey drift ξ = 2% c) Displacement ξ = 6.5% d) Inter-storey drift ξ = 6.5%

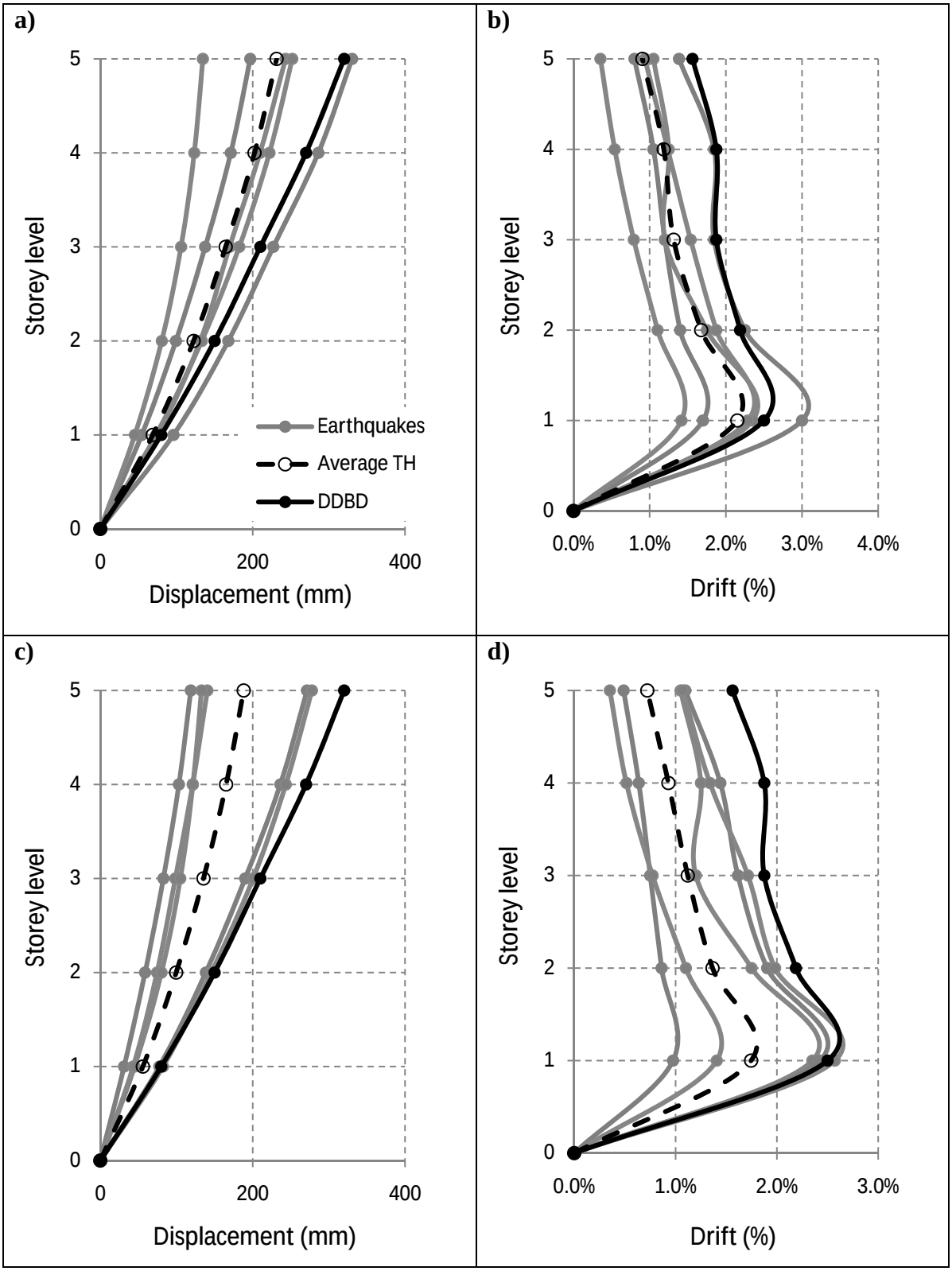

Figure 8-13 Time-history analyses compared to DDBD, 5-storey building: a) Floor displacement ξ = 2% b) Inter-storey drift ξ = 2% c) Displacement ξ = 6.5% d) Inter-storey drift ξ = 6.5%

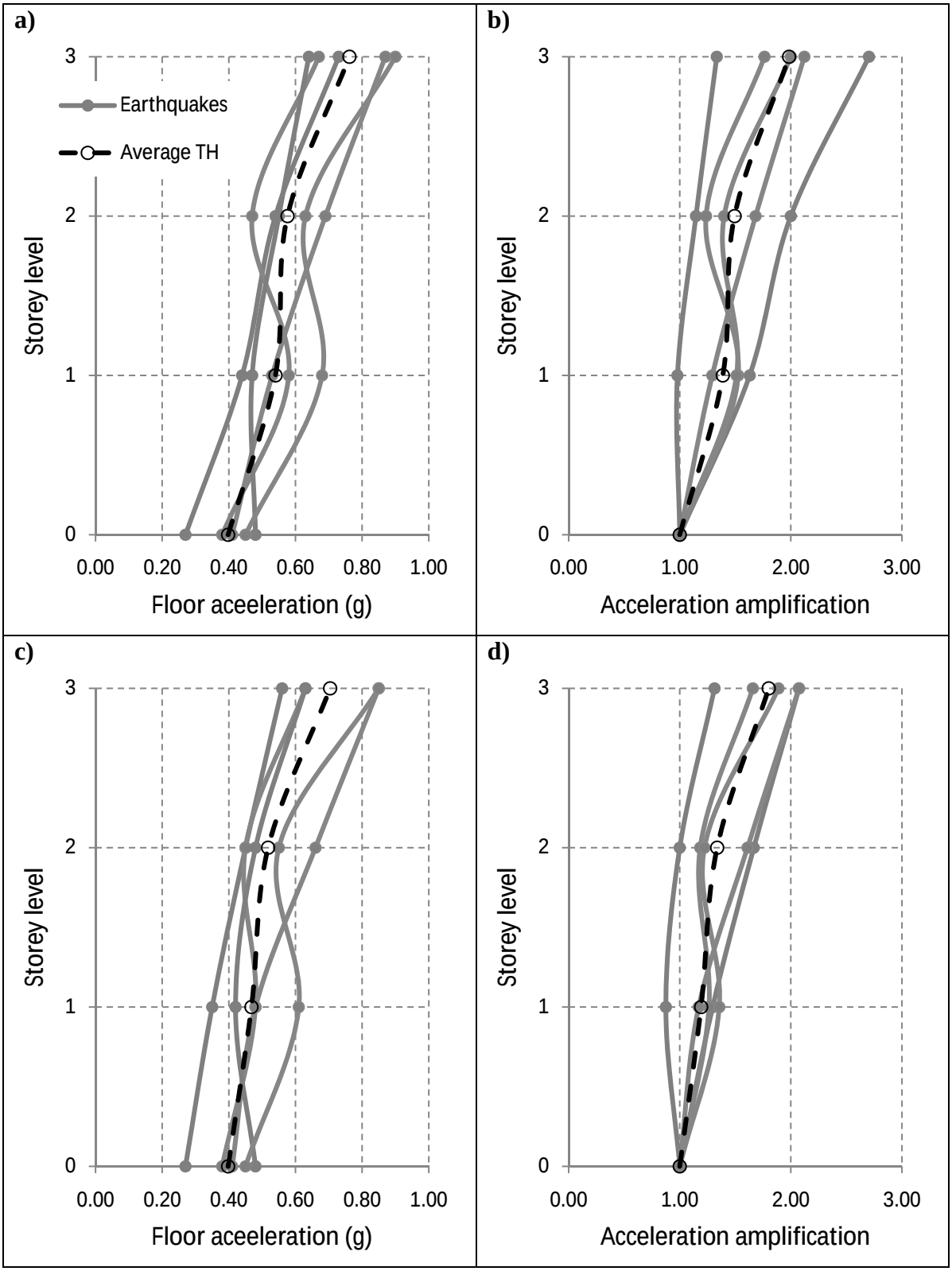

Figure 8-14 Time-history analyses, 3-storey building: a) Floor acceleration ξ = 2% b) Acceleration amplification ξ = 2% c) Floor acceleration ξ = 6.5% d) Acceleration amplification ξ = 6.5%

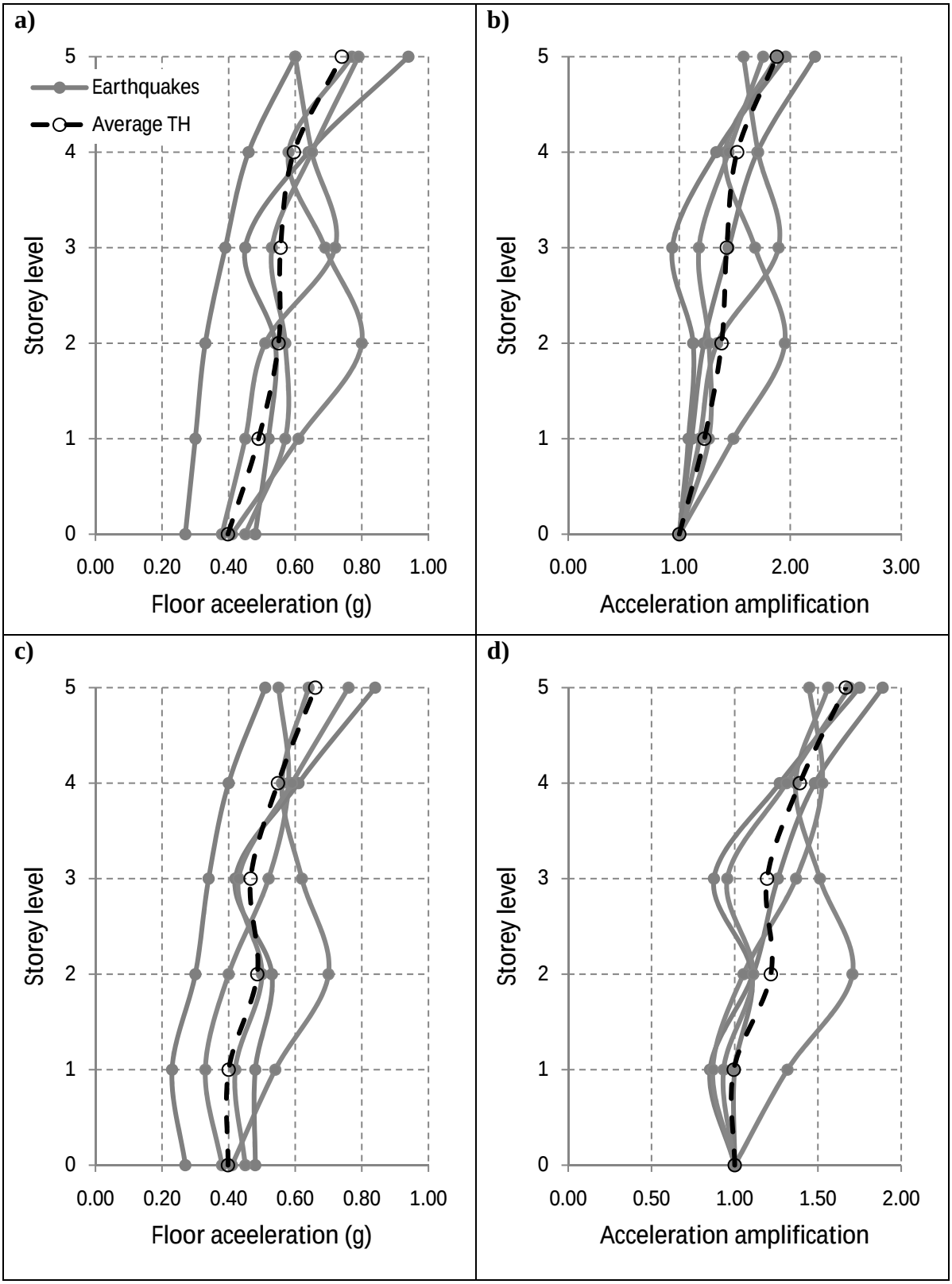

Figure 8-15 Time-history analyses, 5-storey building: a) Floor acceleration ξ = 2% b) Acceleration amplification ξ = 2% c) Floor acceleration ξ = 6.5% d) Acceleration amplification ξ = 6.5%

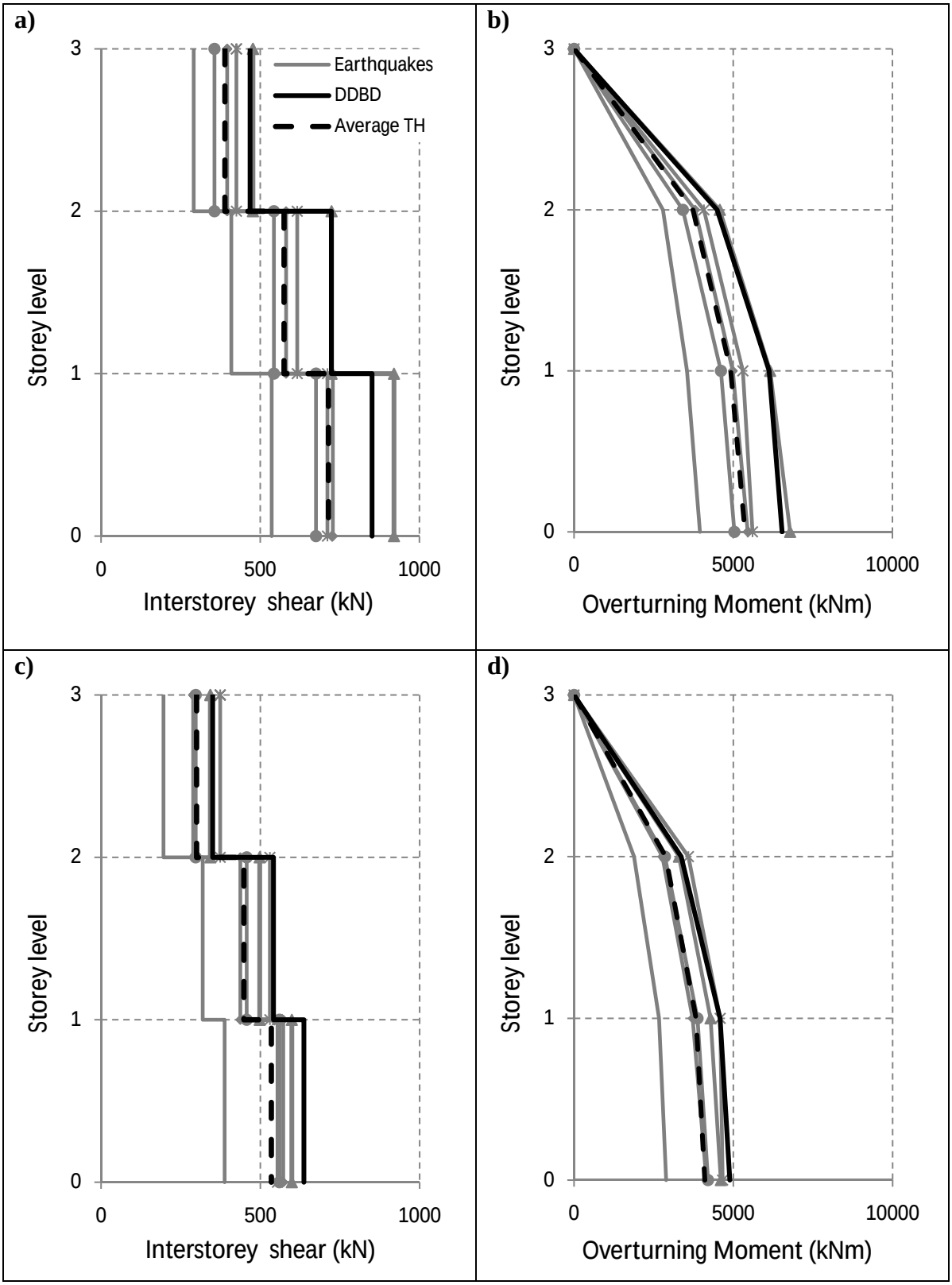

Figure 8-16 Time-history analyses compared to DDBD, 3-storey building: a) Interstorey shear ξ = 2% b) Overturning moment ξ = 2% c) Interstorey shear ξ = 6.5% d) Overturning moment ξ = 6.5%

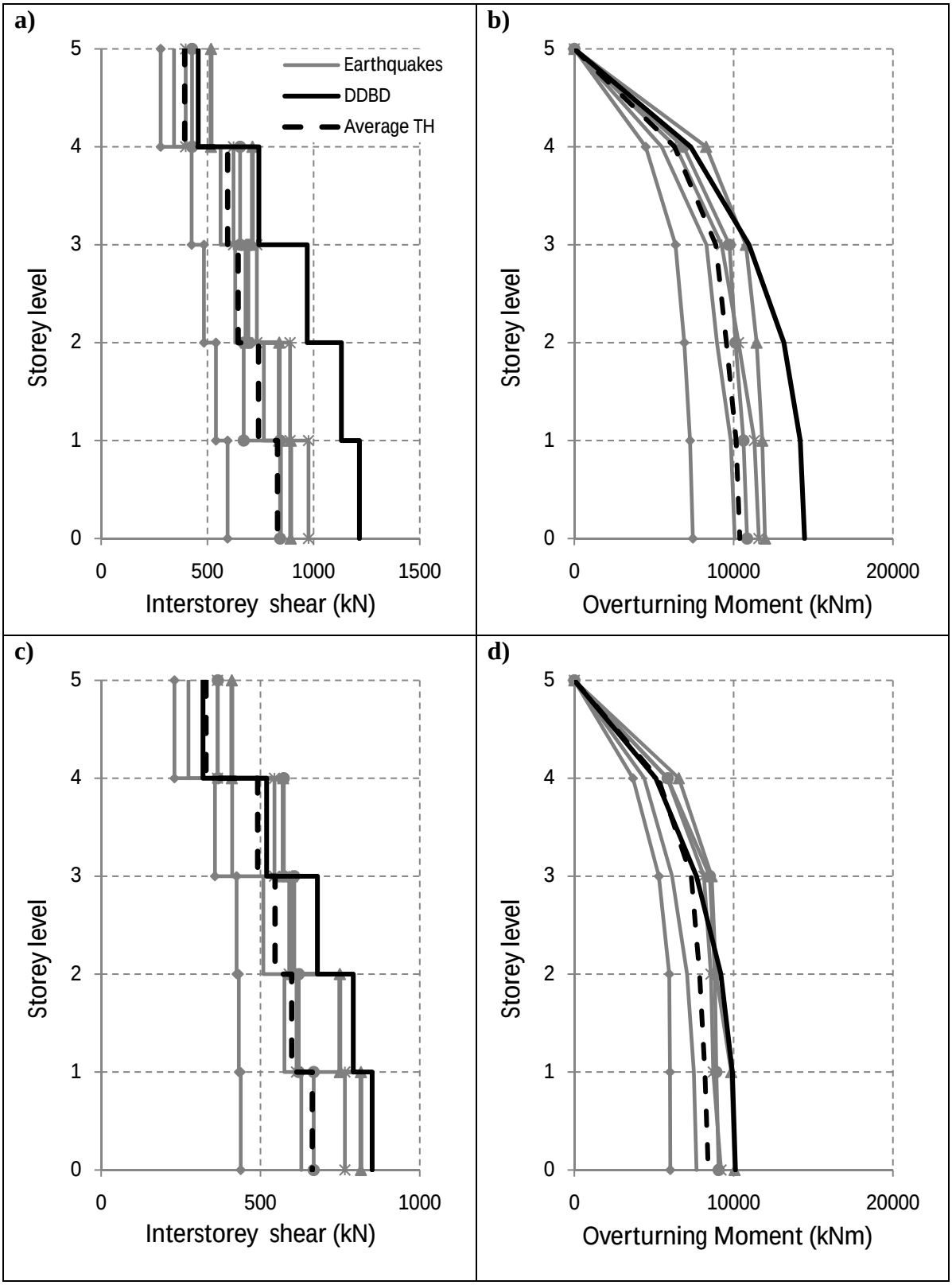

Figure 8-17 Time-history analyses compared to DDBD, 5-storey building: a) Interstorey shear ξ = 2% b) Overturning moment ξ = 2% c) Interstorey shear ξ = 6.5% d) Overturning moment ξ = 6.5%

Finally, Table 8-4 shows the moment requirement, during time-history analysis, at the first level beam-column joint. The table includes the values obtained for both buildings using ξ = 2% and ξ = 6.5%. Depending on the seismic record considered, moment demand (M*) based on equivalent viscous damping ξ = 2% was 5% to 43% greater than the moment demand based on ξ = 6.5%.

It is also possible to notice that in general, moment capacity (ϕM_n) for ξ = 2% is considerably greater than the average moment demand (56% on average). For ξ = 6.5% moment capacity is 27% greater than the average moment demand. In theory, moment demands and moment capacities should be similar, because buildings were designed for a target drift value. However, differences between earthquake spectra and design spectra plus section overstrength during design are the reason for the mentioned differences. For most of the earthquake tests the maximum drift level was less than the target design (θ_d = 2.5%), therefore a connection moment demand was expected to be smaller than moment capacity. During three earthquakes the drift exceeded the target drift limit; the maximum drift reached was around 3%. In this case a moment demand greater than the moment capacity was expected to happen, nevertheless, moment demand was still smaller than moment capacity. This may be the result of moment redistribution and redundancy.

Table 8-4 First level moment capacity (ϕM_n) and connection moment demand during time-history analysis

Nº Level	ξ (%)	øMn (kNm)	First level connection moment demand (KNm)				
			L. Prieta	Kobe	Northridge	Corralitos	Sylmar
3	2.0	165	96	77	127	93	92
3	6.5	101	82	61	89	83	83
5	2.0	211	129	158	165	151	171
5	6.5	165	105	134	157	131	140

8.9 Conclusions

- Analyzing the frame with a combination of DDBD and Monolithic Beam Analogy showed that an equivalent damping value of ξ = 6.5% over the previously assumed ξ = 2%, may produce an important savings on member sizing.

- Dynamic response of post-tensioned timber buildings can be accurately estimated through the utilization of DDBD. In general DDBD design provides a conservative result.

Chapter Nine: **CONCLUSIONS AND RECOMMENDATIONS FOR FUTURE RESEARCH**

Introduction

- Seismic requirements are becoming more demanding as time goes on, and performance based design is moving forward to increase buildings capacity of outstanding seismic events.
- High performance structural systems are required to minimize damage during earthquakes in order to avoid business downtime that leads to financial losses.
- Structural collapse is considered unacceptable in contemporary structures.
- The proposed structural system combines the increasing necessity for environmentally friendly solutions with high levels of seismic performance and minimal damage following seismic events.

Recent investigation into behaviour of post-tensioned timber buildings

- Post-tensioned timber systems have been analytically and numerically studied and responses to high lateral demand of beam-column, wall, and column connections have been verified for numerous experimental quasi-static subassembly tests.
- Extensive experimental results have proven low levels of damage and significant re-centering capacity as a result of using post-tensioned connections.

Shake-table test of 3-storey and 5-storey post-tensioned timber buildings

- Shake-table tests were performed on post-tensioned timber frame buildings, confirming their outstanding seismic response. Minimal levels of damage, no residual deformations, and low levels of post-tensioning force losses were some of the main results obtained during dynamic testing.
- Sinusoidal tests were carried out and equivalent viscous damping computed. The obtained values corresponded to elastic damping values appropriate for the analyses of post-tensioned timber buildings with no added dissipater devices or column armouring.

- Area-based damping values were not considered valid at drift values smaller than 1%. At greater than 1% of lateral drift, area-based damping exhibited a good agreement with one-cycle decay damping.

Quasi-static testing of a post-tensioned timber frame

- Quasi-static tests were also performed and a 3-storey post-tensioned timber frame was taken up to 4.5% of inter-storey drift, considering three levels of post-tensioning force. Again the high capacity of the system at large lateral deformations with minimal damage was proved.
- Frame elongation was verified to not represent a significant problem on post-tensioned timber frames. Frame elongation measured could be easily accommodated by minimal slab cracking.
- Area-based damping obtained during quasi-static testing showed a reasonable similitude with damping values obtained during dynamic testing.

Main contributors to the inter-storey drift

- There are four main contributors to inter-storey drift; connection rotation, joint-panel shear deformation, beam rotation, and column rotation.
- Influence of post-tensioning force was proven to be insignificant over the percentage of contribution of the four components. In general for different levels of post-tensioning forces the percentages of contribution obtained for the four components to the drift were similar.
- Connection rotation (gap opening) was identified as the major contributor to inter-storey drift in normal circumstances at ULS. At SLS, the major contributor to inter-storey drift depends on the particular considered configuration of the beam-column joint.
- The inclusion of column armouring may imply that at SLS the greater contribution to drift is controlled by the joint-panel zone rotation.

Modelling monotonic and dynamic response of post-tensioned timber frames

- Satisfactory predictions were achieved when dynamic response was modelled using linear-rotational-springs combined with an equivalent viscous damping value.
- Values obtained through numerical models were compared to dynamic responses obtained from shake-table tests. In general values obtained with numerical analyses were conservative compared to experimental dynamic responses.
- Non-linear elastic rotational-spring models were the easiest and fastest numerical model to implement. No evident benefit, specifically, no more accurate dynamic prediction response, was achieved when more complex numerical models were used, such as multi-springs (axial elastic springs) or inelastic spring models, to represent the post-tensioned only frames. The advantage of the multi-axial spring model would be on the local behaviour allowing for example a more accurate computation of the neutral axis position.

Sensitivity analysis of modelling and frame configuration

- Sensitivity analyses were carried out to analyse the influence of the stiffness matrix used on Rayleigh damping models. It turned out that given that post-tensioned timber buildings remain primarily elastic and variations of lateral stiffness are not significant, the dynamic response obtained was independent of the stiffness matrix used.
- Post-tensioning force was also checked out, and even when a change of it means a small variation of lateral stiffness, it may imply a change of the dynamic response.
- Incorporation of column armouring increases dramatically the initial lateral stiffness. The increase in lateral stiffness in a frame without armouring reduces quickly once the decompression point is reached. At ULS, the increase of lateral stiffness may still be significant. Therefore, the inclusion of steel column armouring may lead to a considerable change of dynamic response.

Post-tensioned timber frame analysis and design

- The design method utilized, the DBDD, proved to be consistent and easy to follow for post-tensioned timber frame structures.
- The advantages of knowing the equivalent viscous damping to be used with DDBD methods provided the capacity of comparing that design approach with numerical models.
- DDBD was found to provide a good design applicable to post-tensioned timber frame buildings. Monolithic beam analogy was then used to compute connection moment capacity to complete the design process.

Recommendations for future research

- Incorporation of column armouring should be investigated through dynamic testing. It is expected that adding column armouring would result in an increase of frame lateral stiffness, thus reduction of lateral displacement demand. On the other hand column armouring could potentially reduce the amount of damping as a consequence of relocation of the neutral axis and changes on timber strain patterns.

- An investigation of higher mode responses needs to be included when considering medium-rise and high-rise buildings. Damping values computed in Chapter three considered only the first mode response.

- The dynamic response of post-tensioned timber walls needs to be studied. Post-tensioned walls have proved to be an effective structural alternative due to levels of lateral stiffness and energy dissipation [Iqbal *et al.*, 2007]. Computation of damping values for wall-based structural systems is required in order to estimate earthquake response of these systems.

REFERENCES

Amaris, A., Pampanin, S., Bull, D., & Carr, A. (2008). *Experimental performance of hybrid frames systems with non-tearing floor connections*. Proceedings 14th World Conference in Earthquake Engineering, WCTE, Beijing, China.

Baumert, K. A., Blanchard, O., Llosa, S., & Perkaus, J. F. (2002). *Building on Kyoto Protocol: Options for protecting our environment* (No. ISBN 1-56973-524-7). Washington: World Resourses Institute.

Blandon, C. A., & Priestley, M. J. N. (2005). *Equivalent viscous damping equations for Direct Displacement-Based Design*. Journal of Earthquake Engineering, 9(2), pp 257-278.

Buchanan, A. H. (2008). *Timber design guide* (Third Edition ed.). Christchurch, New Zealand: New Zealand Timber Industry Federation

Buchanan, A. H., Deam, B. L., & Dean, J. A. (1991). *Multi-Storey timber buildings.* Proceedings of Institute of Professional Engineers New Zealand Conference, Auckland, New Zealand.

Buchanan, A. H., Pampanin, S., Newcombe, M. P., & Palermo, A. (2009). *Non-conventional multi-storey timber buildings using post-tensioning.* Proceedings of the 11th International Conference on Non-conventional Materials and Technologies (NOCMAT 2009), Bath, UK.

Cattanach, A. & Pampanin, S. (2008). *21st century precast: The detailing and manufacture of New Zealand's first multi-storey PRESSS building*. Proceedings of the 2008 New Zealand concrete industry conference. 2-4 October, 2008. Rotorua, New Zealand.

Carr, A. (2008). RUAUMOKO (Inelastic Dynamic Analysis Software). Christchurch, New Zealand: Department of Civil Engineering, University of Canterbury.

Ceccotti, A. (1990). *Structural behaviour of timber constructions in seismic zones*. Florence, Italy: Commission of the European Communities, Universita de Firenze.

Chopra, A. K., & Goal, R. K. (2001). Direct Displacement-Based Design: *Use of inelastic vs. elastic design spectra*. Earthquake spectra, 17(1), pp. 47-65.

Cusiel, M. (2009). *The effect of joint flexibility on the seismic response of timber frames.* 3rd professional year research project, University of Canterbury, Christchurch.

Cusiel, M., Newcombe, M., Pampanin, S., & Buchanan, A. (2010). *The effect of joint flexibility on the seismic response of post-tensioned LVL frames.* Paper presented at the ECEE.

Durham, J. P. (1998). *Seismic response of wood shear walls with oversized oriented strand board panels.* Masters Dissertation, University of British Columbia, Vancouver, Canada.

Durham, J. P., Lam, H. G. L., & He, M. (1999). *Seismic response of shear walls with oversized sheathing panels.* Proceedings 8th Canadian Conference on Earthquake Engineering, Vancouver, Canada.

Dwairi, H., & Kowalsky, M. (2004, August 1-6, 2004). *Investigation of Jacobsen's equivalent viscous damping approach as applied to Displacement Based Seismic Design.* Proceedings 13th World Conference on Earthquake Engineering, Vancouver, Canada.

EC8 Euro Code 8, (2003) Final draf to Euro Code 8: *Design of structures for earthquake resistance*, European Committee for Standardization, Bruxelles

Fairweather, R. H. (1992). *Beam-column connections for multi-storey timber buildings.* Masters Dissertation, University of Canterbury, Christchurch, New Zealand.

Filiatrault, A., ASCE M., & Folz, B. (2002). *Performance-based design of wood framed buildings*. Journal of Structural Engineering, 128(1), pp. 39-47.

Foliente, G. C. (1995). *Hysteresis modeling of wood joints and structural systems.* Journal of Structural Engineering, 121(6), pp. 1013-1022.

Ghee, A. B. (1985). *Seismic shear strenght of circular bridge piers*, Research Report, Department of Civil Engineering, University of Canterbury, Christchurch.

Grant, D. N., Blandon, C. A., & Priestley, M. J. N. (2005). *Modelling inelastic response in Direct Displacement-Based Design* (No. Report 2005/03). Pavia: IUSS Press.

Hall, J. F. (1995). *Northridge earthquake of January 17, 1994, reconnaissance report, vol 1* (No. Publication 95-03): Earthquake Spectra.

Halliday, M. A. (1991). *Feasibility of using timber for medium rise office structures*, Masters Dissertation, Department of civil engineering, University of Canterbury, Christchurch.

Heiduschke, A., Kasal, B., & Haller, P. (2008). *Shake table tests of small-and full-scale laminated timber frames with moment connections*.. Bulletin of Earthquake Engineering, Vol 7, N., pp. 323-339.

Iqbal, A., Pampanin, S., & Buchanan, A. (2010). *Seismic performance of prestressed timber beam-column sub-assemblies*. Proceedings NZSEE, Christchurch, paper n. 27

Iqbal, A., Pampanin, S., Buchanan, A., Fragiacomo, M., & Palermo, A. (2007). *Application of hysteretic dampers in LVL coupled walls for improved seismic performance.* Proceedings, 8th Pacific Conference of Earthquake Engineering, Singapore.

Iwan, W. D., & Gates, N. C. (1979). *The effective period and damping of a class of hysteretic structures*. Journal of Earthquake Engineering and Structural Dynamics, 7(2), pp 199-211.

Jacobsen, L. S. (1960). *Damping in composite structures.* Proceedings 2nd World Conference on Earthquake Engineering, Tokyo and Kyoto, Japan.

Judi, H. J., Fenwick, R. C., & Davidson, B. J. (2001). *Direct Displacement-Based Design - a definition of damping.* NZSEE Technical Conference, Auckland, New Zealand.

Kircher, C. A. (2003). *It makes dollars and sense to improve nonstructural systems performance*. ATC 29-2 Seminar on Seismic Design, Performance, and Retrofit of Nonstructural Components in Critical Facilities, Newport Beach, California, October 23-24, 2003.

Kircher, C. A., Holmes, W. T., & Whitman, V. (2006). *HAZUS®MH Earthquake loss estimation methods*. American Society of Civil Engineers.

Krawinkler, H. (1999). *Challenges and progress in performance-based earthquake engineering.* Proceedings of International Seminar on Seismic Engineering for Tomorrow - In honour of Professor Hiroshi Akiyama, Tokyo, Japan.

Lindt, J. W. v. d. (2010). *The NEESWood project in review*. Proceedings Canadian Conference on Earthquake Engineering, EERI, Toronto, Canada.

NelsonPine (2003). *Introduction to Nelson Pine LVL*. Auckland, New Zealand: Nelson Pine.

Marriot, D (2009). *The development of high-performance post-tensioned rocking systems for seismic design of structures.* Doctorate Thesis, Department of civil engineering, University of Canterbury, New Zealand.

Newcombe, M. P. (2005). *Seismic resisting structural systems using laminated veneer lumber* (3rd Professional Year Project). Christchurch: University of Canterbury.

Newcombe, M. P. (2008a). *Seismic design of multistorey post-tensioned timber buildings.* Masters Thesis, ROSE School, University of Pavia, Italy.

Newcombe, M. P., Pampanin, S., Buchanan, A., & Palermo, A. (2008b). *Seismic design of post-tensioned timber frames.* Proceedings 14th World Conference in Earthquake Engineering, WCTE, Beijing, China

Newcombe, M., Pampanin, S., Buchanan, A., Palermo, (2008c) *Section analysis and cyclic behavior of post-tensioned jointed ductile connections for multi-storey timber buildings*, Journal of Earthquake Engineering, Special Issue, 12 (S1) , pp. 83-110 ISSN: 1363-2469

Newcombe, M. P., Carradine, D., Pampanin, S., Buchanan A., van-Beerschoten, W. A., & Fragiacomo M. (2009). *In-plane experimental testing of timber-concrete composite floor diaghragms*, Proceedings New Zealand Society of Earthquake Engineering Conference, Christchurch, New Zealand.

Newcombe, M., Pampanin, S., & Buchanan, A. (2010a). *Design, fabrication and assembly of a two-storey post-tensioned timber building*. Proceedings 14th World Conference in Earthquake Engineering, WCTE , Beijing, China

Newcombe, M. P., Pampanin, S., & Buchanan, A. H. (2010b). *Experimental testing of a two-storey post-tensioned timber building.* Proceedings 9th US National and 10th Canadian Conference on Earthquake Engineering, Toronto, Canada.

Newcombe, M. P., Pampanin, S., & Buchanan, A. H. (2010c). *Global response of a two storey pres-lam timber building.* Proceedings New Zealand Society of Earthquake Engineering Conference, Wellington, New Zealand.

Newcombe, M. (2010d). *Numerical modelling and analysis of a two-storey post-tensioned timber frame with floor diaphragms.* Proceedings 14th European Conference on Earthquake Engineering, Ohrid, Macedonia

Newcombe, M., Cusiel, M., Pampanin, S., Palermo, A., & Buchanan, A. (2010e). *Simplied design of post-tensioned timber frames.* Proceedings CIB W18 , Nelson, August

NZCS, (2010) *PRESSS Design Handbook* (S. Pampanin Ed.), New Zealand Concrete Society, Wellington, New Zealand

NZS1170.5:2004 *Structural design actions - Part 5 - Earthquake actions.* Wellington: New Zealand Standards.

NZS3101:2006 *Concrete structures standard.* Wellington: New Zealand Standards.

NZS3603:1999 *Timber structures standard.* Wellington: New Zealand Standards.

NZS4357:1995 *Structural laminated veneer lumber.* Wellington: New Zealand Standards.

Palermo, A. (2004). *Use of controlled rocking in the seismic design of bridges.* Doctorate Thesis, Technical Institute of Milan, Milan.

Palermo, A., Pampanin, S., Buchanan, A., & Newcombe, M. (2005a). *Seismic design of multi-storey buildings using Laminated Veneer Lumber (LVL).* Proceedings New Zealand Society of Earthquake Engineering Conference, Wairaki, New Zealand.

Palermo, A., Pampanin, S., & Carr, A. (2005b). *Efficiency of simplified alternative modelling approaches to predict the seismic response of precast concrete hybrid systems.* fib Symposium, Budapest.

Palermo, A., Pampanin, S., & Buchanan, A. (2006a). *Experimental investigations on LVL* Palermo, A., Pampanin, S., & Buchanan, A. (2006a). *Experimental investigations on LVL seismic resistant wall and frame subassemblies.* Proceedings 1st European Conference in Seismic Engineering and Seismology, Geneva, Switzerland.

Palermo, A., Pampanin, S., Fragiacomo, M., Buchanan, A., & Deam, B. (2006b). *Innovative seismic solutions for multi-storey LVL timber buildings.* Proceedings World Conference in Timber Engineering, Portland, USA.

Palermo, A., Pampanin, S., Fragiacomo, M., Buchanan, A., Deam, B., & Pasticier, L. (2006c). *Quasi-static cyclic tests on seismic-resistant beam-to-column and column-to-foundation subassemblies using Laminated Veneer Lumber (LVL).* Proceedings Australasian Conference on the Mechanics of Structures and Materials, Christchurch.

Pampanin, S. (2005). *Emerging solutions for high seismic performance of precast/prestressed concrete buildings*. Journal of Advanced Concrete Technology, "High Performance Systems" 3(2), pp. 202-223.

Pampanin, (2010) *Damage-control self-centering structures: from laboratory testing to on site applications*, Chapter 28 in the book Advancements in Performance-Based Earthquake Engineering (M Fardis Editor) Publisher Springer, Part 3, pp. 297-308

Pampanin, S., Priestley, M. J. N., & Sritharan, S. (2000). *PRESSS Phase 3: The five-storey precast test building* (Research No. SSRP-2000/08): Department of Structural Engineering, University of California, San Diego, La Jolla, California.

Pampanin, S., Priestley, M. J. N., & Sritharan, S. (2001). *Analytical modelling of the seismic behavior of precast concrete frames designed with ductile connections.* Journal of Earthquake Engineering, 5(3), pp. 329-367.

Peng, B. H. H., Dhakal, R., & Fenwick, R. (2006). *Causes of elongation in reinforced concrete beams subject to cyclic loading.* Proceedings 10th Asia-Pacific Conference on Structural Engineering & Construction, Bangkok, Thailand.

Popovski, M., Prion, H. G. L., & Karacabeyli, E. (2002). *Seismic performance of connections in heavy timber construction.* Canadian Journal of Civil Engineering, 29(3), pp. 389-399.

Priestley, M. J. N. (1991). *Overview of the PRESSS research programme. PCI Journal, 36*(4), pp. 50-57.

Priestley, M.J.N., Sritharan, S., Conley, J., Pampanin, S., (1999). *Preliminary results and conclusions from the PRESSS precast 5-Story test building*, PCI Journal (Precast/Prestressed Concrete Institute), Vol. 44, No.6, pp.42-67.

Priestley, M. J. N., & Grant, D. N. (2005). *Viscous Damping in seismic design and analysis.* Journal of Earthquake Engineering, 9 (Special Issue 2), pp. 229-255.

Priestley, M. J. N., Calvi, G. M., & Kowalsky, M. J. (2007). *Displacement-based seismic design of structures.* Pavia, Italy: IUSS PRESS.

Rodriguez, M. E., Restrepo, J. I., & Carr, A. J. (2002). *Earthquake-induced floor horizontal accelerations in buildings.* Journal of Earthquake Engineering and Structural Dynamics, 31(3), pp. 693-718.

SEAOC (1995). *Vision 2000: Performad based Seismic engineering of buildings*. California Office of Emergengy Services, Structural Engineers Association of California.

Smith, T. (2006). *LVL Rocking shear walls: with external dissipater attachment.* 3rd Professional Year Project, Department of Civil Engineering, University of Canterbury, Christchurch.

Smith, T. (2008a). *Feasibility of multi storey post tensioned timber buildings: detailing, cost and construction.* Master Dissertation, Department of Civil and Natural Resources Engineering, University of Canterbury, Christchurch.

Smith, T., Ludwig, F., Pampanin, S., Fragiacomo, M., Buchanan, A., & Deam, B. (2007). *Seismic response of hybrid-LVL coupled walls under quasi-static and pseudo-dynamic testing.* Proceedings of NZSEE Conference, Palmerston North, New Zealand.

Smith, T., Pampanin, S., Buchanan, A. H., & Fragiacomo, M. (2008b). ***Feasibility and detailing of post-tensioned timber buildings for seismic areas.*** Proceedings of NZSEE Conference, Wairakei.

Spieth, H. A., Carr, A. J., Murahidy, A. G., Arnolds, D., Davies, M., & Mander, J. B. (2004). ***Modelling of post-tensioned precast reinforced concrete frame structures with rocking beam-column connections***, Proceedings New Zealand Society of Earthquake Engineering Conference, Rotorua, New Zealand.

Sullivan, T. J., Pinho, R., & Pavese, A. (2004). ***An introduction to structural testing techniques in earthquake engineering***. Pavia, Italy: IUSS Press.

Yeoh, E. C., Fragiacomo, M., Buchanan, A., Crews, K., Haskell, J., & Deam, B. (2008, June 2-5). ***Development of semi-prefabricated timber-concrete composite floors in Australasia.*** Proceedings 10th World Conference of Timber Engineering, Miyazaki, Japan.

APPENDIX A: MODEL BUILDING GEOMETRY

LEVEL 0

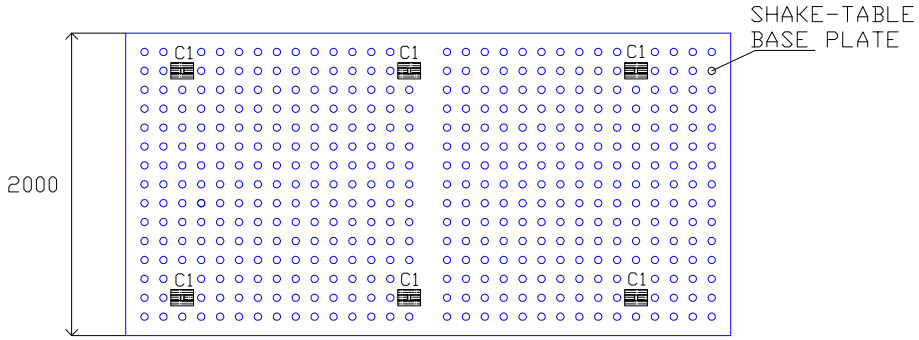

LEVELS 1 TO 5

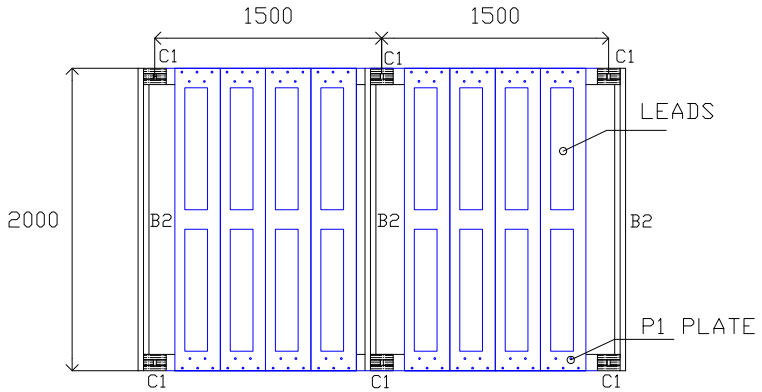

Project
Multi-storey Post-tensioned Timber frame building

DWG. TITLE
STRUCTURAL FLOOR LAYOUT PLANS

SCALE (A4)	1:50	PROJECT No: 001
SCALE (A3)	1:100	DWG. No.
DESIGN	DP	S01
DRAWN	DP	
DATE	2011	

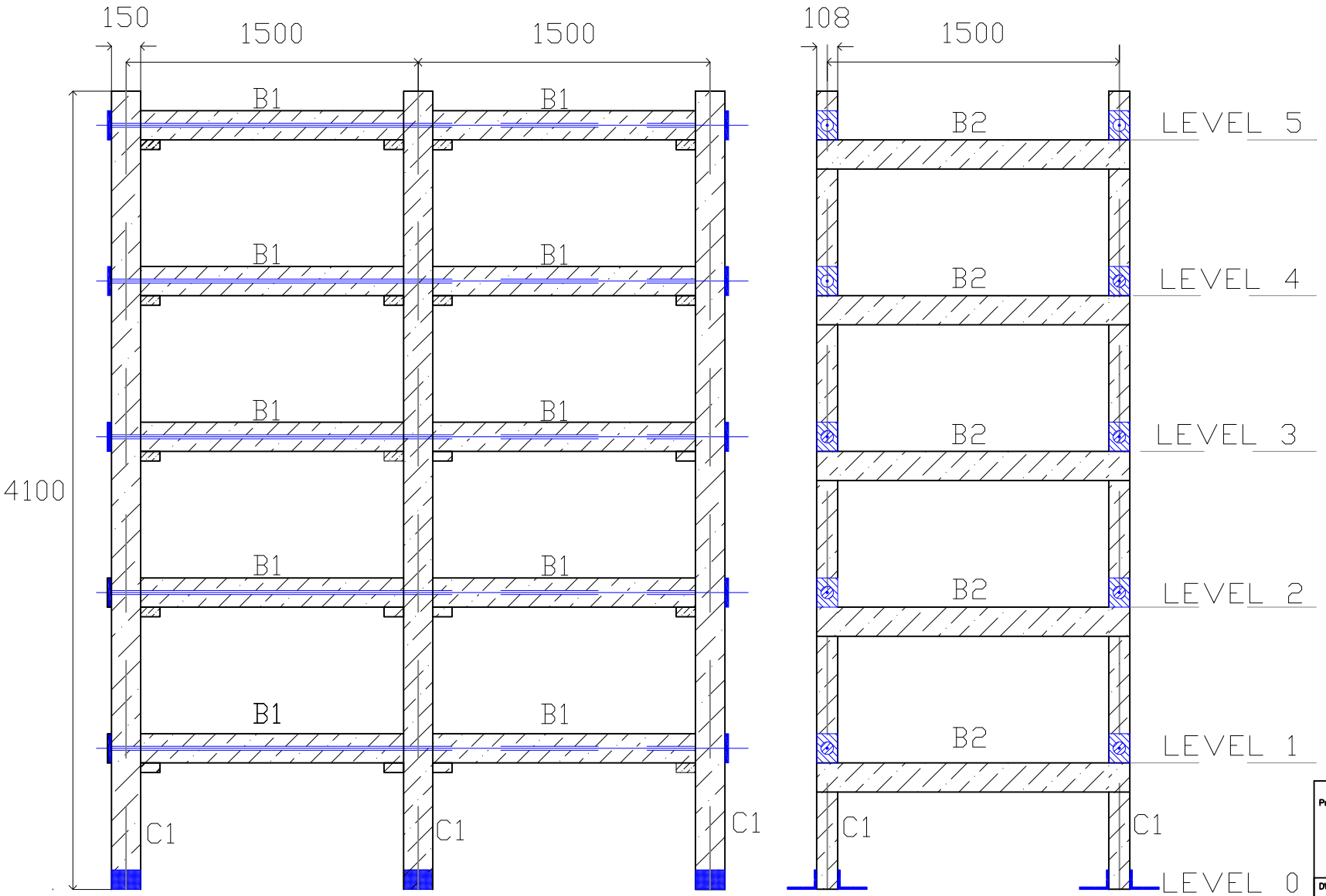

Project

Multi-storey
Post-tensioned
Timber frame building

DWG. TITLE

STRUCTURAL
ELEVATIONS

SCALE (A4)	1:30	PROJECT No: 001
SCALE (A3)	1:60	DWG. No.
DESIGN	DP	S02
DRAWN	DP	
DATE	2011	

COLUMN ELEVATIONS

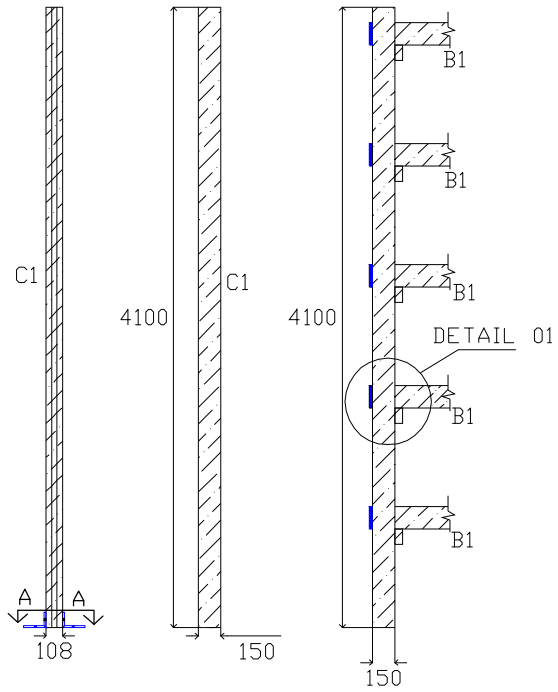

SCALE 1:50 (A4)

COLUMN SECTION A-A

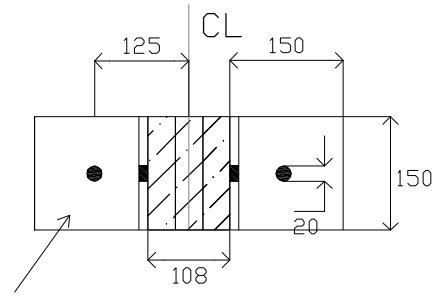

DETAIL 01

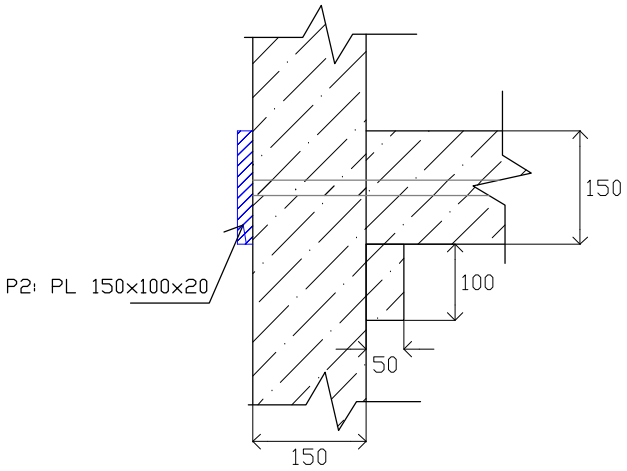

SCALE 1:10 (A4)

Project: *Multi-storey Post-tensioned Timber frame building*		
DWG. TITLE: COLUMN DETAILS		
SCALE (A4)	VARY	PROJECT No: 001
SCALE (A3)	VARY	DWG. No.
DESIGN	DP	S03
DRAWN	DP	
DATE	2011	

B1:LONGITUDINAL BEAM

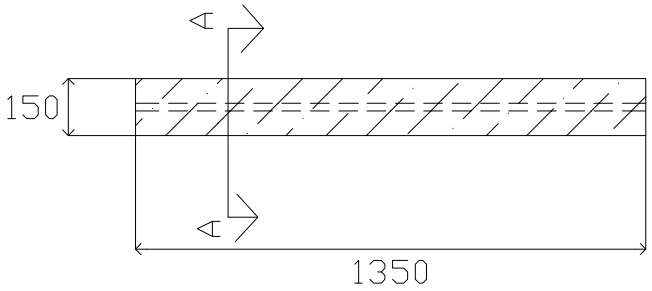

B2:TRANSVERSAL BEAM

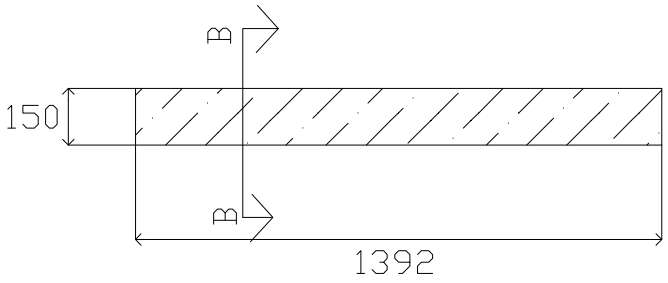

SCALE 1:20 (A4)

BEAM SECTION A-A

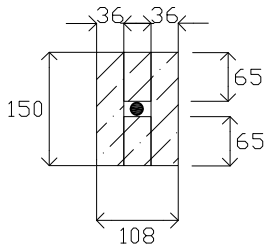

2 pieces of 150x36
2 pieces of 65x36
1 tendon

BEAM SECTION B-B

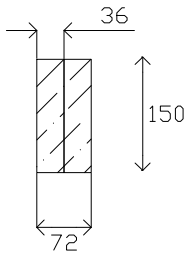

2 pieces of 150x36

SCALE 1:10 (A4)

Project
Multi-storey Post-tensioned Timber frame building

DWG. TITLE
BEAMS
DETAILS

SCALE (A4)	VARY	PROJECT No: 001
SCALE (A3)	VARY	DWG. No.
DESIGN	DP	S04
DRAWN	DP	
DATE	2011	

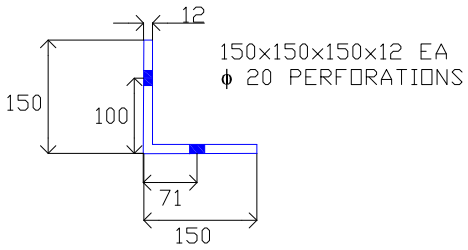

P2: PL 150x100x20

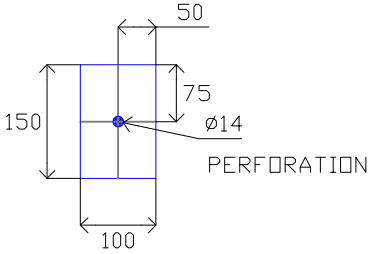

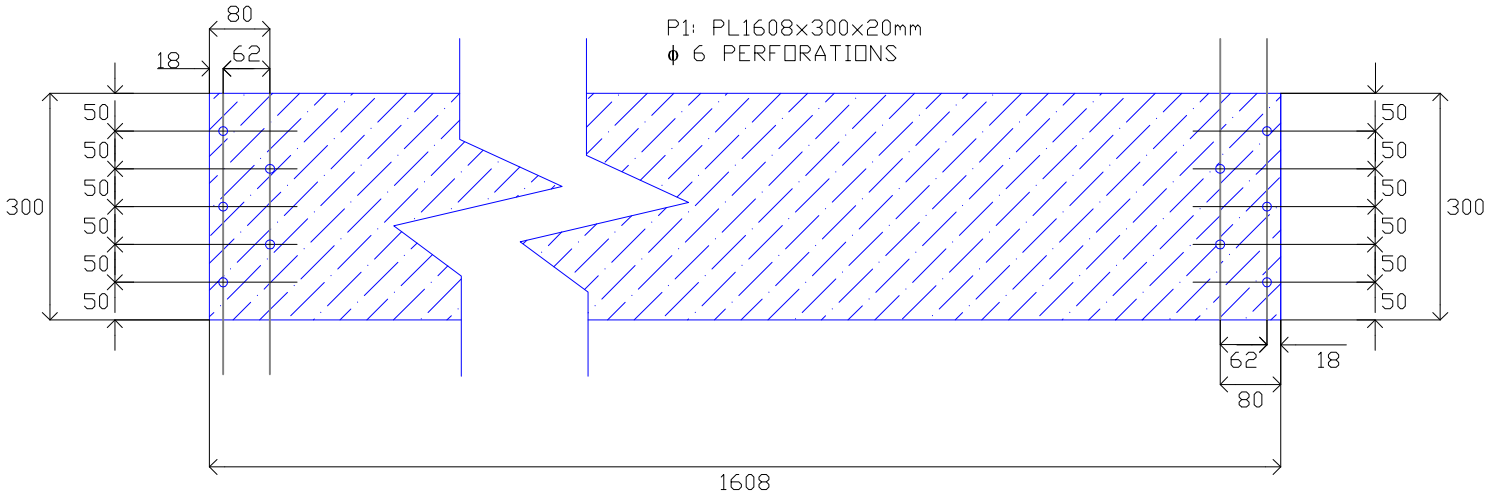

Project	***Multi-storey Post-tensioned Timber frame building***
DWG. TITLE	STEELWORK DETAILS

SCALE (A4)	1:10	PROJECT No: 001
SCALE (A3)	1:20	DWG. No.
DESIGN	DP	**S05**
DRAWN	DP	
DATE	2011	

APPENDIX B: INTRUMENTATION SET-UP FOR 5-STOREY SHAKE-TABLE TESTS

Nomenclature: XX-YY XX: Device YY: Channel

A: Accelerometer
LC: Load cell
LP: Linear potentiometer
RP: Rotational potentiometer
SP: Spring potentiometer

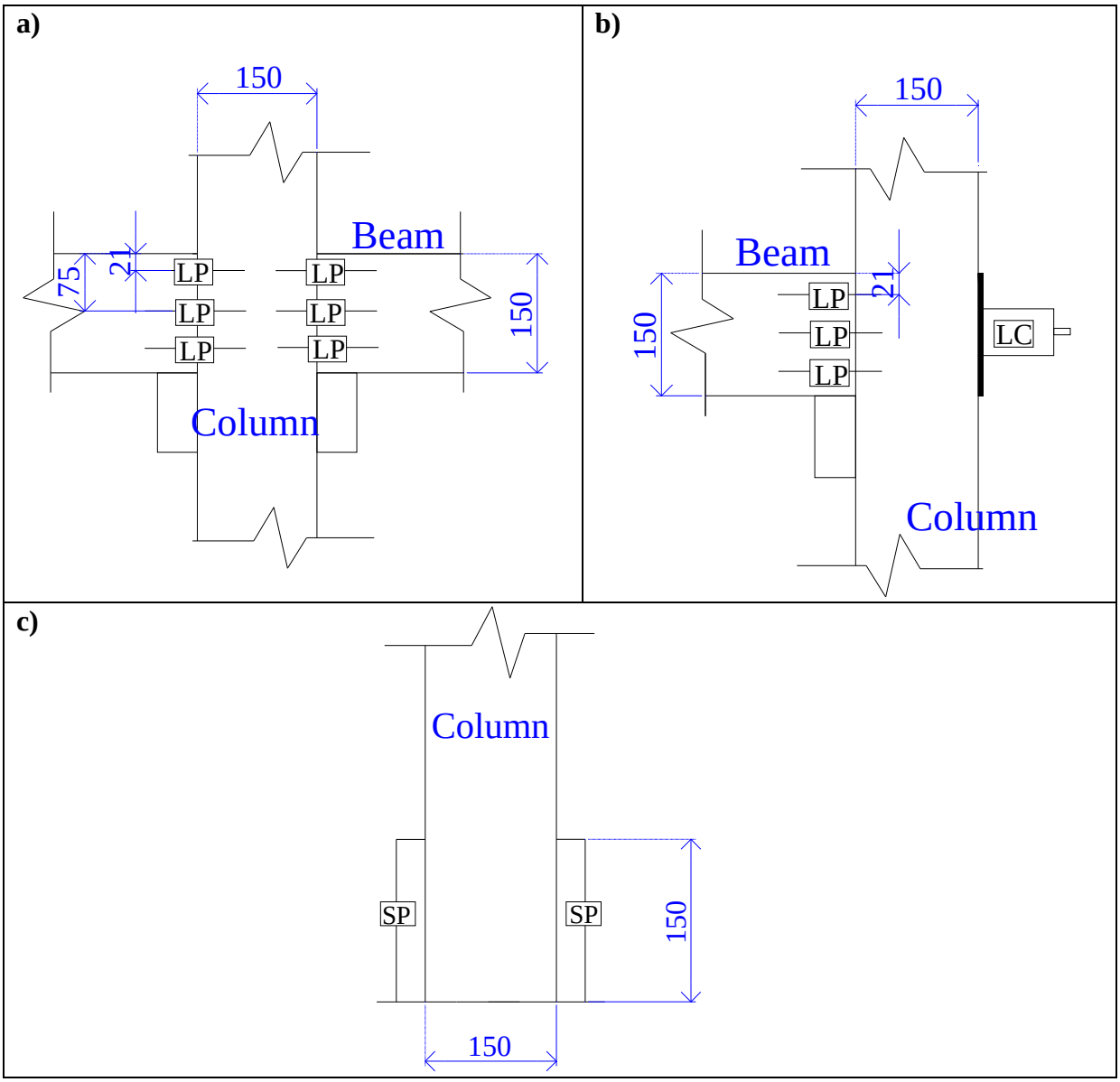

Figure B-1 a) Internal beam-column instrumentation configuration b) External beam-column instrumentation configuration c) Column instrumentation configuration

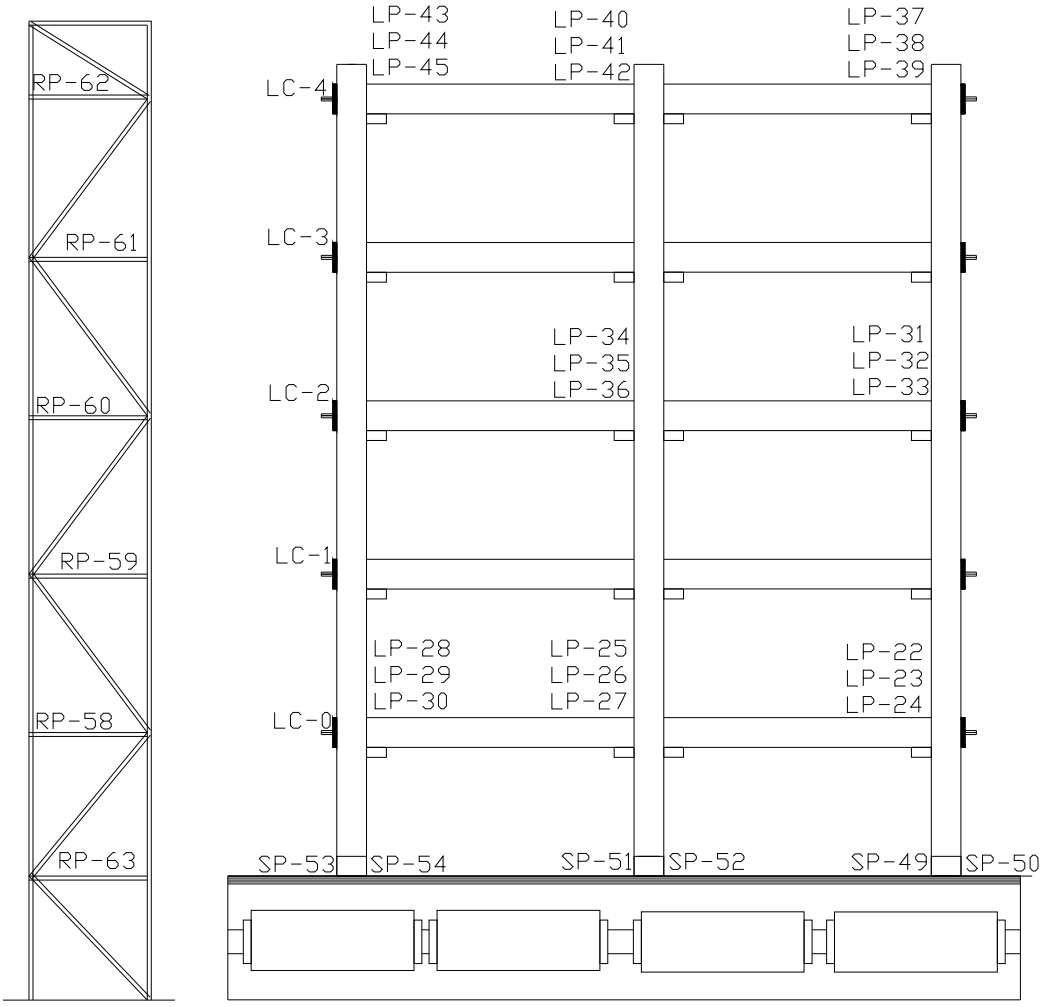

Figure B-2 Instrumentation for 5-storey North frame, shake table test

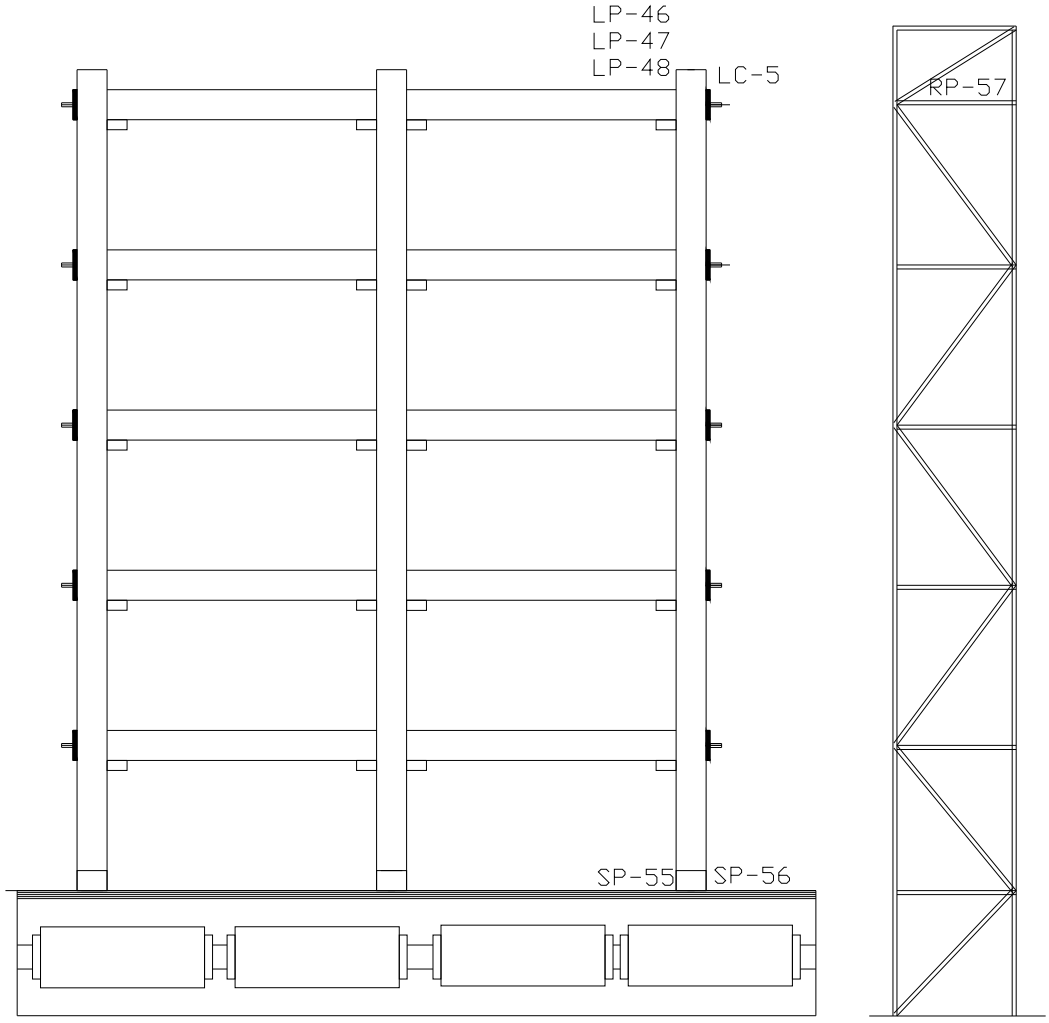

Figure B-3 Instrumentation for 5-storey South frame, shake table test

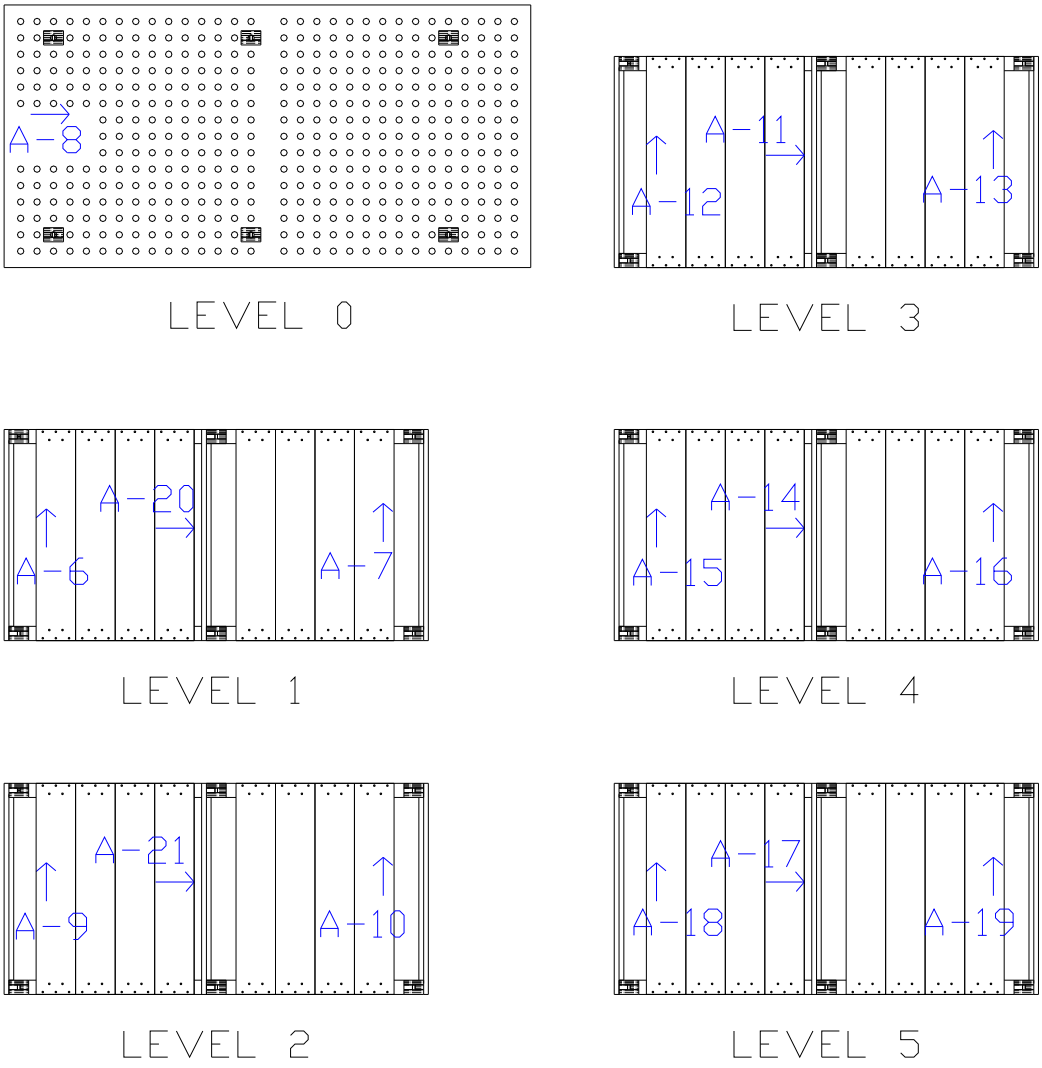

Figure B-4 Instrumentation on 5-storey floor levels

Table B-1 5-storey modelled building instrumentation, shake-table test

Channel	Device	Instrument ID	Calibration Factor
0	Load Cell	LC-Q	0.06725
1	Load Cell	LC-M	0.07427
2	Load Cell	LC-S	0.06553
3	Load Cell	LC-H	0.06944
4	Load Cell	LC-U	0.06777
5	Load Cell	LC-D	0.06861
6	Accelerometer	ACC-6	0.00202
7	Accelerometer	ACC-7	0.00198
8	Accelerometer	ACC-8	0.00154
9	Accelerometer	ACC-9	0.00139
10	Accelerometer	ACC-10	0.00150
11	Accelerometer	ACC-11	0.00148
12	Accelerometer	ACC-12	0.00151
13	Accelerometer	ACC-13	0.00152
14	Accelerometer	ACC-14	0.00153
15	Accelerometer	ACC-15	0.00146
16	Accelerometer	ACC-16	0.00145
17	Accelerometer	ACC-17	0.00148
18	Accelerometer	ACC-18	0.00147
19	Accelerometer	ACC-19	0.00000
20	Accelerometer	ACC-20	0.00182
21	Accelerometer	ACC-21	0.00201
22	Linear Potentiometer	LP-101	0.00712
23	Linear Potentiometer	LP-188	0.00721
24	Linear Potentiometer	LP-189	0.00716
25	Linear Potentiometer	LP-190	0.00712
26	Linear Potentiometer	LP-191	0.00719
27	Linear Potentiometer	LP-192	0.00720
28	Linear Potentiometer	LP-193	0.00711
29	Linear Potentiometer	LP-194	0.00710
30	Linear Potentiometer	LP-195	0.00711
31	Linear Potentiometer	LP-196	0.00706
32	Linear Potentiometer	LP-197	0.00716
33	Linear Potentiometer	LP-198	0.00721
34	Linear Potentiometer	LP-199	0.00715
35	Linear Potentiometer	LP-200	0.00708
36	Linear Potentiometer	LP-201	0.00712
37	Linear Potentiometer	LP-202	0.00713
38	Linear Potentiometer	LP-203	0.00706
39	Linear Potentiometer	LP-204	0.00720
40	Linear Potentiometer	LP-205	0.00717
41	Linear Potentiometer	LP-206	0.00717
42	Linear Potentiometer	LP-207	0.00723
43	Linear Potentiometer	LP-208	0.00719

Table B-1 (continued) 5-storey modelled building instrumentation, shake-table test

Channel	Device	Instrument ID	Calibration Factor
44	Linear Potentiometer	LP-209	0.00709
45	Linear Potentiometer	LP-210	0.01464
46	Linear Potentiometer	LP-165	0.01175
47	Linear Potentiometer	LP-165	0.01180
48	Linear Potentiometer	LP-166	0.01179
49	Spring Potentiometer	SP-2c	0.02368
50	Spring Potentiometer	SP-3c	0.02351
51	Spring Potentiometer	SP-4c	0.02379
52	Spring Potentiometer	SP-5c	0.02338
53	Spring Potentiometer	SP-6c	0.02355
54	Spring Potentiometer	SP-7c	0.02398
55	Spring Potentiometer	SP-8c	0.02353
56	Spring Potentiometer	SP-9c	0.02384
57	Rotary Potentiometer	RP-57	0.08351
58	Rotary Potentiometer	RP-58	0.08435
59	Rotary Potentiometer	RP-59	0.08379
60	Rotary Potentiometer	RP-60	0.08386
61	Rotary Potentiometer	RP-61	0.08393
62	Rotary Potentiometer	RP-62	0.08375
63	Rotary Potentiometer	RP-63	0.08518

APPENDIX C: DAMPING COMPUTATION METHODS

C.1 Damping computed from response decay

To compute damping values, a variety of sinusoidal displacements were applied to the shake table for a certain amount of time. The excitation was stopped and the decay of the modelled building response (acceleration and displacement) measured.
The sinusoidal excitation (*Figure C-1*), represented by *Equation C-1*, was applied during an appropriate amount of time until the scaled building reached a pure steady state response. At the beginning a composed response conformed by the transient and the steady state solutions was observed *(Figure C-2a).* A pure response is required in order to compute the damping values.

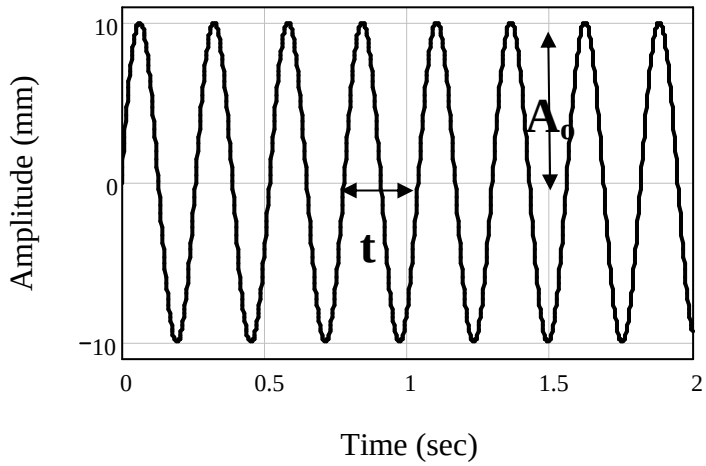

Figure C-1 Sinusoidal excitation

$$P(t) = Ao \cdot \sin(\omega \cdot t) \qquad \textit{Equation C-1}$$

A_o: Wave amplitude
ω: Frequency
t: Time

The damping was obtained based on the decay of the response following the cessation of table movement. For this computation *Equation C-2* was used. The formula considers the amplitude of an initial point and "*m*" cycles after the amplitude of the final excitation point. Damping values are small; hence the formula can be simplified to *Equation C-3*.

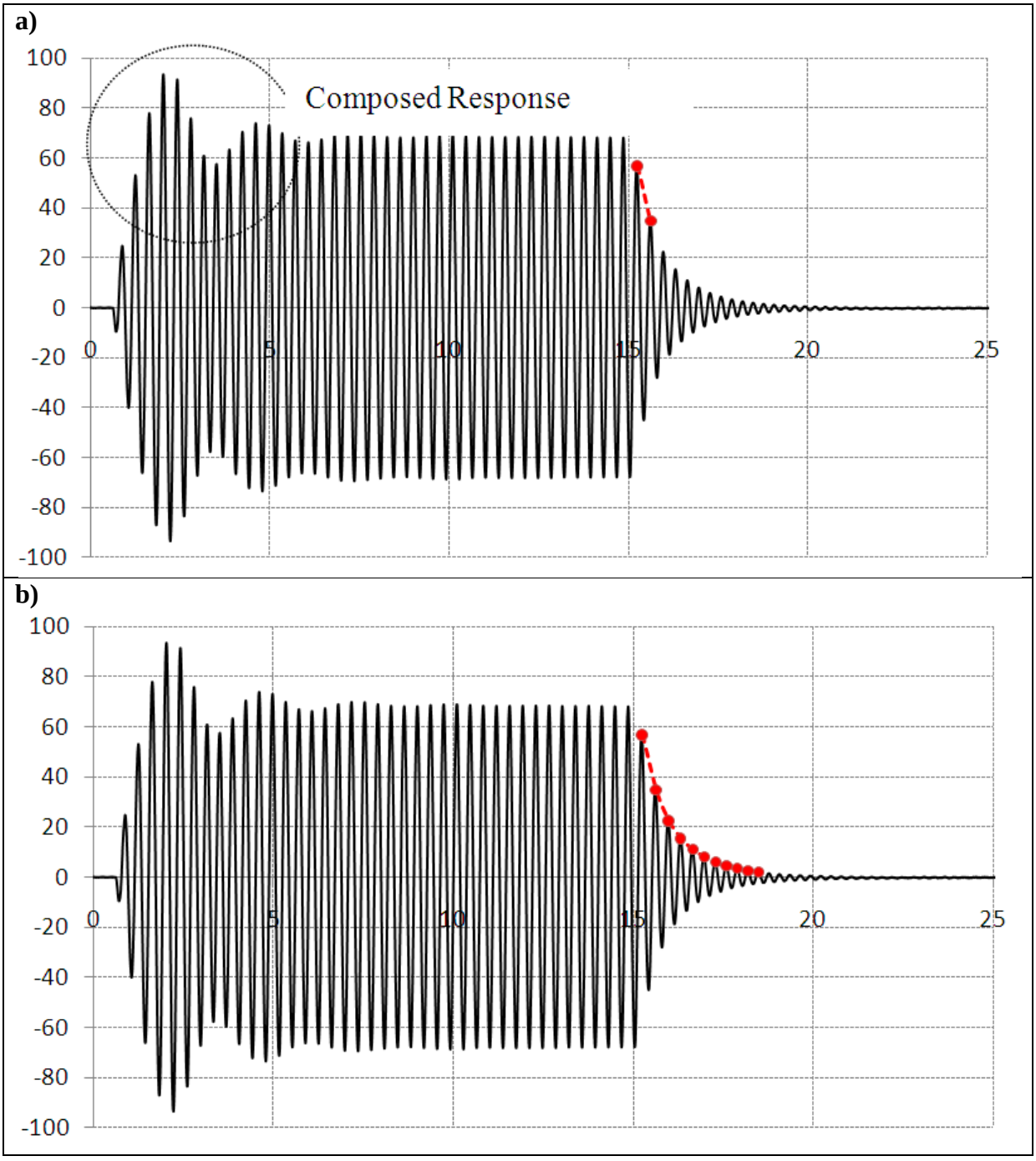

Figure C-2 a) Damping computed using one-decay cycle (shown in red) b) Damping computed using ten-decay cycle (shown in red)

As mentioned in Chapter three damping of post-tensioned timber frame buildings depends highly on inter-storey drift level. Therefore, damping computed through this method will vary depending on the number of cycles considered during its calculation.

$$\ln\left(\frac{x_n}{x_{n+m}}\right) = \frac{2 \cdot m \cdot \pi \cdot \xi}{\sqrt{1-\xi^2}}$$ *Equation C-2*

$$\xi = \frac{\ln\left(\frac{x_n}{x_{n+m}}\right)}{2 \cdot m \cdot \pi}$$ *Equation C-3*

Xn = Initial amplitude considered
Xn+m = Final amplitude considered
m = Number of considered cycles
ξ = Fraction of critic damping

In Chapter three, damping values were presented considering one-cycle decay and ten-cycle decay (***Figure C-2***). To illustrate, the equivalent viscous values obtained during the test 5S-M1-85 (defined in Appendix D) are shown in ***Figure C- 3***.
In this case damping values decreased from 8% to 5%.

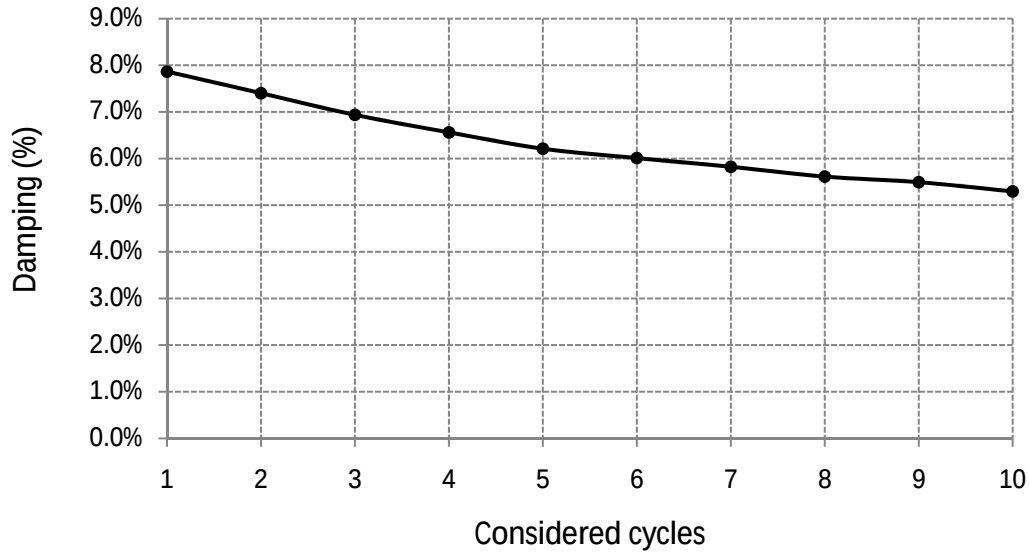

Figure C- 3 Variation of damping values depending of considered cycles

C.2 Area-based damping

Hysteresis damping was simply computed as a function of displayed areas on *Figure C-4*. The damping value was then obtained from *Equation C-4*.

$$\xi = \frac{1}{4 \cdot \pi} \cdot \frac{E_D}{E_s}$$ *Equation C-4*

Where:
E_D = Total energy dissipated during a complete cycle
E_S = Equivalent strain energy at the maximum displacement of the cycle

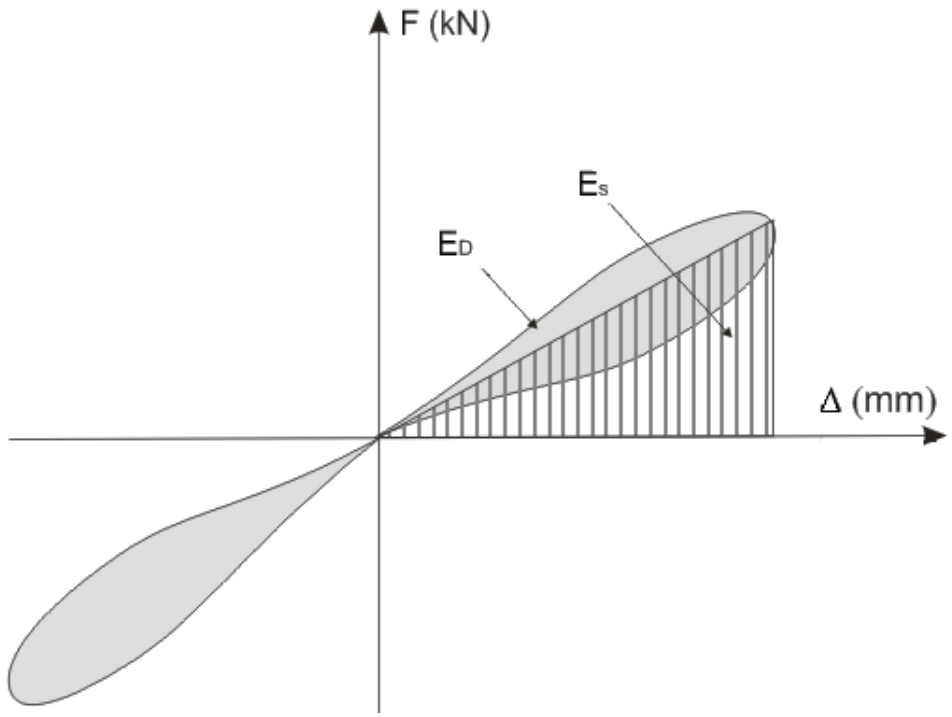

Figure C-4 Area-based damping

APPENDIX D: PERFORMED DYNAMIC TESTS

Table D-1 Sinusoidal 5-storey shake-table tests

Test	Test inputs					Response period (sec.)	Maximum level displacement (mm)					Maximum level acceleration (g)				
	Percentage of required weight	Amplitude (mm)	Period (sec.)	Duration (sec.)	Ground accel. (g)		L1	L2	L3	L4	L5	L1	L2	L3	L4	L5
5S-M1-01	31%	1.6	0.25	10.0	0.29	0.28	2.3	5.2	6.6	8.7	11.4	0.4	0.5	0.5	0.4	0.8
5S-M1-02	31%	1.6	0.22	10.0	0.29	0.27	1.2	3.2	4.6	5.7	7.0	0.2	0.3	0.3	0.4	0.5
5S-M1-03	31%	1.6	0.25	10.0	0.31	0.28	1.3	3.3	4.8	5.9	7.4	0.3	0.3	0.3	0.4	0.5
5S-M1-04	31%	3.9	0.26	10.0	0.59	0.30	4.0	8.7	11.9	13.8	18.4	0.4	0.5	0.6	0.7	1.0
5S-M1-05	31%	5.0	0.25	10.0	0.64	0.30	3.8	8.4	12.4	14.8	19.5	0.4	0.4	0.6	0.7	0.9
5S-M1-06	31%	5.0	0.25	10.0	0.62	0.30	3.6	7.8	11.7	14.1	17.6	0.5	0.3	0.5	0.7	0.8
5S-M1-07	31%	6.5	0.26	10.0	0.52	0.33	4.9	9.5	14.0	17.4	-19.3	0.4	0.4	0.7	0.7	0.8
5S-M1-08	31%	6.5	0.26	10.0	0.53	0.33	4.4	9.6	14.0	17.3	23.3	0.4	0.4	0.7	0.7	0.8
5S-M1-09	31%	6.5	0.27	10.0	0.47	0.32	5.2	10.9	15.8	19.3	22.0	0.4	0.4	0.8	0.8	0.9
5S-M1-10	31%	8.0	0.27	10.0	0.55	0.33	6.3	13.0	18.9	23.3	26.9	0.4	0.4	0.8	0.8	1.0
5S-M1-11	31%	3.0	0.27	10.0	0.46	0.30	3.7	7.5	10.2	12.0	13.5	0.5	0.6	0.6	0.6	1.0
5S-M1-12	31%	6.5	0.17	8.7	0.94	0.29	2.0	5.0	8.3	11.1	12.9	0.8	0.4	0.4	0.8	1.0
5S-M1-13	31%	6.5	0.20	9.9	0.78	0.29	2.4	5.9	9.6	12.7	15.2	0.5	0.2	0.4	0.7	0.9
5S-M1-14	31%	6.5	0.22	11.1	0.60	0.31	3.5	7.9	12.0	15.2	17.8	0.4	0.2	0.4	0.7	0.9
5S-M1-15	31%	6.5	0.25	12.3	0.67	0.31	4.4	9.1	13.7	17.2	20.1	0.5	0.3	0.6	0.8	0.9
5S-M1-16	31%	6.5	0.27	13.5	0.46	0.32	4.8	10.5	15.2	18.4	20.7	0.4	0.6	0.8	0.8	0.9
5S-M1-17	31%	6.5	0.29	14.7	0.45	0.33	5.0	11.7	17.6	22.3	26.5	0.6	0.9	0.9	0.8	1.4

Table D-1(continued) Sinusoidal 5-storey shake-table tests

Test	Test inputs					Response period (sec.)	Maximum level displacement (mm)					Maximum level acceleration (g)				
	Percentage of required weight	Amplitude (mm)	Period (sec.)	Duration (sec.)	Ground accel. (g)		L1	L2	L3	L4	L5	L1	L2	L3	L4	L5
5S-M1-18	31%	6.5	0.32	15.9	0.42	0.35	6.0	13.4	20.8	26.7	31.1	0.4	0.7	0.8	0.8	1.2
5S-M1-19	31%	6.5	0.34	17.1	0.41	0.36	9.0	17.2	25.9	32.6	37.8	0.5	0.6	0.8	0.9	1.2
5S-M1-20	31%	6.5	0.37	18.3	0.47	0.38	7.9	17.6	27.3	34.7	40.6	0.5	0.6	0.9	1.0	1.3
5S-M1-21	31%	6.5	0.39	19.5	0.40	0.39	9.4	20.7	31.4	39.7	46.1	0.5	0.6	0.9	1.0	1.2
5S-M1-22	31%	6.5	0.15	7.5	1.17	0.30	1.8	4.1	6.9	9.9	11.8	0.9	0.5	0.4	0.7	1.2
5S-M1-23	31%	6.5	0.17	8.7	0.91	0.30	2.4	5.4	8.3	11.1	12.8	0.8	0.4	0.5	0.8	1.0
5S-M1-24	31%	6.5	0.20	9.9	1.15	0.30	2.9	5.9	9.2	12.1	14.3	0.8	0.2	0.8	0.8	1.2
5S-M1-25	31%	6.5	0.22	11.1	0.68	0.31	3.7	7.8	11.6	14.7	16.7	0.4	0.2	0.5	0.8	0.9
5S-M1-26	31%	6.5	0.25	12.3	0.91	0.31	4.6	9.4	13.8	17.1	19.5	0.7	0.5	0.9	0.9	1.1
5S-M1-27	31%	6.5	0.27	13.5	0.56	0.32	6.6	12.4	17.0	20.6	23.0	0.5	0.8	0.9	0.9	1.3
5S-M1-28	31%	6.5	0.29	14.7	0.53	0.33	7.6	15.0	21.4	26.1	29.5	0.4	0.6	0.9	1.0	1.3
5S-M1-29	31%	6.5	0.32	15.9	0.47	0.33	9.2	18.2	26.1	32.0	35.8	0.5	0.7	1.0	1.1	1.3
5S-M1-30	31%	6.5	0.34	17.1	0.59	0.35	11.0	21.8	31.1	38.0	42.6	0.6	0.8	1.0	1.2	1.4
5S-M1-31	31%	6.5	0.37	18.3	0.43	0.37	14.0	27.5	39.2	48.1	54.1	0.6	0.8	1.1	1.4	1.6
5S-M1-32	31%	6.5	0.39	19.5	0.31	0.39	15.4	30.6	44.4	54.8	62.1	0.6	0.9	1.1	1.3	1.6
5S-M1-33	31%	1.6	0.25	10.0	0.54	0.30	4.5	9.0	12.3	14.3	15.9	0.5	0.8	0.7	0.7	1.1
5S-M1-34	31%	3.9	0.26	10.0	0.54	0.30	4.5	9.0	12.3	14.3	15.9	0.5	0.8	0.7	0.7	1.1
5S-M1-35	31%	5.0	0.25	10.0	0.61	0.31	4.7	9.2	13.0	15.9	18.2	0.5	0.5	0.8	0.9	1.0
5S-M1-36	31%	8.0	0.27	10.0	0.63	0.32	8.7	15.2	21.0	24.6	27.0	0.8	1.1	1.1	1.0	1.6
5S-M1-37	31%	9.0	0.26	10.0	0.75	0.32	7.7	15.2	21.4	25.8	28.7	0.6	0.7	1.1	0.9	1.3
5S-M1-38	31%	1.6	0.25	10.0	0.35	0.28	2.5	5.2	7.1	8.5	9.3	0.3	0.4	0.6	0.6	0.6
5S-M1-39	31%	3.9	0.26	10.0	0.74	0.30	5.6	10.5	14.2	16.8	18.6	0.6	0.9	1.0	0.9	1.3

Table D-1 (continued) Sinusoidal 5-storey shake-table tests

Test	Test inputs					Response period (sec.)	Maximum level displacement (mm)					Maximum level acceleration (g)				
	Percentage of required weight	Amplitude (mm)	Period (sec.)	Duration (sec.)	Ground accel. (g)		L1	L2	L3	L4	L5	L1	L2	L3	L4	L5
5S-M1-40	31%	5.0	0.25	10.0	0.74	0.30	5.6	10.5	14.2	16.8	18.6	0.6	0.9	1.0	0.9	1.3
5S-M1-41	31%	8.0	0.27	10.0	0.63	0.31	8.4	16.4	23.0	27.7	30.8	0.5	0.9	0.9	1.2	1.5
5S-M1-42	31%	9.0	0.26	10.0	0.78	0.31	9.1	17.1	23.2	27.0	29.4	0.7	1.2	1.2	1.1	1.7
5S-M1-43	31%	3.5	0.15	7.5	0.90	0.27	1.4	2.9	4.6	6.0	6.9	0.7	0.3	0.4	0.5	0.7
5S-M1-44	31%	3.5	0.17	8.7	0.56	0.28	1.7	3.7	5.4	7.0	8.9	0.6	0.3	0.5	0.6	0.7
5S-M1-45	31%	3.5	0.20	9.9	0.51	0.28	2.0	4.4	6.6	8.4	9.5	0.3	0.2	0.4	0.5	0.6
5S-M1-46	31%	3.5	0.22	11.1	0.49	0.29	3.0	5.9	8.3	10.3	11.6	0.3	0.3	0.5	0.6	0.7
5S-M1-47	31%	3.5	0.25	12.3	0.60	0.29	4.0	7.9	10.6	12.6	13.7	0.7	0.8	0.8	0.8	1.3
5S-M1-48	31%	3.5	0.27	13.5	0.42	0.30	4.9	9.8	13.8	16.4	18.4	0.3	0.6	0.8	0.8	0.9
5S-M1-49	31%	3.5	0.29	14.7	0.33	0.31	6.5	13.2	18.2	22.0	24.5	0.4	0.6	0.9	0.9	1.0
5S-M1-50	31%	3.5	0.32	15.9	0.33	0.32	9.1	17.8	24.5	29.4	32.6	0.5	0.7	1.0	1.1	1.3
5S-M1-51	31%	3.5	0.34	17.1	0.39	0.29	2.7	5.9	8.2	9.8	10.8	0.4	0.4	0.5	0.6	0.7
5S-M1-52	31%	3.5	0.37	18.3	0.32	0.27	1.6	3.2	4.5	5.1	5.8	0.3	0.4	0.4	0.3	0.5
5S-M1-53	31%	3.5	0.39	19.5	0.32	0.27	1.2	2.6	3.5	4.6	5.7	0.7	0.7	0.4	0.4	0.8
5S-M1-54	31%	5.0	0.15	7.5	1.20	0.28	1.8	4.1	6.5	8.9	10.5	0.9	0.5	0.5	0.7	1.2
5S-M1-55	31%	5.0	0.17	8.7	0.82	0.29	2.0	4.7	7.3	9.7	11.2	0.7	0.4	0.5	0.8	1.0
5S-M1-56	31%	5.0	0.20	9.9	0.68	0.29	2.9	6.1	8.9	11.3	12.8	0.5	0.2	0.5	0.7	0.8
5S-M1-57	31%	5.0	0.22	11.1	0.64	0.29	4.0	7.8	10.9	13.7	15.2	0.4	0.3	0.6	0.7	0.9
5S-M1-58	31%	5.0	0.25	12.3	0.75	0.30	4.8	11.0	13.3	16.0	18.2	0.8	0.9	0.9	1.0	1.4
5S-M1-59	31%	5.0	0.27	13.5	0.54	0.31	6.0	12.0	16.9	20.4	22.8	0.4	0.7	0.9	0.9	1.1
5S-M1-60	31%	5.0	0.29	14.7	0.57	0.31	8.1	16.1	22.2	26.8	29.5	0.5	0.7	1.0	1.1	1.3
5S-M1-61	31%	5.0	0.32	15.9	0.41	0.32	10.4	21.3	28.3	33.9	37.6	0.5	0.8	1.1	1.2	1.4

Table D-1(continued) Sinusoidal 5-storey shake-table tests

Test	Test inputs					Response period (sec.)	Maximum level displacement (mm)					Maximum level acceleration (g)				
	Percentage of required weight	Amplitude (mm)	Period (sec.)	Duration (sec.)	Ground accel. (g)		L1	L2	L3	L4	L5	L1	L2	L3	L4	L5
5S-M1-62	31%	5.0	0.34	17.1	0.44	0.34	12.8	24.9	34.4	41.4	46.0	0.6	0.9	1.3	1.5	1.7
5S-M1-63	31%	5.0	0.37	18.3	0.38	0.29	3.2	6.9	9.4	11.2	12.6	0.4	0.5	0.5	0.6	0.7
5S-M1-63	31%	5.0	0.37	18.3	0.38	0.29	3.2	6.9	9.4	11.2	12.6	0.4	0.5	0.5	0.6	0.7
5S-M1-64	31%	5.0	0.39	19.5	0.29	0.29	2.0	4.0	5.4	6.8	7.9	0.4	0.6	0.6	0.5	0.7
5S-M1-65	31%	6.5	0.15	15.9	1.76	0.29	2.2	5.4	8.9	11.9	13.6	1.5	0.5	0.8	1.0	1.5
5S-M1-66	31%	6.5	0.17	17.1	0.98	0.27	2.4	6.0	9.6	12.8	14.7	0.8	0.4	0.5	1.0	1.2
5S-M1-67	31%	6.5	0.20	18.3	0.77	0.28	3.1	7.5	11.4	14.8	16.9	0.5	0.2	0.5	0.9	1.1
5S-M1-68	31%	6.5	0.22	19.5	0.66	0.28	4.4	9.6	14.8	18.6	21.2	0.4	0.4	0.7	1.0	1.2
5S-M1-69	31%	6.5	0.25	20.7	0.81	0.30	5.9	12.4	17.6	22.0	25.1	0.9	0.9	1.2	1.2	1.5
5S-M1-70	31%	6.5	0.27	21.9	0.58	0.31	7.9	16.0	22.6	27.3	30.2	0.5	0.9	1.0	1.2	1.4
5S-M1-71	31%	6.5	0.29	23.1	0.47	0.32	10.2	20.3	28.8	34.8	38.8	0.4	0.9	1.1	1.3	1.6
5S-M1-72	31%	6.5	0.32	24.3	0.47	0.33	12.7	25.3	35.5	43.0	48.1	0.5	0.9	1.3	1.5	1.7
5S-M1-73	31%	6.5	0.34	25.5	0.45	0.34	15.0	29.9	41.9	50.7	56.3	0.7	1.0	1.3	1.6	1.9
5S-M1-74	31%	6.5	0.37	26.7	0.42	0.36	19.6	38.6	54.7	66.0	73.6	0.8	1.2	1.6	1.9	2.2
5S-M1-75	31%	6.5	0.39	27.9	0.35	0.28	2.3	5.6	8.2	9.8	11.2	0.4	0.5	0.6	0.5	0.6
5S-M1-76	31%	8.0	0.22	8.9	0.99	0.32	6.4	13.2	19.0	23.5	26.7	0.8	0.7	1.0	1.1	1.4
5S-M1-77	31%	8.0	0.25	9.8	0.63	0.32	8.3	16.4	22.8	27.2	30.0	0.7	1.0	1.0	1.1	1.5
5S-M1-78	31%	8.0	0.27	10.8	0.57	0.33	9.9	19.8	28.0	34.0	37.7	0.4	0.8	1.0	1.3	1.5
5S-M1-79	31%	8.0	0.29	11.8	0.59	0.34	12.6	24.9	34.9	42.0	46.7	0.5	0.9	1.2	1.4	1.6
5S-M1-80	31%	8.0	0.32	12.7	0.67	0.36	15.3	30.4	42.9	52.0	57.7	0.7	1.0	1.4	1.6	1.8
5S-M1-81	31%	8.0	0.34	13.7	0.60	0.37	17.4	34.7	49.1	59.3	65.8	0.7	1.0	1.5	1.7	2.0
5S-M1-82	31%	8.0	0.39	15.6	0.43	0.29	4.3	8.6	12.3	14.9	16.5	0.5	0.6	0.7	0.7	0.8

Table D-1(continued) Sinusoidal 5-storey shake-table tests

Test	Test inputs					Response period (sec.)	Maximum level displacement (mm)					Maximum level acceleration (g)				
	Percentage of required weight	Amplitude (mm)	Period (sec.)	Duration (sec.)	Ground accel. (g)		L1	L2	L3	L4	L5	L1	L2	L3	L4	L5
5S-M1-83	31%	9.0	0.34	13.7	0.69	0.36	15.7	31.4	44.3	54.0	59.9	0.7	1.0	1.4	1.6	1.9
5S-M1-84	31%	9.0	0.37	14.6	0.55	0.37	18.2	36.0	51.3	62.1	69.1	0.7	1.0	1.4	1.8	2.0
5S-M1-85	31%	10.0	0.37	14.6	0.62	0.38	18.2	36.3	51.8	62.7	69.7	0.8	1.0	1.4	1.8	2.1

Table D-2 Sinusoidal 3-storey shake-table tests

Test	Test inputs					Response period (sec.)	Maximum level displacement (mm)			Maximum level acceleration (g)		
	Percentage of required weight	Amplitude (mm)	Period (sec.)	Duration (sec.)	Ground accel. (g)		L1	L2	L3	L1	L2	L3
3S-M1-01	31%	1.6	0.25	10.0	0.28	0.34	0.7	1.5	1.9	0.3	0.3	0.3
3S-M1-02	31%	3.9	0.26	10.0	0.39	0.35	1.4	3.1	4.2	0.4	0.5	0.5
3S-M1-03	31%	5.0	0.25	10.0	0.52	0.20	3.4	6.9	9.3	0.6	0.8	0.9
3S-M1-04	31%	8.0	0.27	10.0	0.69	0.20	6.1	11.4	14.5	1.2	1.3	1.3
3S-M1-05	31%	9.0	0.26	10.0	0.84	0.26	20.2	39.8	57.6	1.4	2.2	3.0
3S-M1-06	31%	3.5	0.15	15.9	0.90	0.21	3.3	6.2	8.8	0.4	0.5	1.0
3S-M1-07	31%	3.5	0.17	17.1	0.59	0.21	4.2	8.7	12.7	0.3	0.6	1.2
3S-M1-08	31%	3.5	0.20	18.3	0.52	0.22	5.7	11.6	16.3	0.5	0.9	1.3
3S-M1-09	31%	3.5	0.22	19.5	0.55	0.23	8.4	16.2	22.0	1.0	1.3	1.6
3S-M1-10	31%	3.5	0.25	20.7	0.54	0.24	11.1	22.0	31.1	0.8	1.4	2.0
3S-M1-11	31%	3.5	0.27	21.9	0.36	0.21	1.7	4.1	5.9	0.4	0.5	0.6
3S-M1-12	31%	3.5	0.29	23.1	0.33	0.20	1.1	2.7	3.5	0.4	0.4	0.4
3S-M1-13	31%	3.5	0.32	24.3	0.34	0.20	1.0	1.9	2.7	0.4	0.4	0.4
3S-M1-14	31%	3.5	0.34	25.5	0.45	0.37	0.8	1.4	2.1	0.4	0.4	0.4
3S-M1-15	31%	3.5	0.37	26.7	0.26	0.37	0.6	1.3	1.6	0.3	0.3	0.3
3S-M1-16	31%	3.5	0.39	27.9	0.23	0.20	0.8	1.4	1.4	0.3	0.2	0.2
3S-M1-17	31%	5.0	0.15	15.9	1.18	0.22	3.6	7.5	11.1	0.5	0.6	1.3
3S-M1-18	31%	5.0	0.17	17.1	0.77	0.22	6.1	11.3	16.4	0.4	0.7	1.4

Table D-2(continued) Sinusoidal 3-storey shake-table tests

Test	Test inputs					Response period (sec.)	Maximum level displacement (mm)			Maximum level acceleration (g)		
	Percentage of required weight	Amplitude (mm)	Period (sec.)	Duration (sec.)	Ground accel. (g)		L1	L2	L3	L1	L2	L3
3S-M1-18	31%	5.0	0.17	17.1	0.77	0.22	6.1	11.3	16.4	0.4	0.7	1.4
3S-M1-19	31%	5.0	0.20	18.3	0.67	0.23	7.2	14.5	20.3	0.5	1.1	1.6
3S-M1-20	31%	5.0	0.22	19.5	0.70	0.23	10.0	18.8	25.4	1.3	1.8	1.7
3S-M1-21	31%	5.0	0.25	20.7	0.61	0.25	13.4	26.0	36.7	1.0	1.5	2.2
3S-M1-22	31%	5.0	0.29	23.1	0.38	0.21	2.2	4.4	6.1	0.6	0.5	0.7
3S-M1-23	31%	5.0	0.32	24.3	0.47	0.20	1.4	3.1	4.0	0.5	0.5	0.5
3S-M1-24	31%	5.0	0.34	25.5	0.50	0.20	1.0	2.2	3.2	0.4	0.5	0.4
3S-M1-25	31%	5.0	0.37	26.7	0.31	0.37	1.1	1.8	2.1	0.4	0.3	0.4
3S-M1-26	31%	5.0	0.39	27.9	0.30	0.37	0.9	1.8	2.1	0.3	0.3	0.3
3S-M1-27	31%	6.5	0.15	15.9	1.73	0.21	4.6	9.5	13.8	0.7	0.7	1.5
3S-M1-28	31%	6.5	0.17	17.1	0.96	0.23	6.6	13.3	19.3	0.5	0.8	1.7
3S-M1-29	31%	6.5	0.20	18.3	0.88	0.23	8.5	17.2	24.1	0.5	1.1	1.8
3S-M1-30	31%	6.5	0.22	19.5	0.80	0.24	12.1	22.4	29.7	1.4	2.1	1.9
3S-M1-31	31%	6.5	0.25	20.7	0.88	0.25	14.5	28.5	40.6	1.2	1.9	2.3
3S-M1-32	31%	6.5	0.27	21.9	0.50	0.27	19.1	37.1	53.1	1.2	1.8	2.7
3S-M2-01	45%	3.5	0.15	15.9	0.79	0.23	2.9	5.7	7.6	0.4	0.5	0.8
3S-M2-02	45%	3.5	0.17	17.1	0.56	0.23	3.6	7.1	9.5	0.6	0.7	1.0
3S-M2-03	45%	3.5	0.20	18.3	0.62	0.25	5.1	9.7	12.9	0.3	0.7	1.0
3S-M2-04	45%	3.5	0.22	19.5	0.57	0.25	6.1	12.1	15.9	0.4	0.8	1.2
3S-M2-05	45%	3.5	0.25	20.7	0.40	0.26	8.2	15.7	21.4	0.5	0.9	1.3
3S-M2-06	45%	3.5	0.27	21.9	0.40	0.27	11.3	21.4	28.7	0.5	1.1	1.4

Table D-2(continued) Sinusoidal 3-storey shake-table tests

Test	Test inputs					Response period (sec.)	Maximum level displacement (mm)			Maximum level acceleration (g)		
	Percentage of required weight	Amplitude (mm)	Period (sec.)	Duration (sec.)	Ground accel. (g)		L1	L2	L3	L1	L2	L3
3S-M2-07	45%	3.5	0.29	23.1	0.38	0.25	4.6	8.9	11.9	0.7	0.7	1.0
3S-M2-08	45%	3.5	0.32	24.3	0.35	0.22	1.7	3.6	4.6	0.4	0.4	0.4
3S-M2-09	45%	3.5	0.34	25.5	0.29	0.21	1.0	2.6	3.0	0.2	0.3	0.3
3S-M2-10	45%	3.5	0.37	26.7	0.29	0.22	0.9	1.8	2.2	0.3	0.3	0.3
3S-M2-11	45%	5.0	0.15	15.9	1.11	0.24	4.3	8.2	11.3	0.7	0.6	1.1
3S-M2-12	45%	5.0	0.17	17.1	0.83	0.24	4.9	9.4	12.7	0.5	0.7	1.1
3S-M2-13	45%	5.0	0.20	18.3	0.73	0.25	6.1	11.9	16.6	0.4	0.7	1.2
3S-M2-14	45%	5.0	0.22	19.5	0.75	0.26	7.6	15.0	20.2	0.5	1.0	1.5
3S-M2-15	45%	5.0	0.25	20.7	0.49	0.26	10.0	19.5	26.5	0.5	1.1	1.5
3S-M2-16	45%	5.0	0.27	21.9	0.43	0.28	13.1	25.0	33.9	0.7	1.2	1.7
3S-M2-17	45%	5.0	0.29	23.1	0.48	0.29	16.6	31.6	42.8	0.8	1.4	1.9
3S-M2-18	45%	5.0	0.32	24.3	0.47	0.24	4.1	7.3	9.4	0.6	0.6	0.7
3S-M2-19	45%	5.0	0.34	25.5	0.36	0.22	1.9	3.9	5.1	0.3	0.4	0.4
3S-M2-20	45%	5.0	0.37	26.7	0.38	0.21	1.6	3.1	4.0	0.4	0.4	0.4
3S-M2-21	45%	6.5	0.15	15.9	1.31	0.24	5.1	9.3	12.7	0.6	0.6	1.2
3S-M2-22	45%	6.5	0.17	17.1	0.96	0.25	5.7	11.1	15.3	0.5	0.7	1.3
3S-M2-23	45%	6.5	0.20	18.3	0.83	0.27	7.4	14.7	20.3	0.5	0.9	1.4
3S-M2-24	45%	6.5	0.22	19.5	0.99	0.26	9.0	17.4	23.8	0.5	1.2	1.7
3S-M2-25	45%	6.5	0.25	20.7	0.63	0.28	11.3	22.0	30.2	0.6	1.2	1.7
3S-M2-26	45%	6.5	0.27	21.9	0.67	0.28	14.8	27.9	38.3	0.9	1.4	2.0
3S-M2-27	45%	6.5	0.29	23.1	0.57	0.30	19.0	35.2	48.2	0.9	1.5	2.1

Table D-2(continued) Sinusoidal 3-storey shake-table tests

Test	Test inputs					Response period (sec.)	Maximum level displacement (mm)			Maximum level acceleration (g)		
	Percentage of required weight	Amplitude (mm)	Period (sec.)	Duration (sec.)	Ground accel. (g)		L1	L2	L3	L1	L2	L3
3S-M2-28	45%	6.5	0.32	24.3	0.65	0.31	22.7	43.1	59.1	1.3	1.7	2.5
3S-M2-29	45%	6.5	0.37	26.7	0.43	0.23	2.4	4.9	6.7	0.5	0.5	0.6
3S-M2-30	45%	6.5	0.39	27.9	0.38	0.23	1.9	3.6	4.9	0.5	0.5	0.5
3S-M2-31	45%	3.5	0.25	20.7	0.39	0.25	11.6	22.0	29.4	0.7	1.3	1.7
3S-M2-32	45%	3.5	0.27	21.9	0.40	0.26	14.0	26.4	35.4	0.9	1.5	2.0
3S-M2-33	45%	3.5	0.29	23.1	0.43	0.22	2.2	4.7	6.5	0.7	0.5	0.8
3S-M2-34	45%	5.0	0.25	20.7	0.50	0.26	12.8	24.5	33.2	0.8	1.3	2.0
3S-M2-35	45%	5.0	0.27	21.9	0.38	0.27	16.7	31.6	42.7	0.8	1.5	2.2
3S-M2-36	45%	5.0	0.30	23.1	0.42	0.25	6.9	13.4	18.1	0.7	1.0	1.3
3S-M2-37	45%	5.0	0.39	27.9	0.27	0.21	1.2	2.1	2.8	0.4	0.4	0.4
3S-M2-38	45%	5.7	0.29	25.5	0.51	0.29	21.6	41.2	55.9	1.0	1.8	2.4
3S-M2-39	45%	5.7	0.39	27.9	0.33	0.21	1.5	2.7	3.3	0.5	0.5	0.5
3S-M2-40	45%	6.5	0.29	23.1	0.40	0.30	22.1	41.9	57.3	0.9	1.6	2.5
3S-M2-41	78%	3.5	0.15	15.9	0.41	0.25	3.5	7.0	8.8	0.5	0.5	0.6
3S-M3-01	78%	3.5	0.17	17.1	0.82	0.29	2.4	4.9	7.0	0.8	0.4	0.7
3S-M3-02	78%	3.5	0.20	18.3	0.63	0.28	2.7	5.5	7.9	0.3	0.3	0.5
3S-M3-03	78%	3.5	0.22	19.5	0.57	0.28	3.0	6.3	8.3	0.2	0.3	0.5
3S-M3-04	78%	3.5	0.25	20.7	0.58	0.30	3.8	7.5	10.4	0.4	0.5	0.6
3S-M3-05	78%	3.5	0.27	21.9	0.50	0.30	5.1	9.1	12.7	0.3	0.5	0.6
3S-M3-06	78%	3.5	0.29	23.1	0.39	0.31	6.0	11.7	16.0	0.3	0.5	0.7
3S-M3-07	78%	3.5	0.32	24.3	0.34	0.32	7.7	15.2	20.5	0.3	0.6	0.8

Table D-2(continued) Sinusoidal 3-storey shake-table tests

Test	Test inputs					Response period (sec.)	Maximum level displacement (mm)			Maximum level acceleration (g)		
	Percentage of required weight	Amplitude (mm)	Period (sec.)	Duration (sec.)	Ground accel. (g)		L1	L2	L3	L1	L2	L3
3S-M3-08	78%	3.5	0.34	25.5	0.37	0.33	9.8	18.9	25.8	0.4	0.7	0.9
3S-M3-09	78%	3.5	0.37	26.7	0.31	0.34	12.4	24.0	32.2	0.4	0.8	1.0
3S-M3-10	78%	3.5	0.39	27.9	0.26	0.30	4.8	9.6	12.8	0.4	0.5	0.5
3S-M3-11	78%	5.0	0.15	15.9	0.34	0.28	2.0	4.1	5.6	0.3	0.3	0.4
3S-M3-12	78%	5.0	0.17	17.1	1.03	0.30	2.7	6.7	10.1	0.7	0.3	0.8
3S-M3-13	78%	5.0	0.20	18.3	0.81	0.30	3.6	7.5	10.6	0.4	0.3	0.7
3S-M3-14	78%	5.0	0.22	19.5	0.69	0.31	4.0	8.0	11.2	0.3	0.4	0.6
3S-M3-15	78%	5.0	0.25	20.7	0.75	0.31	4.8	9.6	13.2	0.3	0.5	0.7
3S-M3-16	78%	5.0	0.27	21.9	0.50	0.32	7.2	14.1	19.3	0.3	0.5	0.8
3S-M3-17	78%	5.0	0.29	23.1	0.48	0.33	9.1	17.7	24.0	0.3	0.6	0.9
3S-M3-18	78%	5.0	0.32	24.3	0.45	0.34	11.3	22.1	30.3	0.4	0.8	1.0
3S-M3-19	78%	5.0	0.34	25.5	0.43	0.36	14.7	28.1	37.9	0.5	0.8	1.1
3S-M3-20	78%	5.0	0.37	26.7	0.35	0.37	17.4	33.2	45.1	0.5	0.9	1.3
3S-M3-21	78%	5.0	0.39	27.9	0.33	0.32	8.1	15.3	20.5	0.5	0.7	0.7
3S-M3-22	78%	6.5	0.15	15.9	1.29	0.30	3.4	8.2	12.3	0.8	0.3	1.0
3S-M3-23	78%	6.5	0.17	17.1	0.98	0.31	4.1	9.0	13.0	0.6	0.4	0.8
3S-M3-24	78%	6.5	0.20	18.3	0.87	0.32	4.9	9.8	14.1	0.4	0.4	0.8
3S-M3-25	78%	6.5	0.22	19.5	0.96	0.32	5.6	11.3	15.8	0.4	0.7	0.8
3S-M3-26	78%	6.5	0.25	20.7	0.83	0.33	7.0	13.4	18.3	0.6	0.7	0.9
3S-M3-27	78%	6.5	0.27	21.9	0.59	0.34	8.2	16.4	22.5	0.3	0.6	0.9
3S-M3-28	78%	6.5	0.29	23.1	0.59	0.34	10.2	19.8	27.0	0.3	0.7	1.0

Table D-2(continued) Sinusoidal 3-storey shake-table tests

Test	Test inputs					Response period (sec.)	Maximum level displacement (mm)			Maximum level acceleration (g)		
	Percentage of required weight	Amplitude (mm)	Period (sec.)	Duration (sec.)	Ground accel. (g)		L1	L2	L3	L1	L2	L3
3S-M3-29	78%	6.5	0.32	24.3	0.55	0.35	12.6	24.5	33.3	0.4	0.8	1.1
3S-M3-30	78%	6.5	0.34	25.5	0.58	0.36	15.6	30.1	40.5	0.5	0.9	1.2
3S-M3-31	78%	6.5	0.37	26.7	0.38	0.37	19.5	37.1	50.8	0.6	1.0	1.4
3S-M3-32	78%	6.5	0.39	27.9	0.41	0.39	22.0	42.4	58.2	0.6	1.0	1.5
3S-M3-33	78%	8.0	0.25	20.7	0.80	0.34	8.5	16.2	22.1	0.6	0.7	1.1
3S-M3-34	78%	8.0	0.27	21.9	0.65	0.33	9.8	19.3	26.6	0.3	0.6	1.1
3S-M3-35	78%	8.0	0.29	23.1	0.58	0.34	12.1	23.1	31.6	0.4	0.7	1.1
3S-M3-36	78%	8.0	0.32	24.3	0.60	0.36	14.2	27.8	38.1	0.4	0.9	1.3
3S-M3-37	78%	3.5	0.15	15.9	0.81	0.32	1.9	4.4	7.2	0.6	0.2	0.5
3S-M3-38	78%	3.5	0.17	17.1	0.60	0.33	2.0	4.8	7.4	0.4	0.2	0.4
3S-M3-39	78%	3.5	0.20	18.3	0.55	0.33	2.3	5.1	7.6	0.3	0.2	0.4
3S-M3-40	78%	3.5	0.22	19.5	0.58	0.34	2.7	5.7	8.3	0.3	0.4	0.4
3S-M3-41	78%	3.5	0.25	20.7	0.52	0.36	3.2	6.4	9.4	0.6	0.5	0.6
3S-M3-42	78%	3.5	0.27	21.9	0.39	0.34	3.5	7.6	11.2	0.2	0.3	0.4
3S-M3-43	78%	3.5	0.29	23.1	0.36	0.34	4.2	9.0	13.2	0.3	0.3	0.4
3S-M3-44	78%	3.5	0.32	24.3	0.37	0.35	5.5	11.3	15.8	0.2	0.4	0.5
3S-M3-45	78%	3.5	0.34	25.5	0.38	0.37	6.5	13.6	19.2	0.2	0.4	0.6
3S-M3-46	78%	3.5	0.37	26.7	0.33	0.39	7.8	16.2	22.8	0.3	0.4	0.6
3S-M3-47	78%	3.5	0.39	27.9	0.21	0.39	9.4	19.2	27.3	0.3	0.5	0.7
3S-M3-48	78%	5.0	0.15	15.9	0.99	0.33	2.1	5.9	10.1	0.7	0.2	0.7
3S-M3-49	78%	5.0	0.17	17.1	0.78	0.34	2.8	6.5	9.9	0.5	0.2	0.6

Table D-2(continued) Sinusoidal 3-storey shake-table tests

Test	Test inputs					Response period (sec.)	Maximum level displacement (mm)			Maximum level acceleration (g)		
	Percentage of required weight	Amplitude (mm)	Period (sec.)	Duration (sec.)	Ground accel. (g)		L1	L2	L3	L1	L2	L3
3S-M3-50	78%	5.0	0.20	18.3	0.67	0.34	3.3	7.0	10.5	0.3	0.2	0.5
3S-M3-51	78%	5.0	0.22	19.5	0.69	0.33	3.3	6.9	10.1	0.4	0.4	0.5
3S-M3-52	78%	5.0	0.25	20.7	0.64	0.36	4.0	8.0	11.6	0.4	0.5	0.6
3S-M3-53	78%	5.0	0.27	21.9	0.47	0.36	4.7	9.6	14.3	0.2	0.3	0.5
3S-M3-54	78%	5.0	0.29	23.1	0.45	0.37	5.7	11.6	16.8	0.3	0.4	0.5
3S-M3-55	78%	5.0	0.32	24.3	0.44	0.36	6.8	14.0	19.6	0.2	0.4	
3S-M3-56	78%	5.0	0.34	25.5	0.52	0.38	8.0	16.3	23.2	0.3	0.5	0.7
3S-M3-57	78%	5.0	0.37	26.7	0.41	0.40	9.4	19.2	27.2	0.3	0.5	0.7
3S-M3-58	78%	5.0	0.39	27.9	0.31	0.40	11.3	22.9	32.7	0.3	0.6	0.8
3S-M3-59	78%	3.5	0.15	15.9	0.78	0.27	2.4	5.4	7.5	0.6	0.4	0.7
3S-M3-60	78%	3.5	0.17	17.1	0.64	0.28	2.8	5.8	8.1	0.3	0.3	0.6
3S-M3-61	78%	3.5	0.20	18.3	0.57	0.29	3.9	7.7	10.9	0.4	0.6	0.7
3S-M3-62	78%	3.5	0.22	19.5	0.57	0.29	3.9	7.5	10.8	0.4	0.6	0.7
3S-M3-63	78%	3.5	0.25	20.7	0.57	0.30	5.0	9.6	13.2	0.3	0.6	0.7
3S-M3-64	78%	3.5	0.27	21.9	0.40	0.31	6.2	12.4	16.8	0.3	0.5	0.7
3S-M3-65	78%	3.5	0.29	23.1	0.34	0.32	7.9	15.7	21.5	0.3	0.6	0.8
3S-M3-66	78%	3.5	0.32	24.3	0.36	0.33	10.1	19.8	27.0	0.5	0.7	1.0
3S-M3-67	78%	3.5	0.34	25.5	0.35	0.34	12.7	24.4	32.8	0.5	0.8	1.1
3S-M3-68	78%	3.5	0.37	26.7	0.26	0.29	3.7	7.5	10.1	0.3	0.5	0.5
3S-M3-69	78%	3.5	0.39	27.9	0.37	0.29	1.6	3.6	5.1	0.3	0.3	0.4
3S-M3-70	78%	5.0	0.15	15.9	1.05	0.30	3.0	7.0	10.2	0.7	0.3	0.8

Table D-2(continued) Sinusoidal 3-storey shake-table tests

Test	Test inputs					Response period (sec.)	Maximum level displacement (mm)			Maximum level acceleration (g)		
	Percentage of required weight	Amplitude (mm)	Period (sec.)	Duration (sec.)	Ground accel. (g)		L1	L2	L3	L1	L2	L3
3S-M3-71	78%	3.5	0.17	17.1	0.65	0.30	2.7	5.9	8.3	0.4	0.3	0.5
3S-M3-72	78%	3.5	0.20	18.3	0.55	0.31	2.8	5.8	8.0	0.3	0.3	0.5
3S-M3-73	78%	3.5	0.22	19.5	0.57	0.31	3.3	6.9	9.6	0.3	0.5	0.5
3S-M3-74	78%	3.5	0.25	20.7	0.60	0.32	4.3	8.4	11.5	0.4	0.5	0.6
3S-M3-75	78%	3.5	0.27	21.9	0.40	0.32	5.2	10.5	14.5	0.2	0.4	0.6
3S-M3-76	78%	3.5	0.29	23.1	0.36	0.33	6.6	13.2	18.1	0.3	0.5	0.7
3S-M3-77	78%	3.5	0.32	24.3	0.35	0.34	8.4	17.0	23.5	0.3	0.6	0.8
3S-M3-78	78%	3.5	0.34	25.5	0.36	0.35	11.5	22.4	30.5	0.4	0.7	0.9
3S-M3-79	78%	3.5	0.37	26.7	0.38	0.36	13.9	27.3	37.3	0.5	0.9	1.1
3S-M3-80	78%	3.5	0.39	27.9	0.33	0.31	3.4	6.8	10.0	0.6	0.5	0.7
3S-M3-81	78%	5.0	0.15	15.9	1.09	0.31	3.0	6.8	10.2	0.7	0.3	0.8
3S-M3-82	78%	5.0	0.17	17.1	0.81	0.32	3.4	7.3	10.5	0.5	0.3	0.6
3S-M3-83	78%	5.0	0.20	18.3	0.69	0.32	3.9	8.0	11.2	0.3	0.3	0.6
3S-M3-84	78%	5.0	0.22	19.5	0.63	0.32	5.3	10.5	15.0	0.4	0.6	0.8
3S-M3-85	78%	5.0	0.25	20.7	0.63	0.32	5.3	10.5	15.0	0.4	0.6	0.8
3S-M3-86	78%	5.0	0.27	21.9	0.49	0.33	6.4	12.9	18.0	0.2	0.5	0.8
3S-M3-87	78%	5.0	0.30	23.1	0.47	0.34	8.2	16.4	22.5	0.3	0.6	0.8
3S-M3-88	78%	5.0	0.33	24.3	0.44	0.34	10.5	20.7	28.4	0.3	0.7	0.9
3S-M3-89	78%	5.0	0.34	25.5	0.50	0.36	13.2	25.7	35.2	0.5	0.8	1.1
3S-M3-90	78%	5.0	0.37	26.7	0.35	0.37	15.9	31.0	42.6	0.5	0.8	1.1
3S-M3-91	78%	5.0	0.39	27.9	0.36	0.39	18.9	37.1	51.4	0.7	1.0	1.3

Table D-3 Earthquake 5-storey shake-table tests

Shake table input								Maximum displacements per level (mm)					Maximum accelerations per level (g)				
Earthquake Event	PGA (g)	PGV (mm/sec.)	PGD (mm)	Dt (sec.)	T (sec.)	Post-tension (kN)	Mass	L1	L2	L3	L4	L5	L1	L2	L3	L4	L5
Loma Prieta	0.27	240	82	0.002	50	30.4	31%	2.4	5.4	6.8	8.4	9.5	0.31	0.34	0.45	0.49	0.52
Kobe	0.38	165	60	0.002	40	30.5	31%	3.2	7.0	9.4	11.8	13.5	0.40	0.40	0.53	0.58	0.65
Northridge	0.41	273	109	0.002	30	29.9	31%	6.5	11.9	17.3	21.1	23.6	0.45	0.60	0.72	0.79	0.99
C. Mendocino	0.48	269	73	0.002	40	30.0	31%	7.1	14.6	19.6	24.0	27.1	0.66	0.81	0.91	0.87	1.16
Loma Prieta	0.30	264	83	0.002	40	45.9	31%	2.4	5.9	7.5	9.0	10.2	0.37	0.33	0.51	0.54	0.61
Kobe	0.39	166	61	0.002	40	45.9	31%	4.0	8.1	10.3	12.7	14.2	0.43	0.45	0.60	0.65	0.73
Northridge	0.41	263	109	0.002	30	46.0	31%	6.4	11.7	16.5	19.5	21.5	0.44	0.57	0.80	0.82	0.94
C. Mendocino	0.46	278	73	0.002	40	46.0	31%	6.8	12.9	18.1	21.8	24.3	0.55	0.62	0.79	0.90	1.05

Table D-4 Earthquake 3-storey shake-table tests

Shake table input								Maximum displacements per level (mm)			Maximum accelerations per level (g)		
Earthquake Event	PGA (g)	PGV (mm/sec.)	PGD (mm)	Dt (sec.)	T (sec.)	Post-tension (kN)	Mass	L1	L2	L3	L1	L2	L3
Loma Prieta	0.34	242	82	0.002	40	47.0	31%	2.1	3.9	5.2	0.36	0.61	0.60
Kobe	0.45	256	61	0.002	40	47.2	31%	3.4	7.1	9.3	0.60	0.77	0.98
Northridge	0.39	273	108	0.002	30	46.9	31%	3.2	4.3	6.0	0.51	0.59	0.75
C. Mendocino	0.47	288	73	0.002	30	47.5	31%	4.6	9.3	12.4	0.71	1.04	1.22
Loma Prieta	0.32	269	82	0.002	40	45.6	44%	3.2	6.1	8.2	0.42	0.52	0.64
Kobe	0.47	200	60	0.002	80	45.6	44%	5.8	11.6	14.7	0.51	0.79	0.88
Northridge	0.42	275	108	0.002	30	45.6	44%	7.9	14.1	19.8	0.58	0.85	1.13
C. Mendocino	0.49	285	72	0.002	30	45.5	44%	4.8	10.0	13.0	0.65	0.70	1.03
Loma Prieta	0.29	237	82	0.002	40	46.5	78%	4.8	8.5	10.7	0.34	0.44	0.57
Kobe	0.45	194	61	0.002	80	46.6	78%	5.9	12.4	16.0	0.42	0.65	0.75
Northridge	0.50	268	108	0.002	30	46.6	78%	8.5	16.1	22.1	0.58	0.67	0.85
C. Mendocino	0.55	298	73	0.002	40	46.7	78%	10.7	21.4	28.1	0.56	0.79	0.92
Parkfield	0.48	253	76	0.002	40	45.5	78%	14.4	27.5	37.4	0.51	0.84	1.06
Sylmar	0.45	225	30	0.002	40	45.5	78%	12.2	22.5	29.7	0.57	0.77	0.95
Loma Prieta	0.34	212	83	0.002	50	17.2	78%	5.4	12.9	17.6	0.36	0.46	0.60
Kobe	0.46	207	61	0.002	80	17.4	78%	7.3	15.3	21.2	0.36	0.58	0.65
Northridge	0.49	283	109	0.002	30	17.5	78%	7.1	16.1	23.2	0.51	0.60	0.81
C. Mendocino	0.48	279	73	0.002	40	17.4	78%	14.8	32.0	45.6	0.49	0.70	0.98

Table D-4(continued) Earthquake 3-storey shake-table tests

Shake table input								Maximum displacements per level (mm)			Maximum accelerations per level (g)		
Earthquake Event	PGA (g)	PGV (mm/sec.)	PGD (mm)	Dt (sec.)	T (sec.)	Post-tension (kN)	Mass	L1	L2	L3	L1	L2	L3
Parkfield	0.43	245	76	0.002	30	16.2	78%	12.1	24.5	35.2	0.45	0.55	0.81
Sylmar	0.46	213	30	0.002	30	16.2	78%	9.7	19.2	27.1	0.50	0.59	0.79
Loma Prieta	0.32	223	82	0.002	90	45.8	78%	5.8	12.4	15.8	0.45	0.53	0.61
Kobe	0.42	165	60	0.002	80	45.7	78%	8.6	17.5	22.8	0.46	0.72	0.84
Northridge	0.47	238	107	0.002	50	45.7	78%	9.5	20.0	26.6	0.48	0.71	0.92
C. Mendocino	0.50	249	72	0.002	50	45.7	78%	13.3	27.3	36.7	0.64	0.78	1.05
Parkfield	0.51	249	75	0.002	40	45.8	78%	15.1	28.6	38.6	0.56	0.82	1.11
Sylmar	0.42	238	29	0.002	40	45.7	78%	11.7	21.8	29.2	0.66	0.78	0.91

APPENDIX E: POST-TENSIONING FORCES

Table E- 1 Post-tensioning forces during dynamic test of 5-storey modelled building

Test	Initial post-tensioning Force per Level (kN)					Final post-tensioning Force per Level (kN)					Post-tensioning loss per Level (%)				
	L 1	L2	L3	L4	L5	L1	L2	L3	L4	L5	L1	L2	L3	L4	L5
5S-M1-01	15.0	15.0	15.2	13.3	15.2	14.9	14.9	15.1	13.3	15.2	0.90%	0.99%	0.43%	0.00%	0.00%
5S-M1-02	14.9	14.9	15.2	13.3	15.2	14.9	14.9	15.1	13.3	15.2	0.00%	0.00%	0.43%	0.00%	0.00%
5S-M1-03	14.9	14.9	15.1	13.3	15.2	14.9	14.9	15.1	13.3	15.2	0.00%	0.00%	0.00%	0.00%	0.00%
5S-M1-04	14.8	15.0	15.1	10.3	15.6	14.8	14.9	15.1	10.3	15.7	0.00%	0.50%	0.00%	0.00%	0.00%
5S-M1-05	14.3	14.3	14.5	11.0	14.5	14.3	14.3	14.5	11.0	14.6	0.47%	0.00%	0.00%	0.00%	0.00%
5S-M1-06	13.6	13.4	13.8	11.7	13.9	13.6	13.4	13.8	11.7	13.8	0.00%	0.55%	0.00%	0.00%	0.49%
5S-M1-07	13.5	13.1	13.7	12.1	13.8	13.3	13.1	13.6	12.2	13.8	1.00%	0.56%	0.48%	0.00%	0.00%
5S-M1-08	13.5	13.1	13.6	12.2	13.8	13.3	13.0	13.6	12.2	13.7	1.00%	0.57%	0.48%	0.57%	0.49%
5S-M1-09	12.6	14.2	15.1	15.2	15.2	12.7	14.2	15.1	15.3	15.3	0.00%	0.00%	0.00%	0.00%	0.00%
5S-M1-10	12.7	14.1	15.1	15.3	14.7	12.8	14.2	15.1	15.3	14.7	0.00%	0.00%	0.00%	0.00%	0.00%
5S-M1-11	12.9	14.2	15.3	15.3	15.4	12.8	14.2	15.3	15.3	15.3	0.52%	0.00%	0.43%	0.00%	0.44%
5S-M1-12	13.4	14.9	15.9	16.2	15.5	13.3	14.9	15.9	16.1	15.5	0.50%	0.00%	0.41%	0.43%	0.00%
5S-M1-13	13.4	14.9	15.9	16.1	15.5	13.4	14.9	15.9	16.1	15.5	0.00%	0.50%	0.41%	0.00%	0.00%
5S-M1-14	13.4	14.9	15.9	16.1	15.5	13.4	14.9	15.9	16.0	15.6	0.00%	0.00%	0.00%	0.43%	0.00%
5S-M1-15	13.4	14.9	15.9	16.1	15.5	13.4	14.9	15.9	16.1	15.5	0.00%	0.00%	0.00%	0.00%	0.00%
5S-M1-16	13.3	14.9	15.9	16.1	15.5	13.3	14.9	15.9	16.1	15.5	0.00%	0.50%	0.00%	0.00%	0.00%
5S-M1-17	13.3	14.9	15.9	16.1	15.5	13.2	14.9	15.9	16.2	15.5	0.51%	0.50%	0.00%	0.00%	0.00%
5S-M1-18	13.3	14.9	15.9	16.2	15.5	13.2	14.9	15.7	16.1	15.5	1.01%	0.00%	0.83%	0.43%	0.44%
5S-M1-19	13.2	14.6	15.7	16.1	15.5	13.0	14.6	15.5	16.0	15.3	1.52%	0.51%	1.67%	0.43%	0.88%
5S-M1-20	13.1	14.6	15.5	16.0	15.4	12.8	14.5	15.3	16.0	15.2	2.05%	1.02%	1.69%	0.00%	0.88%
5S-M1-21	12.8	14.5	15.3	16.0	15.3	12.4	14.1	14.5	15.9	15.2	3.14%	2.56%	5.15%	0.43%	0.88%
5S-M1-22	30.4	28.8	29.2	30.1	31.5	30.4	28.9	29.2	30.1	31.4	0.00%	0.00%	0.00%	0.00%	0.22%
5S-M1-23	30.4	28.8	29.2	30.1	31.4	30.4	28.8	29.2	30.1	31.4	0.00%	0.00%	0.00%	0.00%	0.00%
5S-M1-24	30.4	28.7	29.2	30.1	31.4	30.4	28.9	29.2	30.1	31.4	0.00%	0.00%	0.00%	0.00%	0.00%

Table E-1(continued) Post-tensioning forces during dynamic test of 5-storey modelled building

Test	Initial post-tensioning Force per Level (kN)					Final post-tensioning Force per Level (kN)					Post-tensioning loss per Level (%)				
	L 1	L2	L3	L4	L 5	L 1	L2	L3	L4	L 5	L 1	L2	L3	L4	L 5
5S-M1-25	30.4	28.8	29.2	30.2	31.4	30.4	28.7	29.2	30.1	31.4	0.00%	0.26%	0.00%	0.23%	0.00%
5S-M1-26	30.3	28.7	29.2	30.1	31.4	30.4	28.7	29.2	30.1	31.4	0.00%	0.00%	0.00%	0.00%	0.00%
5S-M1-26	30.3	28.7	29.2	30.1	31.4	30.4	28.7	29.2	30.1	31.4	0.00%	0.00%	0.00%	0.00%	0.00%
5S-M1-27	30.4	28.7	29.2	30.1	31.4	30.3	28.7	29.2	30.1	31.4	0.22%	0.00%	0.00%	0.00%	0.00%
5S-M1-28	30.3	28.8	29.2	30.1	31.4	30.3	28.7	29.2	30.1	31.4	0.00%	0.26%	0.00%	0.23%	0.00%
5S-M1-29	30.3	28.7	29.2	30.1	31.4	30.3	28.7	29.2	30.1	31.4	0.22%	0.00%	0.22%	0.00%	0.00%
5S-M1-30	30.2	28.5	29.1	30.1	31.4	29.9	28.2	29.0	30.1	31.4	1.11%	1.04%	0.45%	0.23%	0.22%
5S-M1-31	30.6	31.2	28.0	29.2	31.2	30.3	30.6	27.7	29.1	31.2	0.88%	1.90%	1.17%	0.24%	0.00%
5S-M1-32	30.3	30.6	27.7	29.0	31.2	29.5	29.9	27.3	29.0	31.1	2.44%	2.18%	1.42%	0.24%	0.22%
5S-M1-33	30.4	31.4	27.9	29.2	31.2	30.5	31.3	27.9	29.2	31.2	0.00%	0.24%	0.00%	0.00%	0.00%
5S-M1-34	30.4	31.4	27.9	29.2	31.2	30.5	31.3	27.9	29.2	31.2	0.00%	0.24%	0.00%	0.00%	0.00%
5S-M1-35	30.4	31.3	27.9	29.2	31.2	30.5	31.4	27.9	29.1	31.2	0.00%	0.00%	0.00%	0.24%	0.00%
5S-M1-36	30.4	31.3	27.9	29.2	31.2	30.5	31.3	27.9	29.2	31.2	0.00%	0.24%	0.00%	0.00%	0.00%
5S-M1-37	30.5	31.2	27.8	29.3	31.1	30.5	31.2	27.9	29.2	31.2	0.00%	0.00%	0.00%	0.24%	0.00%
5S-M1-38	46.4	44.0	45.0	46.3	48.2	46.3	44.0	45.0	46.3	48.3	0.14%	0.00%	0.00%	0.00%	0.00%
5S-M1-39	46.3	44.0	45.0	46.3	48.3	46.3	43.9	45.0	46.2	48.1	0.15%	0.17%	0.00%	0.15%	0.28%
5S-M1-40	46.3	44.0	45.0	46.3	48.3	46.3	43.9	45.0	46.2	48.1	0.15%	0.17%	0.00%	0.15%	0.28%
5S-M1-41	46.4	44.0	45.0	46.2	48.3	46.2	43.7	45.0	46.2	48.3	0.43%	0.51%	0.15%	0.00%	0.00%
5S-M1-42	46.2	43.7	45.0	46.2	48.0	46.3	43.7	45.0	46.2	48.2	0.00%	0.00%	0.00%	0.00%	0.00%
5S-M1-43	46.2	43.7	45.0	46.2	48.2	46.1	43.6	45.0	46.2	48.1	0.15%	0.34%	0.00%	0.15%	0.14%
5S-M1-44	46.1	43.7	45.0	46.0	48.1	46.1	43.7	44.9	46.2	48.0	0.00%	0.00%	0.15%	0.00%	0.14%
5S-M1-45	46.1	43.6	44.9	46.2	48.0	46.2	43.6	44.9	46.2	48.0	0.00%	0.00%	0.00%	0.00%	0.00%
5S-M1-46	46.2	43.6	44.9	46.1	48.1	46.2	43.7	44.9	46.2	48.2	0.00%	0.00%	0.00%	0.00%	0.00%
5S-M1-47	46.2	43.7	44.9	46.2	48.1	46.1	43.7	44.8	46.0	48.1	0.15%	0.00%	0.15%	0.30%	0.00%
5S-M1-48	46.1	43.6	44.8	46.2	48.0	46.1	43.6	44.9	46.2	48.1	0.00%	0.00%	0.00%	0.00%	0.00%
5S-M1-49	46.1	43.7	44.9	46.2	48.1	46.1	43.6	44.9	46.2	48.0	0.00%	0.17%	0.00%	0.00%	0.14%
5S-M1-50	46.1	43.7	45.0	46.1	48.1	46.2	43.7	44.9	46.1	48.1	0.00%	0.00%	0.15%	0.00%	0.00%

Table E-1(continued) Post-tensioning forces during dynamic test of 5-storey modelled building

Test	Initial post-tensioning Force per Level (kN)					Final post-tensioning Force per Level (kN)					Post-tensioning loss per Level (%)				
	L 1	L2	L3	L4	L 5	L 1	L2	L3	L4	L 5	L 1	L2	L3	L4	L 5
5S-M1-51	46.2	43.7	44.9	46.1	48.0	46.1	43.7	44.9	46.1	48.1	0.15%	0.00%	0.00%	0.00%	0.00%
5S-M1-52	46.1	43.6	44.8	46.1	48.1	46.1	43.6	44.9	46.1	48.1	0.00%	0.00%	0.00%	0.00%	0.00%
5S-M1-53	46.0	43.6	44.8	46.2	48.0	46.2	43.6	44.9	46.1	48.1	0.00%	0.00%	0.00%	0.15%	0.00%
5S-M1-55	46.1	43.6	44.9	46.1	48.1	46.2	43.6	44.9	46.2	48.2	0.00%	0.00%	0.00%	0.00%	0.00%
5S-M1-56	46.1	43.6	44.9	46.1	48.1	46.1	43.5	44.8	46.1	48.0	0.15%	0.17%	0.29%	0.00%	0.28%
5S-M1-57	46.1	43.6	44.8	46.1	48.0	46.1	43.6	44.9	46.1	48.1	0.00%	0.00%	0.00%	0.00%	0.00%
5S-M1-58	46.1	43.5	44.8	46.2	48.0	46.1	43.7	44.9	46.0	48.1	0.00%	0.00%	0.00%	0.45%	0.00%
5S-M1-59	46.2	43.7	44.8	46.1	48.1	46.1	43.6	44.9	46.1	48.1	0.15%	0.34%	0.00%	0.00%	0.00%
5S-M1-60	46.1	43.6	44.8	46.1	48.0	46.1	43.6	44.8	46.2	48.0	0.15%	0.00%	0.00%	0.00%	0.00%
5S-M1-61	46.1	43.6	44.9	46.1	48.2	46.1	43.5	44.8	46.1	48.0	0.00%	0.17%	0.29%	0.00%	0.42%
5S-M1-62	46.1	43.6	44.8	46.1	48.1	45.9	43.4	44.8	46.0	48.1	0.44%	0.51%	0.15%	0.30%	0.00%
5S-M1-63	45.9	43.4	44.8	46.0	48.0	45.9	43.4	44.8	46.0	48.0	0.15%	0.00%	0.00%	0.15%	0.00%
5S-M1-64	45.9	43.3	44.7	46.0	48.0	45.9	43.4	44.7	46.0	48.0	0.00%	0.00%	0.00%	0.15%	0.00%
5S-M1-65	44.7	43.2	44.2	45.6	47.4	44.7	43.2	44.2	45.6	47.4	0.00%	0.17%	0.00%	0.15%	0.00%
5S-M1-66	44.7	43.2	44.1	45.5	47.4	44.7	43.1	44.1	45.5	47.3	0.15%	0.17%	0.00%	0.00%	0.14%
5S-M1-67	44.8	43.2	44.2	45.5	47.4	44.6	43.0	44.1	45.5	47.3	0.45%	0.34%	0.15%	0.00%	0.14%
5S-M1-68	44.6	43.0	44.0	45.6	47.2	44.7	43.2	44.1	45.5	47.4	0.00%	0.00%	0.00%	0.15%	0.00%
5S-M1-69	44.6	43.2	44.1	45.5	47.3	44.7	43.2	44.1	45.5	47.4	0.00%	0.17%	0.00%	0.00%	0.00%
5S-M1-70	44.6	43.1	44.2	45.5	47.3	44.7	43.2	44.2	45.6	47.4	0.00%	0.00%	0.00%	0.00%	0.00%
5S-M1-71	44.5	42.9	43.9	45.5	47.0	44.5	43.0	44.0	45.5	47.0	0.00%	0.00%	0.00%	0.00%	0.00%
5S-M1-72	44.5	43.0	44.0	45.5	47.0	44.5	42.9	44.0	45.4	47.0	0.00%	0.17%	0.00%	0.15%	0.00%
5S-M1-73	44.5	42.9	44.0	45.5	47.0	44.3	42.5	43.6	45.3	47.0	0.60%	1.04%	0.75%	0.31%	0.00%
5S-M1-74	44.3	42.6	43.7	45.3	47.0	44.0	42.2	43.4	45.1	46.9	0.76%	0.87%	0.60%	0.46%	0.14%
5S-M1-75	44.0	42.1	43.4	45.2	46.8	43.9	42.1	43.4	45.2	46.8	0.15%	0.00%	0.15%	0.00%	0.00%
5S-M1-76	43.8	42.1	43.3	45.2	46.9	44.0	42.1	43.3	45.1	46.9	0.00%	0.00%	0.00%	0.15%	0.00%
5S-M1-77	43.8	42.0	43.3	45.1	46.9	43.8	42.0	43.3	45.1	46.9	0.15%	0.00%	0.00%	0.00%	0.00%
5S-M1-78	43.8	42.0	43.3	45.1	46.8	43.9	42.0	43.4	45.1	46.9	0.00%	0.00%	0.00%	0.15%	0.00%

Table E-1(continued) Post-tensioning forces during dynamic test of 5-storey modelled building

Test	Initial post-tensioning Force per Level (kN)					Final post-tensioning Force per Level (kN)					Post-tensioning loss per Level (%)				
	L 1	L2	L3	L4	L 5	L 1	L2	L3	L4	L 5	L 1	L2	L3	L4	L 5
5S-M1-79	43.9	42.0	43.3	45.1	46.8	43.9	42.0	43.3	45.1	46.9	0.00%	0.18%	0.00%	0.15%	0.00%
5S-M1-80	43.8	41.9	43.2	45.2	46.8	43.7	41.7	43.1	45.1	46.8	0.31%	0.53%	0.15%	0.31%	0.00%
5S-M1-81	43.7	41.5	43.1	45.1	46.8	43.1	41.1	42.7	44.9	46.8	1.38%	1.07%	0.91%	0.46%	0.00%
5S-M1-82	44.8	46.8	42.5	44.8	46.8	45.3	46.9	42.5	44.8	46.7	0.00%	0.00%	0.00%	0.00%	0.14%
5S-M1-83	45.3	46.9	42.5	44.8	46.7	45.4	46.5	42.5	44.8	46.8	0.00%	0.95%	0.15%	0.00%	0.00%
5S-M1-84	45.3	46.3	42.4	44.8	46.8	45.1	45.8	42.1	44.6	46.6	0.59%	1.28%	0.62%	0.47%	0.29%
5S-M1-85	45.1	45.8	42.1	44.5	46.6	44.7	45.2	41.7	44.4	46.6	0.75%	1.30%	0.78%	0.16%	0.15%

APPENDIX F: INTRUMENTATION SET-UP FOR QUASI-STATIC TESTING

Nomenclature: XX-YY XX: Device YY: Channel

LC: Load cell
LP: Linear potentiometer
RP: Rotational potentiometer
SP: Spring potentiometer

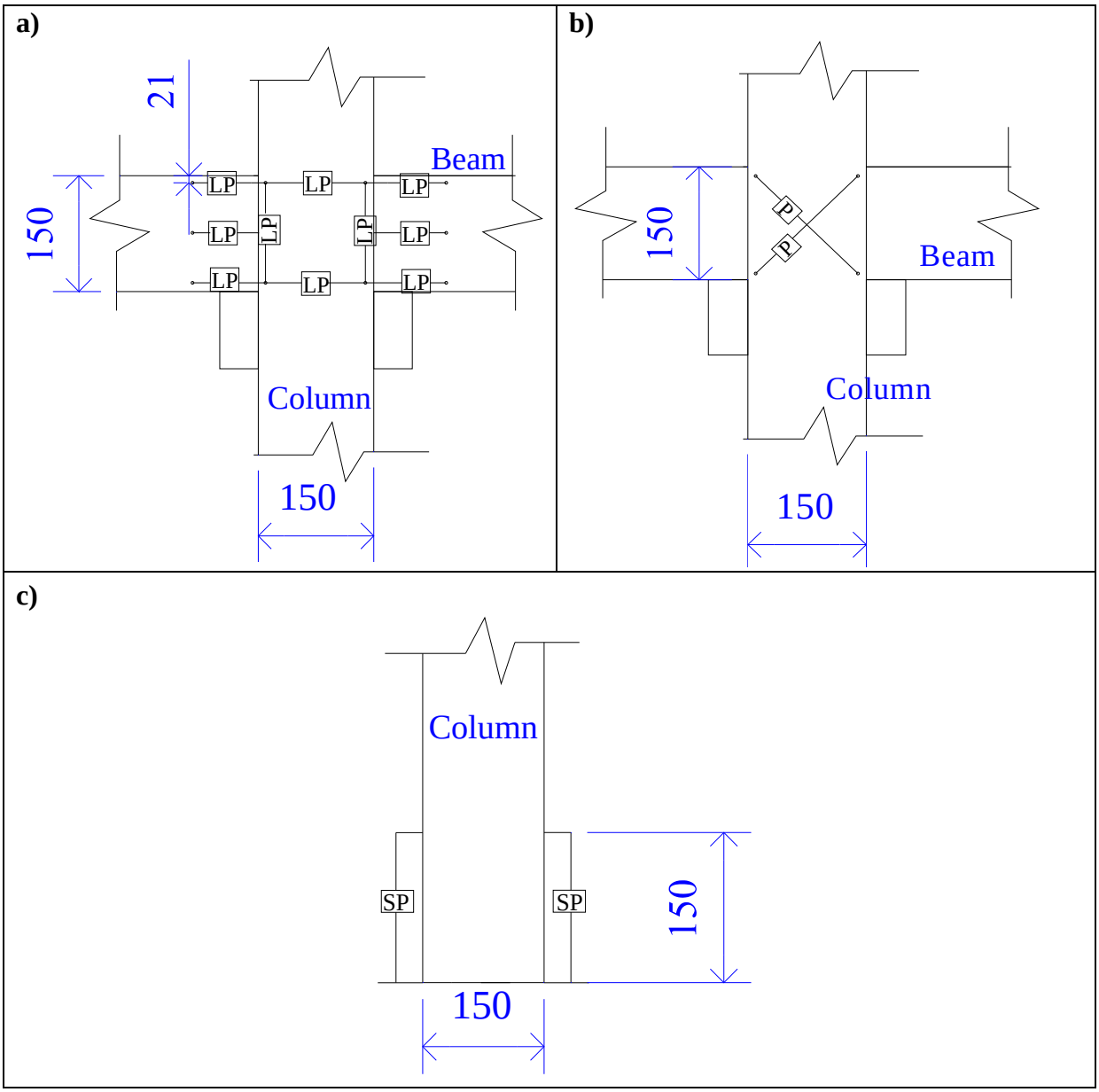

Figure F-1 a) Internal North beam-column instrumentation configuration b) Internal South beam-column instrumentation configuration c) Column instrumentation configuration

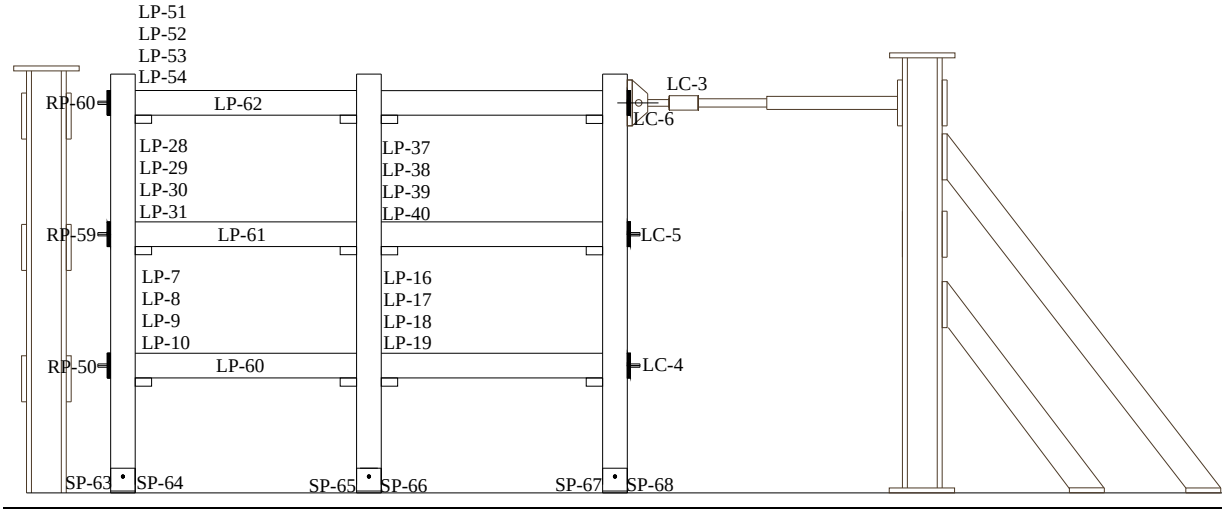

Figure F-2 North side instrumentation set-up quasi-static test

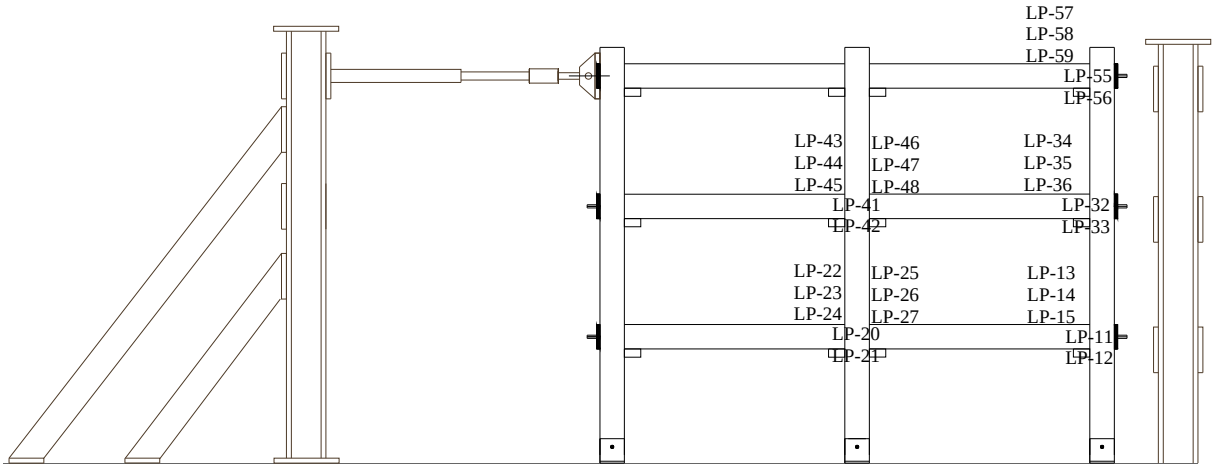

Figure F-3 South side instrumentation set-up quasi-static test

Table F-1 Quasi-static test instrumentation

Channel	Device	Instrument ID	Calibration Factor
1	Load Cell	LC-Q	0.0095
2	Load Cell	LC-M	-0.0230
3	Load Cell	LC-S	0.022
4	Load Cell	LC-H	0.0149
5	Load Cell	LC-U	-0.0159
6	Load Cell	LC-D	-0.0161
7	Linear Potentiometer	LP-81	0.0021
8	Linear Potentiometer	LP-82	0.0021
9	Linear Potentiometer	LP-83	0.0021
10	Linear Potentiometer	LP-84	0.0021
11	Linear Potentiometer	LP-85	0.0021
12	Linear Potentiometer	LP-86	0.0021
13	Linear Potentiometer	LP-87	0.0021
14	Linear Potentiometer	LP-88	0.0021
15	Linear Potentiometer	LP-89	0.0021
16	Linear Potentiometer	LP-90	0.0021
17	Linear Potentiometer	LP-91	0.0021
18	Linear Potentiometer	LP-92	0.0021
19	Linear Potentiometer	LP-93	0.0021
20	Linear Potentiometer	LP-94	0.0021
21	Linear Potentiometer	LP-95	0.0021
22	Linear Potentiometer	LP-96	0.0021
23	Linear Potentiometer	LP-97	0.0021
24	Linear Potentiometer	LP-98	0.0021
25	Linear Potentiometer	LP-99	0.0021
26	Linear Potentiometer	LP-100	0.0021
27	Linear Potentiometer	LP-170	0.0021
28	Linear Potentiometer	LP-171	0.0021
29	Linear Potentiometer	LP-172	0.0021
30	Linear Potentiometer	LP-173	0.0021
31	Linear Potentiometer	LP-174	0.0021
32	Linear Potentiometer	LP-175	0.0021
33	Linear Potentiometer	LP-176	0.0021
34	Linear Potentiometer	LP-177	0.0021
35	Linear Potentiometer	LP-178	0.0021
36	Linear Potentiometer	LP-179	0.0021
37	Linear Potentiometer	LP-180	0.0021
38	Linear Potentiometer	LP-181	0.0021
39	Linear Potentiometer	LP-182	0.0021
40	Linear Potentiometer	LP-183	0.0021
41	Linear Potentiometer	LP-184	0.0021
42	Linear Potentiometer	LP-185	0.0021
43	Linear Potentiometer	LP-186	0.0021
44	Linear Potentiometer	LP-187	0.0021

Table F-1(continued) Quasi-static test instrumentation

Channel	Device	Instrument ID	Calibration Factor
45	Linear Potentiometer	LP-188	0.0021
46	Linear Potentiometer	LP-189	0.0021
47	Linear Potentiometer	LP-190	0.0021
48	Linear Potentiometer	LP-191	0.0021
50	Rotational Potentiometer	RP-1	0.0463
51	Linear Potentiometer	LP-194	0.0021
52	Linear Potentiometer	LP-195	0.0021
53	Linear Potentiometer	LP-197	0.0021
54	Linear Potentiometer	LP-198	0.0021
55	Linear Potentiometer	LP-199	0.0021
56	Linear Potentiometer	LP-200	0.0021
57	Linear Potentiometer	LP-201	0.0021
58	Linear Potentiometer	LP-202	0.0021
59	Linear Potentiometer	LP-203	0.0020
60	Linear Potentiometer	LP-204	0.0021
61	Linear Potentiometer	LP-205	0.0021
62	Linear Potentiometer	LP-206	0.0021
63	Spring Potentiometer	SP-16a	0.0034
64	Spring Potentiometer	SP-17a	0.0034
65	Spring Potentiometer	SP-18a	0.0033
66	Spring Potentiometer	SP-19a	0.0034
67	Spring Potentiometer	SP-20a	0.0034
68	Spring Potentiometer	SP-21a	0.0034
69	Rotational Potentiometer	RP-2	-0.0463
70	Rotational Potentiometer	RP-3	-0.0461